SELECTIVE AEROBIC OXIDATIONS CATALYZED BY MANGANESE(III) COMPLEXES USING REDOX-ACTIVE LIGANDS

A Thesis
Presented to
The Academic Faculty

by

Clarence J. Rolle III

In Partial Fulfillment
of the Requirements for the Degree
Doctorate in the
School of Chemistry and Biochemistry

Georgia Institute of Technology
December, 2011

SELECTIVE AEROBIC OXIDATIONS CATALYZED BY MANGANESE(III) COMPLEXES USING REDOX-ACTIVE LIGANDS

Approved by:

Dr. Jake D. Soper, Advisor
School of Chemistry and Biochemistry
Georgia Institute of Technology

Dr. Angus P. Wilkinson
School of Chemistry and Biochemistry
Georgia Institute of Technology

Dr. E. Kent Barefield
School of Chemistry and Biochemistry
Georgia Institute of Technology

Dr. Christopher W. Jones
School of Chemical and Biomolecular Engineering
Georgia Institute of Technology

Dr. Christoph J. Fahrni
School of Chemistry and Biochemistry
Georgia Institute of Technology

Date: October 11th, 2011

ACKNOWLEDGEMENTS

I would like to thank Dr. Jake Soper for being a great advisor over the past few years. His passion for science is inspirational and made my time in lab enjoyable. I would also like thank my research group members, Aubrey Smith, Michael Bayless and Cameron Lippert for their encouragement and friendship during my time in graduate school. I would also like to thank my wife, Hilda Castillo for her emotional support throughout the course of my studies.

TABLE OF CONTENTS

LIST OF TABLES

LIST OF FIGURES

LIST OF SYMBOLS AND ABBREVIATIONS

NMR	Nuclear magnetic resonance
EPR	Electron paramagnetic resonance
UV-vis	Ultraviolet-visible
FTIR	Fourier transform infrared spectroscopy
MS	Mass spectrometery
FAB	Fast atom bombardment
ESI	Electrospray ionization
EI	Electron impact
GC	Gas chromatography
LC	Liquid chromatography
CV	Cyclic voltammetry
L	Ligand
ap^{2-}	Amidophenolate
isq^{1-}	Iminosemiquinonate
ibq	Iminobenzoquinone
cat^{2-}	Catecholate
sq^{1-}	Semiquninonate
iPr	Isopropyl
tBu	Tertbutyl
Fc	Ferrocene

THF	Tetrahydrofuran
MeOH	Methanol
DMSO	Dimethyl sulfoxide
SCE	Saturated calomel electrode
TMS	Tetramethylsilane
^{o}C	degrees Celcius
ppm	parts per million
λ	wavelength
K	Kelvin
V	Volts
M	Molar
Å	Angstrom
s	second
MHz	megahertz
mL	milliliters
μL	microliters
δ	Chemical shift
^{1}H	Proton
ε	Molar absorbtivity
z	Effective charge
ET	Electron transfer
CT	Charge transfer

LLCT	Ligand-to-ligand charge transfer
MLCT	Metal-to-ligand charge transfer
obs	Observed
equiv	equivalent

Summary

My graduate studies have focused on the development of new manganese-based catalysts for selective aerobic oxidation of organic substrates. These catalysts employ redox-active ligands to accomplish multielectron O_2 reduction, which is required to preserve selectivity. In the catalytic cycles, redox-active ligands act as a reservoir of electrons for net multielectron reaction chemistry at the manganese center.

In the course of my graduate studies, I have prepared a series of new Mn(III) complexes and shown that they are active for aerobic oxidative dehydrogenation of alcohols, and amines, and the oxidative coupling of carbanions. For instance, $[Mn^{III}(Br_4Cat)_2]^-$ is active for the catalytic aerobic oxidation of catechol to quinone at 0.2 mol% catalyst loadings. I was able to isolate $[Mn^{III}(Br_4Cat)_3]^{3-}$ as an intermediate in the reaction. $[Mn^{III}(Br_4Cat)_3]^{3-}$ was previously thought to be inaccessible and isolating it was important in identifying the species that reacts with oxygen. From this study, a detailed understanding of the mechanism was established and allowed me to rationally approach other aerobic organic oxidations.

Other organic oxidations that have successfully been performed include the aerobic oxidation of primary alcohols. I was able to isolate and crystallographically characterize the bridged Mn(III) alkoxide species that reacts with oxygen to extrude 1 equiv of alcohol and 1 equiv of aldehyde. I have shown that this manganese complex is able to oxidize primary alcohols to aldehydes and secondary alcohols to ketones. Primary amines have been oxidized to imines at 2% catalyst loadings using $[Mn^{III}(Br_4Cat)_2]^-$ as a catalyst.

Manganese(III) complexes with redox active amidophenolate ligands have also been prepared. The series of complexes, $Mn^{III}X(isq)_2$, $Mn^{III}(isq)(ap)$ and $[Mn^{III}(ap)_2]^-$ has been isolated and characterized crystallographically. By examining the bond lengths in the crystal structures, it was determined that all three complexes contain Mn(III), with the redox changes occurring at aminophenol ligands. The fully reduced $[Mn^{III}(ap)_2]^-$ reacts with oxygen in the presence of a halide ions to form the $2e^-$ oxidized $Mn^{III}X(isq)_2$. This complex subsequently reacts with aryl Grignard reagents to form new C–C bonds and $[Mn^{III}(ap)_2]^-$. The reaction is catalytic and affords biphenyl in 72% at catalyst loadings as low as 5%. Mechanistic studies show that the C–C bond forming reaction is a concerted $2e^-$ process, whereas the reoxidation by O_2 occurs in a series of $1e^-$ steps.

In sum, I have synthesized new, well-defined manganese(III) complexes that are able to perform selective aerobic oxidations of organic substrates. The use of redox active ligands is important for the multielectronic reaction with O_2. By understanding the mechanistic aspects of the reaction chemistry I have been able to rationally design new complexes and pursue a variety of oxidative transformations.

CHAPTER 1

INTRODUCTION

1.1. Significance of Oxidation Chemistry

Selective oxidations are important tools for the functionalization of compounds in organic synthesis and chemical industry.[1-3] However, approximately 70% of oxidations rely on stoichiometric reagents such as chromate and permanganate to generate products along with metal waste.[1-3]. The scientific community has placed a strong emphasis on reducing the environmental impact of oxidations in fine and commodity chemical synthesis.[4] Molecular oxygen is attractive as an oxidant because it is cheap and produces environmentally benign byproducts (H_2O, H_2O_2).[1-3, 5-10] However, uncatalyzed reactions of dioxygen and organic substrates lead to combustion.[3, 5] The difficulty of using O_2 as a partial oxidant remains a challenging goal within chemistry.[3, 5]

In industry, aerobic oxidations to produce commodity chemicals are typically autoxidations, which are governed by radical pathways. Two successful examples include terephthalic acid and cyclohexanone. Terepthalic acid (TPA) is produced by reacting *p*-xylene and O_2 with a catalytic amount of a trivalent cobalt and manganese acetate salt mixture, and an ammonium bromide cocatalyst in an acetic acid solution **(Scheme 1)**.[11] Bromine free radicals are generated which activate the methyl groups of p-xylene and result in the formation of the aromatic aldehydes, which are further oxidized to carboxylic acids.[11] Nearly all of the 30 million tons of TPA produced each year is used

as precursor for the formation of polyethylene terephthalate, a principal component in plastic bottles and synthetic fibers.[12-13]

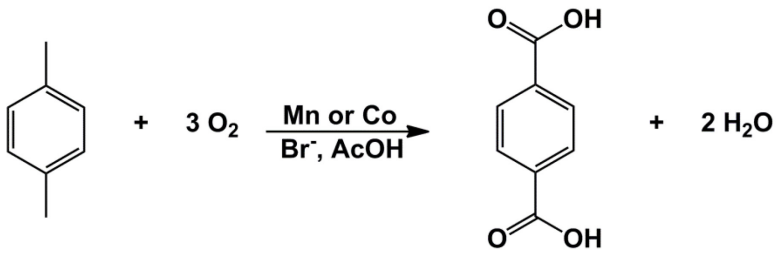

Scheme 1. The aerobic oxidation of p-xylene to terepthalic acid**.**

A mixture of cyclohexanone and cyclohexanol, known as K/A oil, is also produced using air as an oxidant. The reaction of cyclohexane in the presence of a cobalt or manganese acetate salts as catalyst and O_2 affords a cyclohexyl hydroperoxide intermediate, which reacts further to produce the alcohol and the ketone **(Scheme 2)**.[14]

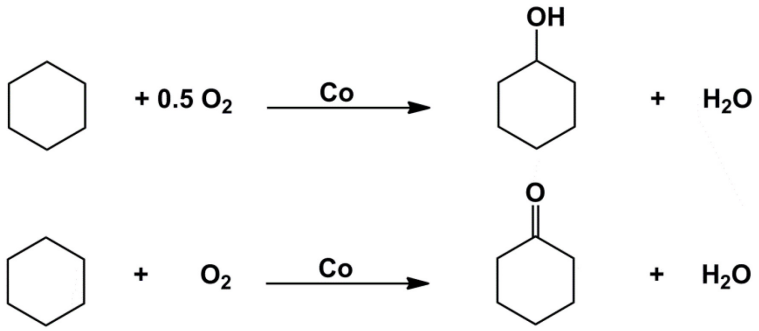

Scheme 2. The aerobic oxidation of cyclohexane.

Most of the K/A mixture produced worldwide is used as a precursor in the preparation of nylon 6,6, which is used in the development of fabrics and materials.[15-16]

Both of these examples of industrial aerobic oxidations are autoxidations and are limited to substrates that are poised to undergo selective radical chemistry. In the case of TPA, the reaction proceeds cleanly because the benzylic C–H bonds are the only reactive

sites in the molecule and the carboxylic acid product that is formed is stable.[3] Whereas, in the reaction of cyclohexane, the conversion to K/A oil is limited to 10–12% in order to prevent overoxidation products such as glutaric and succinic acid from appearing in the mixture.[11] The unreacted cyclohexane must be distilled off and recycled.[11] These cases show that the approach of using O_2 as odd-electron oxidant is both challenging and limited. New methods must be designed that are broadly applicable to a wide range of organic substrates, as the ability to use O_2 as selective oxidant on low carbon feedstocks would have a substantial impact on both fine and commodity chemical syntheses if acheived.

1.2. Palladium Catalyzed Selective Oxidations.

Transition metal catalysts are capable of facilitating selective oxidations by mediating multielectron reactions of organic substrates using dioxygen. One class of metal mediated reactions that has garnered interest is the redox coupling of a $2e^-$ organic substrate oxidation, with the reduction of oxygen to hydrogen peroxide or water.[5] An example of this type of reactivity applied in chemical industry is the Wacker process.[1, 5, 9, 17]. This involves the palladium catalyzed oxidation of alkenes to aldehydes in an aqueous solution and uses a copper cocatalyst **(Scheme 3)**.[1, 5, 9, 17] The reaction is used to make over 4 million tons of aldehyde a year.[18] In this reaction the copper cocatalyst, is necessary to facilitate the reaction with O_2.[1, 19] Without it, the palladium species is prone to decomposition and forms elemental Pd. Other Pd-catalyzed oxidations have been developed to use benzoquinone and alkyl peroxides to facilitate oxidation chemistry.[5]

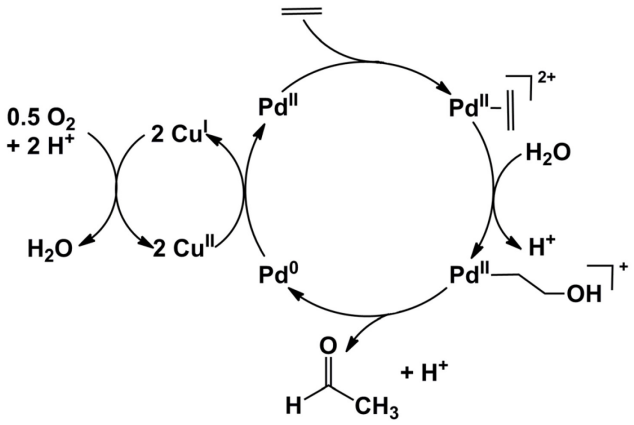

Scheme 3. The Wacker process. [5]

Recent efforts have been made to design palladium oxidation catalysts that undergo direct dioxygen-coupled transfer.[5, 19] This process is more attractive because it is lower in cost, more atom efficient, simplifies product isolation, and helps improve selectivity.[5] The key limitation of previous systems however, was the inability of the reduced Pd^0 to efficiently undergo reoxidation. In these earlier systems, salts such as $Pd(OAc)_2$ and $PdCl_2$ were used for oxidation chemistry. But recently, new Pd systems designed with nitrogen-based and N-heterocyclic carbenes ligands stabilize the Pd^0 state and are resistant to oxidative degradation.[5, 9] These Pd^0 complexes can be efficiently oxidized by O_2. As a result, a host of oxidation chemistry using Pd has been extensively developed over the past 15 years. Some examples include aerobic alcohol oxidation,[20-23] oxidative couplings between alkene substrates with various carbon and heteroatom nucleophiles[24-30] and most recently the aerobic dehydrogenation of substituted cyclohexanones to phenols.[31]

All of these reactions undergo a similar two-step mechanism in which, first Pd^{II} catalyzes the oxidation of an organic substrate by $2e^-$, and, second, the reduced Pd^0 catalyst is oxidized by O_2 to reform the active Pd^{II} species **(Scheme 4)**.[5]

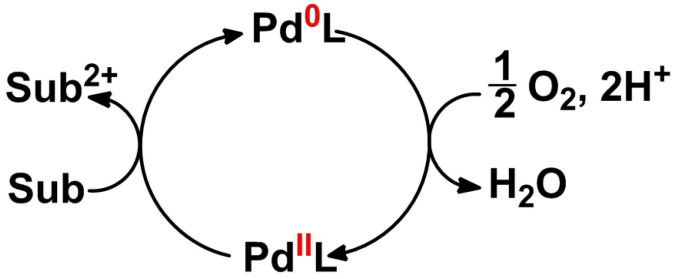

Scheme 4. Aerobic oxidation catalyzed by Pd complexes.

A key feature of both palladium oxidation and cross-coupling catalysts is their tendency to perform $2e^-$ chemistry as opposed to $1e^-$ chemistry.[3, 9, 32-33] This is necessary in order to avoid radical reactions and maintain selectivity. It would be advantageous to use naturally abundant 3d metals such as Mn to perform these selective transformations because they are inexpensive and environmentally friendly. However, 3d metals typically favor $1e^-$ chemistry as opposed to $2e^-$ redox chemistry.[33] In order to do palladium-like aerobic oxidations with 3d metals, systems must be designed to avoid odd electron intermediates when coupling O_2 activation with substrate oxidation.

1.3. Selective Aerobic Oxidation by 3d Metals.

In nature, metalloenzymes are able to mediate selective multielectron reactions with O_2 and/or substrates using 3d metals.[1-3, 34] For instance, active sites at Cu metalloproteins can perform selective oxidations by using multinuclear Cu centers to perform $2e^-$ chemistry or by coupling redox chemistry of Cu to amino acid radical ligands to accomplish multielectron chemistry.[1, 34] Some examples of these active sites can be seen in **Figure 1.1**.

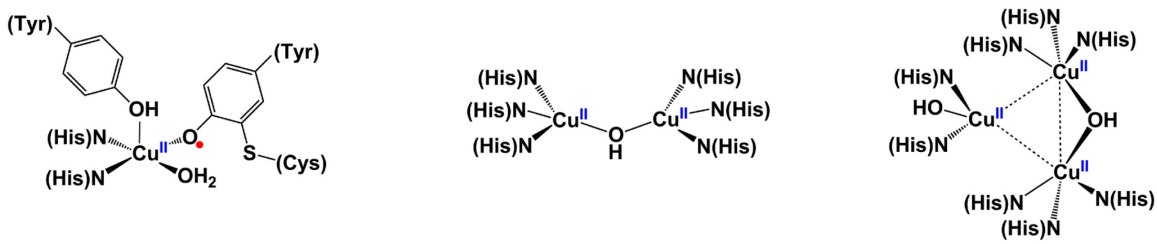

Galactose Oxidase | Catechol Oxidase | Ascorbate Oxidase

Figure 1.1 Structures of the active sites of galactose oxidase, catechol oxidase and ascorbate oxidase

Galactose oxidase is an interesting example because it uses a single Cu that varies between Cu^{I} and Cu^{II} oxidation states with a redox cofactor to accomplish the selective aerobic oxidation of primary alcohols **(Scheme 5).**[1, 3, 34-37]

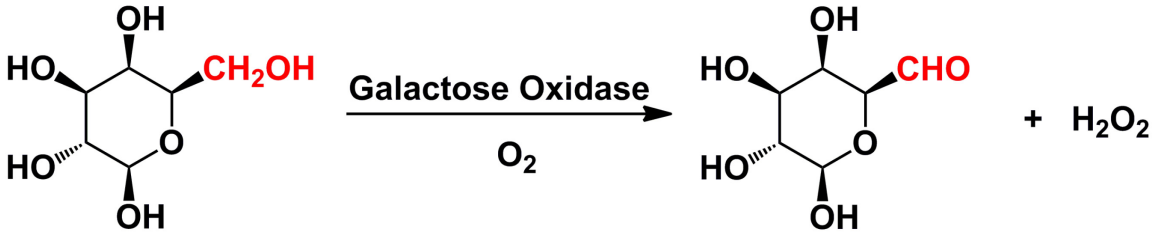

Scheme 5. Aerobic alcohol oxidation catalyzed by Galactose Oxidase

At the active site, copper(II) uses a tyrosyl radical ligand as a redox factor for reaction chemistry **(Scheme 5).** Once an alcohol is bound to the Cu center, it undergoes proton coupled electron transfer to afford a ketyl radical and tyrosine. The ketyl radical can undergo electron transfer to the metal center to yield Cu^{I} and the oxidized aldehyde. The reduced copper metal center and tyrosine undergo selective reoxidation by O_2 to regenerate the starting catalyst.[34]

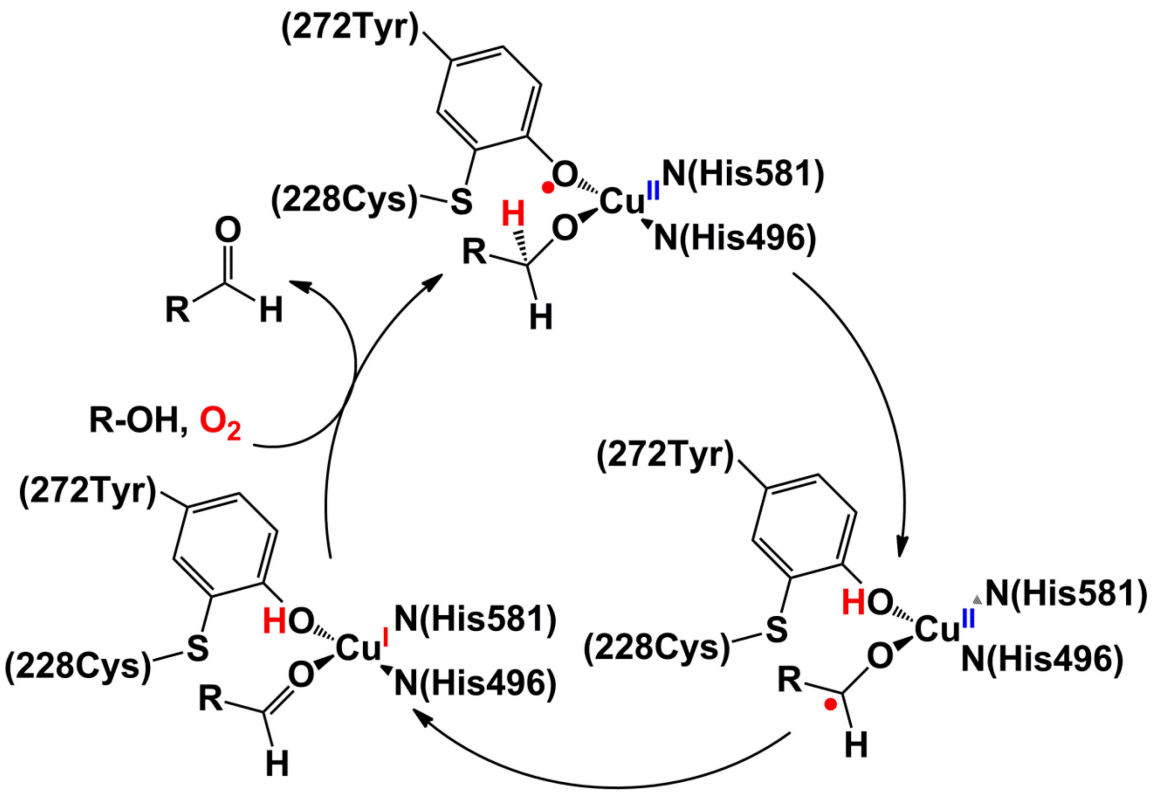

Scheme 6. Mechanism proposed for galactose oxidase.

Another example of radical assisted oxidation is the oxidative deamination of primary amines using copper amine oxidase. This metalloenzyme site converts amines to aldehydes while coupled to the conversion of O_2 to H_2O_2 **(Scheme 6)**.[18, 34, 38]

$$RCH_2NH_2 + O_2 + H_2O \xrightarrow[O_2]{\text{Amine Oxidase}} RCHO + H_2O_2 + NH_3$$

Scheme 7. Oxidative deamination catalyzed by Copper Amine Oxidase.

A look at the proposed mechanism reveals the redox cofactor topaquinone is important for the selective oxidation **(Scheme 8).** The primary amine reacts with the quinone to afford a Schiff base, which is hydrolyzed by water. The overall $2e^-$ reaction

leads to the formation of an aldehyde. It is believed that the reduced species from the resultant reaction is comprised of Cu^{I} and a semiquinone, which is the one electron reduced species of the quinone. This reduced pair then reacts with O_2, in order to regenerate the starting material.

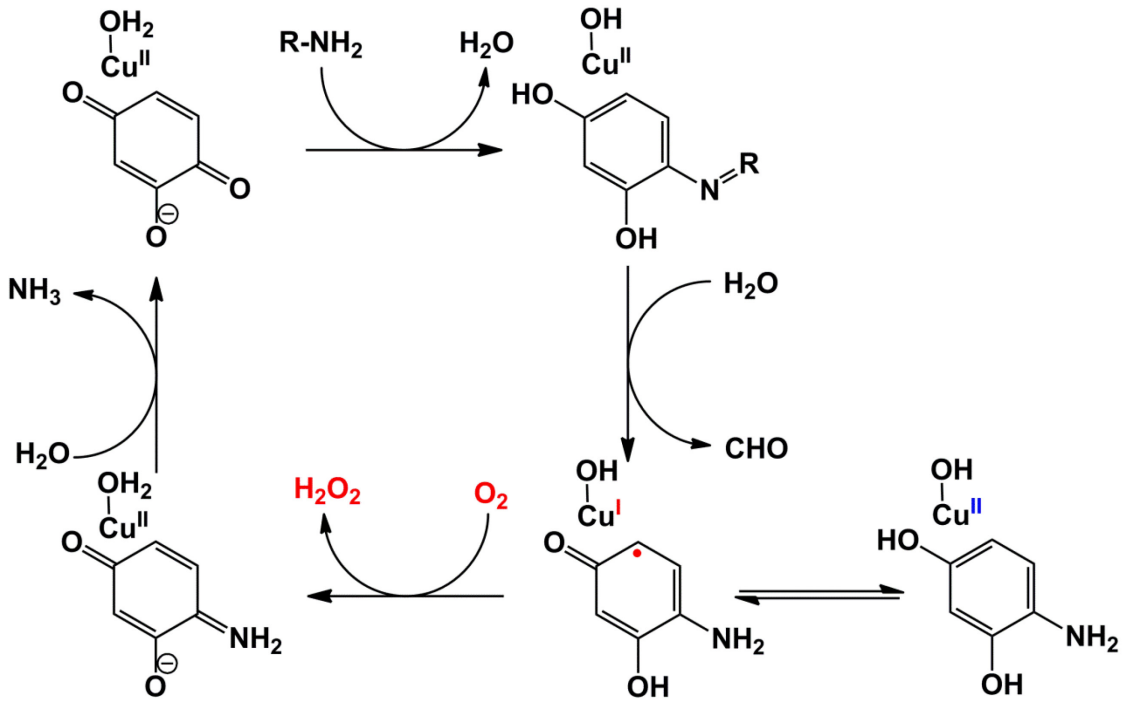

Scheme 8. Detailed mechanism proposed for topa quinone dependent enzymes.

In both reactions, redox cofactors are used in conjunction with copper to facilitate multielectron reactions with organic substrates and O_2.[34] These examples of selective oxidations have inspired the scientific community to build Cu based catalysts that structurally mimic the active sites of enzymes.[39-45] However, rather than mimicking active site structure, an alternative approach to designing an aerobic oxidation catalyst is to translate design elements from these sites that engender catalytic function.

1.4. Redox Active Ligands.

The strategy of using redox cofactors coupled to 3d metals to mediate multielectron redox chemistry can be pursued by using redox active ligands. Redox active ligands undergo low energy ligand-to-metal CT which can facilitate delivery of electrons to the metal center (**Figure 1.2**).

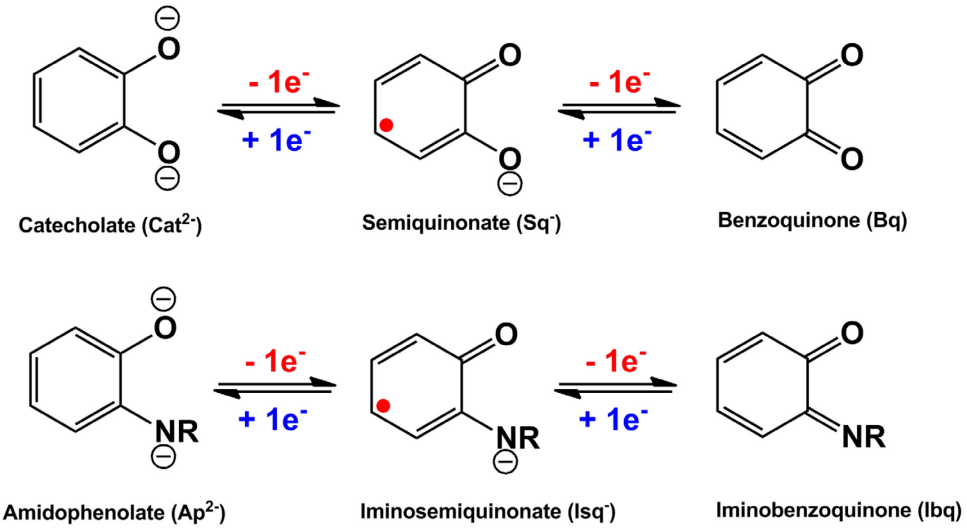

Figure 1.2. The multiple oxidation states of redox active ligands.

Redox active ligands have been studied since the 1960s due to their unusual electronic structures. Gray and co-workers were able to determine that cobalt and nickel dithiolene complexes were best described as M(II) compounds with two ligand centered radicals, rather than complexes with a M(IV) oxidation state.[46-47] Catecholates,[48-49] **(Figure 1.2)** aminophenolates[50-52]**(Figure 1.2)** and diimines[53-55] also have the capacity to act as redox active ligands when coordinated to transition metals. Pierpont[56-62] and Wieghardt[51, 55, 63-66] have used crystallographic, spectroscopic, magnetic data, and theoretical modeling, to assign the correct electronic structure of many transition metal

complexes containing redox active ligands; providing a detailed approach for other chemists to properly assign the correct oxidation states for new complexes.

With a more thorough understanding of electronic structure, recent efforts have focused on using more earth abundant metals in conjunction with redox active ligands to achieve organometallic-type multielectron reactions at coordinatively unsaturated metal centers.[67-82] Some notable examples include, the $2e^-$ oxidative addition and reductive elimination from Zr(IV) complexes,[69, 73] iron catalyzed cycloaddition of dienes,[70] and Negishi type cross-coupling reactions with cobalt.[81]

1.5. Thesis Objective

This thesis describes my successes in developing redox-active ligand catalysts for selective oxidase-type reactions at manganese. I prepared a series of low-coordinate Mn(III) complexes and described their electronic structure. The factors that govern intramolecular ET are elaborated with the aim of utilizing redox-active catechol and aminophenol ligands as reservoirs of electrons for reactions at Mn(III). I expected that these Mn(III) complexes would be stablized over multiple oxidation states by using redox active ligands, which would allow me to activate dioxygen selectively. By designing well defined catalysts, I provided insights and mechanistic details of the role that redox active ligands can play in multielectron catalysis at an earth-abudant metal such as manganese.

1.6. Works Cited

1. F. Meyer, C. L., *Organometallic Oxidation Catalysis*. Springer-Verlag: Heidelberg, 2007; Vol. 22.

2. Borovik, A. S. Z., P. J.; Zart, M. K., Dioxygen Binding and Activation: Reactive Intermediates. In *Activation of Small Molecules: Organometallic and Bioinorganic Perspectives*, Tolman, W. B., Ed. Wiley-VCH: Weinheim, Germany, 2006; pp 187–234.

3. Meunier, B., *Biomimetic Oxidations Catalyzed by Transition Metal Complexes*. Imperial College: London, 2000.

4. Vision 2020 Catalyst Report (http://www.ccrhq.org/Vision2020/Catalysis) September, 2011.

5. Stahl, S. S., Palladium Oxidase Catalysis: Selective Oxidation of Organic Chemicals by Direct Dioxygen-Coupled Turnover. *Angewandte Chemie International Edition* **2004,** *43* (26), 3400-3420, doi:10.1002/anie.200300630.

6. Simándi, L. I., *Advances in Catalytic Activation of Dioxygen by Metal Complexes*. Springer: New York, 2003.

7. Barton, D., H. R., Martell, A. E., Sawyer, D. T.,, *The Activation of Dioxygen and Homogeneous Catalytic Oxidation*. Plenum: New York, 1993.

8. Sawyer, D. T., *Oxygen Chemistry, International Series Of Monographs On Chemistry 26* Oxford University Press: New York, 1991.

9. Stahl, S. S., Palladium-catalyzed oxidation of organic chemicals with O-2. *Science* **2005,** *309* (5742), 1824-1826, doi:10.1126/science.1114666.

10. Zanello, P.; Corsini, M., Homoleptic, mononuclear transition metal complexes of 1,2-dioxolenes: Updating their electrochemical-to-structural (X-ray) properties. *Coordination Chemistry Reviews* **2006,** *250* (15-16), 2000-2022, doi:10.1016/j.ccr.2005.12.017.

11. Weissermel, K., *Industrial organic chemistry*. 3rd ed.; VCH: Weinheim 1997.

12. Wang, Q.; Cheng, Y.; Xu, H.; Wang, L.; Li, X., Aging of Crude Terephthalic Acid Crystals at High Temperatures. *Industrial & Engineering Chemistry Research* **2007,** *46* (22), 7367-7377, doi:10.1021/ie0616139.

13. Raghavendrachar, P.; Ramachandran, S., Liquid-phase catalytic oxidation of p-xylene. *Industrial & Engineering Chemistry Research* **1992,** *31* (2), 453-462, doi:10.1021/ie00002a001.

14. Hendry, D. G.; Gould, C. W.; Schuetzle, D.; Syz, M. G.; Mayo, F. R., Autoxidations of cyclohexane and its autoxidation products. *The Journal of Organic Chemistry* **1976,** *41* (1), 1-10, doi:10.1021/jo00863a001.

15. Hereijgers, B. P. C.; Parton, R. F.; Weckhuysen, B. M., Cyclohexene Epoxidation with Cyclohexyl Hydroperoxide: A Catalytic Route to Largely Increase Oxygenate Yield from Cyclohexane Oxidation. *ACS Catalysis* **2011**, 1183-1192, doi:10.1021/cs200354c.

16. Li, J.; Shi, Y.; Xu, L.; Lu, G., Selective Oxidation of Cyclohexane over Transition-Metal-Incorporated HMS in a Solvent-Free System. *Industrial & Engineering Chemistry Research* **2010,** *49* (11), 5392-5399, doi:10.1021/ie100092x.

17. Keith, J. A.; Henry, P. M., The Mechanism of the Wacker Reaction: A Tale of Two Hydroxypalladations. *Angewandte Chemie International Edition* **2009,** *48* (48), 9038-9049, doi:10.1002/anie.200902194.

18. Crabtree, R., *The Organometallic Chemistry of Transition Metal Complexes* John Wiley & Sons: Hoboken, 2005.

19. Anderson, B. J.; Keith, J. A.; Sigman, M. S., Experimental and Computational Study of a Direct O^2-Coupled Wacker Oxidation: Water Dependence in the Absence of Cu Salts. *Journal of the American Chemical Society* **2010,** *132* (34), 11872-11874, doi:10.1021/ja1057218.

20. Sigman, M. S.; Jensen, D. R., Ligand-Modulated Palladium-Catalyzed Aerobic Alcohol Oxidations. *Accounts of Chemical Research* **2006,** *39* (3), 221-229, doi:10.1021/ar040243m.

21. Pearson, D. M.; Conley, N. R.; Waymouth, R. M., Oxidatively Resistant Ligands for Palladium-Catalyzed Aerobic Alcohol Oxidation. *Organometallics* **2011,** *30* (6), 1445-1453, doi:10.1021/om101037k.

22. Steinhoff, B. A.; Stahl, S. S., Ligand-Modulated Palladium Oxidation Catalysis: Mechanistic Insights into Aerobic Alcohol Oxidation with the Pd(OAc)2/Pyridine Catalyst System. *Organic Letters* **2002,** *4* (23), 4179-4181, doi:10.1021/ol026988e.

23. Nishimura, T.; Onoue, T.; Ohe, K.; Uemura, S., Palladium(II)-Catalyzed Oxidation of Alcohols to Aldehydes and Ketones by Molecular Oxygen. *The Journal of Organic Chemistry* **1999,** *64* (18), 6750-6755, doi:10.1021/jo9906734.

24. Izawa, Y.; Stahl, S. S., Aerobic Oxidative Coupling of o-Xylene: Discovery of 2-Fluoropyridine as a Ligand to Support Selective Pd-Catalyzed C–H Functionalization. *Advanced Synthesis & Catalysis* **2010,** *352* (18), 3223-3229, doi:10.1002/adsc.201000771.

25. Ferreira, E. M.; Stoltz, B. M., Catalytic C–H Bond Functionalization with Palladium(II): Aerobic Oxidative Annulations of Indoles. *Journal of the American Chemical Society* **2003,** *125* (32), 9578-9579, doi:10.1021/ja035054y.

26. Kotov, V.; Scarborough, C. C.; Stahl, S. S., Palladium-Catalyzed Aerobic Oxidative Amination of Alkenes: Development of Intra- and Intermolecular Aza-Wacker Reactions. *Inorganic Chemistry* **2007,** *46* (6), 1910-1923, doi:10.1021/ic061997v.

27. Rogers, M. M.; Wendlandt, J. E.; Guzei, I. A.; Stahl, S. S., Aerobic Intramolecular Oxidative Amination of Alkenes Catalyzed by NHC-Coordinated Palladium Complexes. *Organic Letters* **2006,** *8* (11), 2257-2260, doi:10.1021/ol060327q.

28. Campbell, A. N.; White, P. B.; Guzei, I. A.; Stahl, S. S., Allylic C–H Acetoxylation with a 4,5-Diazafluorenone-Ligated Palladium Catalyst: A Ligand-Based Strategy To Achieve Aerobic Catalytic Turnover. *Journal of the American Chemical Society* **2010,** *132* (43), 15116-15119, doi:10.1021/ja105829t.

29. Bergstad, K.; Grennberg, H.; Bäckvall, J.-E., Aerobic Oxidations of Conjugated Dienes Using a Catalytic Palladium(II) Quinone Heteropolyacid System for Electron Transfer from Organic Substrates to Molecular Oxygen. *Organometallics* **1998,** *17* (1), 45-50, doi:10.1021/om970482w.

30. Nishimura, T.; Araki, H.; Maeda, Y.; Uemura, S., Palladium-Catalyzed Oxidative Alkynylation of Alkenes via C–C Bond Cleavage under Oxygen Atmosphere. *Organic Letters* **2003,** *5* (17), 2997-2999, doi:10.1021/ol0348405.

31. Izawa, Y.; Pun, D.; Stahl, S. S., Palladium-Catalyzed Aerobic Dehydrogenation of Substituted Cyclohexanones to Phenols. *Science* **2011,** *333* (6039), 209-213, doi:10.1126/science.1204183.

32. Stang, P., *Metal-Catalyzed Cross-Coupling Reactions*. Wiley-VCH Verlag GmbH: 1998.

33. Chirik, P. J.; Wieghardt, K., Radical Ligands Confer Nobility on Base-Metal Catalysts. *Science* **2010,** *327* (5967), 794-795, doi:10.1126/science.1183281.

34. Silverman, R., *The Organic Chemistry of Enzyme-Catalyzed Reactions*. Academic Press: San Diego, 2000.

35. Rogers, M. S.; Dooley, D. M., Copper-tyrosyl radical enzymes. *Current Opinion in Chemical Biology* **2003,** *7* (2), 189-196, doi:10.1016/s1367-5931(03)00024-3.

36. Ito, N.; Phillips, S. E. V.; Stevens, C.; Ogel, Z. B.; McPherson, M. J.; Keen, J. N.; Yadav, K. D. S.; Knowles, P. F., Novel thioether bond revealed by a 1.7 [angst] crystal structure of galactose oxidase. *Nature* **1991,** *350* (6313), 87-90,

37. Whittaker, J. W., Galactose oxidase. In *Advances in Protein Chemistry*, Joan Selverstone Valentine, E. B. G., Ed. Academic Press: 2002; Vol. Volume 60, pp 1-49.

38. Mure, M.; Mills, S. A.; Klinman, J. P., Catalytic Mechanism of the Topa Quinone Containing Copper Amine Oxidases†. *Biochemistry* **2002,** *41* (30), 9269-9278, doi:10.1021/bi020246b.

39. Wang, Y.; Stack, T. D. P., Galactose Oxidase Model Complexes: Catalytic Reactivities. *Journal of the American Chemical Society* **1996,** *118* (51), 13097-13098, doi:10.1021/ja9621354.

40. Halfen, J. A.; Jazdzewski, B. A.; Mahapatra, S.; Berreau, L. M.; Wilkinson, E. C.; Que, L.; Tolman, W. B., Synthetic Models of the Inactive Copper(II)−Tyrosinate and Active Copper(II)−Tyrosyl Radical Forms of Galactose and Glyoxal Oxidases. *Journal of the American Chemical Society* **1997,** *119* (35), 8217-8227, doi:10.1021/ja9700663.

41. Peterson, R. L.; Himes, R. A.; Kotani, H.; Suenobu, T.; Tian, L.; Siegler, M. A.; Solomon, E. I.; Fukuzumi, S.; Karlin, K. D., Cupric Superoxo-Mediated Intermolecular

C−H Activation Chemistry. *Journal of the American Chemical Society* **2011,** *133* (6), 1702-1705, doi:10.1021/ja110466q.

42. Wang, Y.; DuBois, J. L.; Hedman, B.; Hodgson, K. O.; Stack, T. D. P., Catalytic Galactose Oxidase Models: Biomimetic Cu(II)-Phenoxyl-Radical Reactivity. *Science* **1998,** *279* (5350), 537-540, doi:10.1126/science.279.5350.537.

43. Chaudhuri, P.; Hess, M.; Müller, J.; Hildenbrand, K.; Bill, E.; Weyhermüller, T.; Wieghardt, K., Aerobic Oxidation of Primary Alcohols (Including Methanol) by Copper(II)− and Zinc(II)−Phenoxyl Radical Catalysts. *Journal of the American Chemical Society* **1999,** *121* (41), 9599-9610, doi:10.1021/ja991481t.

44. Jazdzewski, B. A.; Tolman, W. B., Understanding the copper-phenoxyl radical array in galactose oxidase: contributions from synthetic modeling studies. *Coordination Chemistry Reviews* **2000,** *200-202*, 633-685, doi:10.1016/s0010-8545(00)00342-8.

45. Itoh, S.; Taki, M.; Fukuzumi, S., Active site models for galactose oxidase and related enzymes. *Coordination Chemistry Reviews* **2000,** *198* (1), 3-20, doi:10.1016/s0010-8545(99)00209-x.

46. Gray, H. B.; Williams, R.; Bernal, I.; Billig, E., A Spin-Free Square Planar Cobaltous Complex. *Journal of the American Chemical Society* **1962,** *84* (18), 3596-3597, doi:10.1021/ja00877a045.

47. Billig, E.; Williams, R.; Bernal, I.; Waters, J. H.; Gray, H. B., The Electronic Structures of Square-Planar Metal Complexes. II. The Complexes of Maleonitriledithiolate with Copper(II), Nickel(II), Palladium(II), and Platinum(II). *Inorganic Chemistry* **1964,** *3* (5), 663-666, doi:10.1021/ic50015a013.

48. Pierpont, C. G.; Buchanan, R. M., Transition metal complexes of o-benzoquinone, o-semiquinone, and catecholate ligands. *Coordination Chemistry Reviews* **1981,** *38* (1), 45-87, doi:10.1016/s0010-8545(00)80499-3.

49. Pierpont, C. G.; Lange, C. W., The Chemistry of Transition Metal Complexes Containing Catechol and Semiquinone Ligands. In *Progress in Inorganic Chemistry, Vol 41*, John Wiley & Sons Inc: New York, 1994; Vol. 41, pp 331-442.

50. Poddel'sky, A. I.; Cherkasov, V. K.; Abakumov, G. A., Transition metal complexes with bulky 4,6-di-tert-butyl-N-aryl(alkyl)-o-iminobenzoquinonato ligands:

Structure, EPR and magnetism. *Coordination Chemistry Reviews* **2009,** *253* (3-4), 291-324, doi:10.1016/j.ccr.2008.02.004.

51. Bill, E.; Bothe, E.; Chaudhuri, P.; Chlopek, K.; Herebian, D.; Kokatam, S.; Ray, K.; Weyhermüller, T.; Neese, F.; Wieghardt, K., Molecular and Electronic Structure of Four- and Five-Coordinate Cobalt Complexes Containing Two o-Phenylenediamine- or Two o-Aminophenol-Type Ligands at Various Oxidation Levels: An Experimental, Density Functional, and Correlated ab initio Study. *Chemistry – A European Journal* **2005,** *11* (1), 204-224, doi:10.1002/chem.200400850.

52. Boyer, J. L.; Cundari, T. R.; DeYonker, N. J.; Rauchfuss, T. B.; Wilson, S. R., Redox Activation of Alkene Ligands in Platinum Complexes with Non-innocent Ligands. *Inorganic Chemistry* **2008,** *48* (2), 638-645, doi:10.1021/ic8017248.

53. Lever, A. B. P., Electronic characteristics of an extensive series of ruthenium complexes with the non-innocent o-benzoquinonediimine ligand: A pedagogical approach. *Coordination Chemistry Reviews* **2010,** *254* (13-14), 1397-1405, doi:10.1016/j.ccr.2010.02.022.

54. Nawn, G.; Waldie, K. M.; Oakley, S. R.; Peters, B. D.; Mandel, D.; Patrick, B. O.; McDonald, R.; Hicks, R. G., Redox-Active Bridging Ligands Based on Indigo Diimine ("Nindigo") Derivatives. *Inorganic Chemistry* **2011**, null-null, doi:10.1021/ic200388y.

55. Lu, C. C.; Bill, E.; Weyhermüller, T.; Bothe, E.; Wieghardt, K., Neutral Bis(-iminopyridine)metal Complexes of the First-Row Transition Ions (Cr, Mn, Fe, Co, Ni, Zn) and Their Monocationic Analogues: Mixed Valency Involving a Redox Noninnocent Ligand System. *Journal of the American Chemical Society* **2008,** *130* (10), 3181-3197, doi:10.1021/ja710663n.

56. Bhattacharya, S.; Gupta, P.; Basuli, F.; Pierpont, C. G., Structural Systematics for o-C_6H_4XY Ligands with X,Y= O, NH, and S Donor Atoms. o-Iminoquinone and o-Iminothioquinone Complexes of Ruthenium and Osmium. *Inorganic Chemistry* **2002,** *41* (22), 5810-5816, doi:10.1021/ic025766+.

57. Buchanan, R. M.; Fitzgerald, B. J.; Pierpont, C. G., Semiquinone Radical-Anion Coordination to Divalent Cobalt and Nickel - Strucutral Features of the Bis(3,5-di-tert-butyl-1,2-semiquinone) Cobalt (II) Tetramer. *Inorganic Chemistry* **1979,** *18* (12), 3439-3444,

58. Morris, A. M.; Pierpont, C. G.; Finke, R. G., Synthesis and Characterization of VV(3,6-DBSQ)(3,6-DBCat)2, a d0 Metal Complex with Dioxygenase Catalytic Activity. *Inorganic Chemistry* **2009,** *48* (8), 3496-3498, doi:10.1021/ic802122q.

59. Pierpont, C. G.; Buchanan, R. M., Radical-anion coordination of 9,10-phenanthrenequinone in (pentaoxo)bis(9,10-phenanthrenequinone)dimolybdenum. *Journal of the American Chemical Society* **1975,** *97* (22), 6450-6455, doi:10.1021/ja00855a025.

60. Buchanan, R. M.; Downs, H. H.; Shorthill, W. B.; Pierpont, C. G.; Kessel, S. L.; Hendrickson, D. N., Intramolecular antiferromagnetic exchange in tris(o-semiquinone) complexes of vanadium(III), chromium(III), and iron(III). *Journal of the American Chemical Society* **1978,** *100* (13), 4318-4320, doi:10.1021/ja00481a060.

61. Attia; Pierpont, C. G., Valence Tautomerism within a Linear Polymer Consisting of Pyrazine-Bridged Manganese−Quinone Subunits. Synthesis and Characterization of [MnIII(μ-pyz)(3,6-DBSQ)(3,6-DBCat)]n. *Inorganic Chemistry* **1997,** *36* (27), 6184-6187, doi:10.1021/ic970781d.

62. Buchanan, R. M.; Pierpont, C. G., Tautomeric catecholate-semiquinone interconversion via metal-ligand electron transfer. Structural, spectral, and magnetic properties of (3,5-di-tert-butylcatecholato)(3,5-di-tert-butylsemiquinone)(bipyridyl)cobalt(III), a complex containing mixed-valence organic ligands. *Journal of the American Chemical Society* **1980,** *102* (15), 4951-4957, doi:10.1021/ja00535a021.

63. Chun, H.; Chaudhuri, P.; Weyhermüller, T.; Wieghardt, K., o-Iminobenzosemiquinonato Complexes of Mn(III) and Mn(IV). Synthesis and Characterization of [MnIII(LISQ)2(LAP)] (St = 1) and [MnIV(LISQ)2(LAP-H)] (St = 1/2). *Inorganic Chemistry* **2002,** *41* (4), 790-795, doi:10.1021/ic010860w.

64. Ray, K.; Bill, E.; Weyhermüller, T.; Wieghardt, K., Redox-Noninnocence of the S,S‘-Coordinated Ligands in Bis(benzene-1,2-dithiolato)iron Complexes. *Journal of the American Chemical Society* **2005,** *127* (15), 5641-5654, doi:10.1021/ja040237l.

65. Herebian, D.; Wieghardt, K. E.; Neese, F., Analysis and Interpretation of Metal-Radical Coupling in a Series of Square Planar Nickel Complexes:Correlated Ab Initio and Density Functional Investigation of [Ni(LISQ)2] (LISQ=3,5-di-tert-butyl-o-diiminobenzosemiquinonate(1-)). *Journal of the American Chemical Society* **2003,** *125* (36), 10997-11005, doi:10.1021/ja030124m.

66. Chaudhuri, P.; Verani, C. N.; Bill, E.; Bothe, E.; Weyhermüller, T.; Wieghardt, K., Electronic Structure of Bis(o-iminobenzosemiquinonato)metal Complexes (Cu, Ni, Pd). The Art of Establishing Physical Oxidation States in Transition-Metal Complexes Containing Radical Ligands. *Journal of the American Chemical Society* **2001,** *123* (10), 2213-2223, doi:10.1021/ja003831d.

67. Bart, S. C.; Bowman, A. C.; Lobkovsky, E.; Chirik, P. J., Iron Diazoalkane Chemistry: N−N Bond Hydrogenation and Intramolecular C−H Activation. *Journal of the American Chemical Society* **2007,** *129* (23), 7212-7213, doi:10.1021/ja070056u.

68. Blackmore, K. J.; Lal, N.; Ziller, J. W.; Heyduk, A. F., Catalytic reactivity of a zirconium(IV) redox-active ligand complex with 1,2-diphenylhydrazine. *Journal of the American Chemical Society* **2008,** *130* (9), 2728-+, doi:10.1021/ja710611v.

69. Blackmore, K. J.; Ziller, J. W.; Heyduk, A. F., "Oxidative addition" to a Zirconium(IV) redox-active ligand complex. *Inorganic Chemistry* **2005,** *44* (16), 5559-5561, doi:10.1021/ic050997c.

70. Bouwkamp, M. W.; Bowman, A. C.; Lobkovsky, E.; Chirik, P. J., Iron-Catalyzed [2π + 2π] Cycloaddition of α,ω-Dienes: The Importance of Redox-Active Supporting Ligands. *Journal of the American Chemical Society* **2006,** *128* (41), 13340-13341, doi:10.1021/ja064711u.

71. Bowman, A. C.; Milsmann, C.; Atienza, C. C. H.; Lobkovsky, E.; Wieghardt, K.; Chirik, P. J., Synthesis and Molecular and Electronic Structures of Reduced Bis(imino)pyridine Cobalt Dinitrogen Complexes: Ligand versus Metal Reduction. *Journal of the American Chemical Society* **2010,** *132* (5), 1676-1684, doi:10.1021/ja908955t.

72. Chaudhuri, P.; Wieghardt, K.; Weyhermuller, T.; Paine, T. K.; Mukherjee, S.; Mukherjee, C., Biomimetic metal-radical reactivity: aerial oxidation of alcohols, amines, aminophenols and catechols catalyzed by transition metal complexes. *Biol. Chem.* **2005,** *386* (10), 1023-1033, doi:10.1515/bc.2005.118.

73. Haneline, M. R.; Heyduk, A. F., C-C bond-forming reductive elimination from a zirconium(IV) redox-active ligand complex. *Journal of the American Chemical Society* **2006,** *128* (26), 8410-8411, doi:10.1021/ja061107a.

74. Hull, K. L.; Sanford, M. S., Mechanism of Benzoquinone-Promoted Palladium-Catalyzed Oxidative Cross-Coupling Reactions. *Journal of the American Chemical Society* **2009,** *131* (28), 9651-9653, doi:10.1021/ja901952h.

75. Manuel, T. D.; Rohde, J.-U., Reaction of a Redox-Active Ligand Complex of Nickel with Dioxygen Probes Ligand-Radical Character. *Journal of the American Chemical Society* **2009,** *131* (43), 15582-15583, doi:10.1021/ja9065943.

76. Mukherjee, C.; Pieper, U.; Bothe, E.; Bachler, V.; Bill, E.; Weyhermüller, T.; Chaudhuri, P., Ligand-Derived Oxidase Activity. Catalytic Aerial Oxidation of Alcohols (Including Methanol) by Cu(II)-Diradical Complexes. *Inorganic Chemistry* **2008,** *47* (19), 8943-8956, doi:10.1021/ic8009767.

77. Mukherjee, C.; Weyhermuller, T.; Bothe, E.; Chaudhuri, P., Mimicking the function of amine oxidases and phenoxazinone synthase by a manganese(IV)-monoradical complex. *C. R. Chim.* **2007,** *10* (4-5), 313-325, doi:10.1016/j.crci.2006.11.006.

78. Mukherjee, C.; Weyhermüller, T.; Bothe, E.; Chaudhuri, P., Targeted Oxidase Reactivity with a New Redox-Active Ligand Incorporating N2O2 Donor Atoms. Complexes of Cu(II), Ni(II), Pd(II), Fe(III), and V(V). *Inorganic Chemistry* **2008,** *47* (24), 11620-11632, doi:10.1021/ic8011734.

79. Nguyen, A. I.; Blackmore, K. J.; Carter, S. M.; Zarkesh, R. A.; Heyduk, A. F., One- and Two-Electron Reactivity of a Tantalum(V) Complex with a Redox-Active Tris(amido) Ligand. *Journal of the American Chemical Society* **2009,** *131* (9), 3307-3316, doi:10.1021/ja808542j.

80. Smith, A. L.; Clapp, L. A.; Hardcastle, K. I.; Soper, J. D., Redox-active ligand-mediated Co-Cl bond-forming reactions at reducing square planar cobalt(III) centers. *Polyhedron* **2010,** *29* (1), 164-169, doi:10.1016/j.poly.2009.06.046.

81. Smith, A. L.; Hardcastle, K. I.; Soper, J. D., Redox-Active Ligand-Mediated Oxidative Addition and Reductive Elimination at Square Planar Cobalt(III): Multielectron Reactions for Cross-Coupling. *Journal of the American Chemical Society* **2010,** *132* (41), 14358-14360, doi:10.1021/ja106212w.

82. Zarkesh, R. A.; Ziller, J. W.; Heyduk, A. F., Four-electron oxidative formation of aryl diazenes using a tantalum redox-active ligand complex. *Angew. Chem.-Int. Edit.* **2008,** *47* (25), 4715-4718, doi:10.1002/anie.200800812.

CHAPTER 2

REACTIONS OF TETRABROMOCATECHOLATE COMPLEXES WITH DIOXYGEN

2.1 Introduction.

Significant recent attention has been directed towards the development of new redox catalysts that functionally mimic enzymes that mediate selective aerobic oxidation reactions.[1-16] These catalysts may function as oxygenases, by incorporating one or both oxygen atoms from O_2 into organic substrates, or oxidases, which couple substrate oxidation with the reduction of dioxygen to water or hydrogen peroxide.[2-14]Any catalyst that couples selective bond-activation and functionalization to O_2 reduction must incorporate a multielectron capacity to avoid the loss of specificity that typically accompanies odd-electron autoxidation.[2-3, 6, 17] Traditional inorganic and organometallic catalysts for such reactions often utilize second- and third-row transition metal ions with redox-inert ancillary ligands.[2-3, 5-8] In these systems, the multielectron redox activity is entirely metal-derived. In contrast, redox-active "non-innocent" ligands may impart a multielectron redox capacity to mononuclear first-row metal complexes, which typically prefer only single-electron redox changes.[4, 9, 18] Aside from metalloporphyrin complexes, such ligand-derived multielectron reaction chemistry has been largely unexplored for redox transformations of small-molecules substrates but is receiving increased interest.[4, 9, 18-38]

A goal of this thesis research was to develop new multielectron redox cycles based on the ability of quinoid (*ortho*-dioxolene) ligands and their derivatives to store and deliver charge in reactions with oxygen and other small-molecule substrates.[39-41] In this regard, we were intrigued by previously reported reactions of dioxygen with complexes containing the anionic bis(catecholato)manganese(III) core, particularly the selective and catalytic production of hydrogen peroxide from O_2 by $[Mn^{III}(Cl_4cat)_2(EtOH)(H_2O)]^-$ (Cl_4cat^{2-} = tetrachloro-1,2-catecholate) using hydroxylamine as a sacrificial reductant **(Scheme 1).**[42-47]

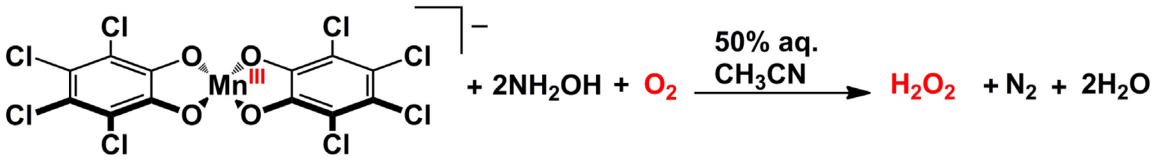

Scheme 1. H_2O_2 production catalyzed by a $[Mn^{III}(Cl_4cat)_2]^-$ complex.[44]

It was postulated that a vacant coordination site at the manganese center was a prerequisite to reaction with O_2.[42-43, 46] However, there was ambiguity regarding the mechanism of the reaction, particularly the speciation of the O_2-sensitive complexes and the possibility of ligand-based redox events during catalytic turnover.[44, 46] Presented herein are the syntheses of new five- and six-coordinate complexes based on the $[Mn^{III}(Br_4cat)_2]^-$ fragment (Br_4cat^{2-} = tetrabromo-1,2-catecholate), and studies of their reaction with O_2.

2.2 Results.

2.2.1 Preparation and Characterization of Mn^{III} Catecholate Complexes.

The complex, ($^{n}Bu_4N$)[$Mn^{III}(Br_4cat)_2(EtOH)(H_2O)$] ($[Br_4Cat]^{2-}$ = tetrabromocatechol) was the precursor used for the studies of reactions with O_2 with manganese(III) catecholate complexes. This complex was prepared based on an adaptation of the literature procedure for the synthesis of $[Mn^{III}(Cl_4cat)_2(EtOH)(H_2O)]^-$.[44] Reactions of $Mn^{II}Cl_2 \bullet 4H_2O$ with 2 equiv Br_4catH_2 in a 4:1 ethanol/water solution with aqueous $^{n}BuN_4OH$, heated to reflux for 1 hr in air to afford a brown solution. Upon cooling, green crystals suitable for X-ray analysis precipitated from solution in 33% yield (**Scheme 2**).

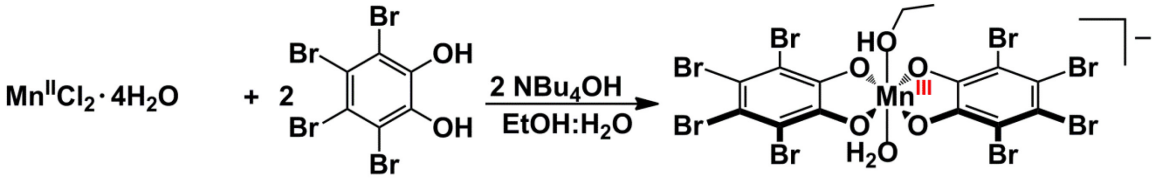

Scheme 2. Synthesis of ($^{n}Bu_4N$)[$Mn^{III}(Br_4cat)_2(EtOH)(H_2O)\bullet(EtOH)$].

A low quality crystal structure was obtained and confirmed that ($^{n}Bu_4N$)[$Mn^{III}(Br_4cat)_2(EtOH)(H_2O)\bullet(EtOH)$] was formed in the reaction **(Figure 2.1)**. The structure contains a six-coordinate manganese anion bound to two coplanar tetrabromocatecholate ligands with one ethanol molecule and one water molecule bound axially. The structure differs from the literature complex, ($^{n}Bu_4N$)[$Mn^{III}(Cl_4Cat)_2(EtOH)(H_2O)$], which also has a manganese ion coordinated to two coplanar catecholate ligands, but has two distinct Mn molecules with either two water molecules or two ethanol molecules bound to the Mn center.[44] The Mn–O bond lengths for the catecholate ligands in $[Mn^{III}(Br_4cat)_2(EtOH)(H_2O)]^-$ have an average distance of 1.906(12) Å. The bond distances between the EtOH and H_2O solvent molecules have an average length of 2.350(12) Å. This axial elongation is typical for

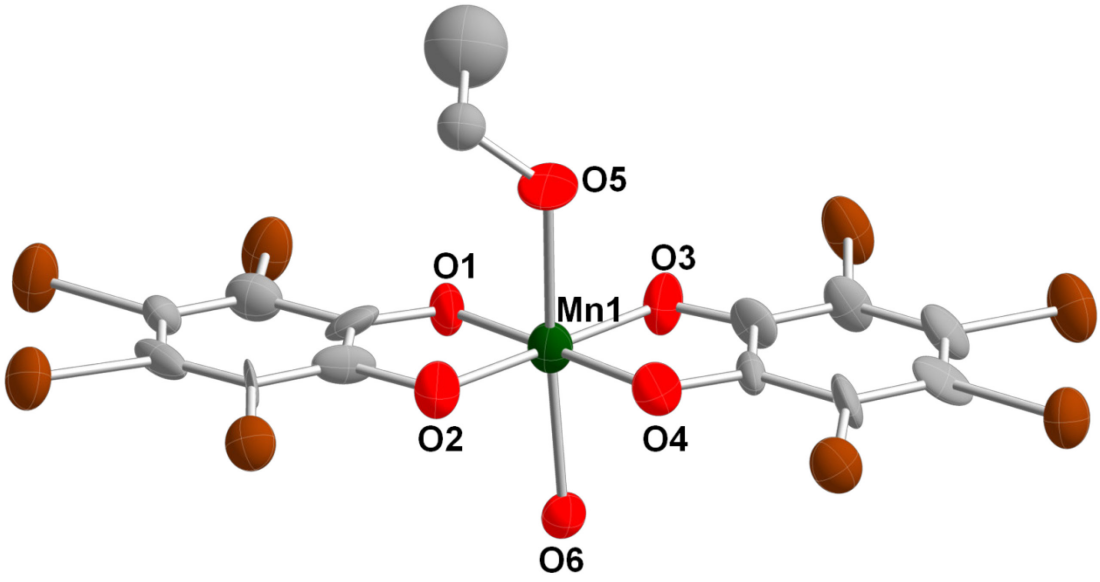

Figure 2.1. Solid-state structure of the anion in (^{n}Bu$_4$N)[Mn^{III}(Br$_4$cat)$_2$(EtOH)(H$_2$O)•(EtOH)] shown with 50% probability ellipsoids. (^{n}Bu$_4$N) countercation, EtOH solvent molecule and H atoms are omitted for clarity. Selected bond lengths (Å) and angles (deg): Mn1–O1 1.884(12), Mn1–O2 1.917 (12), Mn1–O3 1.904(13), Mn1–O4 1.920(12), Mn1–O5 2.359(15), Mn1–O6 2.340(12), O1–Mn1–O2 85.93(5), O1–Mn1–O5 94.91(5), O2–Mn1–O5 87.33 (5).

high spin d^4 metals.[48] The perbrominated catecholates have an average C–O bond lengths of 1.334 Å respectively, which indicate that they are fully reduced.[49] The low quality crystals were not useful for determining the C–C bond lengths, which can also be used to assign the oxidation states of the ligands.

To improve the yield of desired Mn product and the quality of crystals for X-ray analysis, an alternative procedure for synthesis of molecules containing the $[Mn^{III}(Br_4cat)_2]^-$ core was developed. Heating acetone solutions of $Mn^{II}(ClO_4)_2 \bullet 6H_2O$ with 2 equiv Br_4catH_2 and $^nBuN_4OH$ to reflux in air generates an olive green solution, which on cooling to –20 °C deposits analytically pure, dark green solids in ca. 60% yield **(Scheme 3**).

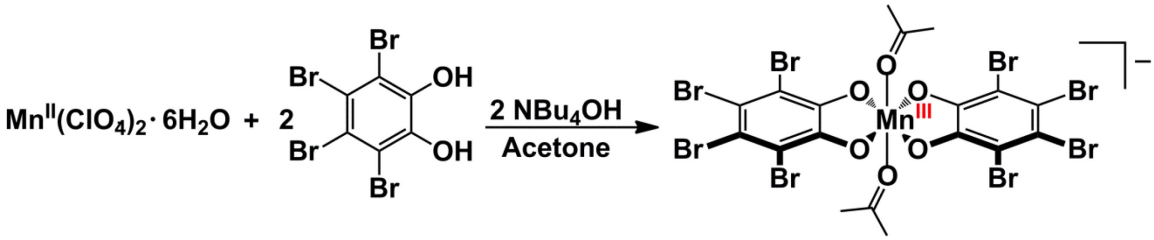

Scheme 3. Synthesis of $(^nBu_4N)[Mn^{III}(Br_4cat)_2(Me_2C{=}O)_2]$.

Recrystallization from acetone gave crystals suitable for X-ray diffraction **(Figure 2.2)**. The crystal structure shows a six-coordinate manganese anion located on a crystallographically defined inversion center and bound to two coplanar *o*-dioxolene ligands and two acetone molecules. The catecholate ligands have C–C and C–O bond lengths averaging 1.396 Å and 1.337 Å respectively, which best match those expected for $[Br_4cat]^{2-}$.[49] The axial $Mn–O_{acetone}$ bond distance of 2.403(4) Å is elongated relative to the 1.901(6) Å averaged $Mn–O_{Br_4cat}$ bond lengths, consistent with a high-spin $3d^4$

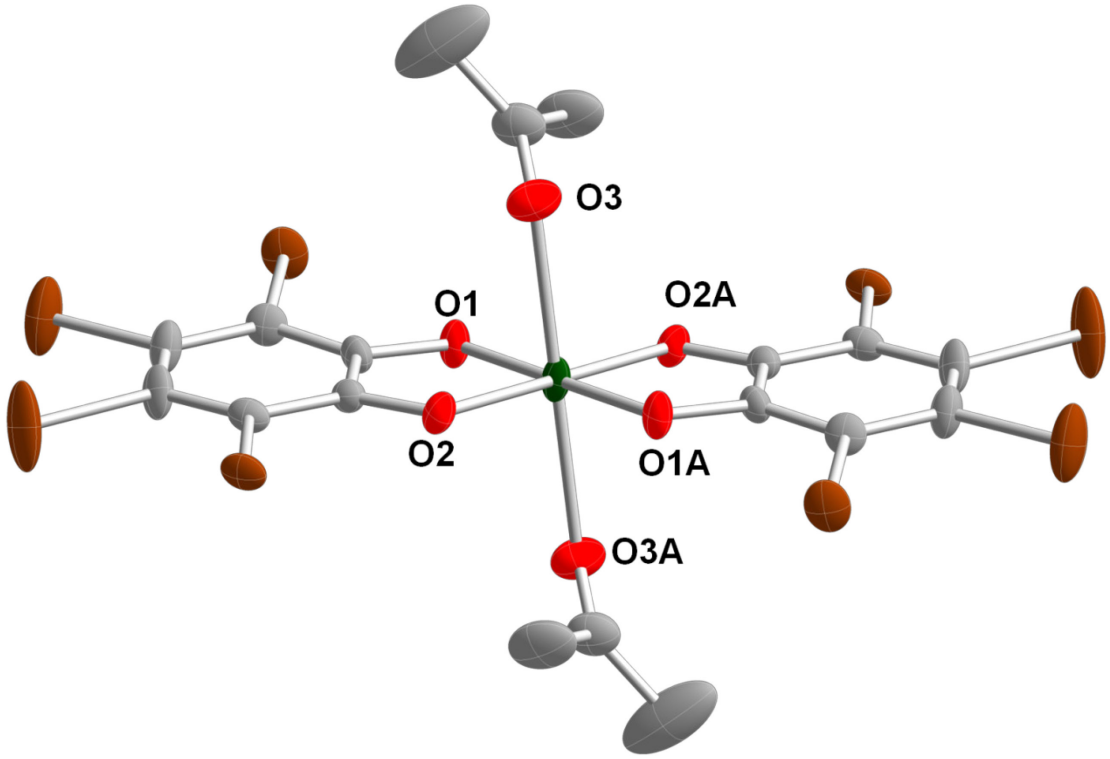

Figure 2.2. Solid-state structure of the anion in (^{n}Bu$_4$N)[Mn^{III}(Br$_4$cat)$_2$(Me$_2$C=O)$_2$] (^{n}Bu$_4$N) and H atoms have been omitted for clarity. Selected bond lengths (Å) and angles (deg): Mn1–O1 1.905(4), Mn1–O2 1.897(4), Mn1–O3 2.403(4), O1–Mn1–O2 86.17(15), O1–Mn1–O3 93.41(16), O2–Mn1–O3 95.27(17).

electron configuration.[48] With the observations the product is best described as ($^{n}Bu_4N$)[$Mn^{III}(Br_4cat)_2(Me_2C{=}O)_2$].

The synthesis of $[Mn^{III}(Br_4cat)_2]^-$ core was also performed in MeOH. Refluxing $Mn^{II}Cl_2{\bullet}4H_2O$ with 2 equiv Br_4catH_2 and $^{n}BuN_4OH$ in a MeOH solution in air for 1 hr affords a yellow solution **(Scheme 4).**

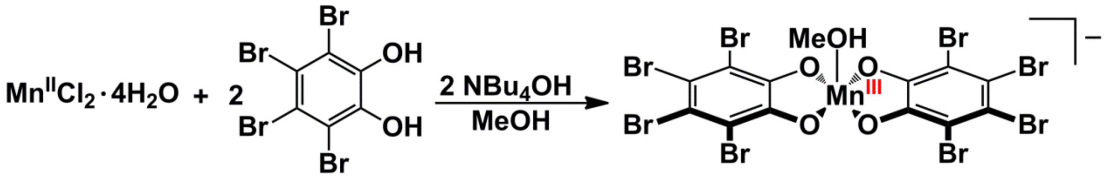

Scheme 4. Synthesis of ($^{n}Bu_4N$)[$Mn^{III}(Br_4cat)_2(MeOH)$].

Slow evaporation of the solution from MeOH leads to green crystals suitable for x-ray crystallography. In this case, the reaction afforded a five-coordinate methanol adduct with distorted square-pyramidal geometry **(Figure 2.3).** The quinoid chelates have C–C and C–O bond lengths averaging 1.399 Å and 1.345 Å respectively, which best match those expected for $[Br_4cat]^{2-}$.indicative of fully reduced catecholate ligands.[49] The catecholate ligands have an average Mn–O bond distance of 1.901(2) Å, which is shorter than the Mn–O bond distance of the methanol adduct, which is 2.119 (2) Å. This is also consistent with a high-spin $3d^4$ electron configuration.[48] ($^{n}Bu_4N$)[$Mn^{III}(Br_4cat)_2(MeOH)$] is the best electronic description of the complex.

Concurrent with the synthesis of ($^{n}Bu_4N$)[$Mn^{III}(Br_4cat)_2(Me_2C{=}O)_2$], the preparation of a five coordinate $OPPh_3$ complex was also pursued. Using $Mn(OPPh_3)_2Cl_2$[50] as a precursor and reacting it with 2 equiv of Br_4catH_2 and $^{n}BuN_4OH$ in isopropanol under reflux conditions in air generates a yellow solution, which on

∘

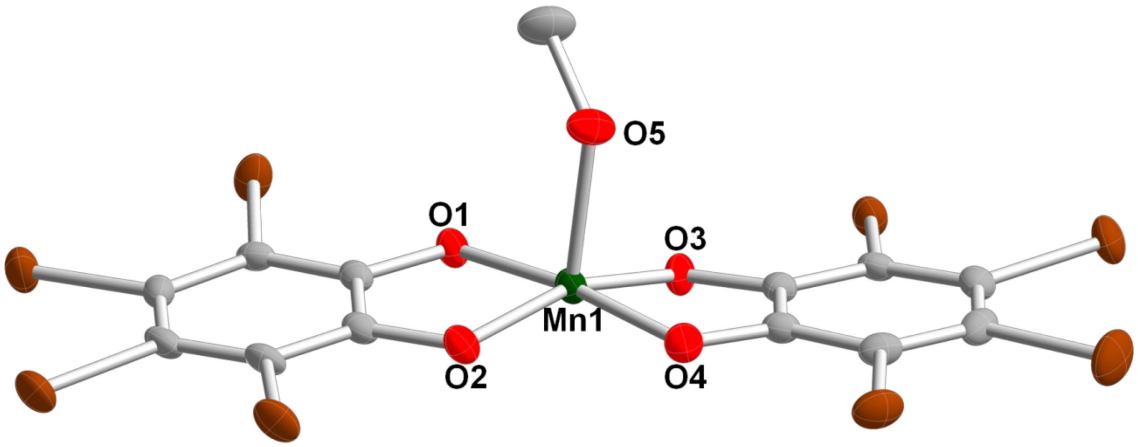

Figure 2.3. Solid-state structure of the anion in ($^{n}Bu_4N$)[$Mn^{III}(Br_4cat)_2(MeOH)$] shown with 50% probability ellipsoids. ($^{n}Bu_4N$) Countercation and H atoms omitted for clarity. Selected bond lengths (Å) and angles (deg): Mn1–O1 1.912(2), Mn1–O2 1.899(2), Mn1–O3 1.886(2), Mn1–O4 1.899(2), Mn1–O5 2.119(3), O5–C13 1.416(4), O1–Mn1–O2 85.22(9), O1–Mn1–O5 101.46(10), O2–Mn1–O5 94.80(10).

to room temperature deposits ($^{n}Bu_4N$)[$Mn^{III}(Br_4cat)_2(OPPh_3)$], as dark green microcrystals in 36% yield **(Scheme 5)**.

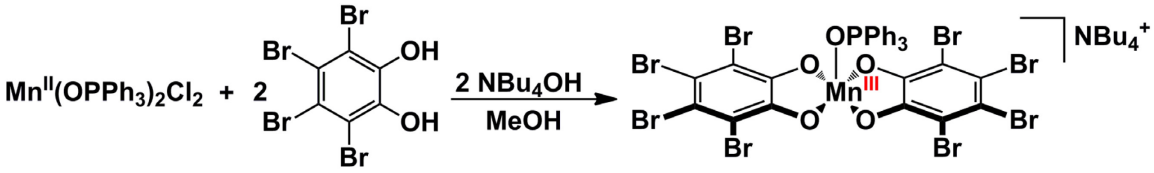

Scheme 5. Synthesis of ($^{n}Bu_4N$)[$Mn^{III}(Br_4cat)_2(MeOH)$].

Crystals suitable for x-ray crystallography were grown by slow diffusion of pentane in to a CH_2Cl_2 solution. The five-coordinate $OPPh_3$ complex is similar to the methanol adduct and also exhibits a distorted square-pyramidal geometry **(Figure 2.4)**. The average Mn–O bond distance for the catecholate ligands is 1.912(13) Å, is shorter than the Mn–O bond distance of the methanol adduct, which is 2.075 (15) Å. This axial elongation is consistent with a high-spin $3d^4$ electron configuration.[48] The crystal was of low quality and could not be used to distinguish the oxidation states of the catecholate ligands by their C–C and C–O bond lengths.

2.2.2. Reactions of $[Mn^{III}(Br_4cat)_2]^-$ with O_2.

The UV–vis spectra of all the complexes containing the $[Mn^{III}(Br_4cat)_2]^-$ core are identical in either acetone or MeCN, suggesting that the axial ligands are all substitution labile, while the $[Mn^{III}(Br_4cat)_2]^-$ fragment is preserved in solution. Exposure of $[Mn^{III}(Br_4cat)_2(Me_2C{=}O)_2]^-$ or $[Mn^{III}(Br_4cat)_2(MeOH]^-$ to 1 atm O_2 in acetone or MeCN solutions affords conversion to a dark blue species over weeks at ambient temperature.

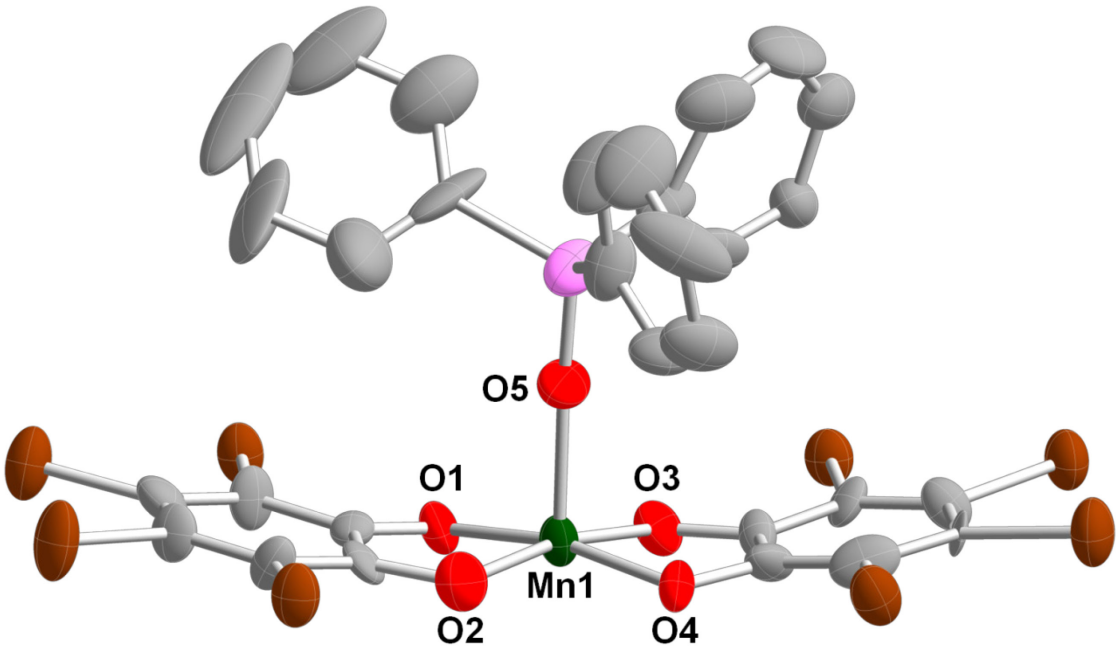

Figure 2.4. Solid-state structure of the anion in ($^{n}Bu_4N$)[Mn^{III}(Br_4cat)$_2$($OPPh_3$] shown with 50% probability ellipsoids. ($^{n}Bu_4N$) Countercation and H atoms omitted for clarity. Selected bond lengths (Å) and angles (deg): Mn1–O1 1.927(13), Mn1–O2 1.899(14), Mn1–O3 1.909(13), Mn1–O4 1.926(12), Mn1–O5 2.075(15), O1–Mn1–O2 85.9(6), O1–Mn1–O5 96.0(6), O2–Mn1–O5 95.3(7).

However, the triphenylphosphine oxide complex ($^{n}Bu_4N$)[$Mn^{III}(Br_4cat)_2(OPPh_3)$] is indefinitely stable under air in MeCN. For O_2 sensitivity studies ($^{n}Bu_4N$)[$Mn^{III}(Br_4cat)_2(OPPh_3)$] was generated *in situ* by the addition of excess $OPPh_3$ to $Mn^{III}(Br_4cat)_2(Me_2C{=}O)_2]^-$. The UV–vis spectrum of ($^{n}Bu_4N$)[$Mn^{III}(Br_4cat)_2(OPPh_3)$] in MeCN is unchanged with air exposure over weeks at ambient temperature. These observations are contrary to previous reports,[42-44, 46-47] which suggested that closely related species underwent facile reactions with O_2. The sluggish reaction of the $[Mn^{III}(Br_4cat)_2]^-$ fragment with dioxygen observed in my hands, led me to thoroughly reexamine its reaction with O_2.

A clue towards the identity of the true air-sensitive species in prior reports came from observation of a second red-orange product in the reaction to prepare $[Mn^{III}(Br_4cat)_2(Me_2C{=}O)_2]^-$. The red-orange product was initially suspected to be tetrabromo-1,2-benzoquinone(Br_4bq), but the UV-Vis spectrum of the unknown product did not agree. However, addition of Br_4cat^{2-} to a solution of Br_4bq afforded a solution whose UV-Vis spectrum matched the unknown product. Previous literature has shown that Br_4bq couples with Br_4cat^{2-} to afford hexabromo-2,3-oxanthrenequinone.[51-52] Accordingly, reactions of Br_4bq with isolated $[Mn^{III}(Br_4cat)_2(Me_2C{=}O)_2]^-$ in MeCN under N_2 leads to the slow formation of bright red crystals and the decomposition of $[Mn^{III}(Br_4cat)_2(Me_2C{=}O)_2]^-$ **(Scheme 6).** The crystals were characterized by X-ray analysis because of the compound's poor solubility in organic solvents for ^{13}C NMR experiments **(Figure 2.5)**.

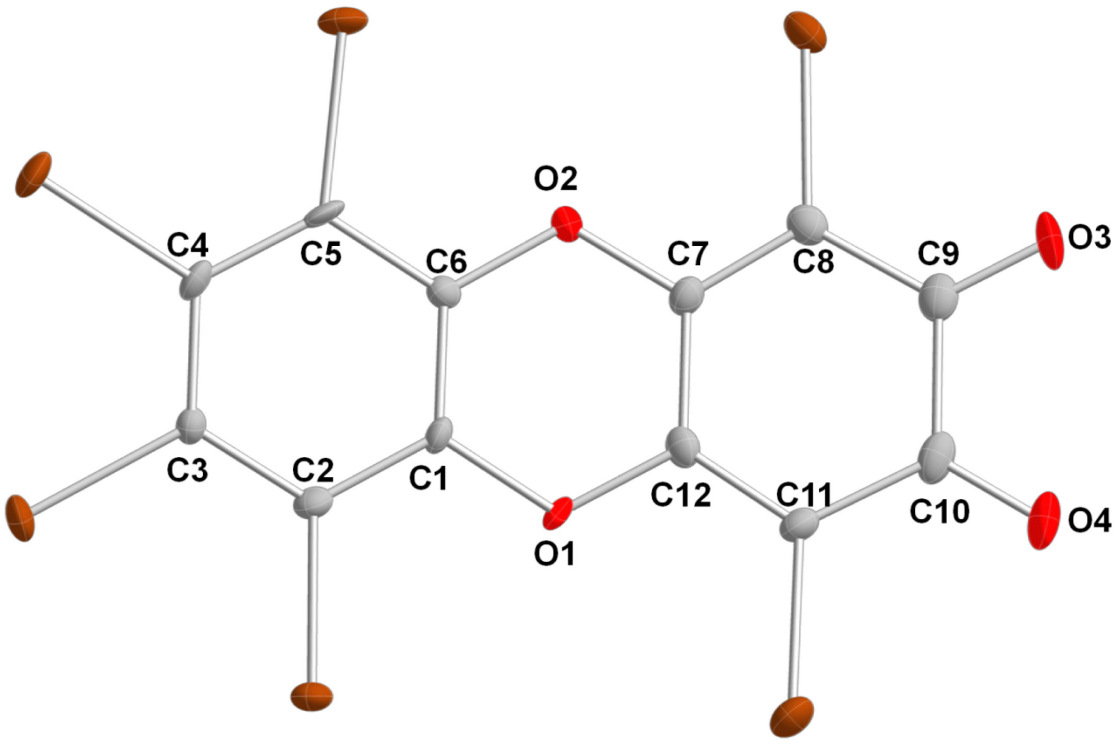

Figure 2.5. Complete solid-state structure of hexabromo-2,3-oxanthrenequinone drawn with 50% probability ellipsoids. Selected bond lengths (Å): O1–C1 1.376(5), O1–C12 1.364(5), O2–C6 1.360(5), O2–C7 1.350(5), O3–C9 1.207(5), O4–C10 1.204(5), C1–C2 1.376(5), C2–C3 1.394(6), C3–C4 1.405(5), C4–C5 1.389(6), C5–C6 1.387(6), C1–C6 1.381(5), C7–C8 1.352(5), C8–C9 1.449(6), C9–C10 1.550(6), C10–C11 1.472(6), C11–C12 1.355(6), C7–C12 1.462(5)

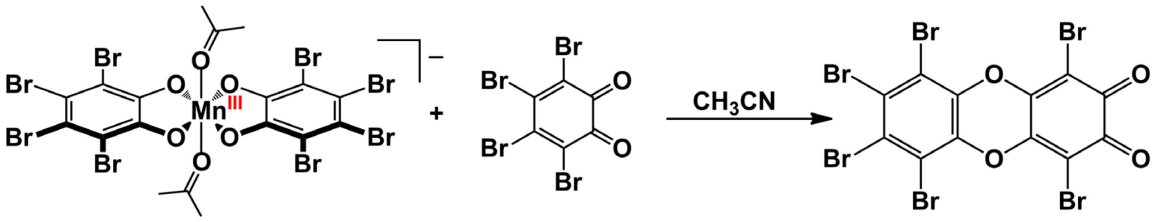

Scheme 6. Decomposition of Mn to form hexabromo-2,3-oxanthrenequinone

The structure confirmed that the red material observed in the reaction was hexabromo-2,3-oxanthrenequinone.

The apparent intermediacy of free Br_4bq under the aerobic conditions employed for the preparation of $[Mn^{III}(Br_4cat)_2(Me_2C{=}O)_2]^-$, and the isolated yields of ~60% for $[Mn^{III}(Br_4cat)_2(Me_2C{=}O)_2]^-$, suggest that 1 equiv Br_4catH_2 is consumed as a sacrificial reductant for each equivalent of $[Mn^{III}(Br_4cat)_2(Me_2C{=}O)_2]^-$ produced **(Scheme 7)**. Assuming Br_4catH_2 is a limiting reagent in the synthesis of $[Mn^{III}(Br_4cat)_2(Me_2C{=}O)_2]^-$, the isolated yields of ~60% for $[Mn^{III}(Br_4cat)_2(Me_2C{=}O)_2]^-$ are close to the theoretical yield of 66%. The discrepancy is likely due to the reaction of Br_4bq with $[Mn^{III}(Br_4cat)_2(Me_2C{=}O)_2]^-$.

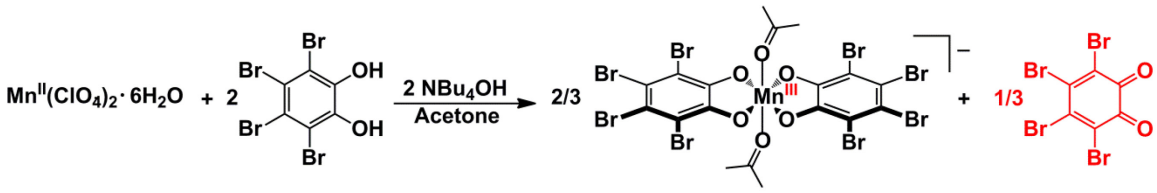

Scheme 7. Secondary product observed in the synthesis of $[Mn^{III}(Br_4cat)_2(Me_2C{=}O)_2]^-$.

Anaerobic addition of Br_4cat^{2-}, generated *in situ* from Br_4catH_2 and LiOMe, to air-stable $[Mn^{III}(Br_4cat)_2(Me_2C{=}O)_2]^-$ in MeCN gives immediate conversion to a dark green, air-sensitive material. The same material can be independently obtained from reaction of $Mn^{II}(ClO_4)_2$ with 3 equiv Br_4catH_2 and 6 equiv LiOMe in MeOH at ambient

temperature, followed by air exposure and precipitation with PPN–Cl (PPN^+ = bis(triphenylphosphine)iminium) **(Scheme 8)**. Recrystallization from THF-pentane under N_2 afforded single crystals suitable for analysis by X-ray crystallography (**Figure 2.6**).

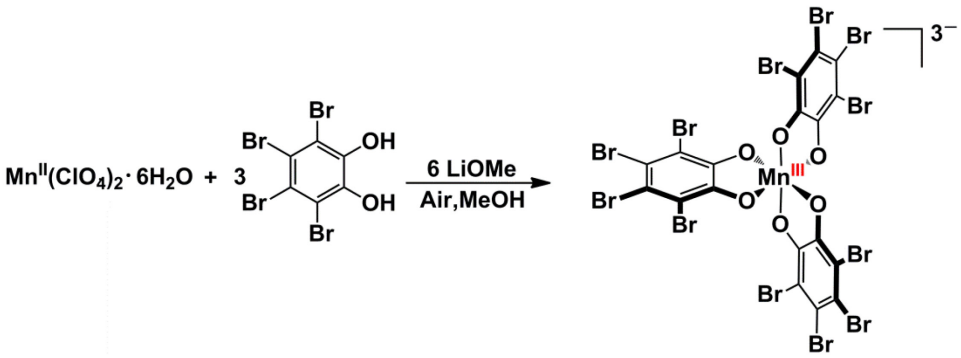

Scheme 8. Synthesis of $[Mn^{III}(Br_4Cat)_3]^{3-}$

The structure reveals a six-coordinate manganese tris(tetrabromo-*o*-catecholato) trianion with two $Li(THF)_2^+$ cations in close contact with the axial oxygen atoms and PPN^+ counterion. The complex has a distorted octahedral geometry with three distinct sets of Mn–O bond lengths. One ligand has short Mn–O bond lengths of 1.898(3) Å and 1.917(3) Å, whereas the other two ligands are coordinated through one short and long Mn–O bond. The bond lengths of 1.970(3) Å and 2.154(3) Å are observed in one ligand and 1.959(3) Å and 2.161(3) Å are observed for the other. The two elongated bonds are arranged in an axial fashion, which is typical of a Jahn-Teller distorted, high-spin Mn(III) ion.[48] The catecholate ligands have C–C and C–O bond lengths averaging 1.398 Å and 1.328 Å respectively, which best match those expected for $[Br_4cat]^{2-}$.[49] The sum of the metrical data are therefore most consistent with formulation $[Mn^{III}(Br_4Cat)_3]^{3-}$. The successful isolation of $[Mn^{III}(Br_4Cat)_3]^{3-}$ refutes earlier reports that suggested that the

°

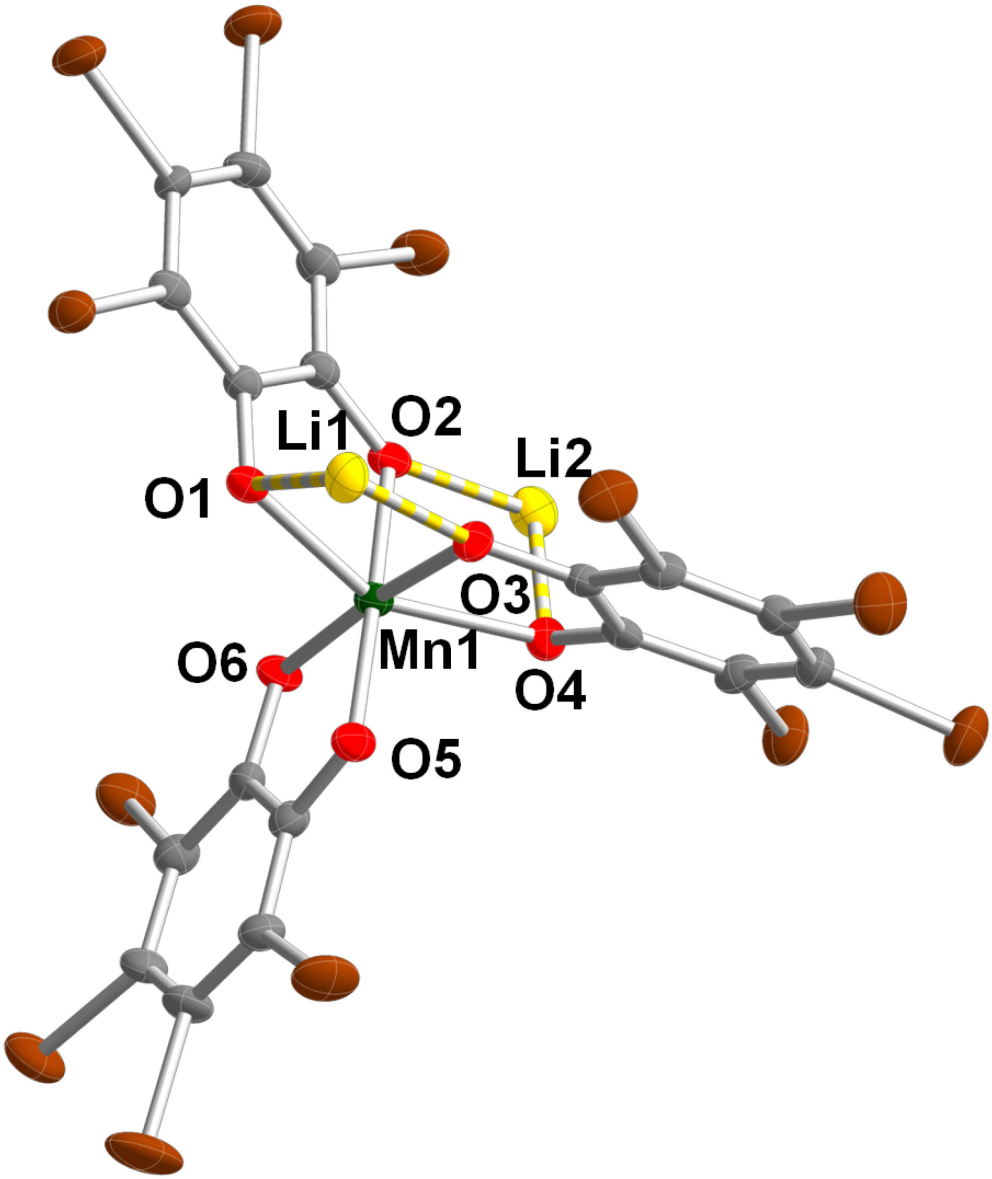

Figure 2.6. Solid-state structures of the anion (PPN)$Li_2[Mn^{III}(Br_4cat)_3]$•5THF shown with 50% probability ellipsoids. Hydrogen atoms, THF solvate molecules and PPN countercation omitted for clarity. Selected bond lengths (Å) and angles (deg): Mn1–O1 1.970(3), Mn1–O2 2.154(3), Mn1–O3 2.161(3), Mn1–O4 1.959(3), Mn1–O5 1.898(3), Mn1–O6 1.917(3), O1–Mn1–O2 85.05(13), O3–Mn1–O4 79.96(11), O5–Mn1–O6 79.84(11), O1–Mn1–O3 102.28(12), O1–Mn1–O6 96.79(11).

homoleptic tris(catecholato)manganese(III) complexes are inaccessible due to geometric constraints imposed by the ligands.[43-44, 46-47, 53]

Exposure of $[Mn^{III}(Br_4Cat)_3]^{3-}$ to O_2 in MeCN, acetone or THF results in an immediate color change from green to dark blue in MeCN or acetone, and violet in THF. The UV–vis spectrum of the blue species is nearly identical to the previously reported dianion $[Mn^{IV}(Cl_4cat)_3]^{2-}$,[42, 44] and was therefore formulated as $[Mn^{IV}(Br_4cat)_3]^{2-}$ **(Figure 2.7)**. Consistent with this assignment, $[Mn^{IV}(Br_4cat)_3]^{2-}$ is independently generated *in situ* from addition of 1.0 equiv $AgPF_6$ to $[Mn^{III}(Br_4cat)_3]^{3-}$ under N_2. $[Mn^{IV}(Br_4cat)_3]^{2-}$ was also prepared and isolated from the reaction of $Mn^{II}(ClO_4)_2$ with 3 equiv Br_4catH_2 and 6 equiv Et_3N in 3:1 CH_2Cl_2/THF solution at ambient temperature **(Scheme 9)**.

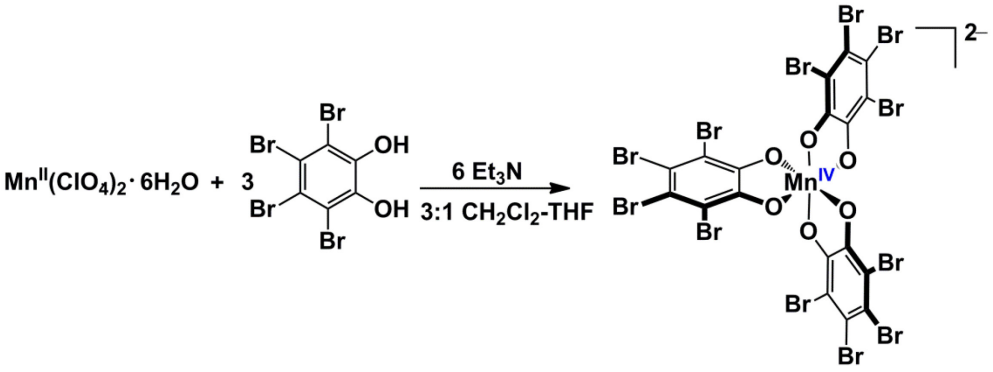

Scheme 9. Synthesis of $2(Et_3NH)[Mn^{IV}(Br_4cat)_3]$.

Slow evaporation affords blue crystals, however a structure could not be obtained. Elemental analysis, ESI–MS and UV–Vis were used to characterize and confirm the identity of the product. Interestingly, the color of $[Mn^{IV}(Br_4cat)_3]^{2-}$ in MeCN is temperature dependent, converting from dark blue at –20 °C to green at 65 °C. This color change may reflect conversion to a $[Mn^{III}(Br_4cat)_2(Br_4sq^{\bullet})]^{2-}$ ($Br_4sq^{\bullet-}$ = tetrabromo-

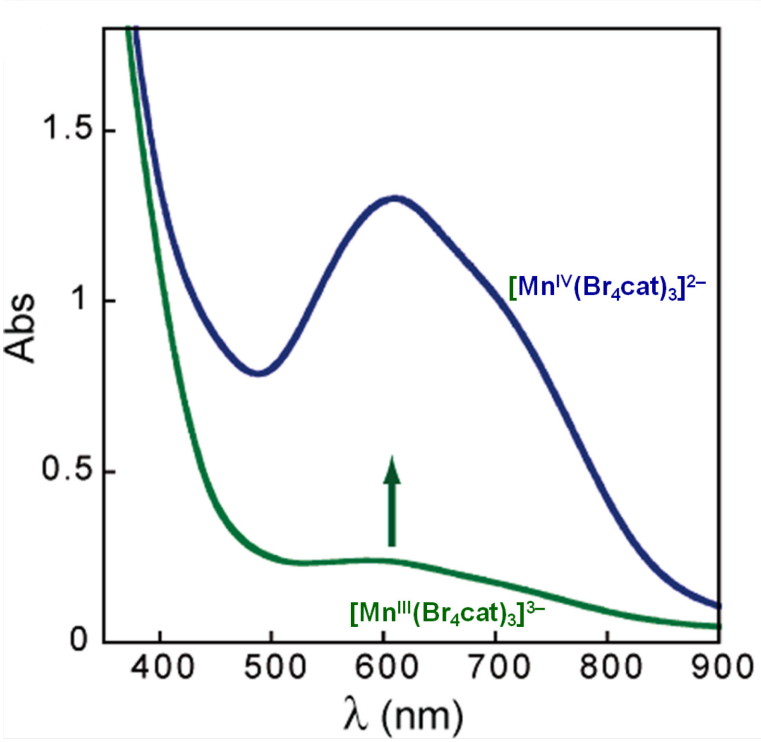

Figure 2.7. UV–vis absorption spectra for a reaction of 2.4×10^{-4} M $[Mn^{III}(Br_4cat)_3]^{3-}$ (green line) with 1 atm O_2 in MeCN to generate$[Mn^{IV}(Br_4cat)_3]^{2-}$ (blue line) in 100 min at 298 K.

1,2-semiquinonate) intravalence isomer. The color change is partially reversible, leading to degradation of the $[Mn^{IV}(Br_4cat)_3]^{2-}$ with repeated trials.

Although $[Mn^{IV}(Br_4cat)_3]^{2-}$ is indefinitely stable under N_2, it is unstable under O_2 over hours at 298 K, affording $[Mn^{III}(Br_4Cat)_2]^-$ and Br_4bq-derived products (**Scheme 10**).

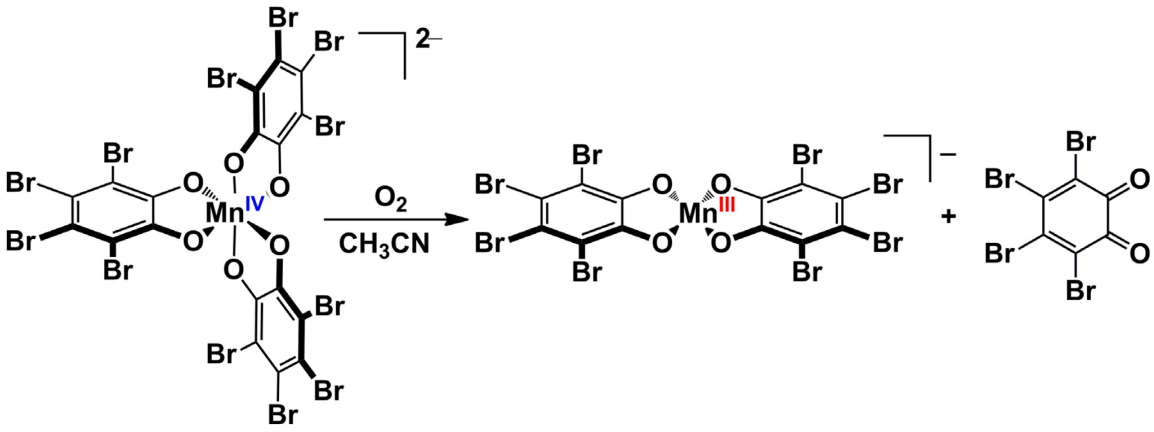

Scheme 10. Oxidative degradation of $[Mn^{IV}(Br_4cat)_3]^{2-}$.

The anionic $[Mn^{III}(Br_4Cat)_2]^-$ fragment was isolated as an insoluble PPN^+ salt from reaction of $(PPN)Li_2[Mn^{III}(Br_4cat)_3]\bullet 5THF$ with O_2 in THF and its identity was confirmed by UV-vis spectroscopy and by ESI-MS in MeCN.

The addition of 1 equiv Cp^*_2Co to $[Mn^{III}(Br_4cat)_2]^-$ in MeCN gives immediate conversion to a light yellow product which rapidly reacts with O_2 to generate green $[Mn^{III}(Br_4cat)_3]^{3-}$ and blue $[Mn^{IV}(Br_4cat)_3]^{2-}$, as evidenced by UV–vis spectroscopy. An identical yellow complex is obtained from combination of $Mn^{II}(ClO_4)_2$, 3 equiv Br_4CatH_2, and $^nBuN_4OH$ in acetone with rigorous exclusion of air. These observations suggest that $[Mn^{II}(Br_4cat)_3]^{4-}$ is the initial product generated in the aerobic synthesis of $[Mn^{III}(Br_4cat)_2]^-$ from Mn(II) salts, and that Br_4cat^{2-} ligand redistribution on reduced $[Mn^{II}(Br_4cat)_2]^{2-}$ is facile.

2.2.3 Catalytic Aerobic Catechol Oxidations

Heating $[Mn^{III}(Br_4cat)_2]^-$ to reflux in air-saturated MeCN with >20 equiv Br_4catH_2, and without base, results in formation of hexabromo-2,3-oxanthrenequinone and degradation of the catalyst. However, quantitative conversion of 3,5-di-*tert*-butylcatechol (3,5-^{t}Bu$_2$catH$_2$) to 3,5-di-*tert*-butylquinone (3,5-^{t}Bu$_2$bq) is achieved with 0.2% $[Mn^{III}(Br_4cat)_2]^-$ in ca. 400 min under 1 atm O_2 at ambient temperature, and without added base **(Scheme 11, Figure 2.8)**.

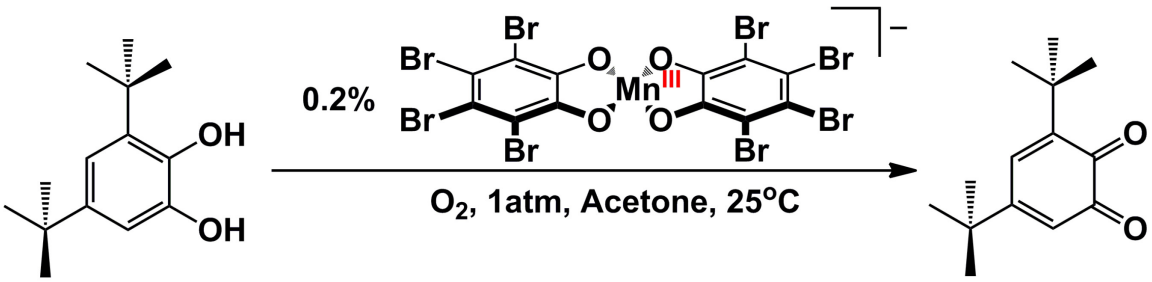

Scheme 11. Catalytic aerobic oxidation of 3,5-di-*tert*-butylcatechol by $[Mn^{III}(Br_4cat)_2]^-$.

Analysis of the products by ^{1}H NMR spectroscopy and GC-MS indicates that 3,5-^{t}Bu$_2$bq is the only catechol-derived species formed, implying $[Mn^{III}(Br_4cat)_2]^-$ is not active for intradiol or extradiol dioxygenase-type activity observed in Fe and V systems.[54-56] Control experiments confirm that $[Mn^{III}(Br_4cat)_2]^-$ is required for catalytic turnover **(Figure 2.8b)**.

2.2.4 Fate of the Reduced O_2.

The fate of the reduced oxygen species was suspected to be H_2O_2 based on literature precedent.[4, 43-44, 46-47] To determine if hydrogen peroxide was formed, catalytic

oxidations of 3,5-di-*tert*-butylquinone were run with 10% $[Mn^{III}(Br_4cat)_2]^-$ loadings to completion in CH_2Cl_2 solutions and extracted with distilled water. The water layer was qualitatively tested for H_2O_2 by using QUANTOFIX peroxide strips and yielded a positive result. A quantitative H_2O_2 yield of 26%, based on the oxidation of 3,5-^{t}Bu$_2$bq, was determined by colormetric titration[57] of the aqueous layer using Ti^{4+} confirming that H_2O_2 is produced during the catalytic oxidation chemistry.

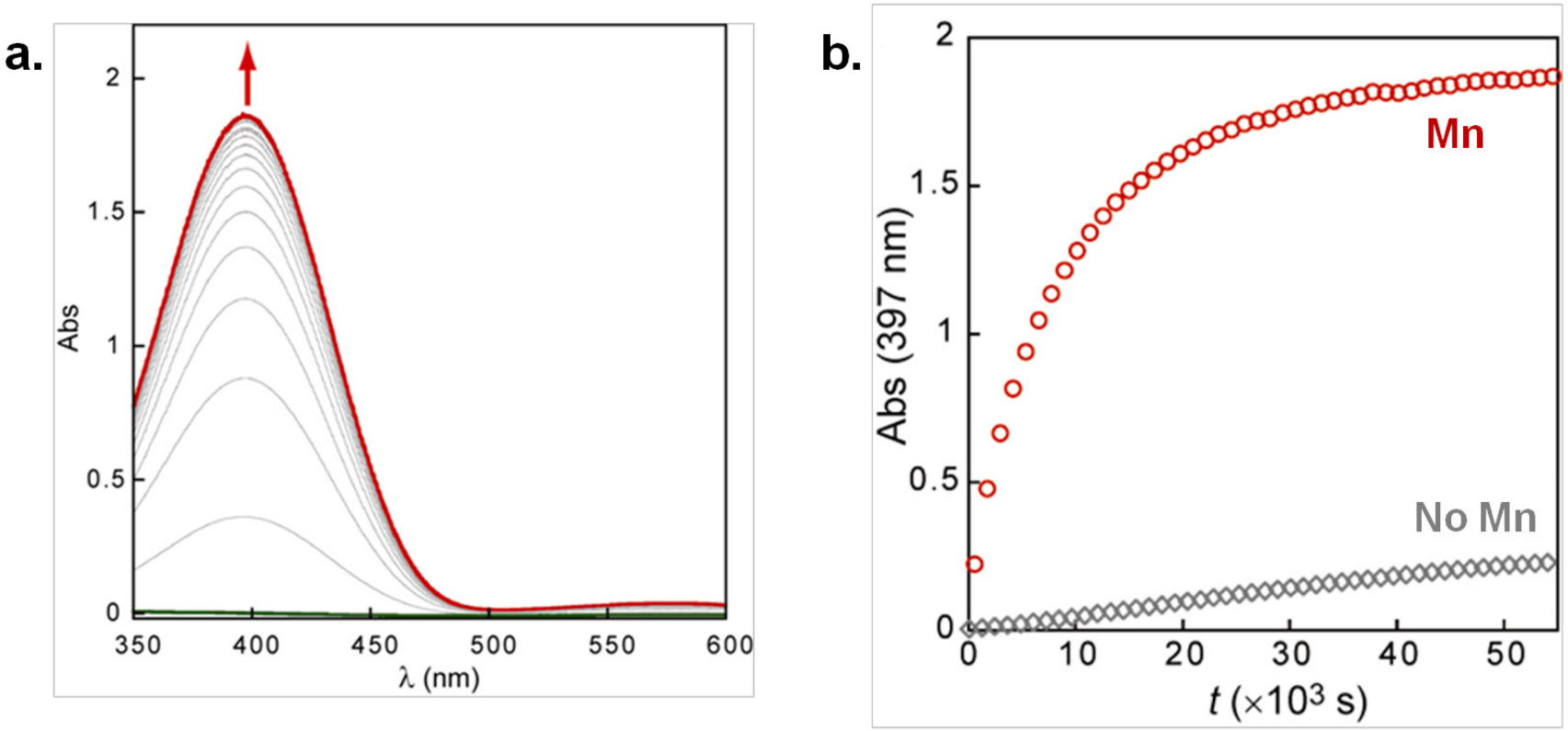

Figure 2.8. (a) Selected UV–vis absorption data for the oxidation of 1.0×10^{-3} M 3,5-^{t}Bu$_2$catH$_2$ to 3,5-^{t}Bu$_2$bq in acetone at 298 K with 1 atm O_2 using 2.1×10^{-6} M [(^{n}Bu$_4$N)[Mn^{III}(Br$_4$cat)$_2$(Me$_2$C=O)$_2$] as a catalyst. Spectra are shown at $t = 0$ under N_2 (green line), and at 60 min intervals from $t = 30$ min to $t = 870$ min (red line) after addition of O_2 **(b)** Selected data for the oxidation of 1.0×10^{-3} M 3,5-^{t}Bu$_2$catH$_2$ to 3,5-^{t}Bu$_2$bq ($\lambda_{max} = 397$ nm) under 1 atm O_2 in acetone at 298 K with 2.1×10^{-6} M (^{n}Bu$_4$N)[Mn^{III}(Br$_4$cat)$_2$(Me$_2$C=O)$_2$] (red ○) and without manganese (gray ◊).

2.3 Discussion.

Five and six coordinate complexes containing the square planar $[Mn^{III}(Br_4cat)_2]^-$ fragment can be prepared with various axial ligands. Previous literature suggested that the closely related $[Mn^{III}(Cl_4cat)_2]^-$ fragment underwent facile reactions with O_2, however in my studies, reactions of the analogous $[Mn^{III}(Br_4cat)_2]^-$ core with O_2 were slow, occurring over the course of weeks. It was determined that the air sensitive species was $[Mn^{III}(Br_4cat)_3]^{3-}$, by addition of Br_4cat^{2-} to the $Mn^{III}(Br_4cat)_2]^-$ core. The relative stability of $[Mn^{III}(Br_4cat)_2]^-$ in oxygen suggest that the slow reaction with O_2 proceeds via an unfavorable preequilibrium ligand redistribution reaction between $[Mn^{III}(Br_4cat)_2]^-$ anions to generate trace amounts of air-sensitive $[Mn^{III}(Br_4cat)_3]^{3-}$**.**

$[Mn^{III}(Br_4cat)_3]^{3-}$ reacts with O_2 to afford the $[Mn^{III}(Br_4cat)_2]^-$ anion and Br_4bq. The net conversion of Br_4catH_2 to Br_4bq by a reaction with $[Mn^{III}(Br_4cat)_2]^-$ and O_2**,** comprises a complete catalytic cycle for aerobic catechol oxidation by the $[Mn^{III}(Br_4cat)_2]^-$ fragment **(Scheme 12)**. The overall reaction of Br_4catH_2 to Br_4bq is a $2e^-$ process, but the oxidation of $[Mn^{III}(Br_4cat)_3]^{3-}$ occurs in a series of $1e^-$ steps and the formation of $[Mn^{IV}(Br_4cat)_3]^{2-}$ as an intermediate is observed. It was suspected that if rate-determining step in catalytic turnover is the oxidation of $[Mn^{IV}(Br_4cat)_3]^{2-}$, then the $[Mn^{III}(Br_4cat)_2]^-$ core could affect rapid catalytic quinone production from a more easily oxidized catechol substrate. Quantitative conversion of 3,5-di-*tert*-butylcatechol (3,5-$^tBu_2catH_2$) to 3,5-di-*tert*-butylquinone can be achieved at 0.2% mol $[Mn^{III}(Br_4cat)_2]^-$. If the catalytic oxidation occurs through a mixed ligand $[Mn^{III}(Br_4cat)_2(3,5\text{-}^tBu_2cat)]^{3-}$

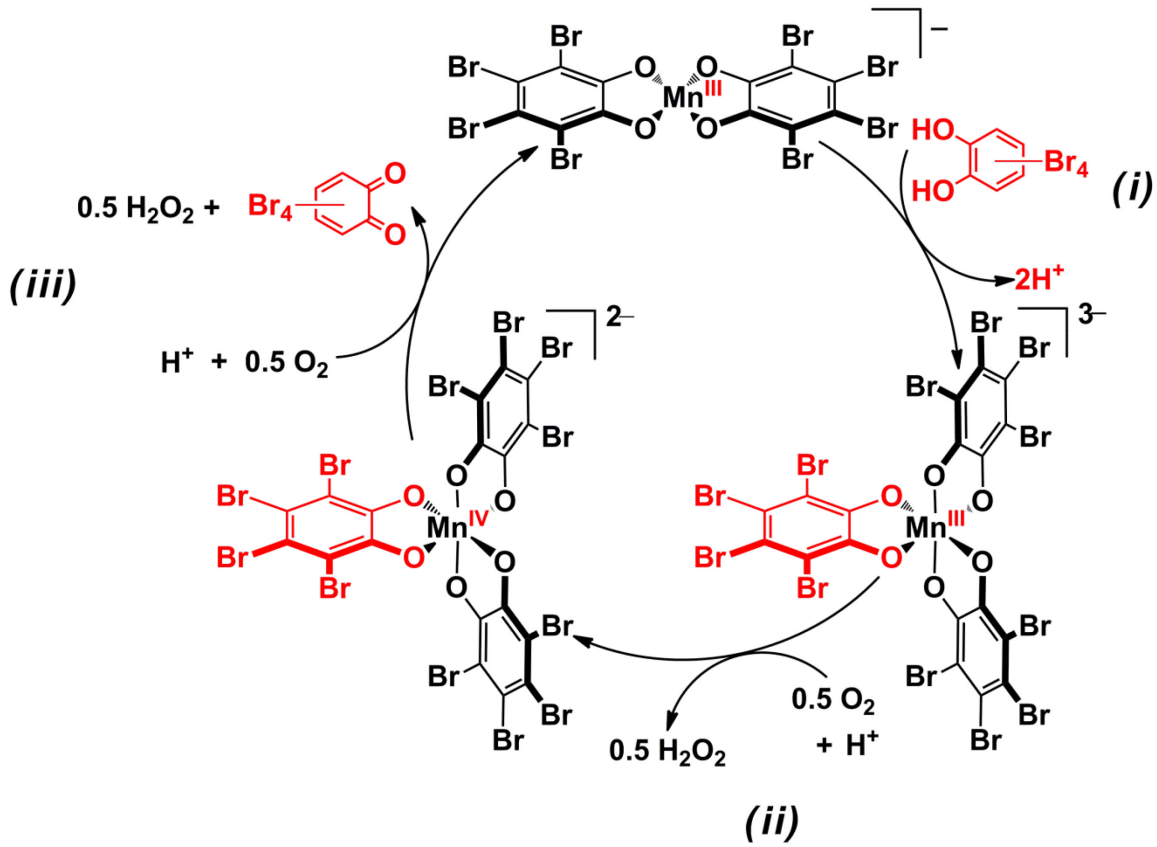

Scheme 12. The catalytic oxidation of Br_4cat by $[Mn^{III}(Br_4cat)_2]^-$. Peroxide was not observed in steps (*ii*) or (*iii*). It is depicted to balance the charge with the observed manganese products.

species analogous to $[Mn^{III}(Br_4cat)_3]^{3-}$, the reaction is >99% selective for internal oxidation of the 3,5-^{t}Bu$_2$catH_2 ligand over Br_4catH_2. This redox selectivity reflects the >500 mV difference in the oxidation potentials of 3,5-^{t}Bu$_2$cat versus Br_4catH_2,[58] which also contributes to the robust nature of the $[Mn^{III}(Br_4cat)_2]^-$ fragment in aerobic catechol oxidation catalysis.

Hydrogen peroxide can be detected as byproduct in the catalytic aerobic oxidations of 3,5-^{t}Bu$_2$cat by $[Mn^{III}(Br_4cat)_2]^-$. Attempts to correlate the yield of quinone formed to the yield of H_2O_2 produced resulted in the detection of only 26% of H_2O_2 for quantitative conversion 3,5-^{t}Bu$_2$cat. It is suspected that $[Mn^{III}(Br_4cat)_2]^-$ may be active for H_2O_2 disproportionation, a reaction common for many transition metals.

2.4 Conclusions.

In conclusion, whereas the robust $[Mn^{III}(Br_4cat)_2]^-$ fragment is itself surprisingly inert to dioxygen, it reacts rapidly with O_2 in the presence of catechol substrates to produce quinone in an oxidase-type dehydrogenation reaction. Although such catecholase chemistry is not rare for metal-quinone complexes,[39, 59-60] our investigations of the $[Mn^{III}(Br_4cat)_2]^-$ complex have already uncovered several significant features of these reactions. In particular, despite proceeding via a series of $1e^-$ steps, the reaction is selective for the $2e^-$ dehydrogenation of catechols. This multielectron capacity apparently derives from both metal- and ligand-centered redox events during catalytic turnover, a consequence of the close match in metal and ligand valence orbital energies. Additionally, the requirement for pre-assembly of a catalyst–substrate complex prior to

reaction O_2 facilitates intramolecular redox processes over competing intermolecular redox events.

2.5. Experimental Details.

2.5.1. General Considerations.

Unless otherwise noted, all manipulations were performed under anaerobic conditions using standard vacuum line techniques, or in an inert atmosphere glove box under purified nitrogen. NMR spectra were acquired on a Varian Mercury 300 spectrometer (300.323 MHz for ^{1}H) at ambient temperatures. All chemical shifts are reported in parts per million (ppm) relative to TMS, with the residual solvent peak serving as an internal reference. UV–visible absorption spectra were obtained using a Varian Cary 50 spectrophotometer equipped with a water-jacketed cell holder fitted to a Peltier temperature controller. Unless otherwise specified, all electronic absorption spectra were recorded at ambient temperatures. IR spectra were obtained in KBr using a Shimadzu 8400S Fourier-transform infrared spectrophotometer. All mass spectra were recorded in the Georgia Institute of Technology Bioanalytical Mass Spectrometry Facility. Electrospray ionization mass spectrometry (ESI-MS) was carried out with acetonitrile solutions using a Micromass Quattro LC spectrometer. GC/MS was performed on GC-HP5890 using a J&W-DB-5 column (30 m × 0.25 mm) equipped with a VG instruments model 70-SE electron impact mass spectrometer. Elemental analyses were performed by Atlantic Microlab, Inc., Norcross, GA. All analyses were performed in duplicate, and the reported compositions are the average of the two runs.

2.5.2. Methods and Materials.

Anhydrous acetonitrile, tetrahydrofuran (THF) and pentane solvents for air- and moisture-sensitive manipulations were purchased from Sigma-Aldrich and further dried by passage through columns of activated alumina, degassed by at least three freeze-pump-thaw cycles, and stored under N_2 prior to use. Methanol (anhydrous, 99.0%) was purchased from Honeywell Burdick and Jackson, and used as received. Acetone (99.8%, extra dry) was purchased from Acros and used as received. Oxygen (ultra high purity) was used as received from Airgas, Inc. Deuterated acetonitrile (CD_3CN) was purchased from Cambridge Isotope Laboratories, degassed by three freeze-pump-thaw cycles, vacuum distilled from CaH_2, and stored under a dry N_2 atmosphere prior to use. $Mn(ClO_4)_2 \cdot 6H_2O$ was purchased from Strem Chemical, Inc. All other reagents were purchased from Sigma-Aldrich and used as received.

2.5.3. Preparation of $(^nBu_4N)[Mn^{III}(Br_4cat)_2(EtOH)(H_2O)\cdot EtOH]$.

$MnCl_2 \cdot 4H_2O$ (0.22 g, 1.1 mmol) and tetrabromo-1,2-catechol (1.064 g, 2.2 mmol)) were combined in a 100 mL evaporating flask and dissolved in 50mL of a 20% aqueous ethanol solution in air. Slow addition of 40% aqueous solution $^nBu_4OH$ in H_2O (1 mL, 2 mmol) over 5 min with vigorous stirring afforded a dark olive-green solution. The flask was fitted to a condenser and the solution heated to reflux for 1 hr, then cooled to ambient temperature and stored at –10 ^oC for 24 hr to deposit green crystals. The solids were collected by vacuum filtration of the cold reaction mixture in air, washed with the filtrate

(3 × 1 mL), and dried *in vacuo* to yield green, microcrystalline ($^{n}Bu_4N$)[$Mn^{III}(Br_4cat)_2(EtOH)(H_2O)$] (0.38 g, 0.31 mmol, 29%). ESI-MS (*m/z*): 902 [M–$^{n}Bu_4N$]$^{-}$.

2.5.4. Preparation of ($^{n}Bu_4N$)[$Mn^{III}(Br_4cat)_2(Me_2C=O)_2$].

$Mn(ClO_4)_2$•$6H_2O$ (0.39 g, 1.1 mmol) and tetrabromo-1,2-catechol (0.91 g, 2.2 mmol)) were combined in a 100 mL evaporating flask and dissolved in 20mL of acetone in air. Slow addition of 1.0 M $^{n}Bu_4OH$ in MeOH (2 mL, 2 mmol) over 5 min with vigorous stirring afforded a dark olive-green solution. The flask was fitted to a condenser and the solution heated to reflux for 2 hr, then cooled to ambient temperature and stored at –10 ^{o}C for 24 hr to deposit green precipitate. The solids were collected by vacuum filtration of the cold reaction mixture in air, washed with acetone (3 × 1 mL, ice cold), and dried *in vacuo* to yield green, microcrystalline ($^{n}Bu_4N$)[$Mn^{III}(Br_4cat)_2(Me_2C=O)_2$] (0.76 g, 6.0 mmol, 56%). UV-vis (acetone) λ_{max}, nm (ε, M^{-1} cm^{-1}): 600 (190), 716 (sh, 170). ESI-MS (*m/z*): 902 [M–$^{n}Bu_4N$]$^{-}$. FT-IR (KBr): 3354 (br), 2966 (s), 2933 (m), 2857 (m), 1479 (m), 1380 (m), 1363 (m), 883 (m) (all $^{n}Bu_4N^{+}$); 1684 (s, acetone C=O), 1427 (vs) 1346 (s), 1261 (s), 1226 (s) 928 (s), 748 (s) 584 (s) cm^{-1}. Anal. Calcd for $C_{34}H_{48}Br_8MnNO_6$: C, 32.38; H, 3.83; N, 1.11; Found: C, 32.44; H, 3.88; N 1.15.

2.5.5. Preparation of ($^{n}Bu_4N$)[$Mn^{III}(Br_4cat)_2(MeOH)$].

A 100 mL round bottom flask was charged with ($^{n}Bu_4N$)[$Mn^{III}(Br_4cat)_2(Me_2C{=}O)_2$] (0.21g, 0.17 mmol), a stir bar, and methanol (30 mL) and fitted to a condenser. The resulting yellow solution was heated to reflux in air for 30 min, then cooled to ambient temperature and evaporated to dryness under a flow of N_2 to give a green powder. The solids were subsequently taken up in MeOH (10 mL) and the volume of the solution was reduced to 2 mL to precipitate green crystals. Vacuum filtration, washing with MeOH (5 mL, ice cold) and drying *in vacuo* afforded ($^{n}Bu_4N$)[$Mn^{III}(Br_4cat)_2(MeOH)$] (0.152 g, 0.129 mmol, 77.6%). FT-IR (KBr): 3375 (br), 2958 (s), 2927 (m), 2871 (m). 1666 (w), 1469 (m) (all $^{n}Bu_4N^{+}$); 3182 (br), 1425 (vs), 1346 (m), 1265 (s), 1227 (s), 927 (s), 752 (s) cm^{-1}. Anal. Calcd for $C_{29}H_{40}Br_8MnNO_5$: C, 29.60; H, 3.43; N, 1.19; Found: C, 29.69; H, 3.42; N 1.17.

2.5.6. Preparation of ($^{n}Bu_4N$)[$Mn^{III}(Br_4cat)_2(OPPh_3)$].

$Mn(OPPh_3)_2Cl_2$ (0.77 g, 1.1 mmol) and tetrabromo-1,2-catechol (1.064 g, 2.5 mmol)) were combined in a 200 mL round bottom flask and dissolved in 100mL of isopropanol in air. Slow addition of 1.0 M $^{n}Bu_4OH$ in MeOH (2 mL, 2 mmol) over 5 min with vigorous stirring afforded a dark olive-green solution with precipitate. The flask was fitted to a condenser and the solution heated to reflux for 2 hr, then cooled to ambient temperature and stored at –10 ^{o}C for 24 hr to deposit green precipitate. The solids were collected by vacuum filtration of the cold reaction mixture in air, washed with

isopropanol (3 × 1 mL, ice cold), and dried *in vacuo* to yield green, microcrystalline ($^{n}Bu_4N$)[$Mn^{III}(Br_4cat)_2(OPPh_3)$] (0.34 g, 6.0 mmol, 56%). %). Samples of ($^{n}Bu_4N$)[$Mn^{III}(Br_4cat)_2(OPPh_3)$] for X-ray crystallography were recrystallized from CH_2Cl_2-hexane. FT-IR (KBr): 2961 (s), 2930 (s), 2897 (m), 2871 (m), 2359 (m), 2342 (m), 1701 (m), 1479 (m), 1479 (m), 1380 (m), 1190 (m) 1153 (w), 1119 (m), 879 (m), 721 (m), 692 (m) (all $^{n}Bu_4N^{+}$); 1425 (vs) 1346 (m), 1263 (m), 1226 (s) 928 (s), 746 (s) 578 (s) cm^{-1}.

2.5.7. Preparation of (PPN)Li_2[$Mn^{III}(Br_4cat)_3$].

$MnCl_2$•$4H_2O$ (0.20 g, 1.0 mmol) and tetrabromo-1,2-catechol (1.28 g, 3.03 mmol) were combined in a 5-dram scintillation vial and dissolved in MeOH (10 mL). Slow addition of 1.0 M LiOMe in MeOH (6.0 mL, 6.0 mmol) with vigorous stirring afforded a dark orange solution. The reaction mixture was fitted with a Teflon-lined cap and stirred for 30 min under N_2, exposed to air, and stirred for an additional 30 min to afford a dark green solution. Addition of PPNCl (0.574 g, 1.00 mmol) yielded a light green precipitate. The suspension was stirred for 15 min, and the solids were collected by vacuum filtration, washed with MeOH (3 × 10 mL) and dried *in vacuo* to give green (PPN)Li_2[$Mn^{III}(Br_4cat)_3$] (1.30 g, 0.69 mmol, 69%). Samples of (PPN)Li_2[$Mn^{III}(Br_4cat)_3$] for elemental analysis were recrystallized from THF-pentane. Analyses performed on multiple samples are most consistent with elemental compositions containing equimolar ratios of PPN^{+} and $Li(THF)_2^{+}$ counter cations, which are also observed in the X-ray crystal structure. The reported analysis is for $(PPN)_{1.5}Li_{1.5}$[$Mn^{III}(Br_4cat)_3$]. UV-vis

(acetone) λ_{max}, nm (ε, M^{-1} cm^{-1}): 597 (610). Anal. Calcd for $C_{84}H_{69}Br_{12}Li_{1.5}MnN_{1.5}O_9P_3$: C, 42.74; H, 2.95; N, 0.89; Found: C, 42.00; H, 2.91; N 0.92.

2.5.8. Preparation of hexabromo-2,3-oxanthrenequinone.

A 20 dram scintillation vial was charged with ($^{n}Bu_4N$)[$Mn^{III}(Br_4cat)_2(Me_2C{=}O)_2$] (0.15g, 0.12 mmol), tetrabromoquinone(0.50g, 1.2 mmol), and acetonitrile (10 mL) under nitrogen . The resulting brown solution was allowed to sit at ambient temperature and precipated out red-orange crystals after 6 hrs. Vacuum filtration, washing with acetonitrile (5 mL, ice cold) and drying *in vacuo* afforded hexabromo-2,3-oxanthrenequinone. (0.098 g, 0.14 mmol, 58%). FT-IR (KBr): 1678 (m), 1659 (w), 1576 (m), 1545 (m). 1402 (s), 1368 (w), 1336 (s), 1324 (s), 1190 (m), 1143 (w), 1003 (s), 956 (w), 862 (m), 831 (w), 780 (w), 681 (w), 609 (m) 553 (m) cm^{-1}.

2.5.9. Preparation of $(Et_3NH)_2[Mn^{IV}(Br_4cat)_3]$.

In air, $Mn(ClO_4)_2{\bullet}6H_2O$ (0.39 g, 1.1 mmol) and tetrabromo-1,2-catechol (1.40 g, 3.3 mmol)) were combined in a 100 mL evaporating flask and dissolved in 20mL of a 1:3 THF/CH_2Cl_2 solution. Addition of Et_3N(0.90 mL, 6.0 mmol) afforded a dark green solution. The solution was then stirred at 25°C for 1hr and reduced in volume by slow evaporation to afford a dark blue crystalline material. The solids were collected by vacuum filtration and washed with CH_2Cl_2 (3×5 mL, ice cold), and dried *in vacuo* to yield $(Et_3N)_2[Mn(Br_4cat)_3]$ (1.27 g, 0.83 mmol, 77%) as dark blue crystals. UV-vis

(CH_3CN) λ_{max}, nm (ε, M^{-1} cm^{-1}): 315 (34000) 610 (7500), ESI-MS (*m/z*): 1326, [M–$2Et_3NH]^-$. 661, $[M–2Et_3NH]^{2-}$. FTIR (ATR): 3056 (w, br), 2978 (w), 1404 (s), 1345 (m), 1260 (m), 1227 (m), 1204 (m), 928 (s), 744 (s) 555 (s) cm^{-1}The reported analysis is for $(Et_3N)_2[Mn(Br_4cat)_3]$. Anal. Calcd for $C_{30}H_{32}N_2O_6Br_{12}Mn$: C, 23.54; H, 2.11; N, 1.83; Found: C, 23.90; H, 2.02.11; N 1.84.

2.5.10. Catalytic Aerobic Catechol Oxidation.

In a representative procedure, a 1.0 cm quartz cuvette fitted with a Kontes brand high-vacuum PTFE valve was charged with an acetone solution containing 3,5-di-*tert*-butylcatechol (1.0×10^{-3} M) and **1** (2.1×10^{-6} M) and sealed under N_2 . The solution was degassed on a high-vacuum line by three freeze-pump-thaw cycles and exposed to 1 atm of O_2 to initiate catalytic turnover. The reaction progress was monitored by UV–vis spectroscopy (350-600 nm) for 870 min at 30 min intervals, and the yield of 3,5-di-*tert*-butylquinone was determined by quantification of a characteristic absorption at λ_{max} = 397 nm with ε = 1830 M^{-1} cm^{-1}. Following completion of the reaction, the solution was analyzed by GC-MS to determine the organic product distribution.

2.5.11. H_2O_2 detection using $Ti^{IV}O(SO_4)$.

Hydrogen peroxide produced from the reaction of $(^nBu_4N)[Mn^{III}(Br_4cat)_2(Me_2C{=}O)_2]$ with 3,5-di-*tert*-butylcatechol was determined spectrophotometrically with titanium(IV) oxysulfate. A CH_2Cl_2 solution of $(^nBu_4N)[Mn^{III}(Br_4cat)_2(Me_2C{=}O)_2]$ (13 mg,0.010

mmol) and 3,5-di-*tert*-butylcatechol (17 mg, 0.39 mmol) was prepared under N_2 in the glovebox. The yellow solution was degassed via 3 FPT cycles and placed under an atmosphere of O_2. The yellow solution turned red corresponding to the formation of 3,5-di-*tert*-butylquinone. After 3 hrs, distilled water (10 mL) was added to the solution. The aqueous layer was separated and a 1mL aliquot was taken. The aliquot was titrated with a $Ti^{IV}O(SO_4)$ solution. The concentration of the hydrogen peroxide was spectroscopically measured from the absorption at 408 nm, and the yield was 26%.

2.5.12. X-Ray Crystallography.

Crystals of $(^nBu_4N)[Mn^{III}(Br_4Cat)_2(EtOH)(H_2O)]$, $(^nBu_4N)[Mn^{III}(Br_4Cat)_2(MeOH)]$, $(^nBu_4N)[Mn^{III}(Br_4Cat)_2(OPPh_3)]$, $(^nBu_4N)[Mn^{III}(Br_4Cat)_2(Me_2C{=}O)_2)]$, $(PPN)Li_2[Mn^{III}(Br_4cat)_3]\bullet 5THF$, and hexabromo-2,3-oxanthrenequinone suitable for X-ray diffraction analysis were coated with Paratone N oil, suspended on small fiber loops and placed in a cooled nitrogen gas stream at 173 K on a Bruker D8 APEX II CCD sealed tube diffractometer. Data for $(^nBu_4N)[Mn^{III}(Br_4Cat)_2(EtOH)(H_2O)]$, $(^nBu_4N)[Mn^{III}(Br_4Cat)_2(MeOH)]$, and $(^nBu_4N)[Mn^{III}(Br_4Cat)_2(Me_2C{=}O)_2)]$ was obtained with graphite monochromated Cu Kα (λ = 1.54178 Å) radiation while diffraction data for $(^nBu_4N)[Mn^{III}(Br_4Cat)_2(OPPh_3)]$, $(PPN)Li_2[Mn^{III}(Br_4cat)_3]\bullet 5THF$, and hexabromo-2,3-oxanthrenequinone were collected using graphite monochromated Mo Kα (λ = 0.71073 Å) radiation. Data collection procedures, data processing and programs were the same for all samples. Frames were measured using a series of combinations of phi and omega scans with 10 s frame exposures and 0.5° frame widths. Data collection, indexing

and initial cell refinements were all carried out using APEX II software.[61] Frame integration and final cell refinements were done using SAINT software.[62] The final cell parameters were determined from least-squares refinement on 6085 reflections for ($^{n}Bu_4N$)[$Mn^{III}(Br_4Cat)_2(EtOH)(H_2O)$], 6972 reflections for ($^{n}Bu_4N$)[$Mn^{III}(Br_4Cat)_2(MeOH)$], 4209 reflections for ($^{n}Bu_4N$)[$Mn^{III}(Br_4Cat)_2(OPPh_3)$], 8071 reflections for ($^{n}Bu_4N$)[$Mn^{III}(Br_4Cat)_2(Me_2C{=}O)_2$)], 9144 reflections for (PPN)Li_2[$Mn^{III}(Br_4cat)_3$]•5THF and 4795 reflections for hexabromo-2,3-oxanthrenequinone. The structures were solved using direct methods and difference Fourier techniques with the SHELXTL program package.[63] Hydrogen atoms were placed in their expected chemical positions using the HFIX command and were included in the final cycles of least-squares with isotropic U_{ij}'s related to the atoms ridden upon. All non-hydrogen atoms in ($^{n}Bu_4N$)[$Mn^{III}(Br_4Cat)_2(MeOH)$], ($^{n}Bu_4N$)[$Mn^{III}(Br_4Cat)_2(OPPh_3)$], ($^{n}Bu_4N$)[$Mn^{III}(Br_4Cat)_2(Me_2C{=}O)_2$)] (PPN)$Li_2$[$Mn^{III}(Br_4cat)_3$]•5THF and hexabromo-2,3-oxanthrenequinone. were refined anisotropically. In ($^{n}Bu_4N$)[$Mn^{III}(Br_4Cat)_2(EtOH)(H_2O)$], only the metal-containing fragments and counterion were refined anisotropically. Scattering factors and anomalous dispersion corrections are taken from the *International Tables for X-ray Crystallography*.[64] Other details of data collection and structure refinement are provided in **Table 2.1**.

Table 2.1. Crystallographic Data and Structure Parameters for ($^{n}Bu_4N$)[$Mn^{III}(Br_4Cat)_2(EtOH)(H_2O)$], ($^{n}Bu_4N$)[$Mn^{III}(Br_4Cat)_2(MeOH)$], and ($^{n}Bu_4N$)[$Mn^{III}(Br_4Cat)_2(OPPh_3)$].

Complex	($^{n}Bu_4N$)[$Mn^{III}(Br_4Cat)_2(EtOH)(H_2O)$]	($^{n}Bu_4N$)[$Mn^{III}(Br_4Cat)_2(MeOH)$]	($^{n}Bu_4N$)[$Mn^{III}(Br_4Cat)_2(OPPh_3)$]
Empirical formula	$C_{29.50}H_{42.25}Br_8MnNO_{6.25}$	$C_{29}H_{40}Br_8MnNO_5$	$C_{46}H_{51}Br_8MnNO_5P$
Formula weight	1205.11	1176.84	1423.07
Temperature (K)	173(2)	173(2)	173(2)
Crystal system	Monoclinic	Monoclinic	Triclinic
Space group	C2/c	P2(1)/n	P-1
Unit cell dimensions			
a (Å)	20.4799(15)	14.9529(7)	9.898(5)
b (Å)	16.9121(10)	14.6956(8)	16.672(8)
c (Å)	25.9554(19)	17.7026(8)	16.912(8)
a (°)	90	90°	98.438(9)
b (°)	110.384(4)	101.797(2)°	β= 106.163(8)
g (°)	90	90°	90.307
Volume ($Å^3$)	8426.9(10)	3807.8(3)	2648(2)
Z	8	4	2
Calculated Density (g cm^{-1})	1.9	2.053	1.785
Absorption coefficient (mm^{-1})	11.748	12.955	6.356
Crystal size (mm)	0.32 x 0.27 x 0.08	0.40 x 0.20 x 0.07	0.36 x 0.21 x 0.06
θ range for data collection (°)	3.48-48.74	3.53-65.97°.	1.24-28.36°.
Index ranges	-19<=h<=18	-15<=h<=17	-13<=h<=13
	15<=k<=16	-17<=k<=17	-22<=k<=22
	-25<=l<=25	-20<=l<=18	-22<=l<=22
Reflections collected/unique	14123/3876	26104/6260	35940/12938
Goodness-of-fit on F2	1.056	1.087	1.606
Final R indices [I>2sigma(I)]	0.0786	0.0271	0.1933
R indices (all data)	0.1168	0.0301	0.2496

Table 2.1 cont.. Crystallographic Data and Structure Parameters for ($^{n}Bu_4N$)[$Mn^{III}(Br_4Cat)_2(Me_2C{=}O)_2$)], (PPN)$Li_2$[$Mn^{III}(Br_4cat)_3$]•5THF, and hexabromo-2,3-oxanthrenequinone.

Complex	($^{n}Bu_4N$)[$Mn^{III}(Br_4Cat)_2(Me_2C{=}O)_2$)]	(PPN)Li_2[$Mn^{III}(Br_4cat)_3$]•5THF	hexabromo-2,3-oxanthrenequinone
Empirical formula	$C_{68}H_{96}Br_{16}Mn_2N_2O_{12}$	$C_{74}H_{70}Br_{12}Li_2MnNO_{11}P_2$	$C_{12}Br_6O_4$
Formula weight	2521.91	2238.99	687.58
Temperature (K)	173(2)	173(2)	172(2)
Crystal system	Monoclinic	monoclinic	Monoclinic
Space group	C2/c	P2(1)/c	P2(1)/c
Unit cell dimensions			
a (Å)	24.9684(19)	12.8717(12)	9.4867(2)
b (Å)	10.9339(8)	29.850(3)	12.5747(3)
c (Å)	19.823(2)	21.778(2)	12.9018(3)
a (°)	90	90	90
b (°)	126.058(2)	102.641(2)	102.759
g (°)	90	90	90
Volume ($Å^3$)	4374.9(7)	8164.5(13)	1501.08(6)
Z	2	4	4
Calculated Density (g cm^{-1})	1.914	1.822	3.042
Absorption coefficient (mm^{-1})	11.345	6.13	16.06
Crystal size (mm)	0.49 x 0.13 x 0.13	0.43 x 0.21 x 0.12	0.20 x 0.11 x 0.10
θ range for data collection (°)	4.38 to 65.02	1.18 to 28.37	2.20 to 30.65°.
Index ranges	-26<=h<=28	-17<=h<=17	-10<=h<=13
	-12<=k<=11	-39<=k<=39	-18<=k<=15
	-23<=l<=21	-29<=l<=29	-18<=l<=18
Reflections collected/unique	11035/3352	124335/20398	19856/4513
Goodness-of-fit on F2	1.017	1.009	1.027
Final R indices [I>2sigma(I)]	0.0501	0.0489	0.0389
R indices (all data)	0.0507	0.0964	0.0731

2.6 Works Cited.

1. Cramer, C. J.; Tolman, W. B., Mononuclear Cu–O2 Complexes: Geometries, Spectroscopic Properties, Electronic Structures, and Reactivity. *Accounts of Chemical Research* **2007,** *40* (7), 601-608, doi:10.1021/ar700008c.

2. Stahl, S. S., Palladium Oxidase Catalysis: Selective Oxidation of Organic Chemicals by Direct Dioxygen-Coupled Turnover. *Angewandte Chemie International Edition* **2004,** *43* (26), 3400-3420, doi:10.1002/anie.200300630.

3. Stahl, S. S., Palladium-catalyzed oxidation of organic chemicals with O-2. *Science* **2005,** *309* (5742), 1824-1826, doi:10.1126/science.1114666.

4. Chaudhuri, P.; Wieghardt, K.; Weyhermuller, T.; Paine, T. K.; Mukherjee, S.; Mukherjee, C., Biomimetic metal-radical reactivity: aerial oxidation of alcohols, amines, aminophenols and catechols catalyzed by transition metal complexes. *Biol. Chem.* **2005,** *386* (10), 1023-1033, doi:10.1515/bc.2005.118.

5. Advances in Catalytic Activation of Dioxygen by Metal Complexes; Simándi, L. I., Ed.; Springer: New York, 2003.

6. Meunier, B., *Biomimetic Oxidations Catalyzed by Transition Metal Complexes*. Imperial College: London.

7. Borovik, A. S.; Zinn, P. J.; Zart, M. K. Dioxygen Binding and Activation: Reactive Intermediates. In Activation of Small Molecules: Organometallic and Bioinorganic Perspectives; Tolman, W. B., Ed.; Wiley-VCH: Weinheim, Germany, 2006; pp 187–234.

8. Acc. Chem. Res. 2007, 7, 465–634.,

9. Tolman, W. B. Metal-Radical Arrays. In Comprehensive Coordination Chemistry II; McCleverty, I. A., Meyer, T. J., Eds.; Elsevier Pergamon: Boston, 2004; Vol. 8, pp 715–737.,

10. Rogers, M. S.; Dooley, D. M., Copper-tyrosyl radical enzymes. *Current Opinion in Chemical Biology* **2003,** *7* (2), 189-196, doi:10.1016/s1367-5931(03)00024-3.

11. Costas, M.; Mehn, M. P.; Jensen, M. P.; Que, L., Dioxygen Activation at Mononuclear Nonheme Iron Active Sites: Enzymes, Models, and Intermediates. *Chemical Reviews* **2004,** *104* (2), 939-986, doi:10.1021/cr020628n.

12. Itoh, S.; Taki, M.; Fukuzumi, S., Active site models for galactose oxidase and related enzymes. *Coordination Chemistry Reviews* **2000,** *198* (1), 3-20, doi:10.1016/s0010-8545(99)00209-x.

13. Silverman, R., *The Organic Chemistry of Enzyme-Catalyzed Reactions*. Academic Press: San Diego, 2000.

14. Korendovych, I. V.; Kryatov, S. V.; Rybak-Akimova, E. V., Dioxygen Activation at Non-Heme Iron: Insights from Rapid Kinetic Studies. *Accounts of Chemical Research* **2007,** *40* (7), 510-521, doi:10.1021/ar600041x.

15. Wang, Y.; DuBois, J. L.; Hedman, B.; Hodgson, K. O.; Stack, T. D. P., Catalytic Galactose Oxidase Models: Biomimetic Cu(II)-Phenoxyl-Radical Reactivity. *Science* **1998,** *279* (5350), 537-540, doi:10.1126/science.279.5350.537.

16. Kieber-Emmons, M. T.; Riordan, C. G., Dioxygen Activation at Monovalent Nickel. *Accounts of Chemical Research* **2007,** *40* (7), 618-625, doi:10.1021/ar700043n.

17. Sheldon, R. A. K., J. K., *Metal-Catalyzed Oxidations of Organic Compounds*. Academic Press: New York.

18. Mirica, L. M.; Ottenwaelder, X.; Stack, T. D. P., Structure and Spectroscopy of Copper−Dioxygen Complexes. *Chemical Reviews* **2004,** *104* (2), 1013-1046, doi:10.1021/cr020632z.

19. Bart, S. C.; Bowman, A. C.; Lobkovsky, E.; Chirik, P. J., Iron diazoalkane chemistry: N-N bond hydrogenation and intramolecular C-H activation. *Journal of the American Chemical Society* **2007,** *129* (23), 7212-+, doi:10.1021/ja070056u.

20. Blackmore, K. J.; Lal, N.; Ziller, J. W.; Heyduk, A. F., Catalytic reactivity of a zirconium(IV) redox-active ligand complex with 1,2-diphenylhydrazine. *Journal of the American Chemical Society* **2008,** *130* (9), 2728-+, doi:10.1021/ja710611v.

21. Blackmore, K. J.; Ziller, J. W.; Heyduk, A. F., "Oxidative addition" to a Zirconium(IV) redox-active ligand complex. *Inorganic Chemistry* **2005,** *44* (16), 5559-5561, doi:10.1021/ic050997c.

22. Bouwkamp, M. W.; Bowman, A. C.; Lobkovsky, E.; Chirik, P. J., Iron-Catalyzed [2π + 2π] Cycloaddition of α,ω-Dienes: The Importance of Redox-Active Supporting Ligands. *Journal of the American Chemical Society* **2006,** *128* (41), 13340-13341, doi:10.1021/ja064711u.

23. Chaudhuri, P.; Hess, M.; Müller, J.; Hildenbrand, K.; Bill, E.; Weyhermüller, T.; Wieghardt, K., Aerobic Oxidation of Primary Alcohols (Including Methanol) by Copper(II)− and Zinc(II)−Phenoxyl Radical Catalysts. *Journal of the American Chemical Society* **1999,** *121* (41), 9599-9610, doi:10.1021/ja991481t.

24. Edison, S. E.; Hotz, R. P.; Baldwin, M. J., Aerobic oxidation of methanol by a Ni(II)-O-2 reaction. *Chem. Commun.* **2004,** (10), 1212-1213, doi:10.1039/b403668a.

25. Haneline, M. R.; Heyduk, A. F., C-C bond-forming reductive elimination from a zirconium(IV) redox-active ligand complex. *Journal of the American Chemical Society* **2006,** *128* (26), 8410-8411, doi:10.1021/ja061107a.

26. Mukherjee, C.; Weyhermuller, T.; Bothe, E.; Chaudhuri, P., Mimicking the function of amine oxidases and phenoxazinone synthase by a manganese(IV)-monoradical complex. *C. R. Chim.* **2007,** *10* (4-5), 313-325, doi:10.1016/j.crci.2006.11.006.

27. Mukherjee, C.; Weyhermüller, T.; Bothe, E.; Chaudhuri, P., Targeted Oxidase Reactivity with a New Redox-Active Ligand Incorporating N2O2 Donor Atoms. Complexes of Cu(II), Ni(II), Pd(II), Fe(III), and V(V). *Inorganic Chemistry* **2008,** *47* (24), 11620-11632, doi:10.1021/ic8011734.

28. Stanciu, C.; Jones, M. E.; Fanwick, P. E.; Abu-Omar, M. M., Multi-electron activation of dioxygen on zirconium(IV) to give an unprecedented bisperoxo complex. *Journal of the American Chemical Society* **2007,** *129* (41), 12400-+, doi:10.1021/ja075396u.

29. Bart, S. C.; Bowman, A. C.; Lobkovsky, E.; Chirik, P. J., Iron Diazoalkane Chemistry: N−N Bond Hydrogenation and Intramolecular C−H Activation. *Journal of the American Chemical Society* **2007,** *129* (23), 7212-7213, doi:10.1021/ja070056u.

30. Bowman, A. C.; Milsmann, C.; Atienza, C. C. H.; Lobkovsky, E.; Wieghardt, K.; Chirik, P. J., Synthesis and Molecular and Electronic Structures of Reduced Bis(imino)pyridine Cobalt Dinitrogen Complexes: Ligand versus Metal Reduction. *Journal of the American Chemical Society* **2010,** *132* (5), 1676-1684, doi:10.1021/ja908955t.

31. Chirik, P. J.; Wieghardt, K., Radical Ligands Confer Nobility on Base-Metal Catalysts. *Science* **2010,** *327* (5967), 794-795, doi:10.1126/science.1183281.

32. Hull, K. L.; Sanford, M. S., Mechanism of Benzoquinone-Promoted Palladium-Catalyzed Oxidative Cross-Coupling Reactions. *Journal of the American Chemical Society* **2009,** *131* (28), 9651-9653, doi:10.1021/ja901952h.

33. Manuel, T. D.; Rohde, J.-U., Reaction of a Redox-Active Ligand Complex of Nickel with Dioxygen Probes Ligand-Radical Character. *Journal of the American Chemical Society* **2009,** *131* (43), 15582-15583, doi:10.1021/ja9065943.

34. Mukherjee, C.; Pieper, U.; Bothe, E.; Bachler, V.; Bill, E.; Weyhermüller, T.; Chaudhuri, P., Ligand-Derived Oxidase Activity. Catalytic Aerial Oxidation of Alcohols (Including Methanol) by Cu(II)-Diradical Complexes. *Inorganic Chemistry* **2008,** *47* (19), 8943-8956, doi:10.1021/ic8009767.

35. Nguyen, A. I.; Blackmore, K. J.; Carter, S. M.; Zarkesh, R. A.; Heyduk, A. F., One- and Two-Electron Reactivity of a Tantalum(V) Complex with a Redox-Active Tris(amido) Ligand. *Journal of the American Chemical Society* **2009,** *131* (9), 3307-3316, doi:10.1021/ja808542j.

36. Smith, A. L.; Clapp, L. A.; Hardcastle, K. I.; Soper, J. D., Redox-active ligand-mediated Co-Cl bond-forming reactions at reducing square planar cobalt(III) centers. *Polyhedron* **2010,** *29* (1), 164-169, doi:10.1016/j.poly.2009.06.046.

37. Smith, A. L.; Hardcastle, K. I.; Soper, J. D., Redox-Active Ligand-Mediated Oxidative Addition and Reductive Elimination at Square Planar Cobalt(III): Multielectron Reactions for Cross-Coupling. *Journal of the American Chemical Society* **2010,** *132* (41), 14358-14360, doi:10.1021/ja106212w.

38. Zarkesh, R. A.; Ziller, J. W.; Heyduk, A. F., Four-electron oxidative formation of aryl diazenes using a tantalum redox-active ligand complex. *Angew. Chem.-Int. Edit.* **2008,** *47* (25), 4715-4718, doi:10.1002/anie.200800812.

39. Pierpont, C. G.; Lange, C. W. The Chemistry of Transition Metal Complexes Containing Catechol and Semiquinone Ligands. In Progress in Inorganic Chemistry; Karlin, K. D., Ed.; Wiley: New York, 1994; Vol. 41, pp 331–442.

40. Chaudhuri, P.; Wieghardt, K. Phenoxyl Radical Complexes. In Progress in Inorganic Chemistry; Karlin, K. D., Ed.; Wiley: New York, 2001; Vol. 50, pp 151–216.,

41. Pierpont, C. G.; Lange, C. W., THE CHEMISTRY OF TRANSITION-METAL COMPLEXES CONTAINING CATECHOL AND SEMIQUINONE LIGANDS. In *Progress in Inorganic Chemistry, Vol 41*, John Wiley & Sons Inc: New York, 1994; Vol. 41, pp 331-442.

42. Ruiz, R.; Caneschi, A.; Gatteschi, D.; Sangregorio, C.; Sorace, L.; Vazquez, M., Counter cation-controlled air oxidation of manganese derivatives of tetrachlorocatechol. *Inorg. Chem. Commun.* **2000,** *3* (2), 76-79,

43. Sheriff, T. S., PRODUCTION OF HYDROGEN-PEROXIDE FROM DIOXYGEN AND HYDROXYLAMINE OR HYDRAZINE CATALYZED BY MANGANESE COMPLEXES. *J. Chem. Soc.-Dalton Trans.* **1992,** (6), 1051-1058,

44. Sheriff, T. S.; Carr, P.; Coles, S. J.; Hursthouse, M. B.; Lesin, J.; Light, M. E., Structural studies on manganese(III) and manganese(IV) complexes of tetrachlorocatechol and the catalytic reduction of dioxygen to hydrogen peroxide. *Inorganica Chimica Acta* **2004,** *357* (9), 2494-2502, doi:10.1016/j.ica.2003.09.032.

45. Tyson, C. A.; Martell, A. E., KINETICS AND MECHANISM OF METAL CHELATE CATALYZED OXIDATION OF PYROCATECHOLS. *Journal of the American Chemical Society* **1972,** *94* (3), 939-&,

46. Sheriff, T. S.; Watkinson, M.; Motevallia, M.; Lesin, J. F., Unexpected formation of a novel pyridinium-containing catecholate ligand and its manganese(III) complex. *Dalton Trans.* **2010,** *39* (1), 53-55, doi:10.1039/b915747f.

47. Sheriff, T. S.; Carr, P.; Piggott, B., Manganese catalysed reduction of dioxygen to hydrogen peroxide: structural studies on a manganese(III)-catecholate complex. *Inorganica Chimica Acta* **2003,** *348*, 115-122, doi:10.1016/s0020-1693(02)01511-6.

48. Krzystek, J.; Yeagle, G. J.; Park, J. H.; Britt, R. D.; Meisel, M. W.; Brunel, L. C.; Telser, J., High-frequency and -field EPR spectroscopy of tris(2,4-pentanedionato)manganese(III): Investigation of solid-state versus solution Jahn-Teller effects. *Inorganic Chemistry* **2003,** *42* (15), 4610-4618, doi:10.1021/ic020712l.

49. Carugo, O.; Castellani, C. B.; Djinovic, K.; Rizzi, M., LIGANDS DERIVED FROM ORTHO-BENZOQUINONE - STATISTICAL CORRELATION BETWEEN OXIDATION-STATE AND STRUCTURAL FEATURES. *J. Chem. Soc.-Dalton Trans.* **1992,** (5), 837-841,

50. Goodgame, D. M.; Cotton, F. A., PHOSPHINE OXIDE COMPLEXES .5. TETRAHEDRAL COMPLEXES OF MANGANESE(II) CONTAINING TRIPHENYLPHOSPHINE OXIDE, AND TRIPHENYLARSINE OXIDE AS LIGANDS. *Journal of the Chemical Society* **1961,** (SEP), 3735-&,

51. Buchanan, R. M.; Fitzgerald, B. J.; Pierpont, C. G., Semiquinone Radical-Anion Coordination to Divalent Cobalt and Nickel - Strucutral Features of the Bis(3,5-di-tert-butyl-1,2-semiquinone) Cobalt (II) Tetramer. *Inorganic Chemistry* **1979,** *18* (12), 3439-3444,

52. Larsen, S. K.; Pierpont, C. G.; DeMunno, G.; Dolcetti, G., Manganese(III)-catecholate coordination in the bis(tetrabromocatecholato)(triphenylphosphine oxide)manganese(III) anionic dimer. *Inorganic Chemistry* **1986,** *25* (27), 4828-4831, doi:10.1021/ic00247a010.

53. Hartman, J. R.; Foxman, B. M.; Cooper, S. R., HIGHER VALENT MANGANESE CHEMISTRY - SYNTHETIC, STRUCTURAL, AND SOLUTION STUDIES ON MN(CATECHOLATE)3 N- (N=2,3) COMPLEXES. *Inorganic Chemistry* **1984,** *23* (10), 1381-1387,

54. Morris, A. M.; Pierpont, C. G.; Finke, R. G., Synthesis and Characterization of VV(3,6-DBSQ)(3,6-DBCat)2, a d0 Metal Complex with Dioxygenase Catalytic Activity. *Inorganic Chemistry* **2009,** *48* (8), 3496-3498, doi:10.1021/ic802122q.

55. Que, L.; Ho, R. Y. N., Dioxygen Activation by Enzymes with Mononuclear Non-Heme Iron Active Sites. *Chemical Reviews* **1996,** *96* (7), 2607-2624, doi:10.1021/cr960039f.

56. Yin, C.-X.; Finke, R. G., Vanadium-Based, Extended Catalytic Lifetime Catechol Dioxygenases: Evidence for a Common Catalyst. *Journal of the American Chemical Society* **2005,** *127* (25), 9003-9013, doi:10.1021/ja051594e.

57. Lee, Y.; Park, G. Y.; Lucas, H. R.; Vajda, P. L.; Kamaraj, K.; Vance, M. A.; Milligan, A. E.; Woertink, J. S.; Siegler, M. A.; Narducci Sarjeant, A. A.; Zakharov, L. N.; Rheingold, A. L.; Solomon, E. I.; Karlin, K. D., Copper(I)/O2 Chemistry with Imidazole Containing Tripodal Tetradentate Ligands Leading to μ-1,2-Peroxo−Dicopper(II) Species. *Inorganic Chemistry* **2009,** *48* (23), 11297-11309, doi:10.1021/ic9017695.

58. Pascaly, M.; Duda, M.; Schweppe, F.; Zurlinden, K.; Muller, F. K.; Krebs, B., The systematic influence of tripodal ligands on the catechol cleaving activity of iron(III) containing model compounds for catechol 1,2-dioxygenases. *J. Chem. Soc.-Dalton Trans.* **2001,** (6), 828-837, doi:10.1039/b0085111.

59. Hitomi, Y.; Ando, A.; Matsui, H.; Ito, T.; Tanaka, T.; Ogo, S.; Funabiki, T., Aerobic catechol oxidation catalyzed by a bis(mu-oxo)dimanganese(III,III) complex via a manganese(II)-semiquinonate complex. *Inorganic Chemistry* **2005,** *44* (10), 3473-3478, doi:10.1021/ic050109d.

60. Triller, M. U.; Pursche, D.; Hsieh, W. Y.; Pecoraro, V. L.; Rompel, A.; Krebs, B., Catalytic oxidation of 3,5-di-tert-butylcatechol by a series of mononuclear manganese complexes: Synthesis, structure, and kinetic investigation. *Inorganic Chemistry* **2003,** *42* (20), 6274-6283, doi:10.1021/ic0347788.

61. APEX II, Analytical X-Ray Systems, Brukers AXS, Inc., Madison, WI, 2005.,

62. SAINT Version 6.45A, Analytical X-ray Systems, Brukers AXS, Inc., Madison, WI,
2003.,

63. SHELXTL Version 6.12, Analytical X-ray Systems, Bruker AXS, Inc., Madison, WI,
2002.,

64. Wilson, J. C., *In International Tables for X-ray Crystallography, Volume C;*. Academic Publishers: Dordrecht, The Netherlands, 1992.

CHAPTER 3

AEROBIC ALCOHOL OXIDATION VIA ALKOXIDE-BRIDGED MANGANESE(III) DIMERS

3.1 Introduction.

Molecular oxygen is the ideal "green" oxidant, but the practical utility of O_2 as a reagent for chemical synthesis is often limited by its propensity for unselective free radical autoxidation.[1-6] Homogeneous "chemical oxidase" catalysts circumvent this issue by coupling multielectron oxidations of organic small molecules—typically dehydrogenation or oxidative coupling reactions—to even-electron O_2 reduction.[1-2, 5, 7-13] Accordingly, the remarkable utility of palladium in oxidase-type aerobic alcohol oxidations is a consequence of its bias for $2e^-$ transfer over potentially competing $1e^-$ radical pathways.[11-13] An alternative, emerging approach to multielectron reaction chemistry utilizes redox "non-innocent" ligands as reservoirs of electrons for reactions at coordinatively unsaturated transition metals, including later first row metal ions.[9, 14-30] Such cooperative redox between metals and ligand radicals is a defining feature of several functional copper oxidase models that catalyze selective aerobic alcohol oxidations.[9, 19, 24-26, 31-32]

In the previous chapter, it was reported that the $[Mn^{III}(Br_4cat)_2]^-$ fragment containing redox-active $[Br_4cat]^{2-}$ ligands ($[Br_4cat]^{2-}$ = tetrabromo-1,2,-catecholate) is a robust catalyst for oxidase-type catechol dehydrogenation.[33] Notably, the $[Mn^{III}(Br_4cat)_2]^-$ core is inert to O_2, but catecholate binding forms a catalyst–substrate

complex and initiates a net $2e^-$ catecholase reaction with O_2. Reported in this chapter are our efforts to utilize a similar strategy for manganese oxidase-type aerobic oxidations of primary alcohols.

3.2. Results.

3.2.1. Preparation of Mn(III) Catecholate Complexes.

The complex, $(^nBu_4N)[Mn^{III}(Br_4cat)_2(THF)_2]\bullet THF$ was used to explore the aerobic oxidations catalyzed by manganese(III) catecholate complexes. This complex was prepared based on an adaptation of the procedure for the synthesis of $(^nBu_4N)[Mn^{III}(Br_4cat)_2(Me_2C{=}O)_2]$.[33] Heating $Mn^{II}(ClO_4)_2\bullet 4H_2O$ with 2 equiv Br_4catH_2 in a neat THF solution with $^nBuN_4OH$ to reflux for 1 hr in air affords a brown solution. Upon cooling to –20 °C, the reaction deposits $(^nBu_4N)[Mn^{III}(Br_4cat)_2(THF)_2]$, as analytically pure, dark green crystals in 29% yield **(Scheme 1, Figure 1**)

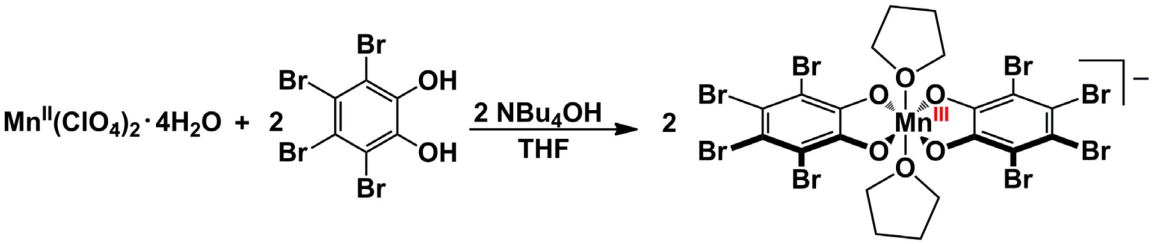

Scheme 1. Synthesis of $(^nBu_4N)[Mn^{III}(Br_4cat)_2(THF)_2)]$

The crystal structure of $(^nBu_4N)[Mn^{III}(Br_4cat)_2(THF)_2]\bullet THF$ contains a six-coordinate manganese anion bound to two coplanar *o*-dioxolene ligands and two THF molecules. The quinoid chelates have C–C and C–O bond lengths averaging 1.397 Å and 1.324 Å respectively, which best match those expected for $[Br_4cat]^{2-}$.[34] The axial Mn–O

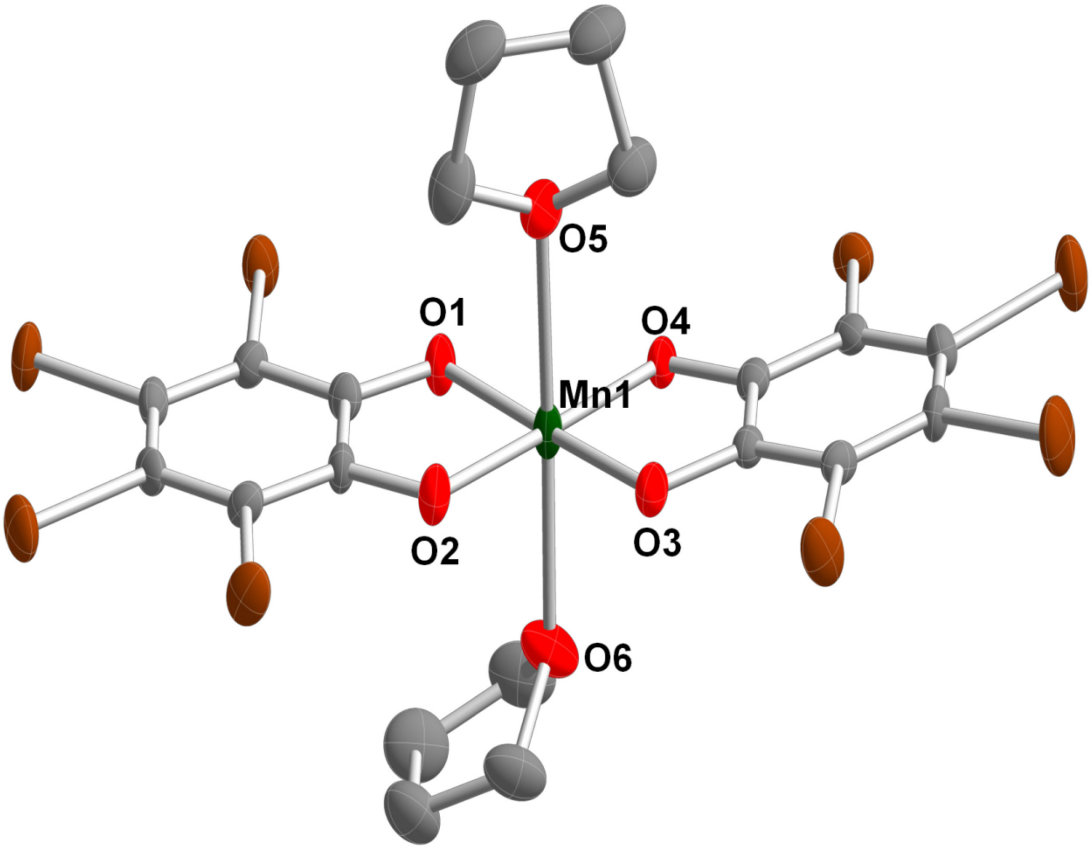

Figure 3.1. Solid-state structure of the anion in ($^{n}Bu_4N$)[$Mn^{III}(Br_4cat)_2(THF)_2$]•(THF) shown with 50% probability ellipsoids. ($^{n}Bu_4N$) countercation , THF solvent molecule and H atoms are omitted for clarity. Selected bond lengths (Å) and angles (deg): Mn1–O1 1.904(3), Mn1–O2 1.903 (3), Mn1–O3 1.898(3), Mn1–O4 1.893(3), Mn1–O5 2.383(3), Mn1–O6 2.364(3), O1–Mn1–O2 84.16(13), O1–Mn1–O5 92.06 (13), O2–Mn1–O5 90.36 (13).

bond distance for THF molecules has an average of 2.374(5) Å and is elongated relative to the average Mn–O bond lengths of 1.900(3) Å for the catecholates ligands. These observations are consistent with a high-spin $3d^4$ electron configuration.[35-37]

The previously prepared MeOH adduct to $[Mn^{III}(Br_4cat)_2]^-$ is the five coordinate square pyramidal $[Mn^{III}(Br_4cat)_2(MeOH)]^-$ anion that is stable for days under 1 atm O_2 at 25 °C. However, addition of strong bases, such as NaH or NaOMe to MeOH solutions of $[Mn^{III}(Br_4cat)_2(MeOH)]^-$ gives a new dark green species that is sensitive to O_2. The same dark green species is isolated in high yield from the reaction of $(^nBu_4N)[Mn^{III}(Br_4cat)_2(THF)_2]$ with 1 equiv NaOMe in MeOH, which deposits crystals suitable for X-ray analysis **(Scheme 2, Figure 3.2)**.

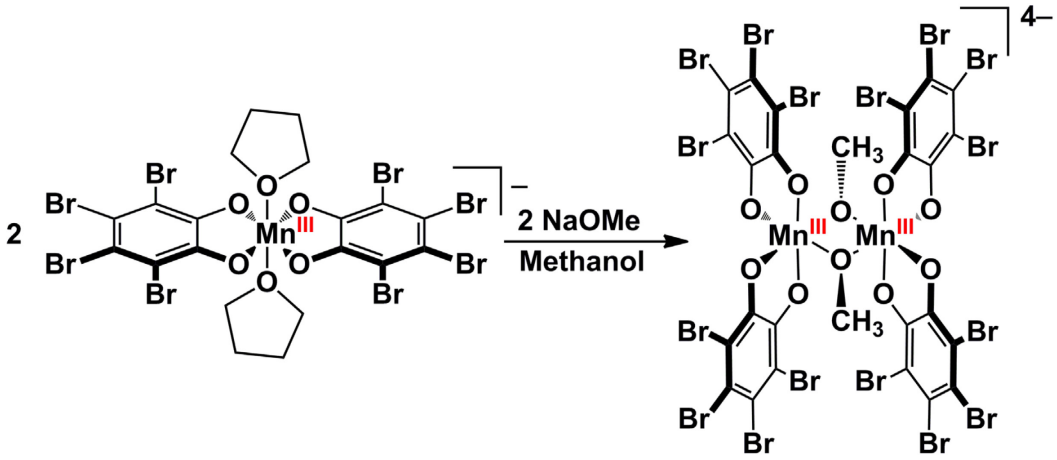

Scheme 2. Synthesis of $[(Br_4cat)_2Mn^{III}(\mu\text{-}OMe)_2Mn^{III}(Br_4cat)_2]^{4-}$.

The anionic component of the structure contains a dimer of six-coordinate manganese ions where each manganese center is ligated by two $[Br_4cat]^{2-}$ ligands and the oxygen atoms of two bridging μ-$[OMe]^-$ ligands. The two halves of the dimer are related by a center of symmetry, so the coordination geometry about both manganese ions is

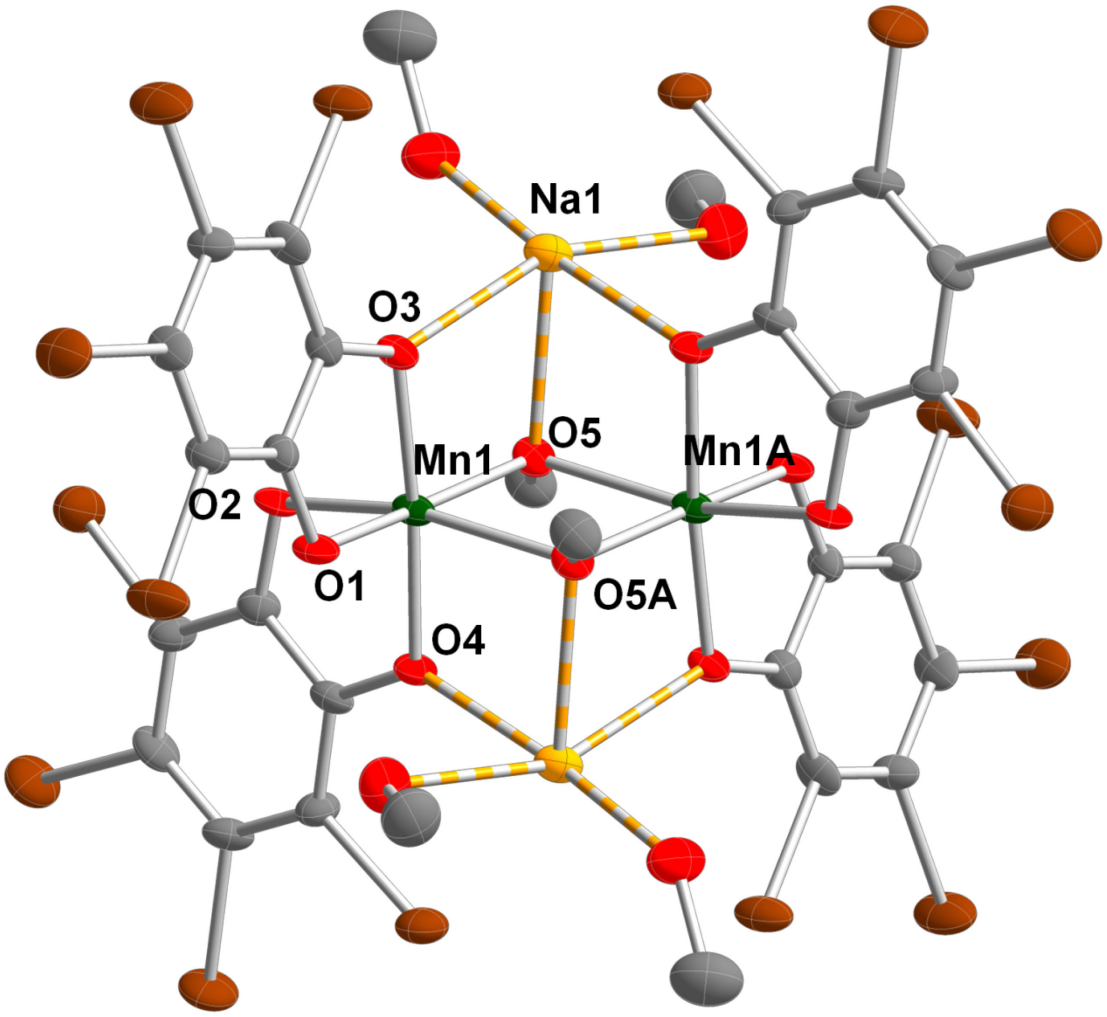

Figure 3.2. Solid-state structure of the sodium salt of anion in $(^{n}Bu_4N)_2[Na(MeOH)_2]_2[(Br_4cat)_2Mn^{III}(\mu\text{-}OMe)_2Mn^{III}(Br_4cat)_2]\bullet MeOH$ **($[Mn^{III}_2(\mu\text{-}OMe)_2]^{4-}$) (1)** drawn with 50% probability ellipsoids. The $[^{n}Bu_4N]^{+}$ countercations, $[Br_4cat]^{2-}$ ligand bromine atoms, and MeOH solvate molecule are omitted for clarity. . Selected bond lengths (Å) and angles (deg): Mn1–O1 1.944(3), Mn1–O2 2.154 (3), Mn1–O3 1.939(3), Mn1–O4 1.944(3), Mn1–O5 1.909 (3), Mn1–O5A 2.258(3), Na1–O3, 2.403(4), Na1–O5, 2.424(3) O1–Mn1–O2 97.25(13), O1–Mn1–O3 84.00(13), O2–Mn1–O5 97.31 (12).

four shorter Mn–O distances averaging 1.934(3) Å and one elongated O_{OMe}–Mn–O_{Br4cat} axis, with an average bond lengths of 2.154 (3) Å and 2.258 (3) Å, consistent with a high-spin $3d^4$ electron configuration.[35-37] Within the dimer, the two long O–Mn–O axes are parallel, resulting in an asymmetric $Mn_2(\mu\text{-}OR)_2$ diamond core that is stabilized by close contact with two $Na(MeOH)_2^+$ cations. The catecholate ligands have C–C and C–O bond lengths averaging 1.398 Å and 1.331 Å respectively, which best match those expected for $[Br_4cat]^{2-}$.[34] The sum of the metrical data are therefore most consistent with formulation of the dimer as $[(Br_4cat)_2Mn^{III}(\mu\text{-}OMe)_2Mn^{III}(Br_4cat)_2]^{4-}$ ($[Mn^{III}{}_2(\mu\text{-}OMe)_2]^{4-}$).

Modifications of the synthetic conditions for preparation of $[Mn^{III}{}_2(\mu\text{-}OMe)_2]^{4-}$ produced analogous dimanganese bis(μ-alkoxo) dimers with varying countercations and catecholate ligands. For instance, the use of 1 equiv LiOMe or LiOPh as a base the reaction of $(^nBu_4N)[Mn^{III}(Br_4cat)_2(THF)_2]$ in MeOH, produced a complex with the same $[Mn^{III}{}_2(\mu\text{-}OMe)_2]^{4-}$ core but $Li(MeOH)^+$ instead of the $Na(MeOH)_2^+$ cations **(Scheme 3, Figure 3)**. The crystal structures were of varying structural fidelity.

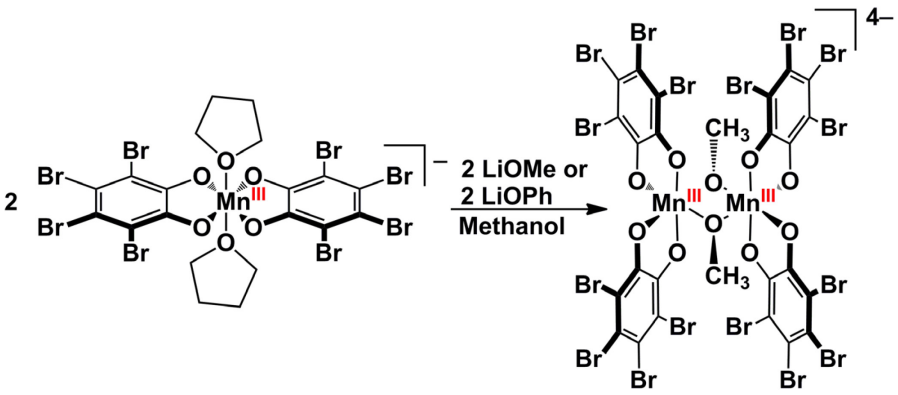

Scheme 3. Synthesis of $[(Br_4cat)_2Mn^{III}(\mu\text{-}OMe)_2Mn^{III}(Br_4cat)_2]^{4-}$.

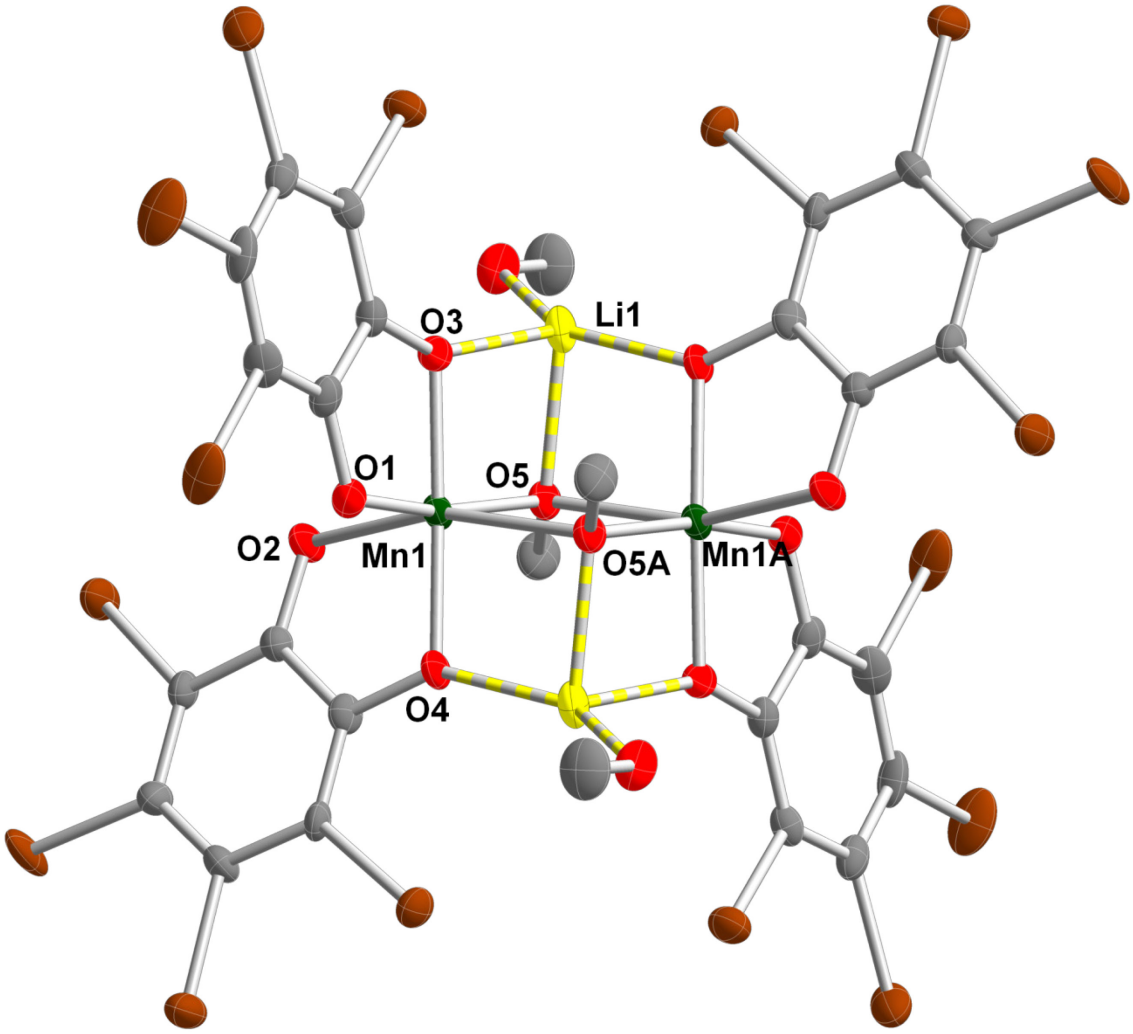

Figure 3.3. Solid-state structure of the lithium salt of the anion in $(^{n}Bu_4N)_2[Li(MeOH)]_2[(Br_4cat)_2Mn^{III}(\mu\text{-}OMe)_2Mn^{III}(Br_4cat)_2]\bullet MeOH$ (**$[Mn^{III}_2(\mu\text{-}OMe)_2]^{4-}$**) **(2)** drawn with 50% probability ellipsoids. The $[^{n}Bu_4N]^{+}$ countercations and MeOH solvate molecule are omitted for clarity. Selected bond lengths (Å) and angles (deg): Mn1–O1 1.906(3), Mn1–O2 2.118 (3), Mn1–O3 1.959(3), Mn1–O4 1.957(3), Mn1–O5 1.913 (3), Mn1–O5A 2.220(3), Li1–O3, 1.969(4), Li1–O5, 2.1364(3) O1–Mn1–O2 94.38(13), O1–Mn1–O3 84.11(12), O2–Mn1–O3 99.86 (12).

The structure contains a dimer of six-coordinate manganese ions where each manganese center is coordinated to two $[Br_4cat]^{2-}$ ligands and the oxygen atoms of two bridging μ-$[OMe]^-$ ligands. The coordination geometry about both manganese ions is crystallographically identical. The geometry at each manganese center consists of a distorted octahedron with four Mn–O distances averaging 1.934(3) Å and one elongated O_{OMe}–Mn–O_{Br4cat} axis, with an average bond lengths of 2.118 (3) Å and 2.220 (3) Å. These Mn–O bond lengths are consistent with a high-spin $3d^4$ electron configuration.[35-37] The dimer also contains two long O–Mn–O axes are parallel to each other, resulting in an asymmetric $Mn_2(\mu\text{-}OR)_2$ diamond core that is stabilized by close contact with two $Li(MeOH)^+$ cations. The catecholate ligands have C–C and C–O bond lengths averaging 1.398 Å and 1.331 Å respectively, which best match those expected for $[Br_4cat]^{2-}$.[34] The sum of the metrical data are therefore most consistent with formulation of the dimer as $[(Br_4cat)_2Mn^{III}(\mu\text{-}OMe)_2Mn^{III}(Br_4cat)_2]^{4-}$ ($[Mn^{III}_2(\mu\text{-}OMe)_2]^{4-}$).

A derivative of the **$[Mn^{III}_2(\mu\text{-}OMe)_2]^{4-}$** core was also prepared by using $(^nBu_4N)[Mn^{III}(Cl_4cat)_2(THF)_2]$ as the precursor complex. The reaction of $[Mn^{III}(Cl_4cat)_2(THF)_2]^-$ with 1 equiv. of LiOMe in MeOH afforded green crystals suitable for x-ray analysis (**Figure 4, Scheme 4**).

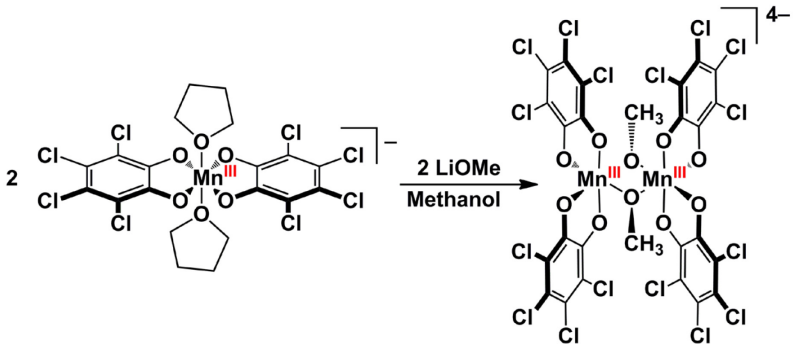

Scheme 4. Synthesis of $[(Br_4cat)_2Mn^{III}(\mu\text{-}OMe)_2Mn^{III}(Br_4cat)_2]^{4-}$.

The structure also contains a dimer of six-coordinate manganese ions where each manganese center is coordinated to two $[Cl_4cat]^{2-}$ ligands and two bridging μ-$[OMe]^-$ ligands. The coordination geometry in this structure about both manganese ions is also crystallographically identical. The geometry of each manganese center is comprised of a distorted octahedron with four Mn–O distances averaging 1.934(3) Å and one elongated O_{OMe}–Mn–O_{Cl4cat} axis, with an average bond lengths of 2.107 (3) Å and 2.222 (3) Å. The Mn–O bond lengths are consistent with a high-spin $3d^4$ electron configuration.[35-37] The dimer also contains two long O–Mn–O axes are parallel to each other, resulting in an asymmetric $Mn_2(\mu\text{-}OR)_2$ diamond core, but no close contact Li^+ ions were observed in the dimer, as in the $[Mn^{III}(Br_4cat)_2]^-$ analog. The catecholate ligands have C–C and C–O bond lengths averaging 1.393 Å and 1.327 Å respectively, which best match those expected for $[Cl_4cat]^{2-}$.[34] The sum of the metrical data are therefore most consistent with formulation of the dimer as $[(Cl_4cat)_2Mn^{III}(\mu\text{-}OMe)_2Mn^{III}(Cl_4cat)_2]^{4-}$ **($[Mn^{III}_2(\mu\text{-}OMe)_2]^{4-}$).**

The reaction of $(^nBu_4N)[Mn^{III}(Br_4cat)_2(THF)_2]$ with 1 equiv NaOBn (Bn = benzyl)—prepared *in situ* from BnOH and NaH—in BnOH solution yields analytically pure dark green crystals containing the $[(Br_4cat)_2Mn^{III}(\mu\text{-}OBn)_2Mn^{III}(Br_4cat)_2]^{4-}$ (**$[Mn^{III}_2(\mu\text{-}OBn)_2]^{4-}$**) anion (**Figure 5, Scheme 5**).

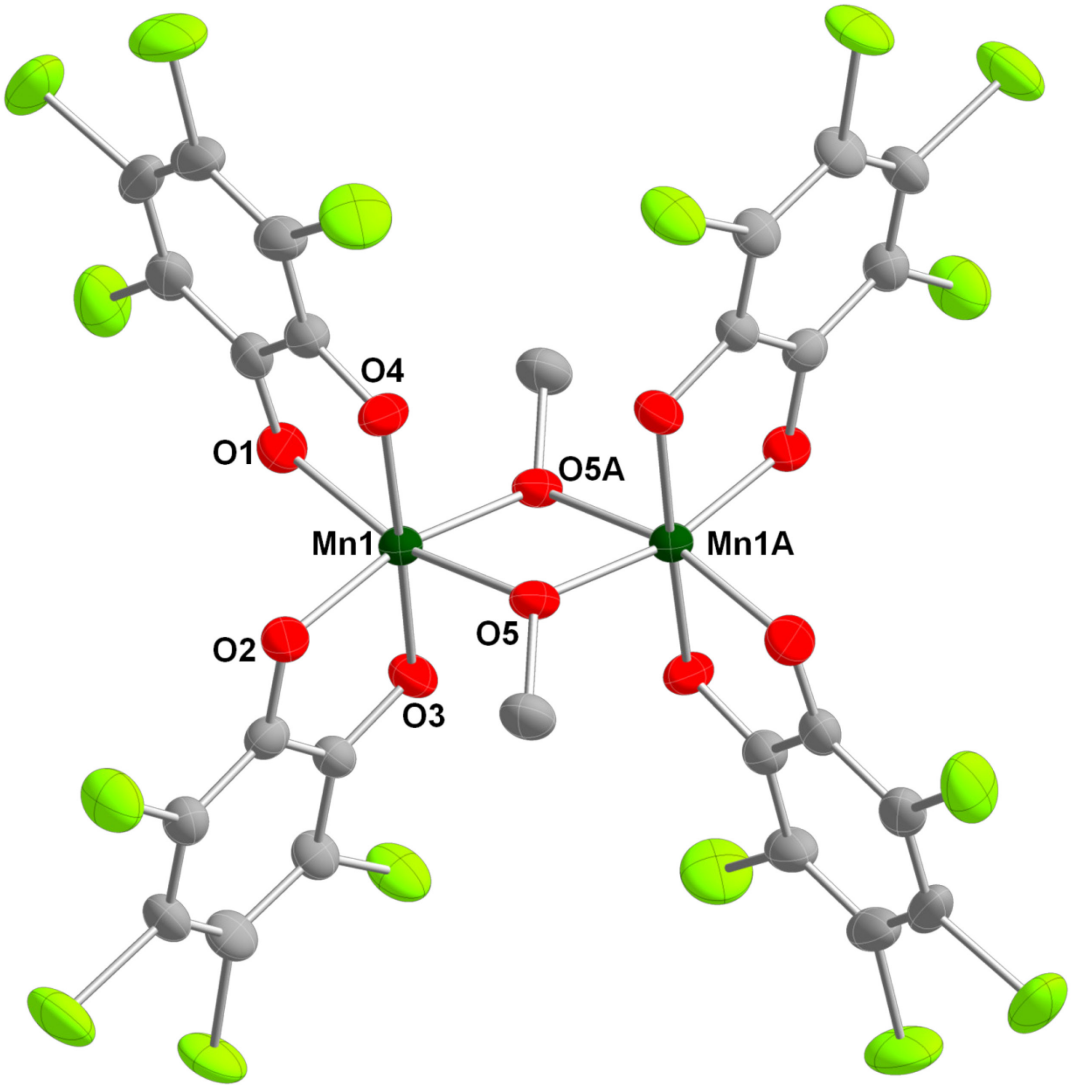

Figure 3.4. Solid-state structure of the of the anion in $(PPN)_2[Li]_2[(Cl_4cat)_2Mn^{III}(\mu\text{-}OMe)_2Mn^{III}(Cl_4cat)_2]\bullet MeOH$ (**$[Mn^{III}_2(\mu\text{-}OMe)_2]^{4-}$**) **(3)** drawn with 50% probability ellipsoids. The $[Li]^+$, $[^nBu_4N]^+$ countercations and H_2O solvate molecule are omitted for clarity. . Selected bond lengths (Å) and angles (deg): Mn1–O1 1.934(3), Mn1–O2 2.107 (3), Mn1–O3 1.953(3), Mn1–O4 1.934(3), Mn1–O5 1.915 (3), Mn1–O5A 2.223(3), O1–Mn1–O2 95.71(13), O1–Mn1–O3 84.35(12), O2–Mn1–O3 97.48 (12).

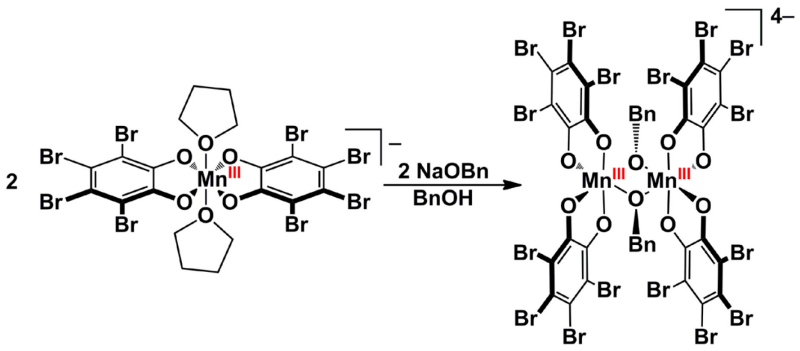

Scheme 5. Synthesis of $[(Br_4cat)_2Mn^{III}(\mu\text{-}OBn)_2Mn^{III}(Br_4cat)_2]^{4-}$.

In the crystal structure of (**$[Mn^{III}_2(\mu\text{-}OBn)_2]^{4-}$**), two unique Mn molecules were determined in each unit cell. Each molecule in the structure contains a dimer of six-coordinate manganese ions where each manganese center is ligated by two $[Br_4cat]^{2-}$ ligands and two bridging μ-$[OBn]^-$ ligands. The geometry at manganese is a distorted octahedron with four shorter Mn–O distances averaging 1.953 (3) Å and two longer Mn–O distances along the O_{OBn}–Mn–O_{Br4cat} axis with average bond lengths of 2.167 (3) Å and 2.301 (3) Å. This is consistent with a high-spin $3d^4$ electron configuration [35-37]. Similarly to **$[Mn^{III}_2(\mu\text{-}OMe)_2]^{4-}$**, the two long O–Mn–O axes are parallel in each molecule, resulting in an asymmetric $Mn_2(\mu\text{-}OR)_2$ diamond core that is stabilized by close contact with two Na^+ cations. In one molecule, 1 eq of BnOH is bound to each Na^+ cation. For the other Mn molecule, the Na^+ cations do not have any free solvent molecules bound. The sum of the metrical data are consistent with formulation of the dimer as $[(Br_4cat)_2Mn^{III}(\mu\text{-}OBn)_2Mn^{III}(Br_4cat)_2]^{4-}$ (**$[Mn^{III}_2(\mu\text{-}OBn)_2]^{4-}$**). All of structures for the (**$[Mn^{III}_2(\mu\text{-}OCH_2R)_2]^{4-}$**) complexes display similar Mn–O distances. A full comparison of the bond lengths for each structure can be observed in **Table 3.1**.

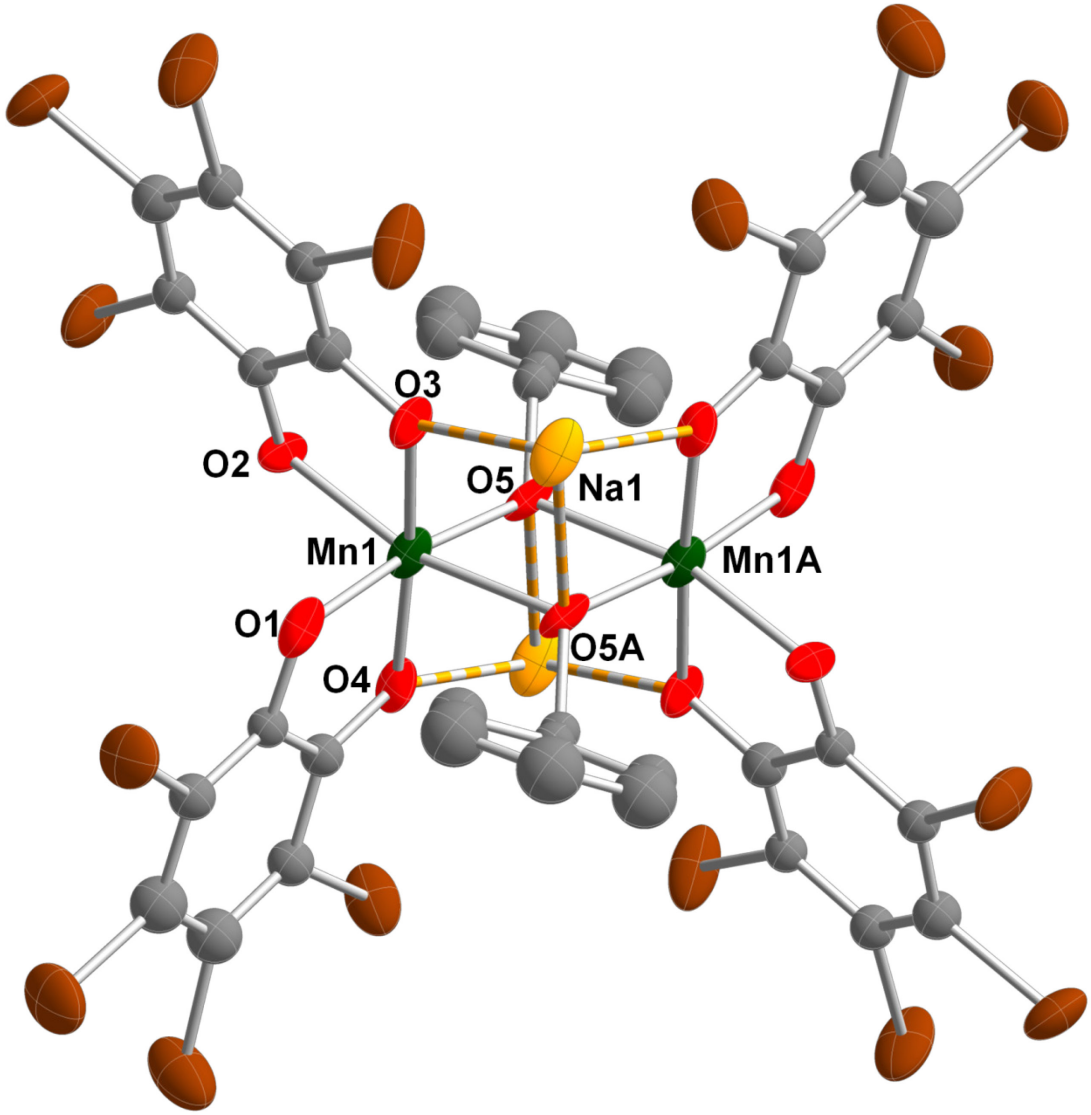

Figure 3.5. Solid-state structure of an anion in $(^{n}Bu_4N)_{1.66}[Na]_{2.33}[(Br_4cat)_2Mn^{III}(\mu\text{-}OBn)_2Mn^{III}(Br_4cat)_2]\bullet BnOH$ (**$[Mn^{III}_2(\mu\text{-}OBn)_2]^{4-}$**) **(4)** drawn with 50% probability ellipsoids. The structure shown represents one of two crystallographically unique, but structurally similar, anionic fragments in the unit cell. The $[^{n}Bu_4N]^{+}$ countercations and BnOH solvate molecule are omitted for clarity. Selected bond lengths (Å) and angles (deg): Mn1–O1 1.936(3), Mn1–O2 2.167 (3), Mn1–O3 1.959(3), Mn1–O4 1.967(3), Mn1–O5 1.949 (3), Mn1–O5A 2.301(3), Na1–O3, 2.277(4), Na1–O5, 2.464(3) O1–Mn1–O2 92.260(13), O1–Mn1–O3 91.264(12), O2–Mn1–O3 80.29 (12).

Table 3.1. Selected bond lengths (Å) for series of ($[Mn^{III}_2(\mu\text{-}OCH_2R)_2]^{4-}$) complexes.

Complex	(1)	(2)	(3)	(4)
Catecholate ligands				
Mn1-O1	1.944(3)	1.906(3)	1.934(3)	1.936(3)
Mn1-O2	2.154 (3)	2.118 (3)	2.107 (3)	2.167 (3)
Mn1-O3	1.939(3)	1.959(3)	1.953(3)	1.959(3)
Mn1-O4	1.944(3)	1.957(3)	1.934(3)	1.967(3)
Alkoxide Ligands				
Mn1–O5	1.909 (3)	1.913 (3)	1.915 (3)	1.949 (3)
Mn1–O5A	2.258(3)	2.220(3)	2.223(3)	2.301(3)

The reaction of ($^{n}Bu_4N$)[$Mn^{III}(Br_4cat)_2(THF)_2$] with 1 equiv NBu_4Cl in CH_3CN solution yields a dark green solution containing the five coordinate chloride adduct ($^{n}Bu_4N)_2[Mn^{III}Cl(Br_4cat)_2]$ dianion (**Scheme 6**). The reaction was precipitated from a THF and pentane solution to yield crystals suitable for X-ray analysis.

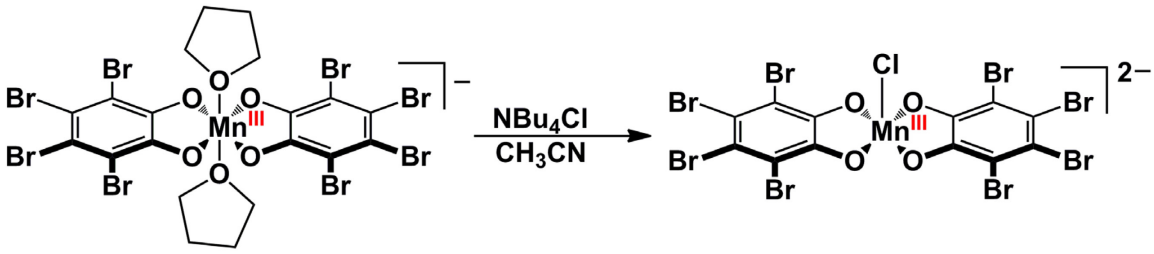

Scheme 6. Synthesis of ($^{n}Bu_4N)_2[Mn^{III}Cl(Br_4cat)_2]$.

The structure obtained from the reaction was of low quality and only good enough for assigining connectivity. Unlike the alkoxide complexes, the chloride adduct does not form a bridged dimer. The structure contains a five-coordinate manganese ion coordinated to two coplanar $[Br_4cat]^{2-}$ ligands and one axial Cl^- ligand. Multiple trials of isolating crystals of ($^{n}Bu_4N)_2[Mn^{III}Cl(Br_4cat)_2]$ using a similar synthetic procedures with varying counterions consistently lead to low quality data being collected.

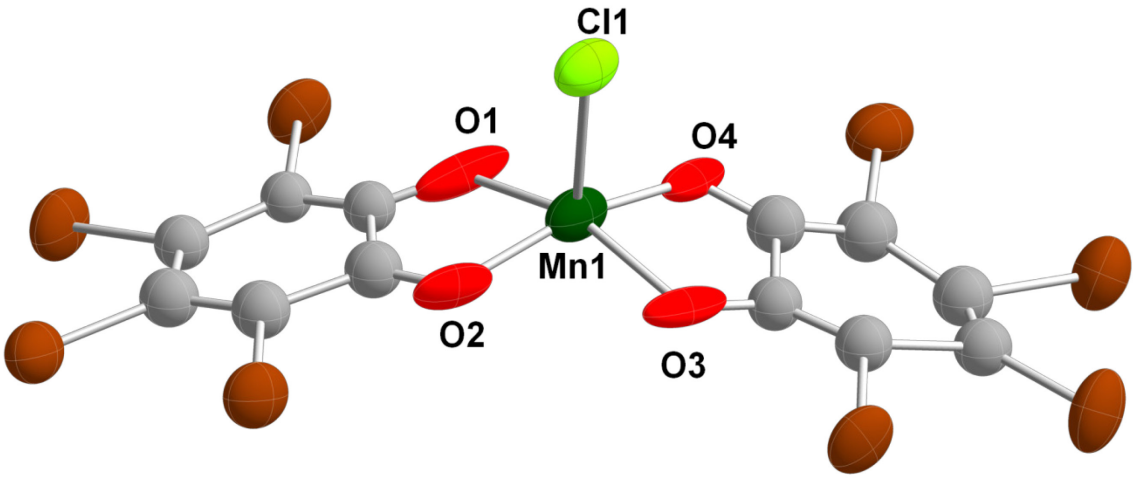

Figure 3.6. Solid-state structure of the anion in $(^{n}Bu_4N)_2[Mn^{III}Cl(Br_4cat)_2]$ shown with 50% probability ellipsoids. $(^{n}Bu_4N)$ countercation and H atoms are omitted for clarity. Selected bond lengths (Å) and angles (deg): Mn1–O1 1.936(30), Mn1–O2 1.939 (19), Mn1–O3 1.940(20), Mn1–O4 1.910(20), Mn1–Cl 2.434(10), O1–Mn1–O2 79.29(11), O1–Mn1–Cl1 105.4(8), O2–Mn1–Cl1 95.8(8).

3.2.2 Reactions of $[Mn^{III}(Br_4Cat)_2X]^{2-}$ with O_2.

The green $\mathbf{[Mn^{III}_2(\mu\text{-}OCH_2R)_2]^{4-}}$ dimers are indefinitely stable in THF, DMSO or CH_3CN under N_2, but all react with O_2. The nature of the bridging alkoxide substituent impacts both the relative reaction rates and the organic product distributions. On addition of 1 atm O_2 to NMR tubes containing $\mathbf{[Mn^{III}_2(\mu\text{-}OMe)_2]^{4-}}$ in MeCN–d_3, the green solutions slowly become blue and then darker green over 12 h at 25 °C. During the entire course of the reaction, no aldehyde resonances are observed by ^{1}H NMR spectroscopy. The UV–vis spectrum of the blue intermediate species observed in the reaction matches the spectrum of the known tris(tetrabromo-*o*-catecholato) dianion $[Mn^{IV}(Br_4cat)_3]^{2-}$, and analysis of the final green solution by ESI–MS indicated that the green product is the monomeric $[Mn^{III}(Br_4cat)_2]^-$ fragment. Formation of this ion was additionally confirmed by isolation and recrystallization of the reaction products from THF–pentane, which afforded a mixture of red-orange solids and green single crystals of $[Mn^{III}(Br_4cat)_2(THF)_2]^-$. Accordingly, the reaction of $\mathbf{[Mn^{III}_2(\mu\text{-}OMe)_2]^{4-}}$ with O_2 apparently proceeds via slow ligand redistribution to afford $[Mn^{IV}(Br_4cat)_3]^{2-}$, which is known to undergo further oxidation by O_2 to give $[Mn^{III}(Br_4cat)_2]^-$ and red-orange Br_4bq-derived products (Br_4bq = tetrabromo-1,2-benzoquinone) **(Scheme 7)**.

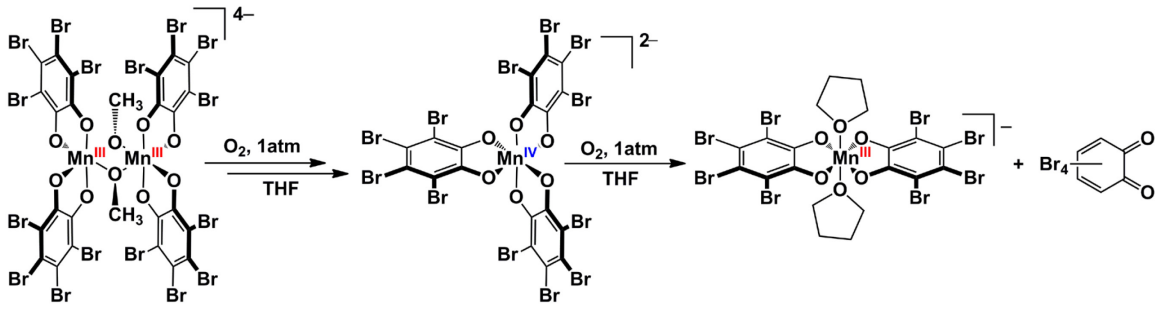

Scheme 7. Oxidative Degradation of $\mathbf{[Mn^{III}_2(\mu\text{-}OMe)_2]^{4-}}$.

The dianion $[Mn^{III}Cl(Br_4cat)_2]^{2-}$ is also air sensitive and behaves similarly to **$[Mn^{III}_2(\mu\text{-}OMe)_2]^{4-}$.** Reactions of $(^nBu_4N)_2[Mn^{III}Cl(Br_4cat)_2]$ with O_2 were examined by preparing solutions of $[Mn^{III}Cl(Br_4cat)_2]^{2-}$ *in situ* by adding 1 equiv. of NBu_4Cl to CH_3CN solutions of the well defined $(^nBu_4N)[Mn^{III}(Br_4cat)_2(THF)_2]$. The dark green solutions turn blue upon air exposure with a UV-vis spectrum that matches $[Mn^{IV}(Br_4cat)_3]^{2-}$, which is known to undergo further oxidation by O_2 to give $[Mn^{III}(Br_4cat)_2]^-$.[33] The blue solutions of $[Mn^{IV}(Br_4cat)_3]^{2-}$eventually turned green and examination of these green solutions by ESI-MS revealed that the core $[Mn^{III}(Br_4cat)_2]^-$ was present. **(Scheme 8)**.

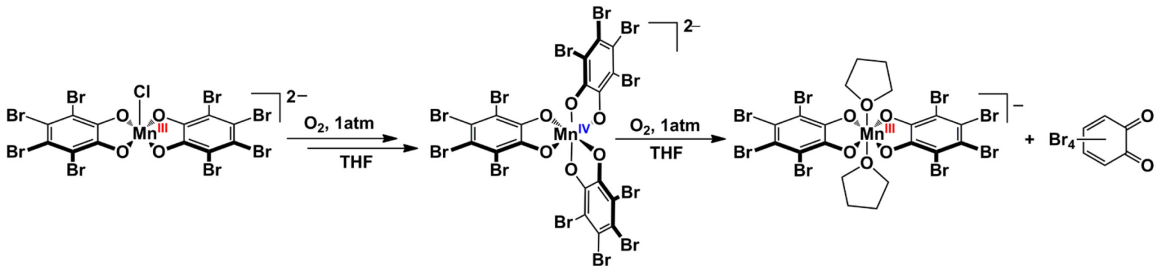

Scheme 8. Oxidative Degradation of $(^nBu_4N)_2[Mn^{III}Cl(Br_4cat)_2]$.

In contrast to both **$[Mn^{III}_2(\mu\text{-}OMe)_2]^{4-}$** and $[Mn^{III}Cl(Br_4cat)_2]^{2-}$, exposure of the benzyl alkoxide dimer **$[Mn^{III}_2(\mu\text{-}OBn)_2]^{4-}$** to 1 atm O_2 in MeCN–d_3 or THF–d_8 initially yields a darker green solution over 2 h at 25 °C. During this time period, the ^1H NMR spectra show concomitant, quantitative formation of BnOH and benzaldehyde (PhCHO) in a 1:1 ratio. The organic ligands bound to manganese are ^1H NMR silent, but integration against the resonances for the $[^nBu_4N]^+$ countercation confirms that the $[OBn]^-$ ligands are quantitatively converted to PhCHO and BnOH **(Scheme 9)**.

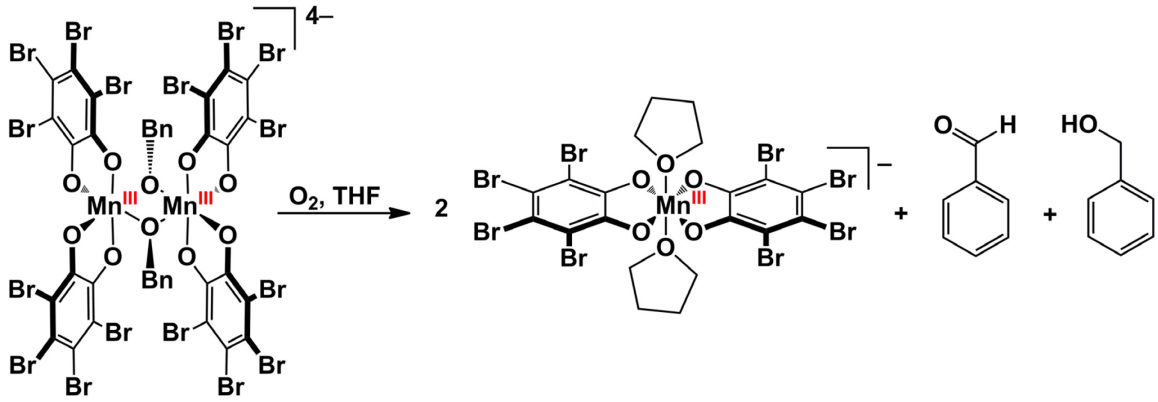

Scheme 9. Aerobic oxidation of benzyl alcohol

Control experiments indicate that NaOBn is not oxidized to PhCHO under the same conditions, suggesting that the reaction to generate PhCHO does not occur by liberation of free $[OBn]^-$ from the $\mathbf{[Mn^{III}_2(\mu\text{-}OBn)_2]^{4-}}$ dimer.

After benzaldehyde is formed, the green solution also turns blue and then darker green over 10 h at 25 °C. The UV–vis spectrum of the blue intermediate species matches the spectrum of the known tris(tetrabromo-*o*-catecholato) trianion $[Mn^{IV}(Br_4cat)_3]^{2-}$, and analysis of the final green solution by ESI–MS indicated that the green product is the monomeric $[Mn^{III}(Br_4cat)_2]^-$ fragment. It was suspected that the reduced oxygen species sodium peroxide, was decomposing the $[Mn^{III}(Br_4cat)_2]^-$ core in similar fashion to other anions, such as Cl^-, Br^-, SCN^- and OMe^-. Independent reactions of $[Mn^{III}(Br_4cat)_2]^-$ with the dianionic Li_2O_2 in the presence of air afford blue solutions of $[Mn^{IV}(Br_4cat)_3]^{2-}$, determined by UV-vis and ESI-MS (**Scheme 10**).

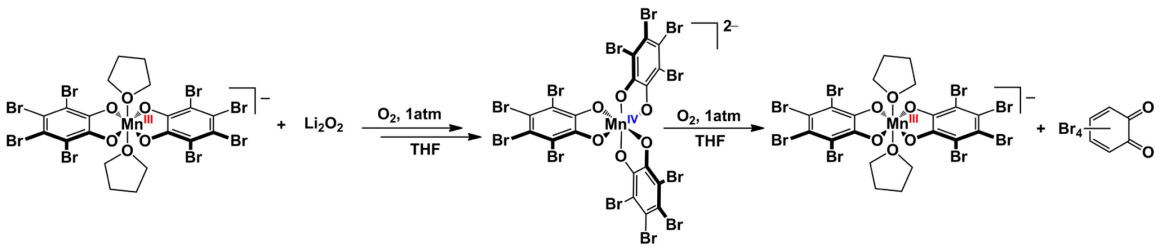

Scheme 10. Oxidative degradation of $[Mn^{III}(Br_4cat)_2]^-$ catalyzed by lithium peroxide.

These results show that peroxide anion is also capable of the oxidative rearrangement reaction observed with Cl^-, Br^-, SCN^- and OMe^-. Similar reactions performed with H_2O_2 do not form blue solutions of $[Mn^{IV}(Br_4cat)_3]^{2-}$. The $[Mn^{III}(Br_4cat)_2]^-$ core is preserved in solutions containing excess hydrogen peroxide in the presence of air over the course of days.

The net conversion of **$[Mn^{III}_2(\mu\text{-}OBn)_2]^{4-}$** to PhCHO, BnOH and $[Mn^{III}(Br_4cat)_2]^-$ requires a $2e^-$ oxidant, but the reaction is surprisingly specific for O_2. Titrations of MeCN–d_3 and THF–d_8 solutions of **$[Mn^{III}_2(\mu\text{-}OBn)_2]^{4-}$** with 1-2 equiv of chemical oxidants including $AgBF_4$ or $NOBF_4$ gave no benzaldehyde by ^1H NMR spectroscopy over 24 h. Addition of larger excess $NOBF_4$ led to decomposition of the complex without aldehyde formation. The specificity for oxygen in the reaction suggests that the $[OBn]^-$ oxidation likely proceeds via an inner-sphere reaction of **$[Mn^{III}_2(\mu\text{-}OBn)_2]^{4-}$** with O_2, affording peroxide salts.

3.2.3 Catalytic Aerobic Oxidation Reactions with $[Mn^{III}(Br_4cat)_2(THF)_2]^-$

The gentle conditions and high selectivity for $[OBn]^-$ oxidation at **$[Mn^{III}_2(\mu\text{-}OBn)_2]^{4-}$** prompted us to pursue catalytic oxidase-type benzylic alcohol oxidations. Our

efforts have yielded mixed results. Using $[Mn^{III}(Br_4cat)_2(THF)_2]^-$ as a catalyst, the alcohol oxidation in **Scheme 11** gives conversion to the corresponding aldehyde.. Control experiments show that without $[Mn^{III}(Br_4cat)_2(THF)_2]^-$ the activated alcohol is not consumed under the reaction conditions, but a mixture of products is observed by GC–MS with the aldehyde accounting only for a trace (≥5%) amount of the benzyl-derived materials.

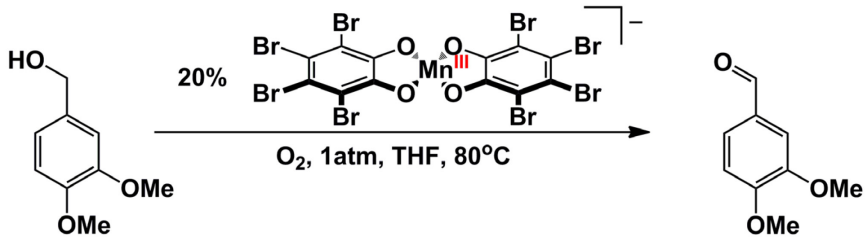

Scheme 11. Aerobic alcohol oxidation catalyzed by $[Mn^{III}(Br_4cat)_2(THF)_2]^-$.

In contrast to the activated alcohol, addition of 10 equiv of the parent BnOH and 1 atm O_2 to NMR tubes containing $[Mn^{III}(Br_4cat)_2(THF)_2]^-$ in MeCN–d_3 gives no observable PhCHO over days at 25 °C, and only trace quantities of PhCHO are formed after 12 h at 80 °C. Analogous reactions performed with 10 mol % **$[Mn^{III}_2(\mu\text{-}OBn)_2]^{4-}$** gave only stoichiometric extrusion of one PhCHO from the dimer.

Without an exogenous base, the resulting alcohol adduct $[Mn^{III}(Br_4cat)_2(BnOH)]^-$ is inert to O_2. Reactions were therefore performed in the presence of stoichiometric bases to regenerate **$[Mn^{III}_2(\mu\text{-}OBn)_2]^{4-}$**, but none facilitated catalytic turnover. For instance, addition of excess alkoxides (≥10 equiv), including NaOtBu or NaOBn, to $(^nBu_4N)[Mn^{III}(Br_4cat)_2(THF)_2]$ in MeCN results in decomposition of the metal complex, apparently via displacement of $[Br_4cat]^{2-}$ ligands. Alkylamines, such as Et_3N, reduce the

$[Mn^{III}(Br_4cat)_2]^-$ fragment, leading to rapid ligand redistribution and formation of $[Mn^{IV}(Br_4cat)_3]^{2-}$ in O_2. Pyridines are apparently not sufficiently basic to deprotonate $[Mn^{III}(Br_4cat)_2(BnOH)]^-$.

3.3 Discussion.

3.3.1. Formation of $[Mn^{III}_2(\mu\text{-}OCH_2R)_2]^{4-}$ Dimers.

$[Mn^{III}(Br_4cat)_2(THF)_2]^-$ acts a convenient precursor for the synthesis of **$[Mn^{III}_2(\mu\text{-}OCH_2R)_2]^{4-}$** complexes. The axial THF ligands in $[Mn^{III}(Br_4cat)_2(THF)_2]^-$ are substitution labile, so dissolution in MeOH likely affords initial conversion to the $[Mn^{III}(Br_4cat)_2(MeOH)]^-$ adduct. This complex can then be deprotonated using bases such as LiOMe, LiOPh to and NaH to afford the bridging μ-OMe complexes. Reactions in neat benzyl alcohol afforded the analgous μ-OBn. All of the dimers derived from $[Mn^{III}(Br_4cat)_2(MeOH)]^-$ were characterized crystallographically and display similar structural features, such as axial elongation across an O_{Br4Cat}–Mn–$O_{\mu\text{-}OR}$ and close contact Li^+ or Na^+ counterions. Reactions using $[Mn^{III}(Cl_4cat)_2(MeOH)]^-$ also afforded dimers when using LiOMe. However, close contact of the lithium was not observed which shows that the close contact interactions are not need for the stabilization of the dimer.

3.3.2 Reactions with $[Mn^{III}(Br_4Cat)_2X]^{2-}$ with Oxygen

The addition of anionic ligand to $[Mn^{III}(Br_4cat)_2]^-$ core afford species that are air sensitive. In the cases of $[Mn^{III}_2(\mu\text{-}OCH_2R)_2]^{4-}$ and $[Mn^{III}(Br_4Cat)_2X]^{2-}$, these complexes

react in air to form $[Mn^{IV}(Br_4cat)_3]^{2-}$, which degrades in air to form $[Mn^{III}(Br_4cat)_2]^-$ and free quinone over time. The observation of $[Mn^{IV}(Br_4cat)_3]^{2-}$ as an intermediate been reported in previous literature.[38] The preparation of the analogous $(PPh_4)_2[Mn^{IV}(Cl_4cat)_3]$ was performed by adding PPh_4Cl to the a solution of $K[Mn^{III}(Cl_4cat)_2]$ in air. The authors ascribe the formation of $[Mn^{IV}(Cl_4cat)_3]^{2-}$ to destabilizing the close contact of the K^+ cations by using PPh_4Cl as K^+ specific chelator **(Scheme 12)**.

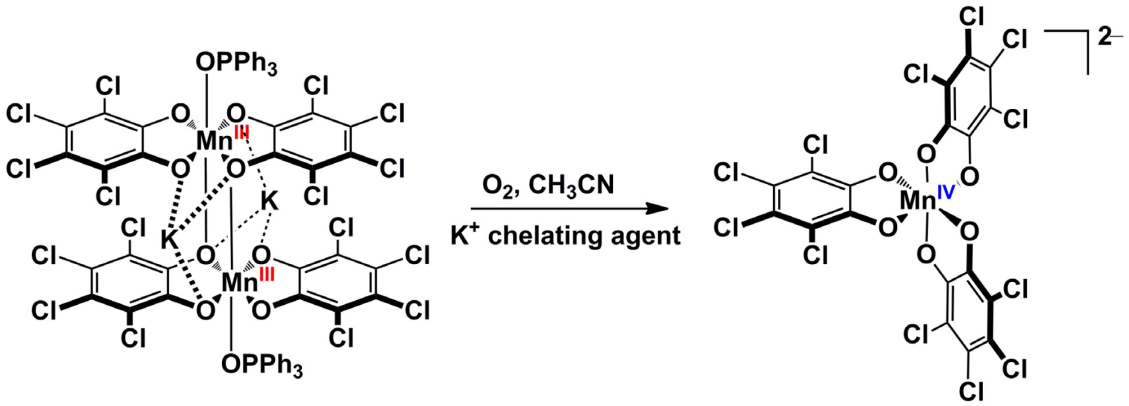

Scheme 12. Synthesis of $[Mn^{IV}(Cl_4cat)_3]^{2-}$.

However, our observation of the formation of $[Mn^{IV}(Br_4cat)_3]^{2-}$ from the addition of PPh_4Cl using $(^nBu_4N)[Mn^{III}(Br_4cat)_2]$, which does not have any close contact interactions, demonstrates that the addition of the chloride anion and exposure to air is responsible for the formation of $[Mn^{IV}(Br_4cat)_3]^{2-}$. This reactivity has also been observed in reactions with other non oxdizable anions such as Br^- and OMe^-. It is possible that $[Mn^{III}(Br_4Cat)_2X]^{2-}$ complexes are labile and rearrange to afford the previously isolated $[Mn^{III}(Br_4cat)_3]^{3-}$ which reacts with O_2 to form $[Mn^{IV}(Br_4cat)_3]^{2-}$.

3.3.3 Aerobic Alcohol oxidation catalyzed by $[Mn^{III}(Br_4cat)_2]^-$

The sum of the reactions leading to formation and oxidation of **$[Mn^{III}_2(\mu\text{-}OBn)_2]^{4-}$** comprise a complete cycle for oxidase-type aerobic oxidation of benzyl alcohols (**Scheme 13**). These reaction steps exhibit strong parallels to aerobic catechol oxidations catalyzed by $[Mn^{III}(Br_4cat)_2]^-$.[33] First, deprotonation of the coordinated alcohol in $[Mn^{III}(Br_4cat)_2(BnOH)]^-$ occurs with isomerization of the *trans* $[Br_4cat]^{2-}$ ligands in $[Mn^{III}(Br_4cat)_2]^-$ to a *cis* conformation, which facilitates binding to two bridging, μ-$[OBn]^-$ ligands in *cis* sites. In the catecholase reactions such isomerization is necessary to accommodate a bidentate $[cat]^{2-}$ ligand, but the stability of the **$[Mn^{III}_2(\mu\text{-}OCH_2R)_2]^{4-}$** dimers suggests that *cis–trans* isomerization at $[Mn^{III}(Br_4cat)_2]^-$ is similarly facile with monodentate strong σ-donors. Second, formation of the six-coordinate catalyst–substrate complex triggers the reaction with O_2. No organic products suggestive of free-radical autoxidation are observed by GC–MS or ^{1}H NMR spectroscopy, implying that the reaction is selective for the net $2e^-$ oxidation of a coordinated $[OBn]^-$ ligand. Third, the peroxide byproduct reacts with $[Mn^{III}(Br_4cat)_2]^-$ core in the presence of O_2 to degrade the complex, limiting turnover. The peroxide anion is capable of binding to $[Mn^{III}(Br_4cat)_2]^-$ which triggers the reaction with O_2. The anion acts as a non-oxidizable substrate, leading to rearrangement and complex degradation.

In the corresponding reactions of the bis(μ-methoxo) dimer **$[Mn^{III}_2(\mu\text{-}OMe)_2]^{4-}$** with O_2, the absence of formaldehyde in reactions with O_2 can be attributed to differences in the oxidation potentials of the alcohols. It is possible that oxidation of the **$[Mn^{III}_2(\mu\text{-}OCH_2R)_2]^{4-}$** dimers generates high-valent manganese species, which oxidizes the most easily oxidized ligand in the primary coordination sphere. Because the reaction

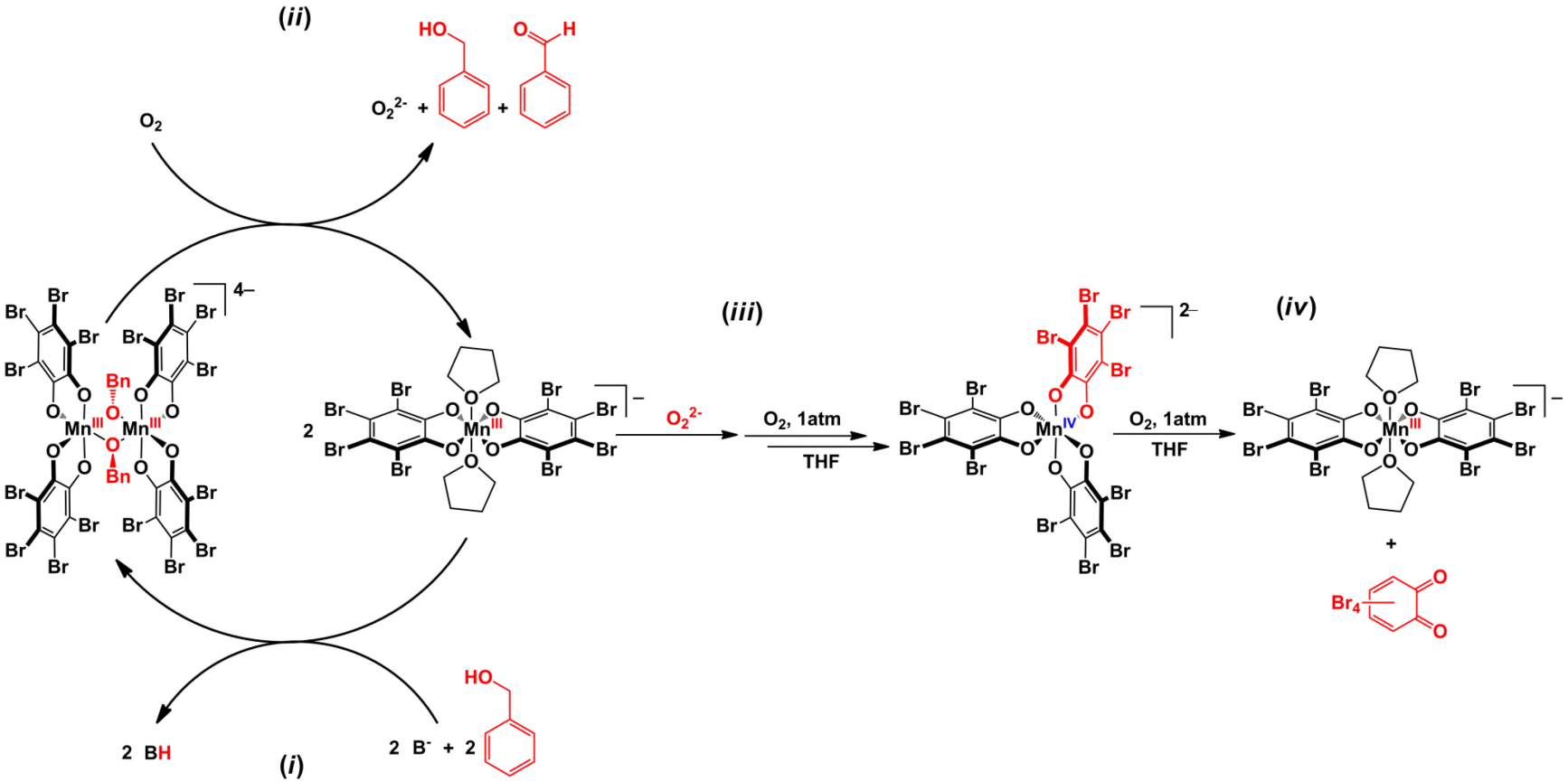

Scheme 13. The $[Mn^{III}(Br_4cat)_2(THF)_2]^-$ aerobic oxidation of benzyl alcohol.

of **$[Mn^{III}_2(\mu\text{-}OMe)_2]^{4-}$** with O_2 results in oxidation of a $[Br_4cat]^{2-}$ ligand rather than a coordinated $[OMe]^-$, the **$[Mn^{III}_2(\mu\text{-}OMe)_2]^{4-}$** complex functions as a catecholase, leading to $[Mn^{III}(Br_4cat)_2]^-$ catabolism.

The reactions of **$[Mn^{III}_2(\mu\text{-}OBn)_2]^{4-}$** with O_2 described above imply that oxidation of coordinated $[OBn]^-$ occurs preferentially to intramolecular $[Br_4cat]^{2-}$ oxidation. Yet the $[Mn^{III}(Br_4cat)_2]^-$ fragment is a catalyst for efficient, base-free aerobic oxidations of catechols, including Br_4catH_2, but not BnOH. This disparate behavior likely reflects differences in the relative substrate acidities.[39-40] Conversion of one $[OBn]^-$ to PhCHO requires net loss of $2e^-$ and $1H^+$. But in the reactions of **$[Mn^{III}_2(\mu\text{-}OBn)_2]^{4-}$** with O_2, the H^+ is transferred to the second bridging $[OBn]^-$ ligand, generating one equiv. of BnOH **(Scheme 14)**.

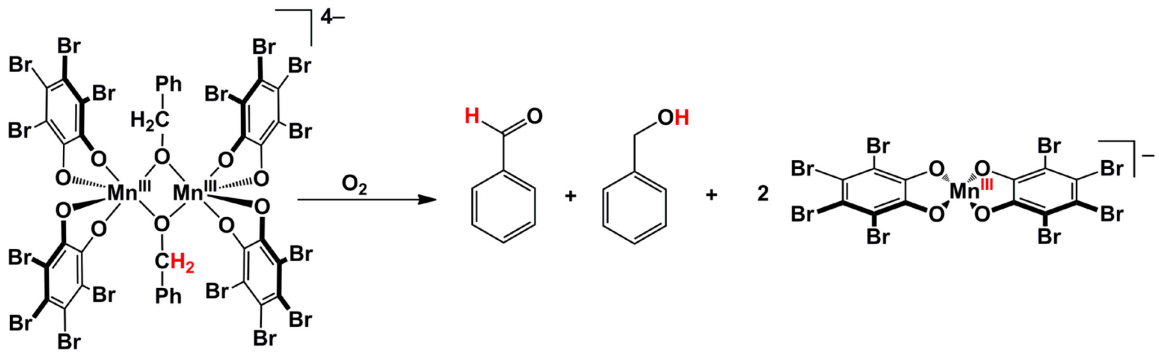

Scheme 14. Proton transfer in the aerobic oxidation of benzyl alkoxide.

Attempts to make the reactions of $Mn^{III}(Br_4cat)_2(BnOH)]^-$ with BnOH catalytic by adding exogenous bases was unsuccessful. Bases such as NaO^tBu and Et_3N result in decomposition of the metal complex while weaker bases such as pyridines do not deprotonate $[Mn^{III}(Br_4cat)_2(BnOH)]^-$ species to initiate the reaction with oxygen. In the previous chapter, the aerobic catechol oxidations formally transfer $2e^-$ and $2H^+$ to O_2,

affording H_2O_2. It is unclear why the reduced O_2 species generated from **$[Mn^{III}_2(\mu\text{-}OBn)_2]^{4-}$** oxidation are not able to efficiently deprotonate $[Mn^{III}(Br_4cat)_2(BnOH)]^-$.

3.4 Conclusions.

In conclusion, the **$[Mn^{III}_2(\mu\text{-}OBn)_2]^{4-}$** anion reacts with O_2 to efficiently oxidize $[OBn]^-$ to PhCHO. Selectivity in the net $2e^-$ reaction apparently derives from the ability of the $[Mn^{III}(Br_4cat)_2]^-$ fragment to bind BnOH and assemble a catalyst–substrate complex that initiates an inner-sphere reaction with O_2. However, the same features that facilitate these stoichiometric reactions are ultimately a detriment to catalytic activity. Dimer formation requires a base to deprotonate the weakly acidic primary alcohols, but excess bases all lead to catalyst degradation. Despite these challenges, the $[Mn^{III}(Br_4cat)_2]^-$ fragment is able to catalyze the selective aerobic oxidation of an activated benzylic alcohol under conditions comparable to those used for some palladium oxidase catalysis.[12] Future efforts to develop modified manganese complexes with redox-active ligands for catalytic oxidase-type oxidations will be pursued.

3.5. Experimental Details.

3.5.1 General Considerations.

Unless otherwise specified, all manipulations were performed under anaerobic conditions using standard vacuum line techniques, or in an inert atmosphere glove box under

purified nitrogen. NMR spectra were acquired on a Varian Mercury 300 spectrometer (300.323 MHz for ^{1}H) at ambient temperature. Chemical shifts are reported in parts per million (ppm) relative to TMS, with the residual solvent peak serving as an internal reference. UV–visible absorption spectra were acquired using a Varian Cary 50 spectrophotometer equipped with a water-jacketed cell holder fitted to a Peltier temperature controller. Unless otherwise specified, all electronic absorption spectra were recorded at 25 °C in 1 cm quartz cells. UV–vis chemical kinetics data were fit by iterative multivariate analysis using the commercially available software Specfit/32 from Spectrum Software Associates. IR spectra were obtained by attenuated total reflection (ATR) through a diamond plate on a Bruker Optics Alpha-P FTIR spectrometer. All mass spectra were recorded in the Georgia Institute of Technology Bioanalytical Mass Spectrometry Facility. Electrospray ionization mass spectrometry (ESI–MS) was carried out with acetonitrile or tetrahydrofuran solutions using a Micromass Quattro LC spectrometer. Gas chromatography–mass spectrometry (GC–MS) analyses used an Agilent 6890 GC equipped with an autosampler and a Restek Rxi-5ms column (30 m x 0.25 mm i.d., 0.25 μm film thickness). 1 μL injections were made at a 50:1 split ratio. The GC oven program consisted of a hold at 30 °C for 1 min, followed by a 15 °C min^{-1} ramp to 300 °C, and then a hold at 300 °C for 11 minutes. The mass spectrometer used in tandem was a Micromass AutoSpec electronionization (EI) detector. Elemental analyses were performed by Atlantic Microlab, Inc., Norcross, GA. All analyses were performed in duplicate, and the reported compositions are the average of the two runs.

3.5.2. Methods and Materials.

Anhydrous acetonitrile (MeCN), tetrahydrofuran (THF), and pentane solvents for air- and moisture-sensitive manipulations were purchased from Sigma-Aldrich, further dried by passage through columns of activated alumina, degassed by at least three freeze-pump-thaw cycles, and stored under N_2 prior to use. Methanol (anhydrous, 99.0%) was purchased from Honeywell Burdick and Jackson, and used as received. Acetone (99.8%, extra dry) was purchased from Acros and used as received. Diethyl ether (Et_2O) was purchased from Sigma-Aldrich and vacuum distilled from sodium/benzophenone prior to use. Oxygen (ultra high purity) was used as received from Airgas, Inc. Deuterated acetonitrile (MeCN–d_3) and tetrahydrofuran (THF–d_8) were purchased from Cambridge Isotope Laboratories, degassed by three freeze-pump-thaw cycles, vacuum distilled from CaH_2 or $Na_{(s)}$, respectively, and stored under a dry N_2 atmosphere prior to use. $Mn(ClO_4)_2 \cdot 6H_2O$ was purchased from Strem Chemical, Inc. All other chemicals were purchased from Sigma-Aldrich and used as received.

3.5.3. Synthesis of ($^{n}Bu_4N$)[$Mn^{III}(Br_4cat)_2(THF)_2$].

In air, $Mn(ClO_4)_2 \cdot 6H_2O$ (0.39 g, 1.1 mmol) and tetrabromo-1,2-catechol (0.91 g, 2.2 mmol)) were combined in a 100 mL evaporating flask and dissolved in 20mL of THF. Slow addition of 1.0 M $^{n}Bu_4OH$ in MeOH (2.0 mL, 2.0 mmol) over 5 min with vigorous stirring afforded a dark olive-green solution. The flask was fitted to a condenser and the solution was heated to reflux for 1 h, then cooled to ambient temperature and stored at –10 °C for 24 h to deposit green precipitate. The solids were collected by vacuum filtration of the cold reaction mixture in air, washed with THF (3 × 1 mL, ice cold), and dried *in*

vacuo to yield ($^{n}Bu_4N$)[$Mn^{III}(Br_4cat)_2(THF)_2$] (0.39 g, 0.30 mmol, 29%) as green microcrystals. UV-vis (THF) λ_{max}, nm (ε, M^{-1} cm^{-1}): 600 (80), 720 (sh, 60). ESI-MS (*m/z*): 902 [M–$^{n}Bu_4N$]$^{-}$. FTIR (ATR): 2958 (m), 2860 (m), 1648 (m) 1480 (m), 1380 (w), 883 (m) (all $^{n}Bu_4N$); 3573 (m), 3518 (m),1424 (vs) 1346 (m), 1260 (s), 1227 (s) 927 (s), 746 (s) cm^{-1}. A single crystal of the same sample of ($^{n}Bu_4N$)[$Mn^{III}(Br_4cat)_2(THF)_2$] used for elemental analysis was determined. It includes one H_2O solvate per manganese, so the reported analysis is for ($^{n}Bu_4N$)[$Mn^{III}(Br_4cat)_2(THF)_2$]•$H_2O$. Anal. Calcd for $C_{36}H_{54}Br_8MnNO_7$: C, 33.08; H, 4.16; N, 1.07; Found: C, 33.13; H, 4.11; N 0.99.

3.5.4. Synthesis of ($^{n}Bu_4N)_2[Na(MeOH)_2]_2[(Br_4cat)_2Mn^{III}(\mu\text{-}OMe)_2Mn^{III}(Br_4cat)_2]$ ($[Mn^{III}_2(\mu\text{-}OMe)_2]^{4-}$).

A 100 mL round bottom flask was charged with ($^{n}Bu_4N$)[$Mn^{III}(Br_4cat)_2(THF)_2$] (0.10 g, 0.076 mmol), a stir bar, and MeOH (15 mL) to afford a yellow solution. Dropwise addition of 0.5 M NaOMe (0.15 mL, 0.075 mmol) with vigorous stirring gave immediate formation of a dark green solution. The reaction was capped and stored at 25 °C for 18 h to deposit dark green crystals that were used for X-ray diffraction analysis. The solids for elemental analysis and reaction studies were collected by vacuum filtration, washed with MeOH (3 mL, ice cold) and dried *in vacuo* to yield single crystals of **$[Mn^{III}_2(\mu\text{-}OMe)_2]^{4-}$** (0.088 g, 0.069 mmol, 90%) without MeOH solvates. UV-vis (MeCN) λ_{max}, nm (ε, M^{-1} cm^{-1}): 579 (520). FT-IR (ATR): 3411 (br), 2954 (w), 2871 (w), 1646 (w), 1457 (s) 1377 (m), (all $^{n}Bu_4N^{+}$); 1425 (vs), 1345 (m), 1265 (s), 1230 (s), 1026(s), 926 (s), 736 (s) cm^{-1}.

Anal. Calcd for $C_{29}H_{39}Br_8MnNNaO_5$: C, 29.06; H, 3.28; N, 1.17; Found: C, 28.83; H, 3.47; N 1.27.

3.5.5 Synthesis of $(^nBu_4N)_2[Na(BnOH)]_2[(Br_4cat)_2Mn^{III}(\mu\text{-}OBn)_2Mn^{III}(Br_4cat)_2]$ ($[Mn^{III}_2(\mu\text{-}OBn)_2]^{4-}$).

A 100 mL round bottom flask was charged with $(^nBu_4N)[Mn^{III}(Br_4cat)_2(THF)_2]$ (0.250 g, 0.191 mmol), a stir bar, and BnOH (6 mL) to generate a yellow solution. Separately, NaH (4.6 mg, 0.191 mmol) and BnOH (2 mL) were combined in a 5 dram scintillation vial to generate a 0.10 M solution of NaOBn, which was slowly added to the vigorously stirring $(^nBu_4N)[Mn^{III}(Br_4cat)_2(THF)_2]$ to give an immediate color change to dark green solution. The reaction mixture was capped and stored at 25 °C for 48 h, resulting in the deposition of green crystals. Single crystals for X-ray diffraction studies were collected by vacuum filtration. Samples for elemental analysis were subsequently washed with Et_2O (3 mL, ice cold) and dried *in vacuo* to remove the excess BnOH solvates from $[Mn^{III}_2(\mu\text{-}OBn)_2]^{4-}$ (0.099 g, 0.077 mmol, 41%). UV-vis (MeCN) λ_{max}, nm (ε, M^{-1} cm^{-1}): 592 (440). FT-IR (ATR): 3358 (br), 2959 (s), 2930 (m), 2871 (m), 1379 (m), (all $^nBu_4N^+$); 1431 (vs), 1347 (m), 1255 (s), 1230 (s), 1009 (s), 929 (s), 734 (s) cm^{-1}. Anal. Calcd for $C_{35}H_{43}Br_8MnNaNO_5$: C, 32.39; H, 3.34; N, 1.08; Found: C, 32.18; H, 3.55; N 1.29.

3.5.6. Aerobic Alcohol Oxidations.

In a representative procedure, a J. Young brand NMR tube with a Teflon screw cap was charged with 0.20 M **$[Mn^{III}_2(\mu\text{-}OBn)_2]^{4-}$** (0.70 mL, 0.014 mmol) in MeCN–d_3 and sealed under N_2 . The solution was degassed on a high-vacuum line by three freeze–pump–thaw cycles and backfilled with to 1 atm of O_2 and shaken vigorously. The reaction progress was monitored by ^{1}H NMR spectroscopy for 36 h, and the yields of benzyl alcohol (BnOH) and benzaldehyde (PhCHO) were determined by integration against the resonances for the $[^nBu_4N]^+$ countercation, as described in the manuscript text. During the course of the reaction, the tube was shaken periodically to ensure that the concentration of dissolved O_2 was maintained. The reaction solution was subsequently transferred to a 2 mL GC autosampler vial and analyzed by GC–MS to determine the organic product distribution. For catalytic oxidations, 3,4-dimethoxybenzyl alcohol (5.4 μL, 0.038 mmol) and $(^nBu_4N)[Mn^{III}(Br_4cat)_2(THF)_2]$ (9.8 mg, 7.5 μmol), were combined in a 50 mL flask fitted with a Kontes brand PTFE valve. The flask was degassed on a high-vacuum line by three freeze–pump–thaw cycles, backfilled with to 1 atm of O_2, and heated by immersion in a silicone fluid bath at 80 °C for 12 h. An aliquot of the reaction mixture was transferred to a 2 mL GC autosampler vial and analyzed by GC–MS using the method described above.

3.5.7. X-Ray Crystallography.

Crystals of $(^nBu_4N)[Mn^{III}(Br_4cat)_2(THF)_2\bullet THF)]$, $(^nBu_4N)_2[Na(MeOH)_2]_2[(Br_4cat)_2Mn^{III}(\mu\text{-}OMe)_2Mn^{III}(Br_4cat)_2]\bullet MeOH$, $(^nBu_4N)_2[Li(MeOH)]_2[(Br_4cat)_2Mn^{III}(\mu\text{-}OMe)_2Mn^{III}(Br_4cat)_2]\bullet MeOH$,

$(PPN)_2[Li]_2[(Cl_4cat)_2Mn^{III}(\mu\text{-}OMe)_2Mn^{III}(Cl_4cat)_2]\bullet MeOH$, $(^nBu_4N)_{1.66}[Na]_{2.33}[(Br_4cat)_2Mn^{III}(\mu\text{-}OBn)_2Mn^{III}(Br_4cat)_2]\bullet BnOH$, and $(^nBu_4N)_2[Mn^{III}Cl(Br_4cat)_2]$, suitable for X-ray diffraction analysis were coated with Paratone N oil, suspended on small fiber loops and placed in a cooled nitrogen gas stream at 173 K on a Bruker D8 APEX II CCD sealed tube diffractometer. Data for $(^nBu_4N)_2[Li(MeOH)]_2[(Br_4cat)_2Mn^{III}(\mu\text{-}OMe)_2Mn^{III}(Br_4cat)_2]\bullet MeOH$, $(PPN)_2[Li]_2[(Cl_4cat)_2Mn^{III}(\mu\text{-}OMe)_2Mn^{III}(Cl_4cat)_2]\bullet MeOH$ and $(^nBu_4N)_2[Mn^{III}Cl(Br_4cat)_2]$ was obtained with graphite monochromated Cu Kα (λ = 1.54178 Å) radiation while diffraction data for $(^nBu_4N)[Mn^{III}(Br_4cat)_2(THF)_2\bullet THF)]$, $(^nBu_4N)_2[Na(MeOH)_2]_2[(Br_4cat)_2Mn^{III}(\mu\text{-}OMe)_2Mn^{III}(Br_4cat)_2]\bullet MeOH$ and $(^nBu_4N)_{1.66}[Na]_{2.33}[(Br_4cat)_2Mn^{III}(\mu\text{-}OBn)_2Mn^{III}(Br_4cat)_2]\bullet BnOH$ were collected using graphite monochromated Mo Kα (λ = 0.71073 Å) radiation. Data collection procedures, data processing and programs were the same for all samples. Frames were measured using a series of combinations of phi and omega scans with 10 s frame exposures and 0.5° frame widths. Data collection, indexing and initial cell refinements were all carried out using APEX II software.[41] Frame integration and final cell refinements were done using SAINT software.[42] The final cell parameters were determined from least-squares refinement on 9939 reflections for $(^nBu_4N)[Mn^{III}(Br_4cat)_2(THF)_2\bullet THF)]$, 7076 reflections for $(^nBu_4N)_2[Na(MeOH)_2]_2[(Br_4cat)_2Mn^{III}(\mu\text{-}OMe)_2Mn^{III}(Br_4cat)_2]\bullet MeOH$, 8619 reflections for $(^nBu_4N)_2[Li(MeOH)]_2[(Br_4cat)_2Mn^{III}(\mu\text{-}OMe)_2Mn^{III}(Br_4cat)_2]\bullet MeOH$, 3747 reflections for $(PPN)_2[Li]_2[(Cl_4cat)_2Mn^{III}(\mu\text{-}OMe)_2Mn^{III}(Cl_4cat)_2]\bullet MeOH$ 9929 reflections for $(^nBu_4N)_{1.66}[Na]_{2.33}[(Br_4cat)_2Mn^{III}(\mu\text{-}OBn)_2Mn^{III}(Br_4cat)_2]\bullet BnOH$, and 1432 reflections for $(^nBu_4N)_2[Mn^{III}Cl(Br_4cat)_2]$. The structures were solved using direct

methods and difference Fourier techniques with the SHELXTL program package.[43] Hydrogen atoms were placed in their expected chemical positions using the HFIX command and were included in the final cycles of least-squares with isotropic U_{ij}'s related to the atoms ridden upon. All non-hydrogen atoms in for $(^nBu_4N)_2[Na(MeOH)_2]_2[(Br_4cat)_2Mn^{III}(\mu\text{-}OMe)_2Mn^{III}(Br_4cat)_2]\bullet MeOH$ and $(^nBu_4N)_2[Li(MeOH)]_2[(Br_4cat)_2Mn^{III}(\mu\text{-}OMe)_2Mn^{III}(Br_4cat)_2]\bullet MeOH$ $(^nBu_4N)_{1.66}[Na]_{2.33}[(Br_4cat)_2Mn^{III}(\mu\text{-}OBn)_2Mn^{III}(Br_4cat)_2]\bullet BnOH$, and $(^nBu_4N)_2[Mn^{III}Cl(Br_4cat)_2]$ were refined anisotropically, but only the metal-containing fragments and counterions in $(^nBu_4N)[Mn^{III}(Br_4cat)_2(THF)_2\bullet THF)]$ and$(PPN)_2[Li]_2[(Cl_4cat)_2Mn^{III}(\mu\text{-}OMe)_2Mn^{III}(Cl_4cat)_2]\bullet MeOH$ were refined anisotropically. Scattering factors and anomalous dispersion corrections are taken from the *International Tables for X-ray Crystallography.*[44] Other details of data collection and structure refinement are provided in **Table 3.2.**

Table 3.2 Crystallographic Data and Structure Parameters for $(^{n}Bu_4N)[Mn^{III}(Br_4cat)_2(THF)_2\bullet THF)]$, $(^{n}Bu_4N)_2[Na(MeOH)_2]_2[(Br_4cat)_2Mn^{III}(\mu\text{-}OMe)_2Mn^{III}(Br_4cat)_2]\bullet MeOH$, and $(^{n}Bu_4N)_2[Li(MeOH)]_2[(Br_4cat)_2Mn^{III}(\mu\text{-}OMe)_2Mn^{III}(Br_4cat)_2]\bullet MeOH$.

Complex	$(^{n}Bu_4N)[Mn^{III}(Br_4cat)_2(THF)_2\bullet THF)]$	$(^{n}Bu_4N)_2[Na(MeOH)_2]_2[(Br_4cat)_2Mn^{III}(\mu\text{-}OMe)_2Mn^{III}(Br_4cat)_2]\bullet MeOH$	$(^{n}Bu_4N)_2[Li(MeOH)]_2[(Br_4cat)_2Mn^{III}(\mu\text{-}OMe)_2Mn^{III}(Br_4cat)_2]\bullet MeOH$
Empirical formula	C36 H52 Br8 Mn N O7	C32 H51 Br8 Mn N Na O8	C31 H47 Br8 Li Mn N O7
Formula weight	1305.01	1294.95	1246.86
Temperature (K)	173(2)	173(2)	173(2)
Crystal system	Monoclinic	Monoclinic	Monoclinic
Space group	C2/c	P2(1)/n	P2(1)/n
Unit cell dimensions			
a (Å)	40.5455(9)	14.6637(4)	9.8990(4)
b (Å)	10.4344(3)	19.5637(6)	25.5790(11)
c (Å)	21.7056(5)	16.0988(4)	17.1264(8)
a (°)	90	90	90
b (°)	96.818(1)	106.288(1)	102.861(2)
g (°)	90	90	90
Volume ($Å^3$)	9118.0(4)	4433.0(2)	4227.7(3)
Z	8	4	4
Calculated Density (g cm^{-1})	1.901	1.94	1.959
Absorption coefficient (mm^{-1})	7.345	7.563	7.915
Crystal size (mm)	0.38 x 0.34 x 0.22	0.20 x 0.18 x 0.05	0.22 x 0.10 x 0.08
θ range for data collection (°)	2.02 to 26.33	1.66 to 26.36	1.46 to 30.45
Index ranges	-50<=h<=50	-18<=h<=18	-10<=h<=14
	-12<=k<=9	-24<=k<=24	-36<=k<=36
	-26<=l<=20	-16<=l<=20	-24<=l<=23
Reflections collected/unique	34175/9185	33792/8995	39194/11563
Goodness-of-fit on F2	1.012	1.003	1.002
Final R indices [I>2sigma(I)]	0.0400	0.0510	0.0666
R indices (all data)	0.0693	0.1232	0.1224

Table 3.2. Crystallographic Data and Structure Parameters for $(PPN)_2[Li]_2[(Cl_4cat)_2Mn^{III}(\mu\text{-}OMe)_2Mn^{III}(Cl_4cat)_2]\bullet MeOH$, $(^nBu_4N)_{1.66}[Na]_{2.33}[(Br_4cat)_2Mn^{III}(\mu\text{-}OBn)_2Mn^{III}(Br_4cat)_2]\bullet BnOH$, and $(^nBu_4N)_2[Mn^{III}Cl(Br_4cat)_2]$.

Complex	$(PPN)_2[Li]_2[(Cl_4cat)_2Mn^{III}(\mu\text{-}OMe)_2Mn^{III}(Cl_4cat)_2]\bullet MeOH$	$(^nBu_4N)_{1.66}[Na]_{2.33}[(Br_4cat)_2Mn^{III}(\mu\text{-}OBn)_2Mn^{III}(Br_4cat)_2]\bullet BnOH$	$(^nBu_4N)_2[Mn^{III}Cl(Br_4cat)_2]$
Empirical formula	C49 H35 Cl8 Li Mn N O7 P2	C77 H94 Br16 Mn2 N2 Na2 O11	C44 H72 Br8 Cl Mn N2 O4
Formula weight	1157.2	2657.96	1422.71
Temperature (K)	173(2) K	173(2)	173(2) K
Crystal system	Triclinic	Monoclinic	Monoclinic
Space group	P-1	P2(1)/c	P2(1)
Unit cell dimensions			
a (Å)	10.8707(3)	25.17(5)	13.084(2)
b (Å)	15.7485(3)	24.40(4)	16.398(3)
c (Å)	16.7817(4)	19(3)	13.084(2)
a (°)	106.490(1)	90	90
b (°)	103.615(1)	95.2	101.50(2)
g (°)	97.221(1)	90	90
Volume ($Å^3$)	2619.57(11)	11432(1835)	2750.8(8)
Z	2	4	2
Calculated Density (g cm^{-1})	1.467	1.544	1.718
Absorption coefficient (mm^{-1})	6.796	5.865	9.51
Crystal size (mm)	0.18 x 0.12 x 0.08	0.28 x 0.19 x 0.16	0.45 x 0.14 x 0.05
θ range for data collection (°)	2.86 to 65.09°.	1.55 to 27.00°.	3.45 to 67.01
Index ranges	-12<=h<=12	0<=h<=32	-13<=h<=13
	-18<=k<=18	-31<=k<=0	-16<=k<=19
	-19<=l<=19	-23<=l<=23	-15<=l<=15
Reflections collected/unique	15801/7891	24680/24680	10115/6073
Goodness-of-fit on F2	1.038	1.003	1.048
Final R indices [I>2sigma(I)]	0.0549	0.1073	0.1726
R indices (all data)	0.0687	0.1931	0.2328

3.6. Works Cited

1. Simándi, L. I., *Advances in Catalytic Activation of Dioxygen by Metal Complexes*. Springer: New York, 2003.

2. Meunier, B., *Biomimetic Oxidations Catalyzed by Transition Metal Complexes*. Imperial College: London, 2000.

3. Borovik, A. S. Z., P. J.; Zart, M. K., Dioxygen Binding and Activation: Reactive Intermediates. In *Activation of Small Molecules: Organometallic and Bioinorganic Perspectives*, Tolman, W. B., Ed. Wiley-VCH: Weinheim, Germany, 2006; pp 187–234.

4. Sheldon, R. A. K., J. K., *Metal-Catalyzed Oxidations of Organic Compounds*. Academic Press: New York.

5. Barton, D., H. R., Martell, A. E., Sawyer, D. T.,, *The Activation of Dioxygen and Homogeneous Catalytic Oxidation*. Plenum: New York, 1993.

6. Sawyer, D. T., *Oxygen Chemistry, International Series Of Monographs On Chemistry 26* Oxford University Press: New York, 1991.

7. Tolman, W. B., Metal-Radical Arrays. In *Comprehensive Coordination Chemistry II*, McCleverty, I. A., Meyer, T. J.,, Ed. Elsevier Pergamon: Boston, 2004; Vol. 8, pp 715–737.

8. Chaudhuri, P.; Wieghardt, K., Phenoxyl radical complexes. In *Progress in Inorganic Chemistry, Vol. 50*, John Wiley & Sons Inc: New York, 2001; Vol. 50, pp 151-216.

9. Chaudhuri, P.; Wieghardt, K.; Weyhermuller, T.; Paine, T. K.; Mukherjee, S.; Mukherjee, C., Biomimetic metal-radical reactivity: aerial oxidation of alcohols, amines, aminophenols and catechols catalyzed by transition metal complexes. *Biol. Chem.* **2005,** *386* (10), 1023-1033, doi:10.1515/bc.2005.118.

10. Mirica, L. M.; Ottenwaelder, X.; Stack, T. D. P., Structure and Spectroscopy of Copper−Dioxygen Complexes. *Chemical Reviews* **2004,** *104* (2), 1013-1046, doi:10.1021/cr020632z.

11. Sigman, M. S.; Jensen, D. R., Ligand-Modulated Palladium-Catalyzed Aerobic Alcohol Oxidations. *Accounts of Chemical Research* **2006,** *39* (3), 221-229, doi:10.1021/ar040243m.

12. Stahl, S. S., Palladium Oxidase Catalysis: Selective Oxidation of Organic Chemicals by Direct Dioxygen-Coupled Turnover. *Angewandte Chemie International Edition* **2004,** *43* (26), 3400-3420, doi:10.1002/anie.200300630.

13. Stahl, S. S., Palladium-catalyzed oxidation of organic chemicals with O-2. *Science* **2005,** *309* (5742), 1824-1826, doi:10.1126/science.1114666.

14. Bart, S. C.; Bowman, A. C.; Lobkovsky, E.; Chirik, P. J., Iron Diazoalkane Chemistry: N−N Bond Hydrogenation and Intramolecular C−H Activation. *Journal of the American Chemical Society* **2007,** *129* (23), 7212-7213, doi:10.1021/ja070056u.

15. Blackmore, K. J.; Lal, N.; Ziller, J. W.; Heyduk, A. F., Catalytic reactivity of a zirconium(IV) redox-active ligand complex with 1,2-diphenylhydrazine. *Journal of the American Chemical Society* **2008,** *130* (9), 2728-+, doi:10.1021/ja710611v.

16. Blackmore, K. J.; Ziller, J. W.; Heyduk, A. F., "Oxidative addition" to a Zirconium(IV) redox-active ligand complex. *Inorganic Chemistry* **2005,** *44* (16), 5559-5561, doi:10.1021/ic050997c.

17. Bouwkamp, M. W.; Bowman, A. C.; Lobkovsky, E.; Chirik, P. J., Iron-Catalyzed [2π + 2π] Cycloaddition of α,ω-Dienes: The Importance of Redox-Active Supporting Ligands. *Journal of the American Chemical Society* **2006,** *128* (41), 13340-13341, doi:10.1021/ja064711u.

18. Bowman, A. C.; Milsmann, C.; Atienza, C. C. H.; Lobkovsky, E.; Wieghardt, K.; Chirik, P. J., Synthesis and Molecular and Electronic Structures of Reduced Bis(imino)pyridine Cobalt Dinitrogen Complexes: Ligand versus Metal Reduction. *Journal of the American Chemical Society* **2010,** *132* (5), 1676-1684, doi:10.1021/ja908955t.

19. Chaudhuri, P.; Hess, M.; Müller, J.; Hildenbrand, K.; Bill, E.; Weyhermüller, T.; Wieghardt, K., Aerobic Oxidation of Primary Alcohols (Including Methanol) by Copper(II)− and Zinc(II)−Phenoxyl Radical Catalysts. *Journal of the American Chemical Society* **1999,** *121* (41), 9599-9610, doi:10.1021/ja991481t.

20. Chirik, P. J.; Wieghardt, K., Radical Ligands Confer Nobility on Base-Metal Catalysts. *Science* **2010,** *327* (5967), 794-795, doi:10.1126/science.1183281.

21. Haneline, M. R.; Heyduk, A. F., C-C bond-forming reductive elimination from a zirconium(IV) redox-active ligand complex. *Journal of the American Chemical Society* **2006,** *128* (26), 8410-8411, doi:10.1021/ja061107a.

22. Hull, K. L.; Sanford, M. S., Mechanism of Benzoquinone-Promoted Palladium-Catalyzed Oxidative Cross-Coupling Reactions. *Journal of the American Chemical Society* **2009,** *131* (28), 9651-9653, doi:10.1021/ja901952h.

23. Manuel, T. D.; Rohde, J.-U., Reaction of a Redox-Active Ligand Complex of Nickel with Dioxygen Probes Ligand-Radical Character. *Journal of the American Chemical Society* **2009,** *131* (43), 15582-15583, doi:10.1021/ja9065943.

24. Mukherjee, C.; Pieper, U.; Bothe, E.; Bachler, V.; Bill, E.; Weyhermüller, T.; Chaudhuri, P., Ligand-Derived Oxidase Activity. Catalytic Aerial Oxidation of Alcohols (Including Methanol) by Cu(II)-Diradical Complexes. *Inorganic Chemistry* **2008,** *47* (19), 8943-8956, doi:10.1021/ic8009767.

25. Mukherjee, C.; Weyhermuller, T.; Bothe, E.; Chaudhuri, P., Mimicking the function of amine oxidases and phenoxazinone synthase by a manganese(IV)-monoradical complex. *C. R. Chim.* **2007,** *10* (4-5), 313-325, doi:10.1016/j.crci.2006.11.006.

26. Mukherjee, C.; Weyhermüller, T.; Bothe, E.; Chaudhuri, P., Targeted Oxidase Reactivity with a New Redox-Active Ligand Incorporating N2O2 Donor Atoms. Complexes of Cu(II), Ni(II), Pd(II), Fe(III), and V(V). *Inorganic Chemistry* **2008,** *47* (24), 11620-11632, doi:10.1021/ic8011734.

27. Nguyen, A. I.; Blackmore, K. J.; Carter, S. M.; Zarkesh, R. A.; Heyduk, A. F., One- and Two-Electron Reactivity of a Tantalum(V) Complex with a Redox-Active Tris(amido) Ligand. *Journal of the American Chemical Society* **2009,** *131* (9), 3307-3316, doi:10.1021/ja808542j.

28. Smith, A. L.; Clapp, L. A.; Hardcastle, K. I.; Soper, J. D., Redox-active ligand-mediated Co-Cl bond-forming reactions at reducing square planar cobalt(III) centers. *Polyhedron* **2010,** *29* (1), 164-169, doi:10.1016/j.poly.2009.06.046.

29. Smith, A. L.; Hardcastle, K. I.; Soper, J. D., Redox-Active Ligand-Mediated Oxidative Addition and Reductive Elimination at Square Planar Cobalt(III): Multielectron Reactions for Cross-Coupling. *Journal of the American Chemical Society* **2010,** *132* (41), 14358-14360, doi:10.1021/ja106212w.

30. Zarkesh, R. A.; Ziller, J. W.; Heyduk, A. F., Four-electron oxidative formation of aryl diazenes using a tantalum redox-active ligand complex. *Angew. Chem.-Int. Edit.* **2008,** *47* (25), 4715-4718, doi:10.1002/anie.200800812.

31. Wang, Y.; DuBois, J. L.; Hedman, B.; Hodgson, K. O.; Stack, T. D. P., Catalytic Galactose Oxidase Models: Biomimetic Cu(II)-Phenoxyl-Radical Reactivity. *Science* **1998,** *279* (5350), 537-540, doi:10.1126/science.279.5350.537.

32. Markó, I. E.; Giles, P. R.; Tsukazaki, M.; Brown, S. M.; Urch, C. J., Copper-Catalyzed Oxidation of Alcohols to Aldehydes and Ketones: An Efficient, Aerobic Alternative. *Science* **1996,** *274* (5295), 2044-2046, doi:10.1126/science.274.5295.2044.

33. Rolle, C. J.; Hardcastle, K. I.; Soper, J. D., Reactions of Tetrabromocatecholatomanganese(III) Complexes with Dioxygen. *Inorganic Chemistry* **2008,** *47* (6), 1892-1894, doi:10.1021/ic702390q.

34. Carugo, O.; Castellani, C. B.; Djinovic, K.; Rizzi, M., Ligands derived from orthobenzoquinone - statistical correlation between oxidation state and structural features *J. Chem. Soc.-Dalton Trans.* **1992,** (5), 837-841,

35. Krzystek, J.; Yeagle, G. J.; Park, J. H.; Britt, R. D.; Meisel, M. W.; Brunel, L. C.; Telser, J., High-frequency and -field EPR spectroscopy of tris(2,4-pentanedionato)manganese(III): Investigation of solid-state versus solution Jahn-Teller effects. *Inorganic Chemistry* **2003,** *42* (15), 4610-4618, doi:10.1021/ic020712l.

36. Figgis, B. N., Hitchman, M. A., *Ligand field theory and its applications* Wiley-VCH: New York, 2000.

37. Tregenna-Piggott, P. L. W., Origin of Compressed Jahn-Teller Octahedra in Sterically Strained Manganese(III) Complexes. *Inorganic Chemistry* **2007,** *47* (2), 448-453, doi:10.1021/ic700968q.

38. Ruiz, R.; Caneschi, A.; Gatteschi, D.; Sangregorio, C.; Sorace, L.; Vazquez, M., Counter cation-controlled air oxidation of manganese derivatives of tetrachlorocatechol. *Inorg. Chem. Commun.* **2000,** *3* (2), 76-79,

39. Bordwell, F. G.; Liu, W.-Z., Equilibrium Acidities and Homolytic Bond Dissociation Energies of N–H and/or O–H Bonds in N -Phenylhydroxylamine and Its Derivatives. *Journal of the American Chemical Society* **1996,** *118* (37), 8777-8781, doi:10.1021/ja960152n.

40. Barrette, W. C.; Johnson, H. W.; Sawyer, D. T., Voltammetric evaluation of the effective acidities (pKa') for Broensted acids in aprotic solvents. *Analytical Chemistry* **1984,** *56* (11), 1890-1898, doi:10.1021/ac00275a030.

41. APEX II, Analytical X-Ray Systems, Brukers AXS, Inc., Madison, WI, 2005.,

42. SAINT Version 6.45A, Analytical X-ray Systems, Brukers AXS, Inc., Madison, WI,
2003.,

43. SHELXTL Version 6.12, Analytical X-ray Systems, Bruker AXS, Inc., Madison, WI,
2002.,

44. Wilson, J. C., *In International Tables for X-ray Crystallography, Volume C;*. Academic Publishers: Dordrecht, The Netherlands, 1992.

CHAPTER 4

OXIDATIVE COUPLING REACTIONS CATALYZED BY MANGANESE(III) AMIDOPHENOLATE COMPLEXES

4.1 Introduction

Carbon-carbon bond forming reactions are extremely important synthetic tool in chemistry.[1-2] Over the past 100 years, organic chemists have developed a plethora of methods for new C–C bond formation with a variety of different substrates.[1] The ability to selectively form new C–C bonds allows chemists to design and assemble elaborate molecular systems, for varying purposes.[1-2] The total synthesis of natural products, medicinal chemistry, industrial process development, supramolecular chemistry, chemical biology, material science, and nanotechnology are all fields that have been substantially impacted by the progress in C–C bond forming chemistry.[1-2]

A significant breakthrough in the field was the advent of transition metal mediated cross coupling reactions during the 1970's.[1, 3] With metal catalyzed cross coupling reactions, a general approach for making C–C bonds, with both sp and sp^2-hybridized carbon atoms was established. Over the past four decades, cross-coupling has emerged as a powerful method in organic synthesis based on the assortment of organometallic reagents that can be used in these reactions.[1-2, 4] The importance of transition metal catalyzed couplings was recognized in 2010, with the awarding of the Nobel prize in chemistry to Richard Heck, Ei-ichi Negishi, and Akira Suzuki "for palladium-catalyzed cross-couplings in organic synthesis".[5]

Traditional palladium catalyzed coupling reactions involve the coupling of a nucleophilic carbon with an electrophilic carbon **(Scheme 1)**.

Scheme 1. Palladium catalyzed cross coupling

This strategy utilizes common nucleophiles such as Grignards, organozinc, organotin or boronic acids and couples them with electrophilic sources of carbon such as alkyl halides or pseudohalides.[1] The reactivity observed in traditional cross coupling reactions results in high yields of products with predictable regioselectivity.[6-7]

One alternative that has garnered some attention from traditional cross coupling methods is oxidative coupling chemistry, which can also be used for assembly of carbon–carbon bonds.[7-13] In oxidative coupling, two nucleophilic sources are coupled to form a new bond with the use of an oxidant **(Scheme 2)**.

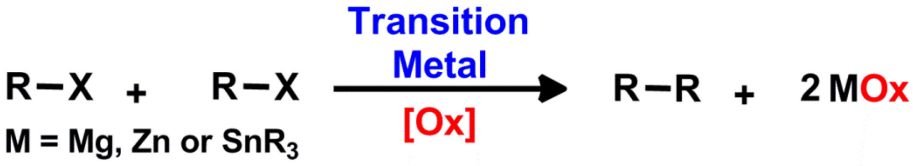

Scheme 2. Oxidative coupling catalyzed by transition metals.

The oxidative coupling of prefunctionalized carbon bonds is an attractive field because coupling reactions can be performed using cheap base metals. For example, the metal-catalyzed homocoupling of aryl Grignard reagents has been known for over 80 years.[14-16] However, its utility in organic synthesis can be limited by the need for stoichiometric

chemical oxidants. A recent resurgence of interest in the development of Earth-abundant metal catalysts for coupling reactions has led to the discovery of new methods for oxidative coupling.[17-21] One example is the remarkable manganese- and iron-catalyzed cross coupling and homocoupling of some Grignard reagents using O_2 as the° oxidant.[18, 22-24] Because selectivity in palladium-catalyzed coupling typically derives from metal-mediated $2e^-$ oxidative addition and reductive elimination reactions,[1, 13] it was proposed that similar steps are involved in the aerobic coupling cycles.[18, 22] However, later first-row metals are typically stable in oxidation states that vary by only $1e^-$,[25] so the true speciation of the catalytically active species, as well as the viability of the proposed $2e^-$ redox steps, remains speculative (**Scheme 3**).

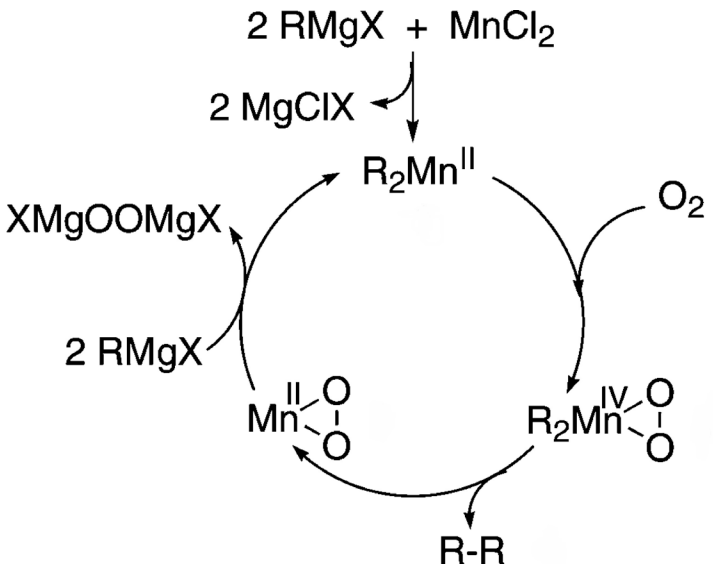

Scheme 3. Proposed mechanism for manganese(II) catalyzed oxidative homocoupling.[18]

An emerging strategy for multielectron chemistry exploits the ability of redox-active ligands to store and deliver charge for reactions at coordinatively-unsaturated metals, including $2e^-$ O_2 activation and C–C reductive elimination.[25-38] In this chapter, I

reported how this approach can be used to effect both of these $2e^-$ redox processes at new four- and five-coordinate manganese(III) redox-active ligand complexes. The sum of the stoichiometric reaction steps comprises a well-defined cycle for catalytic aerobic coupling of aryl Grignard reagents at a naturally abundant metal.

4.2 Results.

4.2.1 Preparation and Characterization of Manganese Amidophenolate Complexes.

The previously reported Mn^{III}(ap)(isq) complex ($[ap]^{2-}$ = 2,4-di-*tert*-butyl-6-(2,6-diisopropylphenylamido)phenolate; $[isq]^{\bullet-}$ = 2,4-di-*tert*-butyl-6-(2,6-diisopropylphenylimino)semiquinonate) is a convenient precursor to the coupling catalysts of present interest.[39-40] Mn^{III}(ap)(isq) was prepared by irradiating a toluene solution containing 1 equiv of Mn_2CO_{10} with 4 equiv of 2,4-di-*tert*-butyl-6-(2,6-diisopropylphenylimino)quinone with UV light over the course of two days to afford a purple species **(Scheme 4).**

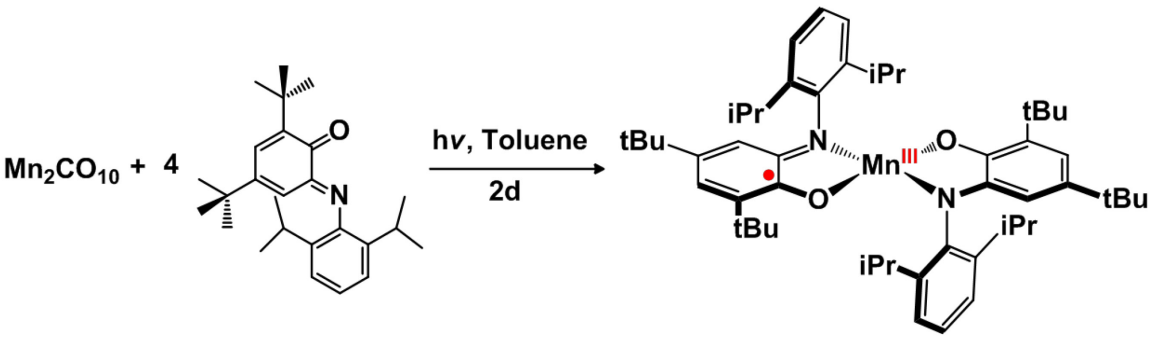

Scheme 4. Synthesis of Mn^{III}(ap)(isq).

Previous literature suggested that complex was a green species in toluene,[40] however in our hands, it was isolated as purple crystals from a purple toluene solution. The crystals were characterized using UV-Vis, elemental analysis and X-ray crystallography **(Figure 4.1)**.

The crystal structure shows that the N1–Mn–N2 and O1–Mn–O2 angles for Mn(isq)(ap) are both 177(1) . The sum of the bond angles around the metal based on N1–Mn–O1, N1–Mn–O2, N2–Mn–O1 and N2–Mn–O2 is 360(1) which is typical for a square planar environment. This was also observed in the previous literature complex.[39] The complex contains two different toluene solvates in the crystal structure which allow for distinct characterization of the bond lengths in each ligand. The C–N bond lengths of 1.374(4) Å and 1.381(4) Å observed in the structure are between the C–N bond lengths commonly observed in reduced amidophenolate(2–) ligands (1.39 Å) and oxidized iminosemiquinonate(1–) (1.34 Å) ligand in transition metal complexes.[41-43] The previous literature crystal structure has an average C–N bond length of 1.368 Å, which is shorter than what I observed in my structure, but also lies between the typical values.[40] The C–O bond lengths of 1.340(4) Å and 1.343(4) observed in my structure also lie between C–O bond lengths commonly observed in amidophenolate(2–) ligands (1.35 Å) and iminosemiquinonate(–)ligands (1.30 Å) in transition metal complexes. The literature crystal structure of has an average C–O bond length of 1.326 Å, which also lies between the typical values.[40-43] Because both ligands display bond lengths that are between in amidophenolate(2–) ligands and iminosemiquinonate(–)ligands we can conclude that a single ligand centered oxidation is delocalized across both ligands. Therefore, the overall oxidation state of the complex is best described as Mn^{III}(ap)(isq).

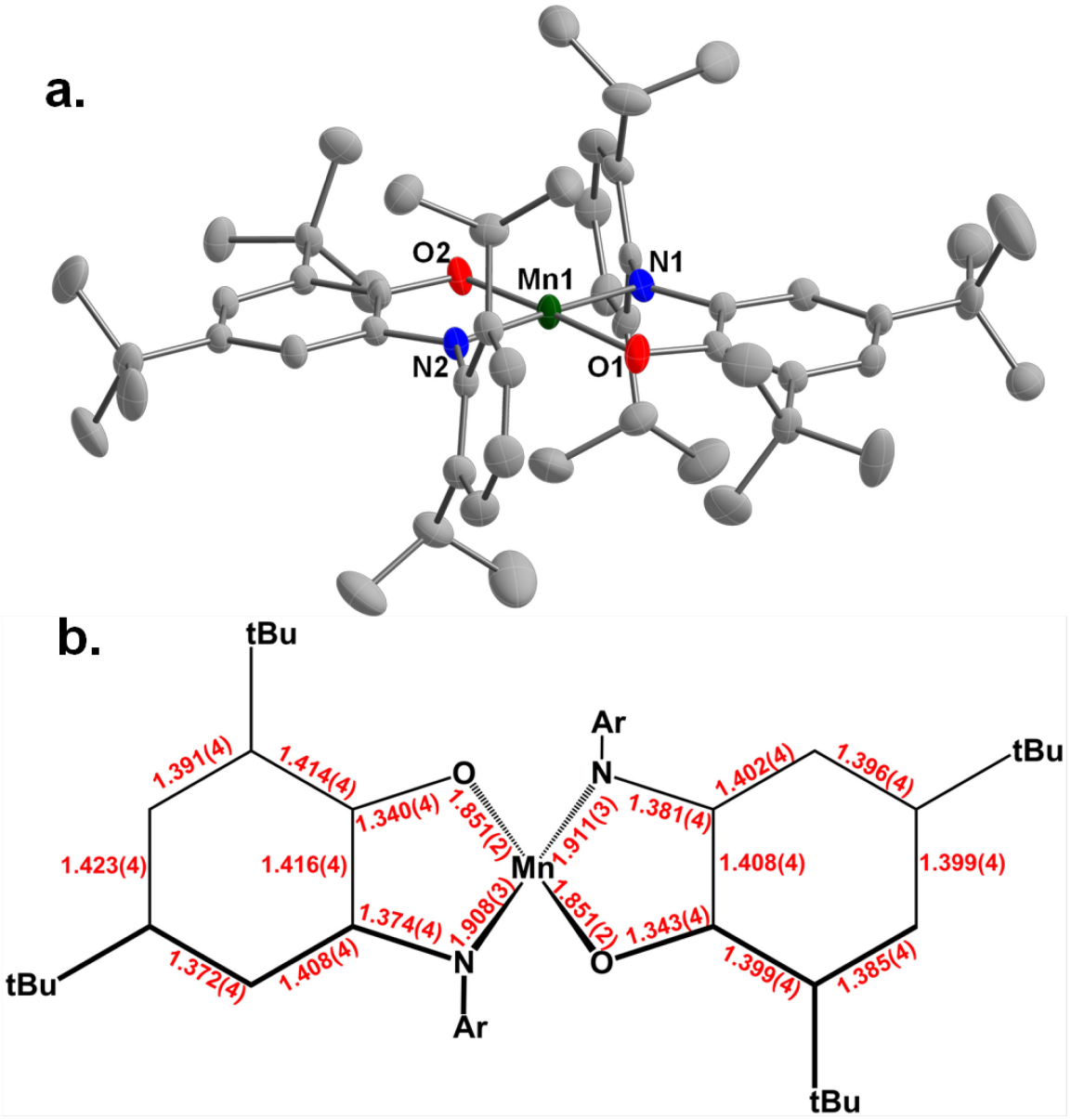

Figure 4.1 (a) Solid-state structure of Mn^{III}(ap)(isq) drawn with 50% probability ellipsoids. The hydrogen atoms and toluene solvate molecule are omitted for clarity. (b) Schematic of selected bond lengths (Å) in Mn^{III}(ap)(isq) drawn to correspond to Figure 4.1a

It was determined that Mn^{III}(ap)(isq) forms a purple species in non-coordinating solvents, such as toluene or hexane, but in coordinating solvents such as THF, MeOH or MeCN, Mn^{III}(ap)(isq) was observed as green species. UV-vis spectra of green solutions of Mn^{III}(ap)(isq) in THF have four distinct peaks at 653 nm (6800 ε), 518nm (4600 ε), 465 nm (4500 ε) and 389 nm (7600 ε) whereas UV-vis spectra of purple solutions in toluene have four peaks at 843 nm (1800 ε) , 655 nm (3300 ε) and 578 nm(5100 ε) and 463 nm (5300 ε) **(Figure 4.2).**

Recrystallization of purple Mn^{III}(ap)(isq) in an MeCN solution resulted in dark green crystals suitable for X-ray analysis. The crystal structure revealed that in MeCN, a five coordinate square pyramidal complex is formed **(Figure 4.3, Scheme 5)**.

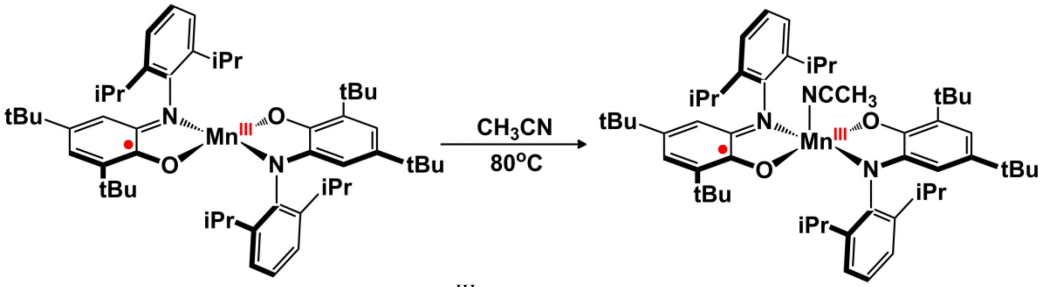

Scheme 5. Recrystallization of Mn^{III}(ap)(isq) in CH_3CN.

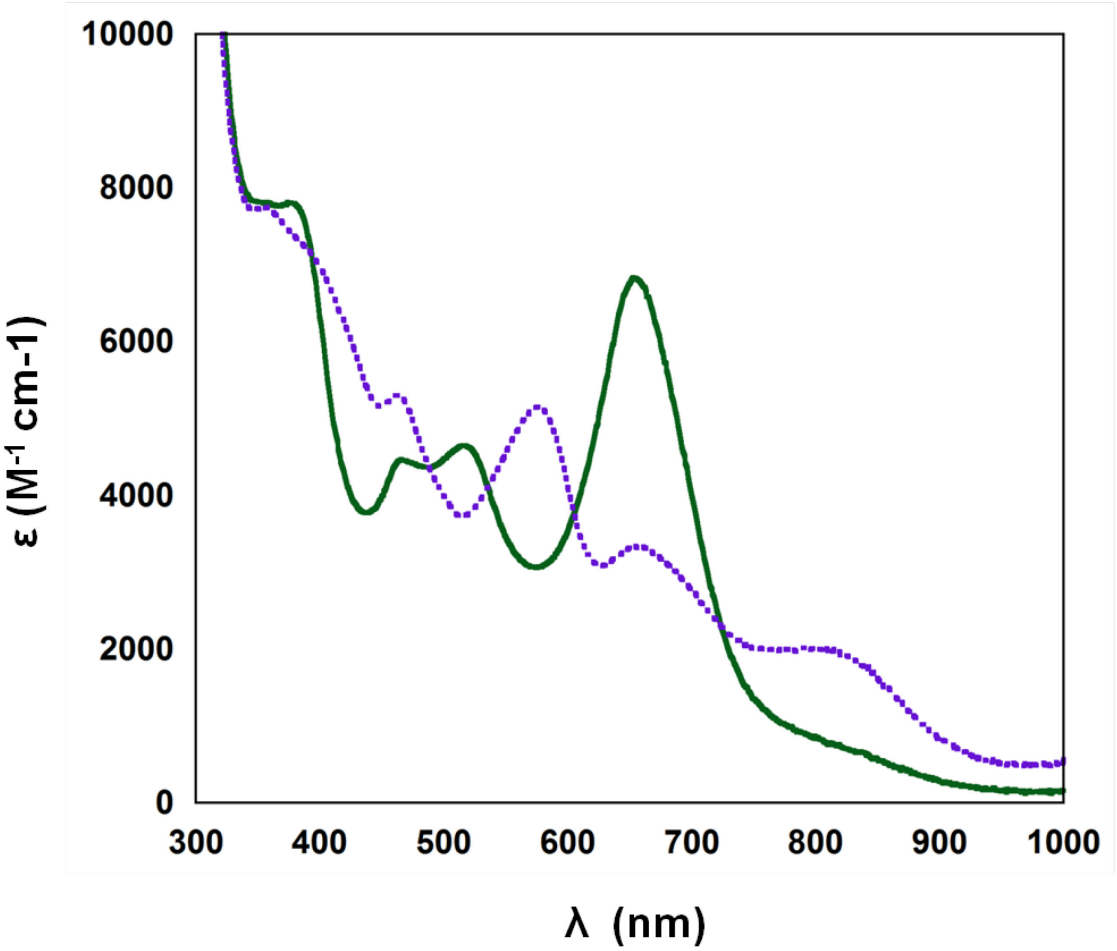

Figure 4.2. UV-Vis spectra showing the spectral changes observed in Mn^{III}(isq)(ap) based on solvent. A 0.09 mM solution of Mn^{III}(ap)(isq) in THF(green) and a 0.08 mM solution toluene(purple) is shown.

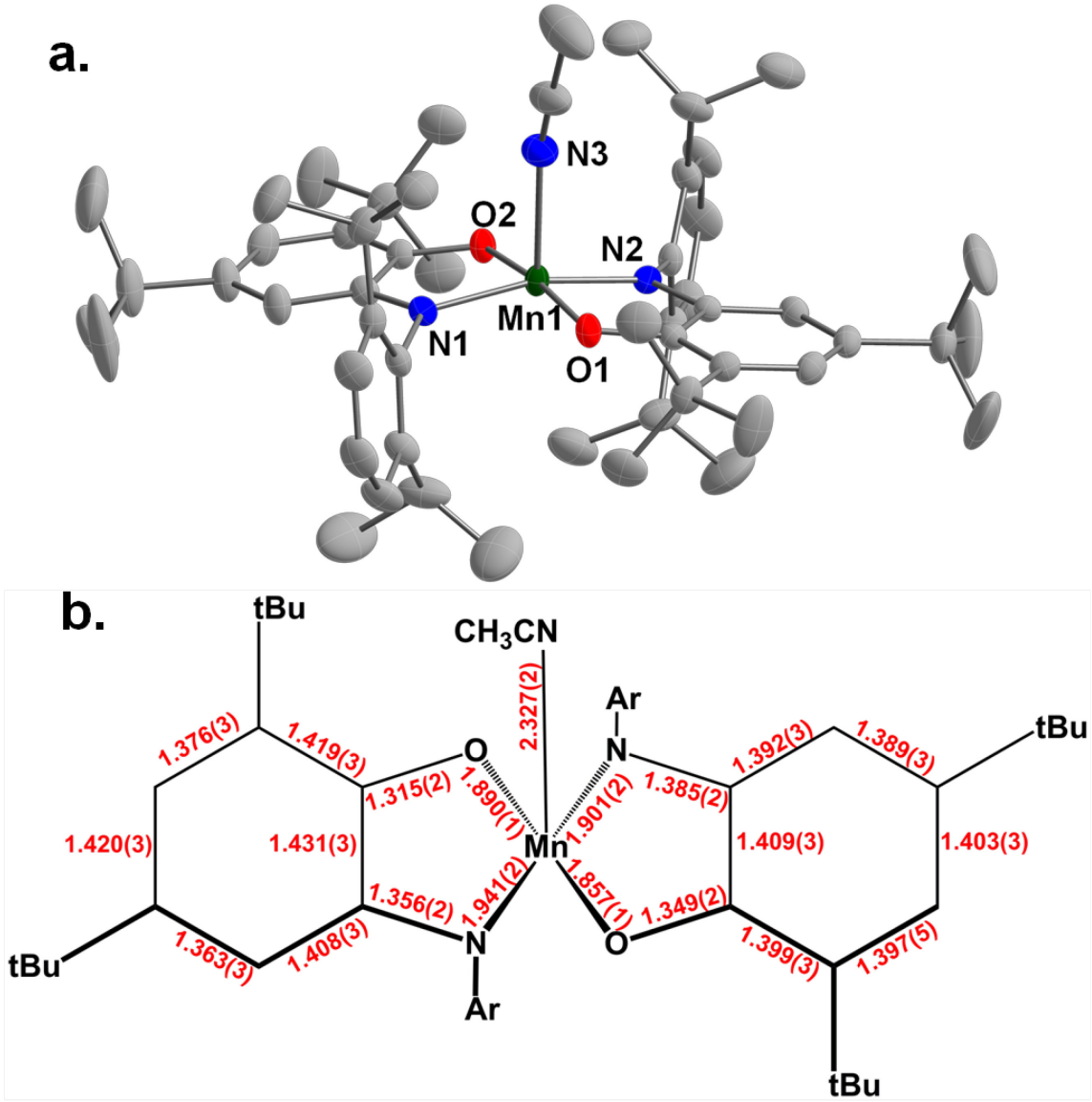

Figure 4.3. (a) Solid-state structure of Mn^{III}(ap)(isq)(CH_3CN) drawn with 50% probability ellipsoids. The hydrogen atoms are omitted for clarity. (b) Schematic of selected bond lengths (Å) in Mn^{III}(ap)(isq)(CH_3CN) drawn to correspond to Figure 4.3a.

The crystal structure shows that the complex is square pyramidal with an acetonitrile bound in the axial position. An analogous THF complex has been reported to adopt this geometry.[39] Additional acetonitrile solvates in the crystal stucture make the two aminophenol ligands symmetry inequivalent. Analaysis of the X-ray metrical data allows assignment of the oxidation states of each ligand. The C–N and C–O bond lengths in each ligand are significantly different from each other. One ligand has C–N and C–O bond lengths of 1.385(2) Å and 1.349(2) Å respectively, which coincide with average C–N (1.39 Å) and C–O (1.35 Å), typically observed for fully reduced amidophenolate(2–) ligands in transition metal complexes. The other ligand has C–N and C–O bond lengths of 1.356(2) Å and 1.315(2) Å respectively, which agree with average C–N (1.34 Å) and C–O (1.30 Å), typically observed for iminosemiquinonate(1–) ligands in transition metal complexes. Unlike the crystal structure of Mn^{III}(ap)(isq) observed in toluene, this structure clearly has two ligands in two different oxidation states. The N1–Mn–N2 and O1–Mn–O2 angles for Mn^{III}(ap)(isq)(CH_3CN) are 164(1) and 171(1) respectively, which are contracted from 177(1) observed in the four coordinate Mn^{III}(ap)(isq) complex. A solution magnetic moment of 4.1 μ_B was observed for Mn^{III}(ap)(isq) in THF at 25°C. This can be rationalized by intramolecular antiferromagnetic coupling between the high spin Mn(III) and one iminobenzosemiquinonate(1–) radical ligand to yield a S=3/2 ground state, as previously assigned.

Electrochemical studies of Mn^{III}(ap)(isq) in MeCN display two reversible $1e^-$ redox couples in cyclic voltammograms at $E_{1/2}$ = –0.294 V and –0.851 V versus Fc^+/Fc **(Figure 4.4)**. The redox event at the more negative potential corresponds to interconversion of Mn^{III}(ap)(isq) and its $1e^-$ reduced congener, whereas the redox event at

the more positive potential to the oxidation of Mn^{III}(ap)(isq). Efforts were made to isolate both the oxidized and reduced species observed in the cyclic voltammagram.

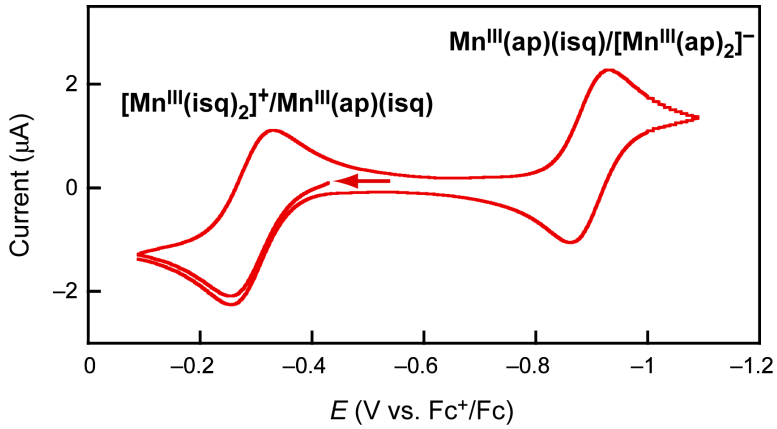

Figure 4.4 Cyclic voltammogram of Mn^{III}(ap)(isq) in MeCN containing 0.1M [$^{n}Bu_4N$][PF_6] at a 10 mm Pt electrode. Scan rate: 10 mV s^{-1}. Temperature: 25 °C.

Addition of 1 equiv Cp^*_2Co to a suspension of Mn^{III}(ap)(isq) in MeCN under N_2 gives a new rust-brown solution over 12 h at ambient temperature **(Scheme 6).**

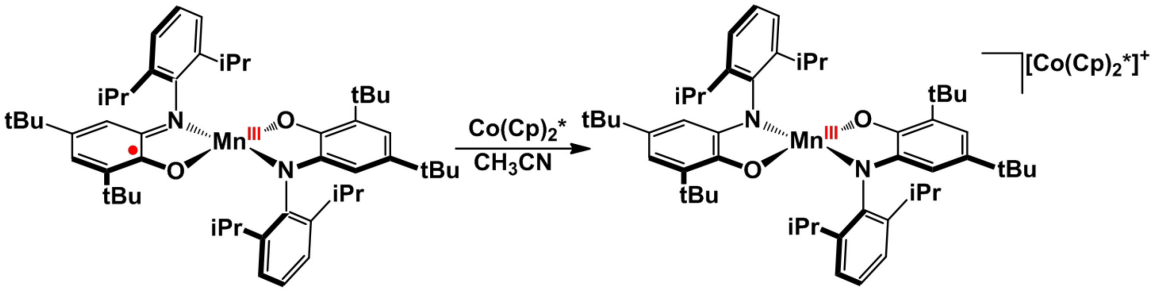

Scheme 6. Synthesis of $[Mn(ap)_2]^-$

Slow evaporation of the rust-brown solution under vacuum affords X-ray quality crystals in a 77% yield. A X-ray structure of the resulting anion is provided in **Figure 4.5a**. In the structure, the N1–Mn–N2 and O1–Mn–O2 angles are 166(1) and 177(1) respectively, which are contracted, in comparison to 177(1) observed in the four

coordinate Mn^{III}(isq)(ap)complex. The sum of the bond angles around the metal based on N1–Mn–O1, N1–Mn–O2, N2–Mn–O1 and N2–Mn–O2 is 359(1) , which is typical for a square planar environment. The manganese center bound to two crystallographically unique aminophenol ligands. The C–N bond lengths of 1.391(4) Å and 1.392(4) Å are typical for fully reduced aminophenolate(2–) ligands (1.39 Å).[41-43] The C–O bond lengths of 1.357(4) Å and 1.345(4) Å are also commonly observed in reduced amidophenolate(2–) ligands (1.35 Å), so the product is best described as $[Mn^{III}(ap)_2]^-$. A solution magnetic moment of 4.6 μ_B was observed for $[Mn^{III}(ap)_2]^-$ in THF at 25°C. This is consistent with a high spin Mn(III) center yielding a S=2 ground state because both amidophenolate(2–) ligands are fully reduced with no intramolecular antiferromagnetic coupling being observed.

The second reversible redox couple in the CV implied that Mn^{III}(ap)(isq) is oxidized at modest potentials. The oxidation product has not been isolated as a four-coordinate cation, but a chloride adduct to the $1e^-$ oxidized species was previously reported as $Mn^{III}Cl(isq)_2$.[44] Modifications of the synthetic procedure using various Mn(II) salts afforded new five-coordinate analogs. (**Scheme 7**).

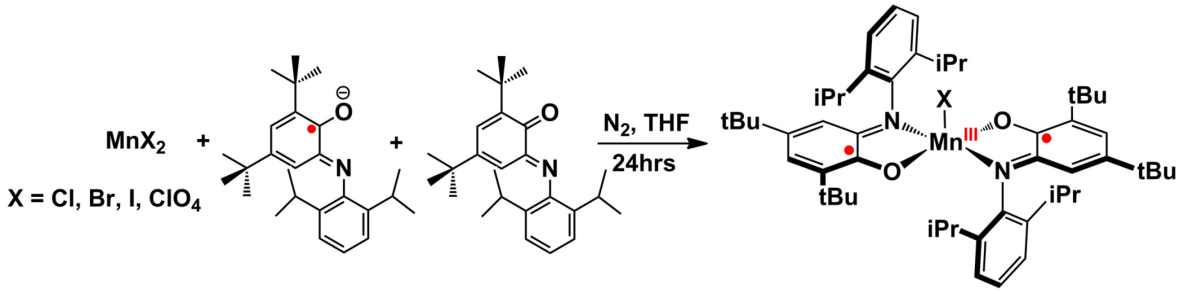

Scheme 7. Synthesis of $Mn(isq)_2X$ complexes.

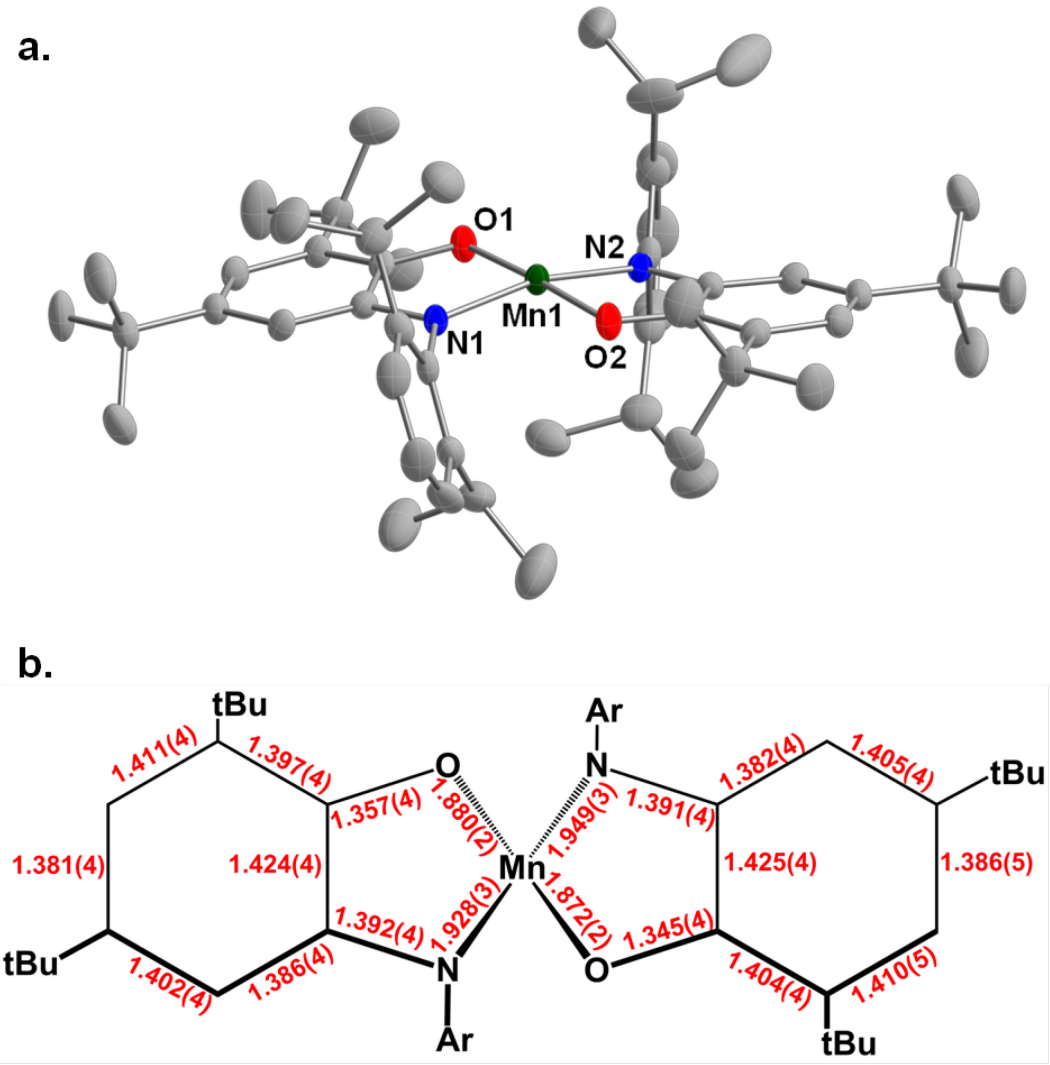

Figure 4.5. **(a)** Solid-state structure of the anion in $(Cp^*_2Co)[Mn^{III}(ap)_2]$•2MeCN drawn with 50% probability ellipsoids. The hydrogen atoms, MeCN solvate molecules and $[Cp^*_2Co]^+$ countercation are omitted for clarity. **(b)** Schematic of selected bond lengths (Å) in $[Mn^{III}(ap)_2]^-$ drawn to correspond to Figure 4.5a.

The solid-state structures of the five coordinate Br^- and ClO_4 adducts were isolated and exhibited high structural homology **(Figures 4.6, 4.7)**. In the bromide adduct, the N1–Mn–N2 and O1–Mn–O2 angles are 144(1) and 165(1) respectively, and the N1–Mn–Br1 and O1–Mn–Br1 angles are 108(1) and 98(1) respectively. These bond angles are indicative of a distorted square pyramidal geometry observed. In the crystal structure of the percholate adduct two unique molecules were determined in each unit cell **(Figure 4.7)**. The N1–Mn–N2 and O1–Mn–O2 angles for $Mn^{III}(OClO_3)(isq)_2$ are 142(1) and 169(1) in both molecules. The square pyramidal geometry of perchlorate complex is more distorted than the bromide analog. The perchlorate anion is larger than bromide and forces one of the iminosemiquinonate ligands to partially twist out of the plane to accommodate the perchlorate anion at the metal center.

In both the Br^- and ClO_4 stuctures, similar patterns in bond length distances are observed. The C–N bond lengths for each ligand in both complexes range from 1.339(6) Å to 1.364(6) Å, which is typical for the C–N bond lengths (1.34 Å) commonly observed in oxidized iminosemiquinonate(1–) ligands.[41-44] The C–O bond lengths for both complexes range from 1.304(4) Å to 1.326(4) Å, which is also typical for oxidized iminosemiquinonate(–1) ligands (1.30 Å).[41-44] The adducts are best described as $Mn^{III}Br(isq)_2$ and $Mn^{III}OClO_3(isq)_2$. A solution magnetic moment of 2.6 μ_B was observed for $Mn^{III}Br(isq)_2$ in THF at 25°C. This consistent with intramolecular antiferromagnetic coupling between the high spin Mn(III) and both iminobenzosemiquinonate(1–) radical ligands to yield a S=1 ground state.

Although a crystal structure of $Mn^{III}I(isq)_2$ was not obtained, the complex was

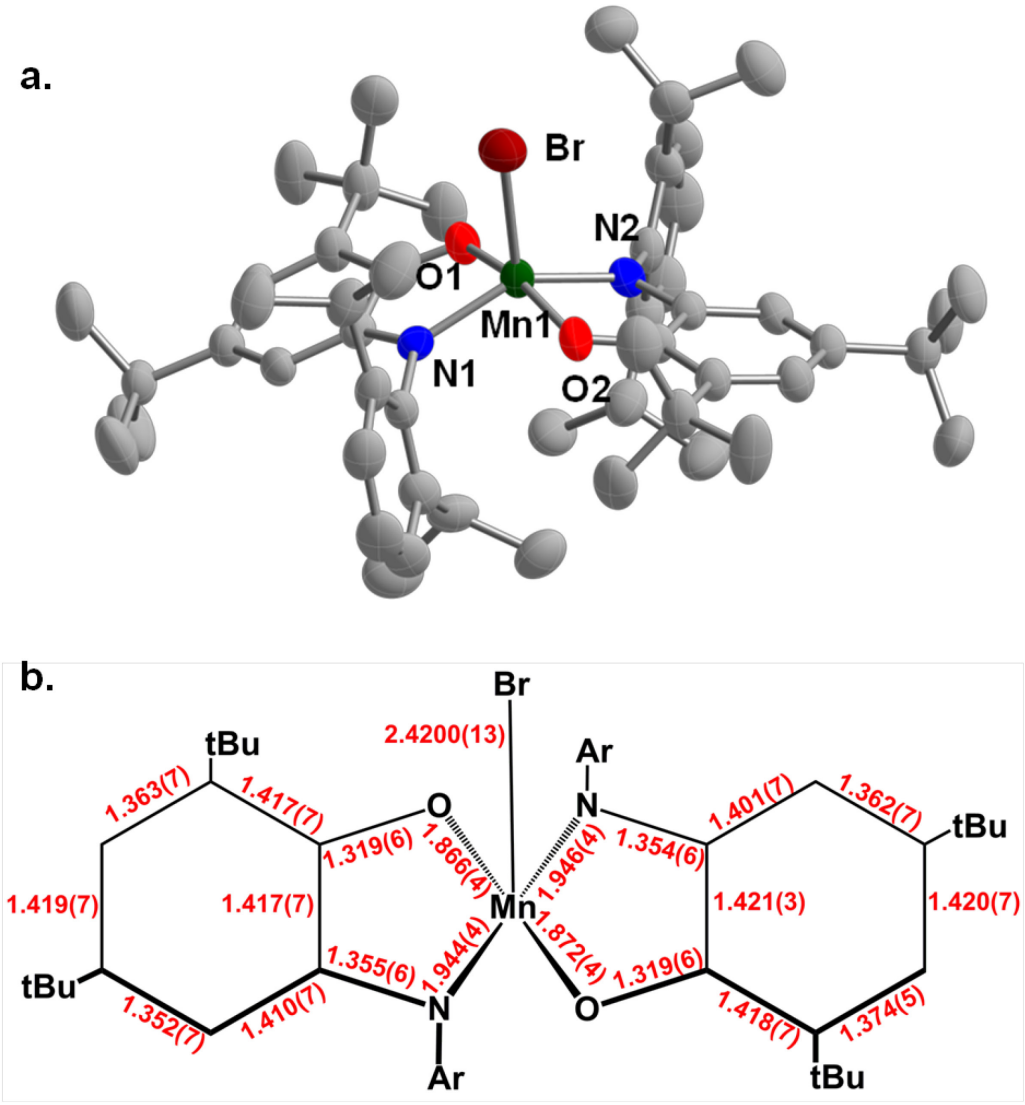

Figure 4.6. (a) Solid-state structure of $Mn^{III}Br(isq)_2 \cdot 0.42C_6H_{14}$ drawn with 50% probability ellipsoids. The hydrogen atoms and *n*-hexane solvate molecule are omitted for clarity. **(b)** Schematic of selected bond lengths (Å) in $Mn^{III}Br(isq)_2$ drawn to correspond to Figure 4.6a

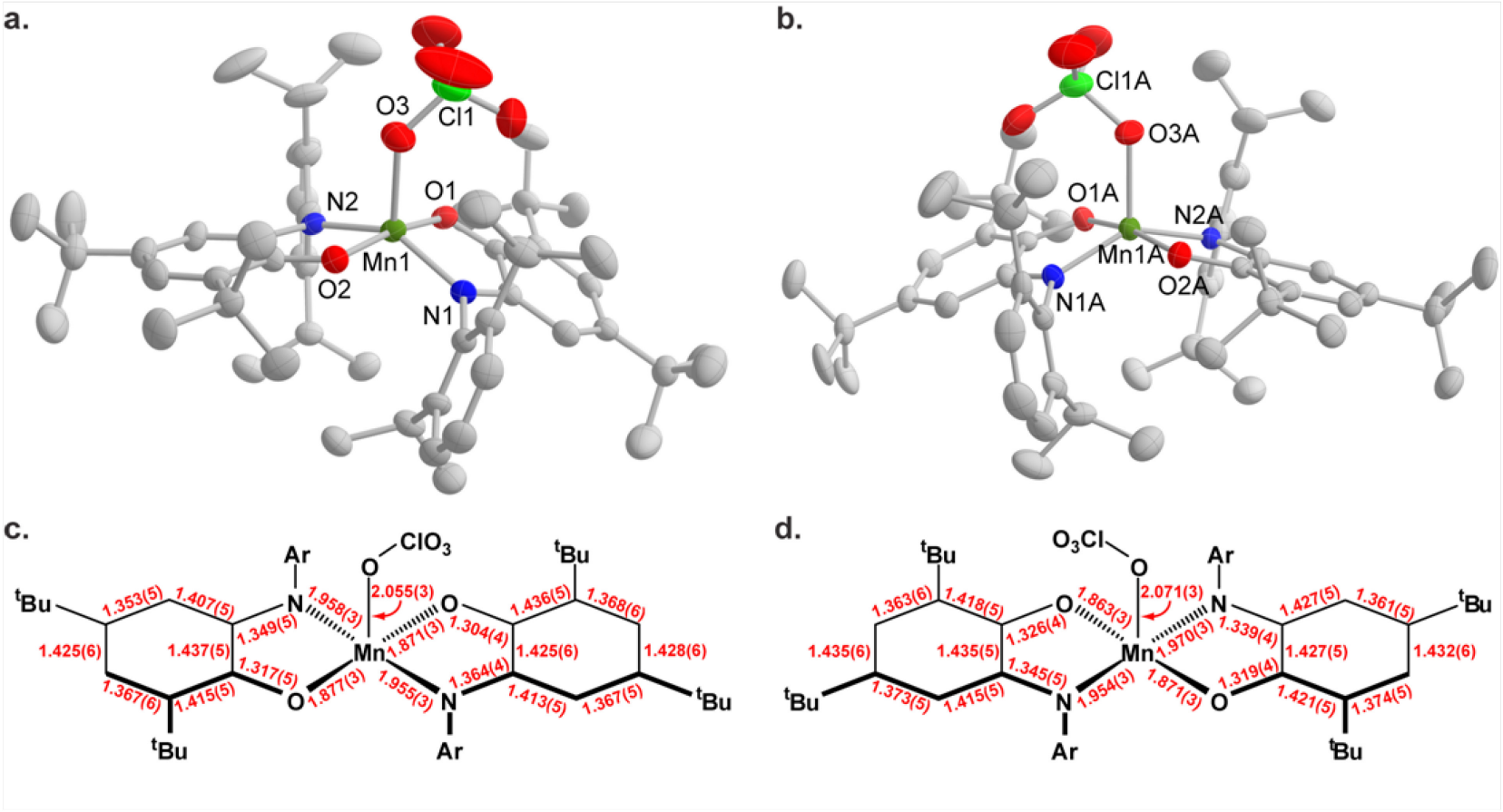

Figure 4.7. (a-b) Solid-state structures of $[Mn^{III}(OClO_3)(isq)_2]$•$0.25CH_2Cl_2$•$0.25C_7H_8$ drawn with 50% probability ellipsoids. The two ellipsoid plots represent two crystallographically unique molecules in the unit cell of the same crystal. The hydrogen atoms and CH_2Cl_2 and toluene solvate molecules are omitted for clarity. **(c-d)** Schematic representations of selected bond lengths (Å) in the two $Mn^{III}(OClO_3)(isq)_2$ structures. Figure 4.7c corresponds to Figure 4.7a, and Figure 4.7d corresponds to Figure 4.7b.

characterized by elemental analysis and ESI-MS. The UV-Vis spectrum of the $Mn^{III}I(isq)_2$ also bears a strong resemblance to the UV- Vis spectra of $Mn^{III}Br(isq)_2$ and $Mn^{III}Cl(isq)_2$**(Figure 4.8)**. $Mn^{III}I(isq)_2$ has a peak at 727 nm (6500 ε) with a shoulder at 670 nm (5000 ε), a sharp, intense band at 497 nm (21000 ε) and another peak at 410 nm (13000 ε). The electronic spectra of $Mn^{III}Br(isq)_2$ displays a hypsochromic shift, with peaks at 686 nm (4600 ε), 627 nm(4100 ε), 482 nm(22000 ε) and 398 nm(11000 ε). A blue shift is also observed with $Mn^{III}Cl(isq)_2$, with peaks at 677 nm (4600 ε), 615 nm (4500 ε), 474 nm (24000 ε), and 397 nm (12000 ε). A solution magnetic moment of 3.0 μ_B was observed for $Mn^{III}I(isq)_2$ in THF at 25°C. This is consistent with intramolecular antiferromagnetic coupling between the high spin Mn(III) and both iminobenzosemiquinonate(1–) radical ligands to yield a S=1 ground state.

As illustrated in **Scheme 8**, both oxidation and reduction of $Mn^{III}(ap)(isq)$ proceeds without a change in oxidation state at the manganese(III) center.

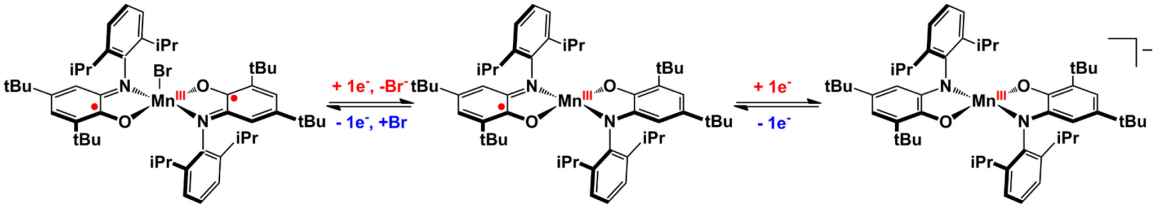

Scheme 8. Redox series of Manganese (III) complexes.

A full comparison of the bond lengths for each structure can be observed in **Table 4.1**.

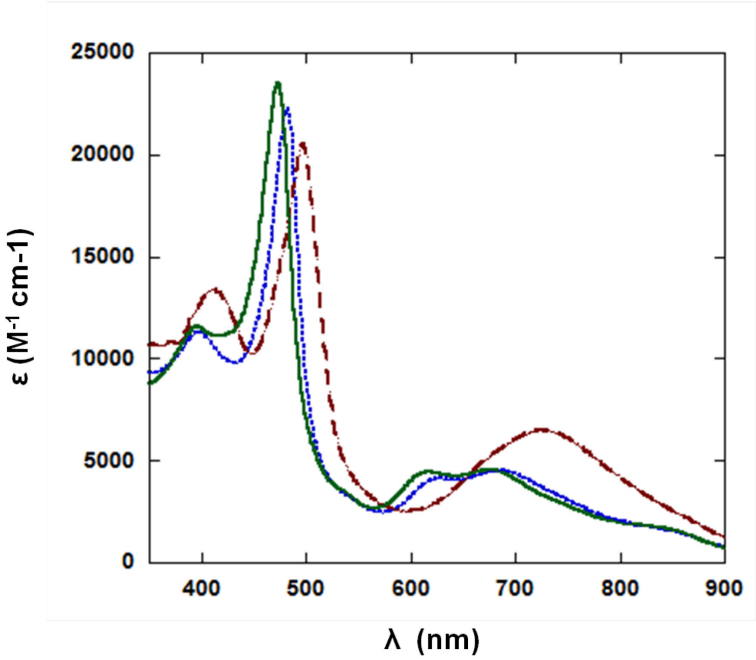

Figure 4.8 UV-Vis spectra showing the spectral differences observed in $Mn^{III}X(isq)_2$ where X = Cl, Br, and I. A 0.07 mM solution of $Mn^{III}Cl(isq)_2$ in THF(green), A 0.06 mM solution of $Mn^{III}Br(isq)_2$ in THF(blue) and a 0.04 mM solution of $Mn^{III}I(isq)_2$ in THF(brown).

Table 4.1. Selected bond lengths (Å) for $Mn^{III}(isq)(ap)\bullet 1.25(C_7H_8)$, $Mn^{III}(isq)(ap)(CH_3CN)$ and $CoCp^*_2[Mn^{III}(ap)_2]\bullet 2(CH_3CN)$.

$Mn^{III}(isq)(ap)\bullet 1.25(C_7H_8)$			
Mn1-O	1.851(2)	Mn1-O2	1.851(2)
Mn1-N	1.908(3)	Mn1-N2	1.911(3)
ap/isq ligands			
C18-O1	1.340(4)	C44-O2	1.343(4)
C13-N1	1.374(4)	C39-N2	1.381(4)
C13-C14	1.408(4)	C39-C40	1.406(4)
C14-C15	1.372(4)	C40-C41	1.396(4)
C15-C16	1.423(4)	C41-C42	1.399(4)
C16-C17	1.391(4)	C42-C43	1.385(4)
C17-C18	1.414(4)	C43-C44	1.399(4)
C13-C18	1.416(4)	C39-C44	1.408(4)
$Mn^{III}(isq)(ap)(CH_3CN)$			
Mn1-O1	1.857(1)	Mn1-O2	1.890(1)
Mn1-N1	1.901(2)	Mn1-N2	1.941(2)
$Mn1\text{-}N3_{CH3CN}$	2.327(2)		
ap ligand		***isq ligand***	
C1-O1	1.349(2)	C27-O2	1.315(2)
C2-N1	1.385(4)	C28-N2	1.356(2)
C2-C3	1.392(3)	C28-C29	1.408(3)
C3-C4	1.389(3)	C29-C30	1.363(3)
C4-C5	1.403(3)	C30-C31	1.420(3)
C5-C6	1.397(3)	C31-C32	1.376(3)
C1-C6	1.399(3)	C27-C32	1.419(3)
C1-C2	1.409(3)	C27-C28	1.431(3)
$CoCp^*_2[Mn^{III}(ap)_2]\bullet 2(CH_3CN)$			
Mn1-O1	1.880(2)	Mn1-O2	1.872(2)
Mn1-N1	1.928(3)	Mn1-N2	1.949(3)
ap ligands			
C1-O1	1.357(4)	C27-O2	1.345(2)
C6-N1	1.392(4)	C32-N2	1.391(2)
C5-C6	1.386(4)	C31-C32	1.382(4)
C4-C5	1.402(4)	C30-C31	1.405(4)
C3-C4	1.381(4)	C29-C30	1.386(5)
C2-C3	1.411(4)	C28-C29	1.410(5)
C1-C2	1.397(4)	C27-C28	1.404(4)
C1-C6	1.424(4)	C27-C32	1.425(4)

Table 4.1 cont. Selected bond lengths (Å) for $Mn^{III}Br(isq)_2 \bullet 0.42(C_6H_{14})$, and $Mn^{III}ClO_4(isq)_2 \bullet 0.25(CH_2Cl_2)0.25(C_7H_8)$.

$Mn^{III}Br(isq)_2 \bullet 0.42(C_6H_{14})$			
Mn1-O1	1.866(3)	Mn1-O2	1.872(4)
Mn1-N1	1.944(4)	Mn1-N2	1.946(4)
Mn1-Br	2.4200(13)		
isq ligands			
C6-O1	1.319(6)	C32-O2	1.319(6)
C1-N1	1.355(6)	C27-N2	1.354(6)
C1-C2	1.410(7)	C27-C28	1.402(7)
C2-C3	1.352(7)	C28-C29	1.363(7)
C3-C4	1.419(7)	C29-C30	1.420(7)
C4-C5	1.363(7)	C30-C31	1.374(7)
C5-C6	1.417(7)	C31-C32	1.422(7)
C1-C6	1.417(7)	C27-C32	1.425(7)
$Mn^{III}ClO_4(isq)_2 \bullet 0.25(CH_2Cl_2)0.25(C_7H_8)$			
Mn1-O1	1.871(3)	Mn1-O2	1.877(3)
Mn1-N1	1.955(3)	Mn1-N2	1.958(3)
Mn1-O3	2.055(3)		
isq ligands			
C1-O1	1.304(4)	C27-O2	1.317(5)
C6-N1	1.364(4)	C32-N2	1.349(5)
C5-C6	1.413(5)	C31-C32	1.407(5)
C4-C5	1.367(5)	C30-C31	1.353(5)
C3-C4	1.428(6)	C29-C30	1.425(6)
C2-C3	1.368(6)	C28-C29	1.367(6)
C1-C2	1.436(5)	C27-C28	1.415(5)
C1-C6	1.425(6)	C27-C32	1.437(5)
Mn1A-O1A	1.863(2)	Mn1-O2	1.871(3)
Mn1A-N1A	1.954(3)	Mn1-N2	1.970(3)
Mn1A-O3A	2.071(3)		
isq ligands			
C1A-O1A	1.326(4)	C27A-O2A	1.319(4)
C6A-N1A	1.345(5)	C32A-N2A	1.339(5)
C5A-C6A	1.415(5)	C31A-C32A	1.427(5)
C4A-C5A	1.373(5)	C30A-C31A	1.361(5)
C3A-C4A	1.435(6)	C29A-C30A	1.432(6)
C2A-C3A	1.363(6)	C28A-C29A	1.374(6)
C1A-C2A	1.418(5)	C27A-C28A	1.421(5)
C1A-C6A	1.435(5)	C27A-C32A	1.427(5)

4.2.2 Oxidative Coupling of Grignard Reagents

Addition of 2 equiv PhMgBr to a NMR tube containing $Mn^{III}Br(isq)_2$ in THF–d_8 resulted in an immediate color change from green to rust-brown with concomitant formation of 1 equiv Ph–Ph, as evidenced by ^1H NMR spectroscopy.

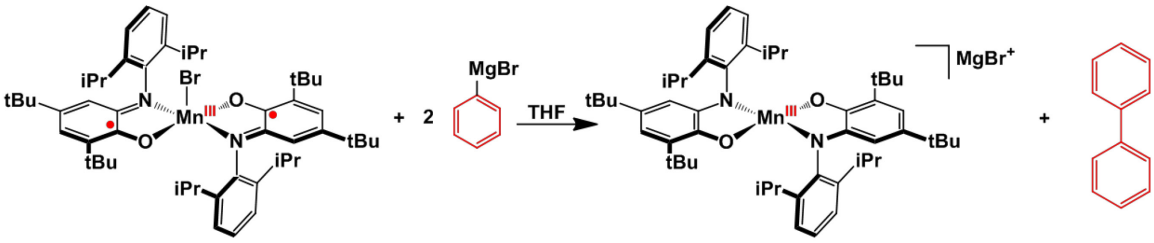

Scheme 9. Oxidative coupling of phenyl grignard by $MnBr(isq)_2$.

The rust-brown product is $[Mn^{III}(ap)_2]^-$. The net $2e^-$ process shown in **Scheme 9** is therefore analogous to stoichiometric oxidative couplings of aryl Grignard reagents by simple metal halides.[14, 16] Reaction of $Mn^{III}Br(isq)_2$ with 1 equiv PhMgBr gives 0.5 equiv Ph–Ph and quantitative formation of $Mn^{III}(ap)(isq)$, and addition of 1 equiv PhMgBr to $Mn^{III}(ap)(isq)$ affords $[Mn^{III}(ap)_2]^-$ and 0.5 equiv Ph–Ph. The sum of these two reactions is therefore consistent with the redox stoichiometry in **Scheme 9**, and suggests that $Mn^{III}(ap)(isq)$ is a kinetically competent intermediate in the net $2e^-$ process.

Reactions with aryl Grignard reagents that are probes of radical intermediates were performed to determine whether the $1e^-$ radical pathway or concerted $2e^-$ pathway followed by comproportionation was responsible for the observed reactivity. Stoichiometric reactions of 1 equiv of 2-(3-butenyl)-phenyl magnesium iodide and $Mn^{III}Br(isq)_2$ afforded 2,2'-bis-(3-butenyl)-biphenyl, in 64% yield without evidence for

5-exo radical cyclization products. This allows us to exclude free radical intermediates in the coupling reaction **(Scheme 10)**.

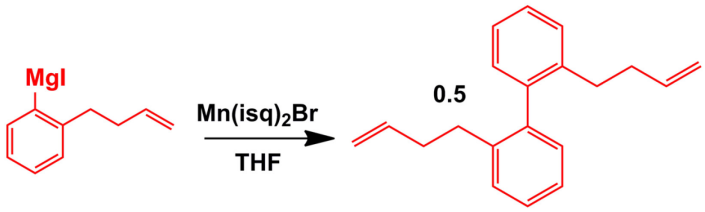

Scheme 10. Oxidative coupling of 2-(3-butenyl)-phenyl magnesium iodide.

4.2.3 Reactions with O_2

THF solutions containing the $[Mn^{III}(ap)_2]^-$ anion are indefinitely stable under N_2, but exposure to 1 atm O_2 affords an immediate color change from the rust-brown color. However, different preparations of $[Mn^{III}(ap)_2]^-$ lead to different products. Reaction of O_2 with samples of $[MgBr][Mn^{III}(ap)_2]$ generated *in situ* from $Mn^{III}Br(isq)_2$ and 2 equiv PhMgBr gives green $Mn^{III}Br(isq)_2$ **(Scheme 11)**.

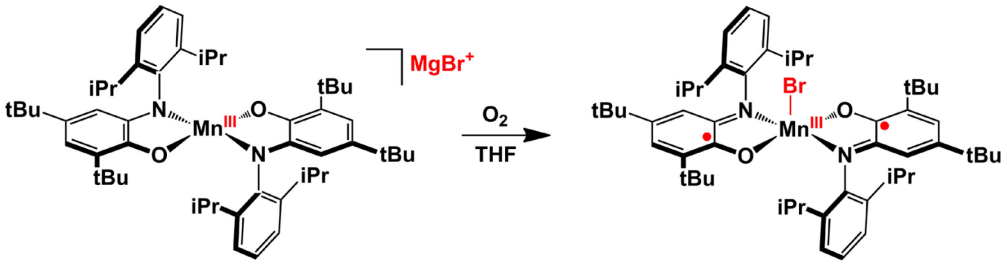

Scheme 11. Oxidation of $[MgBr][Mn^{III}(ap)_2]$ by O_2 to $Mn^{III}Br(isq)_2$

In contrast, addition of 1 atm O_2 to isolated $[Cp^*_2Co][Mn^{III}(ap)_2]$ resulted in decomposition of the metal complex to yield orange solutions containing the free 2,4-di-*tert*-butyl-6-(2,6-diisopropylphenylimino)benzoquinone (**ibq**) form of the ligand (**Scheme 12**).

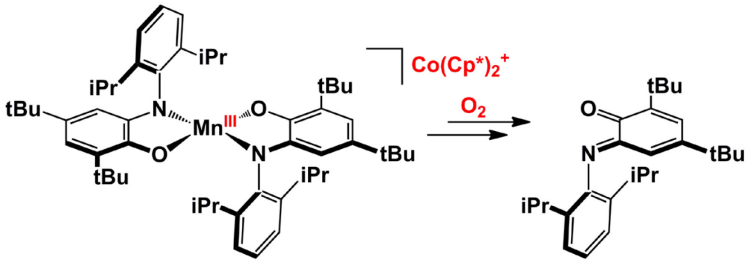

Scheme 12. Oxidative decomposition of $[Cp^*_2Co][Mn^{III}(ap)_2]$ by O_2 to form ibq.

Surprisingly, monitoring by UV–vis spectroscopy reveals that both reactions proceed through a common intermediate. The colored species observed in two reactions of $[MgBr][Mn^{III}(ap)_2]$ with O_2 are shown in **Figures 4.9 and 4.10** . Immediately upon O_2 exposure $[Mn^{III}(ap)_2]^-$ is oxidized by $1e^-$ to $Mn^{III}(ap)(isq)$. In dilute solutions of $[MgBr][Mn^{III}(ap)_2]$ (0.07 mM), a bright red species subsequently accumulates prior to formation of $Mn^{III}Br(isq)_2$ (**Figure 4.9**). But at a higher initial $[MgBr][Mn^{III}(ap)_2]$ concentration (0.28 mM), a fast first reaction forms a mixture of $Mn^{III}(ap)(isq)$ and the red intermediate **(I1)** which is consumed in a second reaction to generate $Mn^{III}Br(isq)_2$ (**Figure 4.10**). Solutions of $[Cp^*_2Co][Mn^{III}(ap)_2]$ react rapidly with O_2 to form a green solution and then the same red transient, which decomposes to lead to the orange free ibq (**Figure 4.11**). Although the red material formed from O_2 oxidation of $[MgBr][Mn^{III}(ap)_2]$ and $[Cp^*_2Co][Mn^{III}(ap)_2]$ is the same, the UV–vis spectra of the initially formed green materials are not identical in **Figures 4.10** and **4.11**. The origin of this difference is not currently known. Notably, an identical red material is obtained from exposure of isolated $Mn^{III}(ap)(isq)$ to 1 atm O_2 in THF, and removal of the O_2 from the red solutions regenerates the green UV–vis spectrum of $Mn^{III}(ap)(isq)$ **(Scheme 13, Figure 4.12)**.

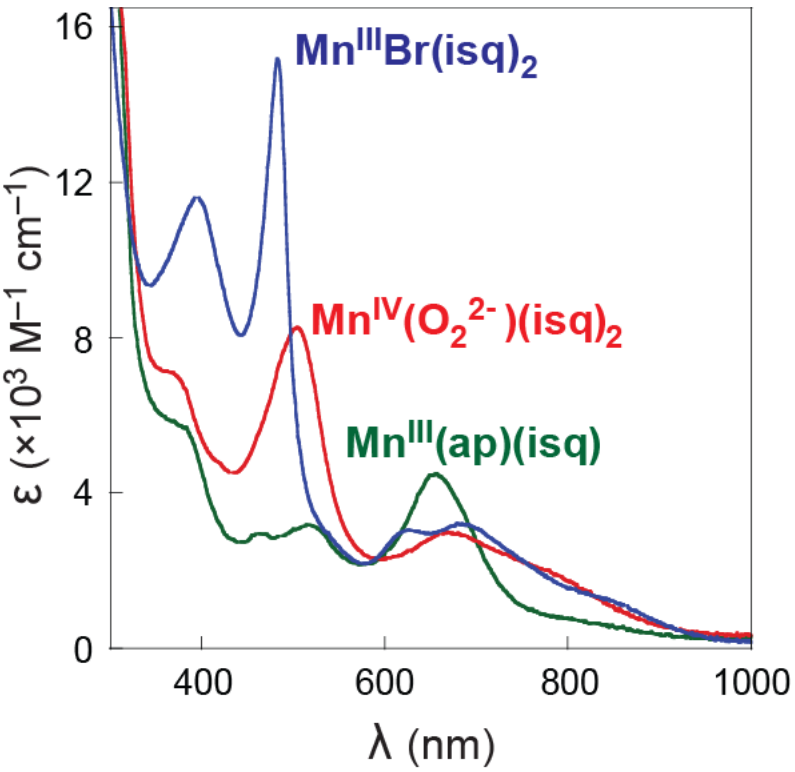

Figure 4.9. Selected UV–vis absorption data from the reaction of $[MgBr][Mn^{III}(ap)_2]$ with 1 atm O_2 in THF at 25 °C $Mn^{III}Br(isq)_2$. Spectra were selected at time points corresponding to the maximum yield of each species, as measured by the change in absorption intensity at their respective λ_{max} values. The reaction of 0.07 mM $[MgBr][Mn^{III}(ap)_2]$ with O_2 proceeds in three phases, through $Mn^{III}(ap)(isq)$ (green line), $Mn^{IV}(O_2^{2-})(isq)_2$ (red line) at t = 25 s, and $Mn^{III}Br(isq)_2$ (blue line) at t = 330 min.

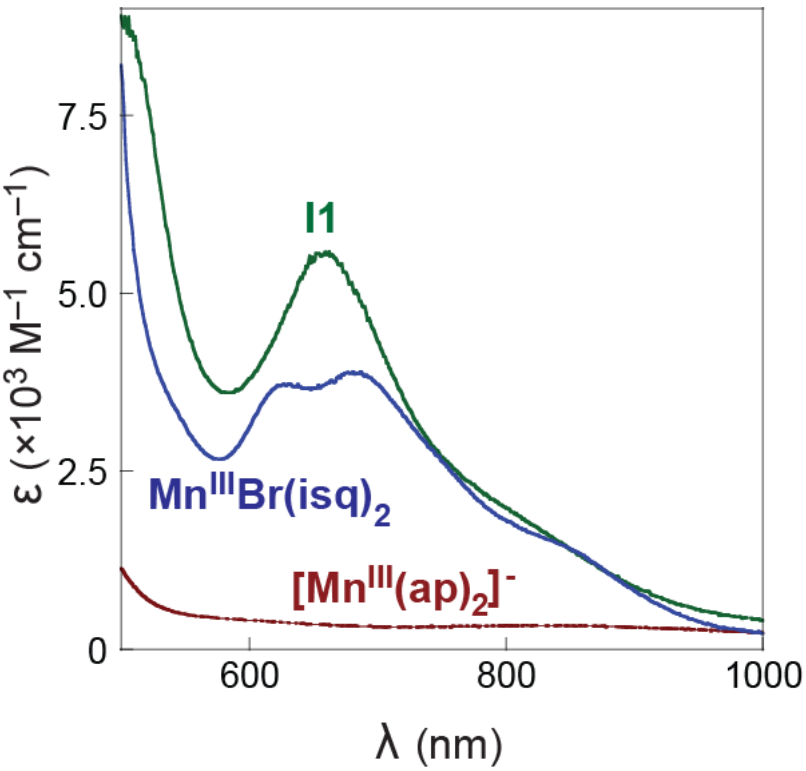

Figure 4.10. Selected UV–vis absorption data from two reactions of [MgBr][$Mn^{III}(ap)_2$] with 1 atm O_2 in THF at 25 °C $Mn^{III}Br(isq)_2$. Spectra were selected at time points corresponding to the maximum yield of each species, as measured by the change in absorption intensity at their respective λ_{max} values. The reaction of 0.28 mM [MgBr][$Mn^{III}(ap)_2$] (brown line) occurs in two phases. The first phase forms a green intermediate (I1) (green line) at t = 60 s that is a mixture of $Mn^{III}(ap)(isq)$ and $Mn^{IV}(O_2^{2-})(isq)_2$, and the second generates $Mn^{III}Br(isq)_2$ (blue line) at t = 20 min.

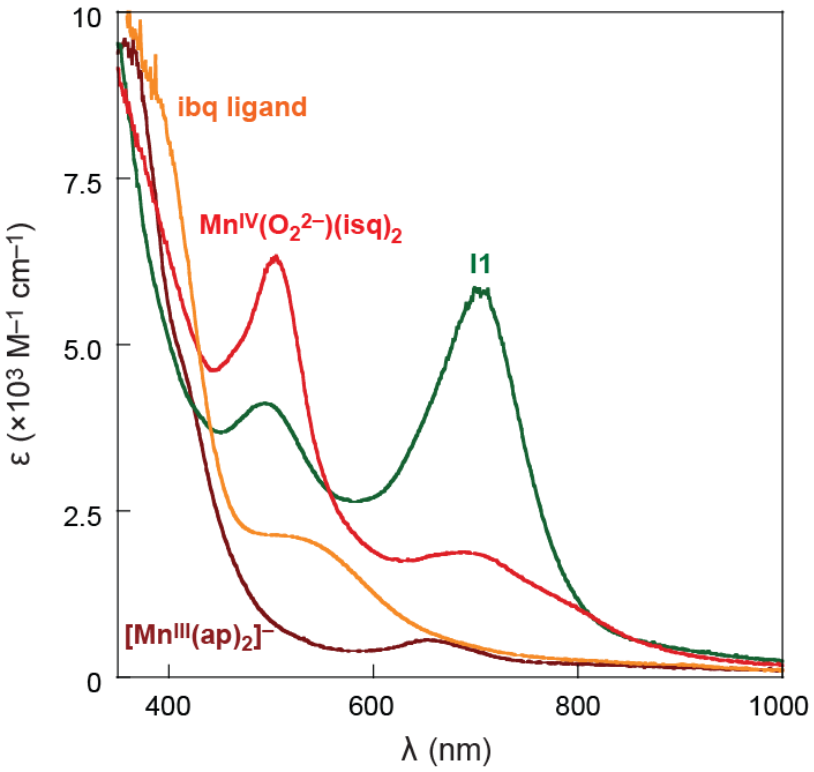

Figure 4.11. Selected UV–vis absorption data for a reaction of 0.28 mM $(Cp^*_2Co)[Mn^{III}(ap)_2]$ with 1 atm O_2 in THF at 25°C to generate free ibq ligand. Spectra were selected at time points corresponding to the maximum yield of each species, as measured by the change in absorption intensity at their respective λ_{max} values. Spectra correspond to $(Cp^*_2Co)[Mn^{III}(ap)_2]$ in degassed THF (rust-brown line), a green intermediate (I1) (green line) at t = 30 s after exposure to O_2, the red O_2 complex $Mn^{IV}(O_2^{2-})(isq)_2$ (red line) at t = 10 min, and free ibq ligand (orange line) at t = 330 min.

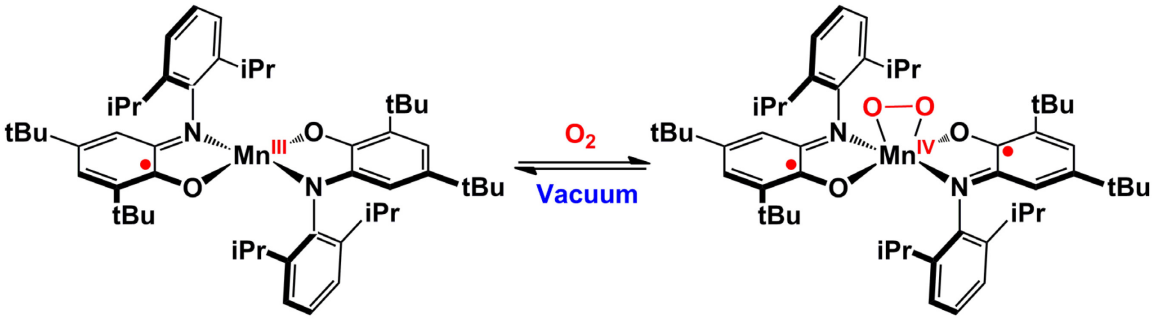

Scheme 13. The reversible binding of O_2 by Mn^{III}(ap)(isq).

This ability of Mn^{III}(ap)(isq) to reversibly bind O_2 was previous reported, where the O_2 adduct to Mn^{III}(ap)(isq) was formulated as an η^2-$[O_2]^{2-}$ peroxo complex $Mn^{IV}(O_2^{2-})(isq)_2$.[39-40] The conversion of Mn^{III}(ap)(isq) to $Mn^{III}Br(isq)_2$ is a $1e^-$ oxidation. However, the O_2 adduct was previously reported as $Mn^{IV}(O_2^{2-})(isq)_2$, implying that O_2 binding occurs with $2e^-$ oxidation of Mn^{III}(ap)(isq). Assuming $MgBr_2$ reacts as a source of Br^-, the reaction with $MgBr_2$ formally reduces the manganese center and displaces $[O_2]^{\bullet-}$, as shown in **Scheme 14**.

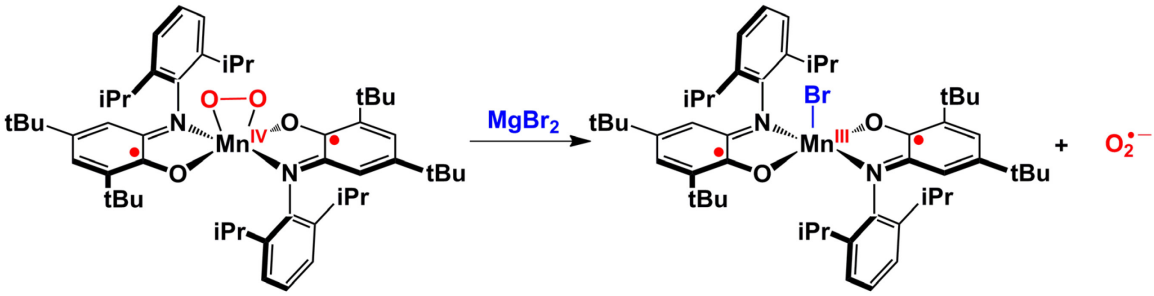

Scheme 14. The displacement of O_2 by magnesium bromide.

A clue to understanding the cation-specific branching behavior came from examination of the solution stabilities of $Mn^{III}Br(isq)_2$ in O_2. Exposure of a THF solution of $Mn^{III}Br(isq)_2$ to 1 atm O_2 results in complete complex degradation and extrusion of free ibq ligand over 5 h at 25 °C. However, addition of excess (10 equiv) $MgBr_2$ to the

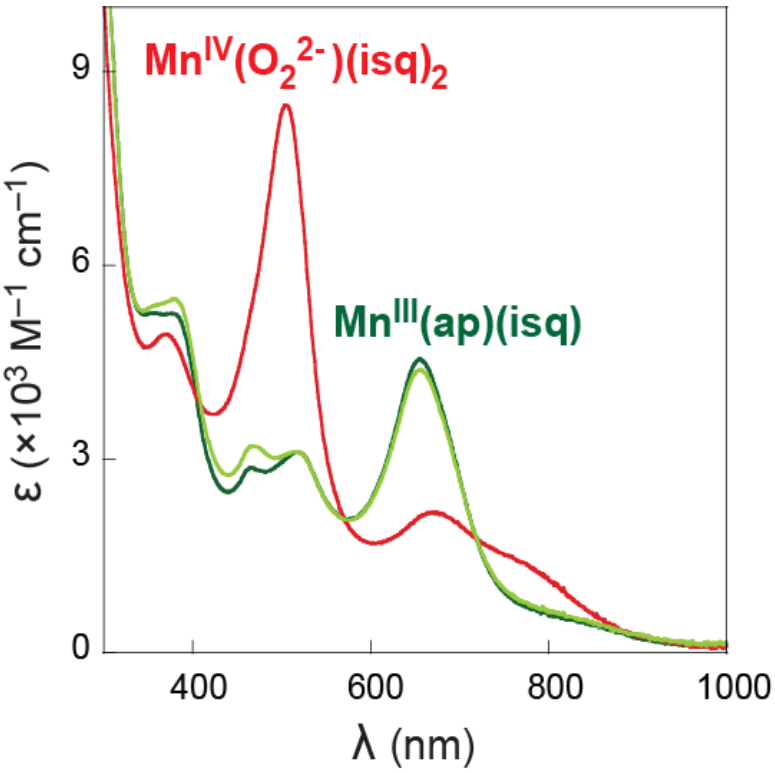

Figure 4.12. UV–vis absorption spectra showing reversible O_2 binding at Mn^{III}(ap)(isq). Addition of 1 atm O_2 to 0.08 mM Mn^{III}(ap)(isq) in THF (dark green line) generates $Mn^{IV}(O_2^{2-})(isq)_2$.(red line). Degassing the solution regenerates Mn^{III}(ap)(isq) (light green line).

$Mn^{III}Br(isq)_2$ solution prior to O_2 exposure significantly inhibits the degradation process; 33% of the $Mn^{III}Br(isq)_2$ is intact after 24 h under the same conditions **(Figure 4.13)**. This suggested that in samples of $[Mn^{III}(ap)_2]^-$ derived from reactions with 2 equiv PhMgBr, the magnesium bromide byproducts trap and stabilize an O_2-sensitive $[Mn^{III}(isq)_2]^+$ fragment, preventing oxidative degradation by formation of a comparatively robust $Mn^{III}Br(isq)_2$ complex. Accordingly, addition of excess $MgBr_2$ to the putative peroxo complex results in an immediate color change from red to green that corresponds to formation of $Mn^{III}Br(isq)_2$ by formal displacement of $[O_2]^{\bullet-}$.

The sum of the reactions observed in oxidative coupling of PhMgBr by $Mn^{III}Br(isq)_2$ and the reoxidation of $[Mn^{III}(ap)_2]^-$ by O_2 constitutes a complete cycle for catalytic aerobic homocoupling of PhMgBr (**Scheme 15**).

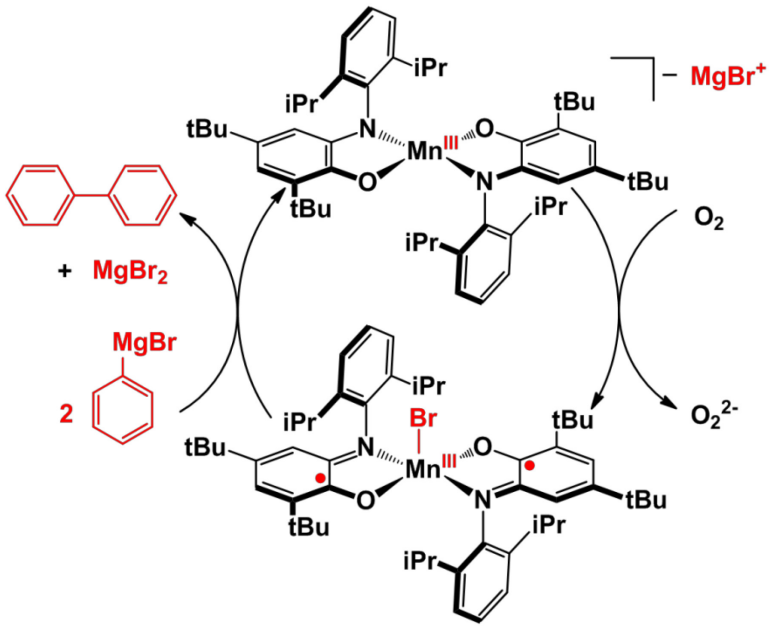

Scheme 15. Catalytic aerobic homocoupling of PhMgBr by $Mn^{III}Br(isq)_2$.

Accordingly, addition of 20 equiv PhMgBr and 1 atm O_2 to NMR tubes containing $Mn^{III}Br(isq)_2$ in THF–d_8 gives Ph–Ph in 72% yield within 10 min at 25 °C, as determined

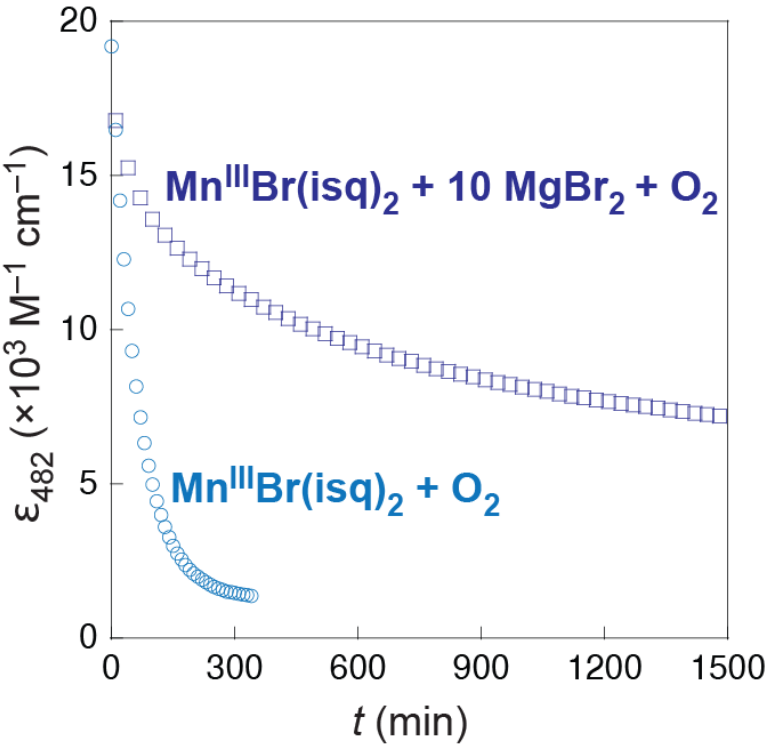

Figure 4.11. Time-resolved data at 482 nm showing the decomposition of 0.08 mM $Mn^{III}Br(isq)_2$ in THF under 1 atm O_2 (light blue ○) and the effect of 10 equiv $MgBr_2$ on the same reaction (dark blue □).

by ^{1}H NMR spectroscopy. A control reaction performed under the same conditions, but without $Mn^{III}Br(isq)_2$, showed complete consumption of PhMgBr, but Ph–Ph comprised less than 5% of the total phenyl-containing products.

4.2.4 Scope of Oxidative Coupling Reactions.

To expand the substrates scope, reactions were performed with different Grignard reagents. A catalytic reaction of 5% $Mn^{III}Br(isq)_2$ and sp hybridized phenylethynylmagnesium bromide was placed under 1 atm O_2 in THF–d_8 and monitored by NMR **(Scheme 16)**. The reaction yielded 1,4-diphenylbutadiyne in 60% yield.

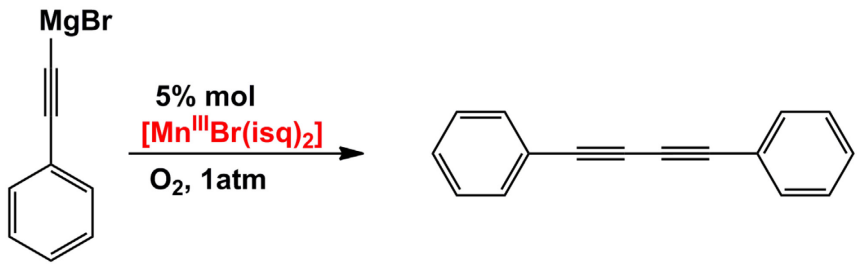

Scheme 16. The oxidative coupling of phenylmagnesium bromide by $Mn^{III}Br(isq)_2$.

Oxidative coupling reactions were also attempted with sp^3 grignard reageants such as pentylmagnesium bromide. Addition of the reagent to catalytic amounts of $Mn^{III}Br(isq)_2$ in THF led to rapid decomposition of the catalyst, forming a black precipitate from solution. The organic products observed from the reaction via GC-MS were a mixture of pentane, pentene and decane, which are indicative of a radical disproportionation mechanism.

Oxidative coupling of organic substrates with acidic C–H bonds was also attempted. Benzoxazole was deprotonated using lithium bis(trimethylsilyl)amide(LiHMDS) and then reacted with with $Mn^{III}Br(isq)_2$ in THF solutions to afford the homocoupled dimer **(Scheme17)**.

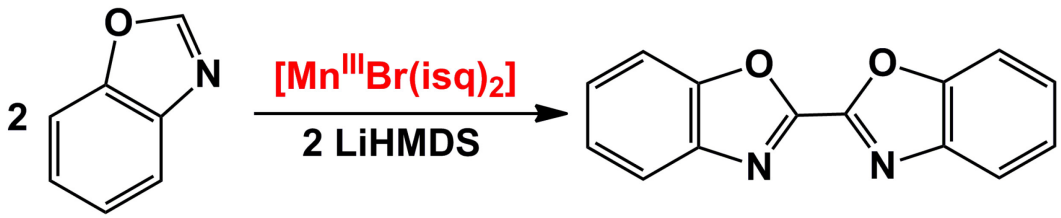

Scheme 17. The oxidative coupling of benzoxazole using $Mn^{III}Br(isq)_2$.

However, the reaction was limited to stoichiometric reactions because $Mn^{III}Br(isq)$ decomposes in the presence of excess LiHMDS, which is needed to deprotonate the acidic C–H bond.

The oxidative homocoupling of anilines to form azo dyes was also attempted. Successful stoichiometric coupling reactions were performed by deprotonation of *p*-toluidine with LiHMDS and reacting with $Mn^{III}Br(isq)_2$ in the presence of O_2 to form azobenzene. (**Scheme 18**).

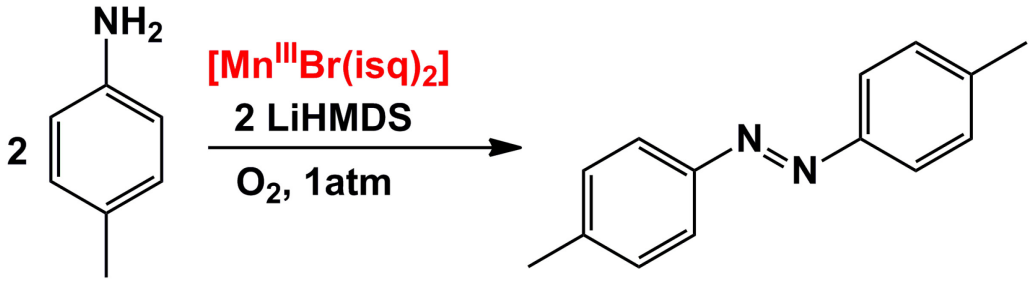

Scheme 18. The oxidative homocoupling of p-toluidine using $Mn^{III}Br(isq)_2$..

This reaction was also limited to stoichiometric reactions because of the difficulty of finding a suitable base to deprotonate p-toluidine. Reactions attempted with Et_3N, DIEA or DABCO were unsuccessful. The magnesium anilide of p-toluidine was prepared by adding stoichiometric amounts of pentylmagnesium bromide. However, the reaction of the magnesium anilide with O_2 in the absence of $Mn^{III}Br(isq)$, rapidly affords a mixture of azobenzene and azoxybenzene which competes with the metal catalyzed process.

4.3 Discussion.

4.3.1 Coupling of PhMgBr by $Mn^{III}Br(isq)$.

A well defined series of manganese(III) amidophenolate complexes was synthesized and characterized crystallographically. The differences in C–O, C–N and aromatic C–C bond lengths observed in each crystal structure showed that the redox chemistry was preferentially occurring at the ligand and were used to assign the oxidation state for each complex. The capacity of the redox-active aminophenol ligands to stabilize four-coordinate manganese(III) over oxidation states spanning two redox equivalents prompted us to pursue $2e^-$ organometallic reactions for coupling catalysis.

Reactions of $Mn^{III}Br(isq)_2$ with 2 equiv of PhMgBr afforded 1 equiv biphenyl and $[Mn^{III}(ap)_2]^-$. This reaction can be performed sequentially by adding 1 equiv of PhMgBr to $Mn^{III}Br(isq)_2$ to form 0.5 equiv of biphenyl and $Mn^{III}(ap)(isq)$ followed by another equiv of PhMgBr to form 0.5 equiv of biphenyl and$[Mn^{III}(ap)_2]^-$. The potential intermediacy of $Mn^{III}(ap)(isq)$ in stepwise reaction implies that aryl–aryl coupling occurs by a radical $1e^-$ mechanism, however a concerted $2e^-$ pathway is also possible. The two

possible pathways are outlined in **Scheme 19**. For the concerted $2e^-$ pathway, the independent reaction of $Mn^{III}Br(isq)_2$ and $[Mn^{III}(ap)_2]^-$ to undergo rapid comproportionation to generate 2 $Mn^{III}(ap)(isq)$ can be viable alternative for the formation of. $Mn^{III}(ap)(isq)$ in reaction of 1 equiv of PhMgBr with $Mn^{III}Br(isq)_2$. To rule out the radical $1e^-$ pathway, we prepared 2-(3-buten-1-yl)phenylmagnesium iodide, containing a pendant double bond, and reacted 1 equiv of the Grignard reagent with 1 equiv of $Mn^{III}Br(isq)_2$. The resulting non-cyclized biphenyl is the only coupled product, and the 5-exo products of intramolecular radical cyclization, which are indicators of free radical intermediates, are formed in only low yield. Also, phenyl radical is known to react with THF with a bimolecular rate constant $>10^6$ M^{-1} s^{-1},[45] suggesting that biphenyl formation via a bimolecular reaction of free aryl radicals in the second step of radical $1e^-$ pathway is statistically implausible in dilute solutions.

The details of the concerted $2e^-$ pathway mechanism regarding the formation of manganese(III) aryl species is not known. It is suspected that transarylation occurs to generate highly reactive, unobservable organomanganese(III) intermediates. In this regard, the previously reported aryl–aryl reductive elimination from redox active ligand d^0 zirconium complexes provides good precedent for the capacity of the [isq]"– ligands to mediate a similar concerted 2e– reaction.[29]

4.3.2 Reduction of O_2.

The oxidation $[Mn^{III}(ap)_2]^-$ by dioxygen is cation specific, with different counterions leading to different products. Reactions of $CoCp^*_2[Mn^{III}(ap)_2]$ with O_2

Observed reaction pathway.

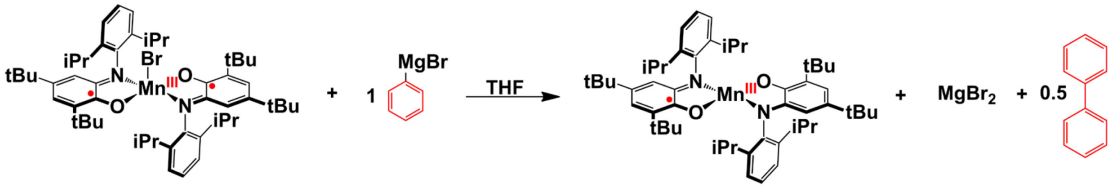

Radical 1e⁻ pathway.

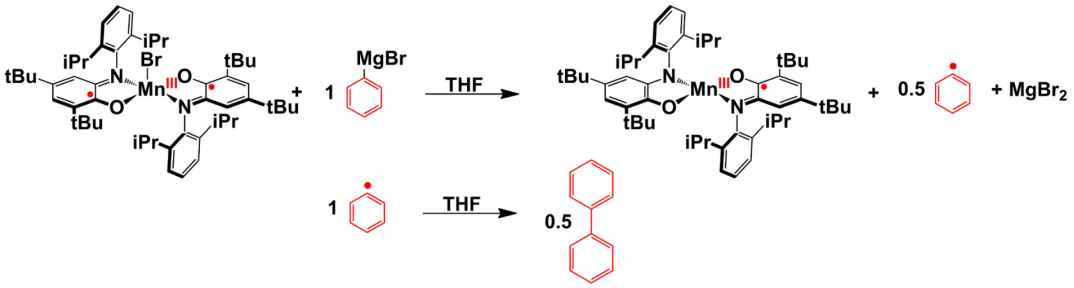

Concerted 2e⁻ pathway followed by comproportionation.

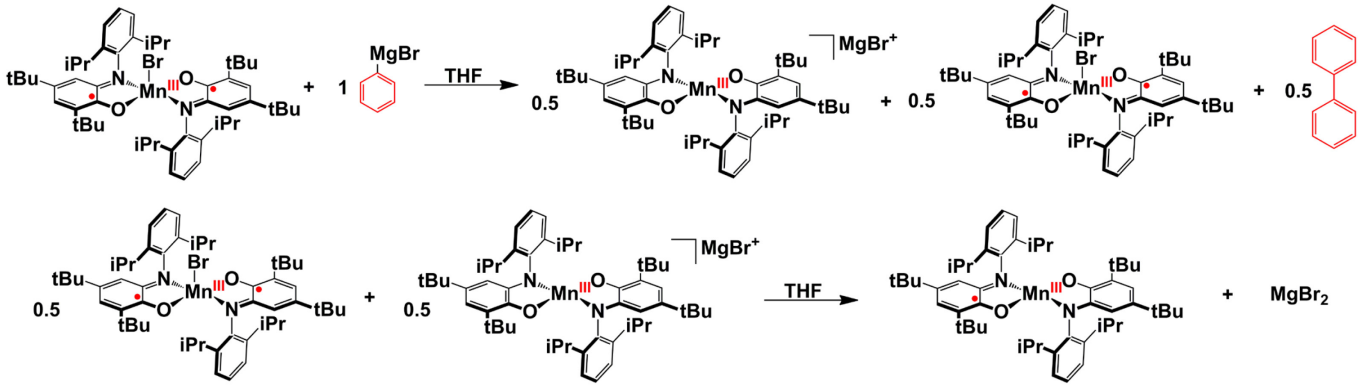

Scheme 19. Balanced equation for the reaction of $Mn^{III}Br(isq)_2$ with 1 PhMgBr to generate $Mn^{III}(ap)(isq)$ and 0.5 Ph–Ph and two plausible mechanisms

proceeds through a series of intermediates to form $Mn^{IV}O_2(isq)_2$ which rapidly decomposes to form free ibq. $MgBr[Mn^{III}(ap)_2]$, which is generated in situ with 2 equiv of PhMgBr, reacts with O_2 and also proceeds through the same intermediates, however the end product is $Mn^{III}Br(isq)_2$. Independent reactions of $Mn^{IV}O_2(isq)_2$ with $MgBr_2$ show that Br^- can displace the O_2 adduct to afford $Mn^{III}Br(isq)_2$. All of these results are rationalized by the proposed reaction sequence in **Scheme 20**, in which all $[Mn^{III}(ap)_2]^-$ samples are oxidized by O_2 via the same two steps. In step (*i*) an irreversible reaction of $[Mn^{III}(ap)_2]^-$ with O_2 generates the products of outer-sphere $1e^-$ transfer. A second reaction with O_2 in step (*ii*) generates the red dioxygen complex, $Mn^{IV}O_2(isq)_2$. Because Br^- substitutes the reduced O_2 ligand, reactions performed in the presence of $MgBr_2$ are converted to $Mn^{III}Br(isq)_2$ in step (*iii*). In the absence of a Br^- trap, the putative peroxo complex is unstable toward oxidative extrusion of the quinone ligand.

Note that the net conversion of $Mn^{III}(ap)(isq)$ to $Mn^{III}Br(isq)_2$ is a 1e– oxidation. However, the O_2 adduct was previously reported as $Mn^{IV}O_2(isq)_2$, implying that O_2 binding occurs with 2e– oxidation of $Mn^{III}(ap)(isq)$. Assuming $MgBr_2$ reacts as a source of Br–, the reaction of $Mn^{IV}O_2(isq)_2$ with $MgBr_2$ to make $Mn^{III}Br(isq)_2$ formally reduces the manganese center and displaces superoxide. At this time, the fate of the reduced O_2 is unknown. We have no evidence for formation of superoxide in the reactions, but we note that salts precipitate from the THF solutions during the reaction. It is reasonable that these may contain superoxide and/or peroxides.

4.3.3 Advantages of using $Mn^{III}Br(isq)_2$ as a catalyst.

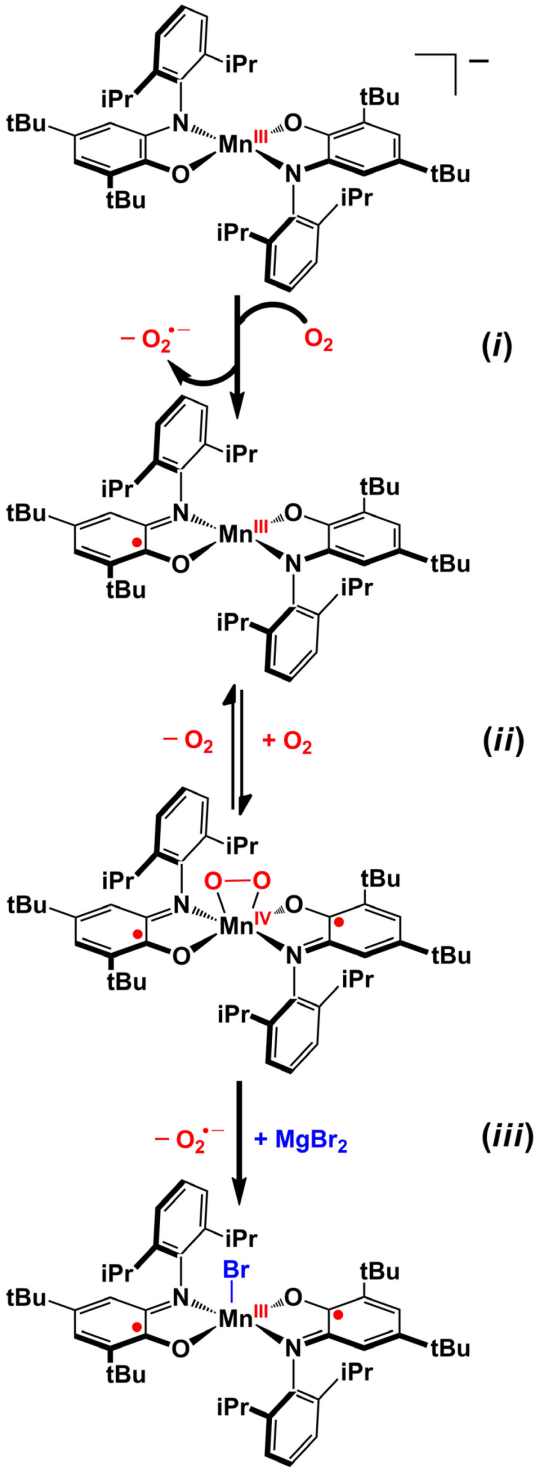

Scheme 20. The stepwise oxidation of $[Mn^{III}(ap)_2]^-$. Superoxide $[O_2]^{\bullet-}$ was not observed in steps (*i*) or (*iii*). It is depicted as $[O_2]^{\bullet-}$ to balance the charge with the observed manganese products. The O_2 adduct formed in step (*ii*) is depicted as containing an η^2-peroxo ligand in $[Mn^{IV}(O_2^{2-})(isq)_2]$ to be consistent with previous reports.[39-40]

The ability of $Mn^{III}Br(isq)_2$ to catalytically mediate coupling of aryl Grignard reagents parallels well-established oxidative coupling reactions using simple di- and trivalent metal halides. In the case of $MnCl_2$, which is catalytically active for aerobic coupling of Grignard reagents, little is known about the intermediates involved in the reaction. The reduced fragment is suspected to be an organomanganese(II) fragment but no evidence is presented to support these claims.[18] Little is known about the nature of the oxidized species responsible for the coupling reaction.[18]

The main advantage of using $Mn^{III}Br(isq)_2$ as catalyst for aerobic homocoupling of aryl Grignard reagents versus the recently reported coupling reaction using manganese and iron salts is its unique stability over a range of oxidation states, affording opportunities to investigate and optimize each of the reaction steps. For example, we are able to observe that the selectivity in the $2e^-$ reaction with O_2 derives from the ability of magnesium bromides to trap and stabilize the $[Mn^{III}(isq)2]^+$ fragment against oxidative catalyst degradation. In the PhMgBr coupling reagents, the Br^- trap derives from the substrate itself. But the successful demonstration of facile trapping by exogenous $MgBr_2$ provides a template to pursue other oxidative coupling reactions whereby X^- trapping provides a mechanism for redox control in $2e^-$ reactions of $[Mn^{III}(ap)_2]^-$ with O_2. Furthermore, the surprising ability of $Mn^{III}Br(isq)_2$ to mediate $2e^-$ aryl–aryl coupling without forming free radical intermediates opens new avenues to pursue oxidative cross coupling reactions. In using this well defined system, future experiments can be aimed at expanding the scope of the aerobic coupling reactions, as well as evaluating the capacity of modified redox-active ligands with varying steric and electronic properties to engender substrate selectivity that would not be feasible using simple metal halide catalysts.

4.4. Conclusions.

In conclusion, $Mn^{III}Br(isq)_2$ is a uniquely well-defined Earth-abundant metal catalyst for aerobic homocoupling of PhMgBr. The capacity of the redox-active aminophenol-derived ligands to mediate the net $2e^-$ reaction without a change in manganese(III) oxidation state makes the reduced metal complex unusually stable in solution. This stabilizing effect in turn facilitates a series of slower redox-active ligand-mediated reactions wherein $[Mn^{III}(ap)_2]^-$ is oxidized by O_2 to regenerate $Mn^{III}Br(isq)_2$. Because O_2 functions as a net $2e^-$ oxidant, the catalyst functions without the need for a sacrificial chemical oxidant. Selectivity in the $2e^-$ reaction with O_2 derives from the ability of magnesium bromides to trap and stabilize the $[Mn^{III}(isq)_2]^+$ fragment against oxidative catalyst degradation. In the PhMgBr coupling reagents, the Br^- trap derives from the substrate itself. However, the successful demonstration of facile trapping by exogenous $MgBr_2$ provides a template to pursue other oxidative coupling reactions whereby X^- trapping provides a mechanism for redox control in $2e^-$ reactions of $[Mn^{III}(ap)_2]^-$ with O_2.

4.5 Experimental Details.

4.5.1. General Considerations.

Unless otherwise specified, all manipulations were performed under anaerobic conditions using standard vacuum line techniques, or in an inert atmosphere glove box under purified nitrogen. NMR spectra were acquired on a Varian Mercury 300

spectrometer (300.323 MHz for ^{1}H) at ambient temperature. Chemical shifts are reported in parts per million (ppm) relative to TMS, with the residual solvent peak serving as an internal reference. UV–visible absorption spectra were acquired using a Varian Cary 50 spectrophotometer equipped with a water-jacketed cell holder fitted to a Peltier temperature controller. All electronic absorption spectra were recorded at 25 °C in 1 cm quartz cells unless specified otherwise. IR spectra were obtained by attenuated total reflection (ATR) through a diamond plate on a Bruker Optics Alpha-P FTIR spectrometer. Elemental analyses were performed by Atlantic Microlab, Inc. in Norcross, GA. All analyses were performed in duplicate, and the reported compositions are the average of the two runs.

4.5.2. Methods and Materials.

Anhydrous acetonitrile (MeCN), tetrahydrofuran (THF), dichloromethane (CH_2Cl_2), toluene, and pentane solvents for air- and moisture-sensitive manipulations were purchased from Sigma-Aldrich, further dried by passage through columns of activated alumina, degassed by at least three freeze-pump-thaw cycles, and stored under N_2 prior to use. Oxygen (ultra high purity) was used as received from Airgas, Inc. Deuterated tetrahydrofuran (THF–d_8) was purchased from Cambridge Isotope Laboratories, degassed by three freeze-pump-thaw cycles, vacuum distilled from CaH_2 or $Na_{(s)}$, respectively, and stored under a dry N_2 atmosphere prior to use. Mn^{III}(ap)(isq)[40] and 2,4-di-*tert*-butyl-6-(2,6-diisopropylphenylimino)benzoquinone (**ibq**) [46] were prepared by literature methods. All characterization data matched those referenced. $Mn(ClO_4)_2$•$6H_2O$ and $MnBr_2$•$4H_2O$

were purchased from Strem Chemical, Inc. All other chemicals were purchased from Sigma-Aldrich and used as received.

4.5.3. Synthesis of $(Cp^*_2Co)[Mn^{III}(ap_2)]$.

A 100 mL round bottom flask was charged with Mn^{III}(ap)(isq) (0.140 g, 0.170 mmol), a stir bar, and MeCN (20 mL) to afford a dark green suspension. Addition of Cp^*_2Co (55 mg, 0.17 mmol) to the vigorously stirring Mn^{III}(ap)(isq) mixture gave a rust-brown solution over 12 h. The solution was filtered, reduced in volume, and stored at –25 °C for 48 h to deposit $(Cp^*_2Co)[Mn^{III}(ap)_2]$ (0.150 g, 0.131 mmol, 77%) as brown single crystals suitable for X-ray diffraction analysis. UV-vis (THF) λ_{max}, nm (ε, M^{-1} cm^{-1}): 650 (560). A single crystal of the same sample of $(Cp^*_2Co)[Mn^{III}(ap)_2]$ used for elemental analysis was determined. It includes two MeCN solvate molecules per manganese, so the reported analysis is for $(Cp^*_2Co)[Mn^{III}(ap)_2]$•2MeCN. Anal. Calcd for $C_{76}H_{110}CoMnN4O_2$: C, 74.48; H, 9.05; N, 4.57; Found: C, 72.94; H, 8.92; N 4.86.

4.5.4. Synthesis of $Mn^{III}Br(isq)_2$.

A 5 dram scintillation vial was charged with ibq (0.19 g, 0.50 mmol) and THF (10 mL), and the resulting red solution was stirred for 4 h over excess freshly cut sodium metal to afford a pale yellow solution containing the 2,4-di-*tert*-butyl-6-(2,6-diisopropylphenylamido)phenolate ($[ap]^{2-}$) dianion. A second aliquot of ibq (0.19 g, 0.50 mmol) was added to yield a dark blue solution of the comproportionation product 2,4-di-

tert-butyl-6-(2,6-diisopropylphenylimino)semiquinonate ([isq]$^{\bullet-}$). In a separate 100 mL evaporating flask, $MnBr_2 \bullet 4H_2O$ (0.39 g, 1.0 mmol) and ibq (0.38 g, 1.0 mmol)) were dissolved in THF (10 mL) to form a red solution. The blue [isq]$^{\bullet-}$ radical anion was then combined with the red manganese solution to immediately generate a dark green mixture. The solution was stirred for 12 h, filtered to remove salts, and reduced to dryness *in vacuo* to yield a green powder. The solids were taken up in minimal hexane, filtered, and stored at –10 °C for 24 h to deposit a green precipitate. The solids were collected by vacuum filtration of the cold reaction mixture and dried *in vacuo* to yield $Mn^{III}Br(isq)_2$ (0.42 g, 0.47 mmol, 47%) as green single crystals suitable for X-ray diffraction. UV-vis (THF) λ_{max}, nm (ε, M^{-1} cm^{-1}): 400 (10000), 482 (22000), 627(3800), 685(4200). FTIR (ATR): 2960 (s), 2924 (m), 2866 (m), 1462 (m), 1438 (m), 1402 (m), 1385 (m), 1362 (m), 1325 (m), 1305 (m), 1251 (m), 1240 (sh), 1199 (m), 1168 (m), 1100 (w), 1028 (w), 935 (w), 914 (w), 891 (m), 863 (m), 826 (w), 799 (m), 767 (w), 716 (m), 672 (m), 651 (w), 579 (m), 544 (m), 499 (m), 425 (w) cm^{-1}. A single crystal of the same sample of $Mn^{III}Br(isq)_2$ used for elemental analysis was determined. It includes 0.42 hexane solvate molecules per manganese, so the reported analysis is for $Mn^{III}Br(isq)_2 \bullet 0.42C_6H_{14}$. Anal. Calcd for $C_{54.52}H_{79.88}BrMnN_2O_2$: C, 70.40; H, 8.66; N, 3.01; Found: C, 70.16; H, 8.99; N 2.89.

4.5.5. Synthesis of $Mn^{III}(OClO_3)(isq_2)$.

This complex was prepared using $Mn(ClO_4)_2 \bullet 4H_2O$ (0.39 g, 1.0 mmol) in a procedure directly analogous to that described above for $Mn^{III}Br(isq)_2$. Following isolation of the

green powder the solids were washed with toluene, taken up in minimal CH_2Cl_2, filtered, and pentane (10 mL) was then added to the solution. Storage at –20 °C deposited $Mn^{III}(OClO_3)(isq)_2$ (0.150 g, 0.160 mmol, 16%) as X-ray quality green crystals. UV-vis (THF) λ_{max}, nm (ε, M^{-1} cm^{-1}): 462 (14000), 608 (2700), 650 (2600). FT-IR (ATR): 3498 (br), 2963 (m), 2907 (sh, w), 2867 (w), 1621 (w), 1463 (m), 1440 (w), 1402 (w), 1387 (w), 1363 (m), 1308 (m) 1250 (w), 1159 (s), 1075 (vs), 1010 (vs), 862 (s), 825 (m), 799 (m), 717 (m), 674 (m), 619 (s), 580 (m), 549 (s), 489 (s), 464 (s), 424 (s) cm^{-1}. Samples of $Mn^{III}(OClO_3)(isq)_2$ for elemental analysis were obtained from concentrated CH_2Cl_2 solutions, as described above. The reported analysis is for $Mn^{III}(OClO_3)(isq)_2 \bullet 2.75CH_2Cl_2$, and the presence of CH_2Cl_2 in the sample was confirmed by ^1H NMR spectroscopy. Anal. Calcd for $C_{54.75}H_{79.5}Cl6.5MnN_2O_6$: C, 57.33; H, 6.99; N, 2.44; Found: C, 56.92; H, 7.39; N 2.64.

4.5.6. Synthesis of $Mn^{III}(Cl)(isq_2)$.

This complex was prepared using $Mn(Cl)_2$ (0.305g, 1.0 mmol) in a procedure directly analogous to that described above for $Mn^{III}Br(isq)_2$. The complex has been characterized previously [44].

4.5.7. Synthesis of $Mn^{III}(I)(isq_2)$.

This complex was prepared using $Mn(I)_2$ (0.305g, 1.0 mmol) in a procedure directly analogous to that described above for $Mn^{III}Br(isq)_2$. Following isolation of the brown

powder the solids were taken up in minimal hexane, filtered, and stored at –10 °C for 24 h to deposit a brown precipitate. The solids were collected by vacuum filtration of the cold reaction mixture and dried *in vacuo* to yield $Mn^{III}I(isq)_2$ (0.38 g, 0.40 mmol, 40%) as brown single crystals not suitable for X-ray diffraction. at UV-vis (THF) λ_{max}, nm (ε, M^{-1} cm^{-1}): 410 (13000) 497 (21000), 670 (5000), 727 (6500). FT-IR (ATR): 2959 (m), 2924 (sh, w), 2864 (w), 1530 (w), 1460 (m), 1437 (w), 1400 (w), 1384 (w), 1361 (m), 1321 (w), 1301 (m) 1250 (w), 1239 (w) 1199 (sh, w) 1166 (s), 1100 (w), 1027 (w), 996 (w), 913 (w) 863 (w), 826 (m), 799 (m), 716 (w), 672 (w), 651 (w), 579 (m), 545 (m), 499 (w), 426 (m) cm^{-1}. Samples of $Mn^{III}I(isq)_2$ for elemental analysis were obtained from concentrated *n*-hexane solutions, as described above. The reported analysis is for $Mn^{III}I(isq)_2$• 0.6 C_6H_{14}, and the presence of C_6H_{14} in the sample was confirmed by ^1H NMR spectroscopy. Anal. Calcd for $C_{55.6}H_{80.4}IMnN_2O_2$: C, 67.27; H, 8.37; N, 2.82; Found: C, 67.29; H, 8.34; N 2.87.

4.5.8 X-Ray Crystallography.

Crystals of $Mn^{III}(isq)(ap)$•1.25(C_7H_8), $Mn^{III}(ap)(isq)(CH_3CN)$, ($Cp^*_2Co$)[$Mn^{III}(ap)_2$]•2MeCN, $Mn^{III}Br(isq)_2$•0.42C_6H_{14} and [$Mn^{III}(OClO_3)(isq)_2$]•0.25CH_2Cl_2•0.25C_7H_8, suitable for X-ray diffraction analysis were coated with Paratone N oil, suspended on small fiber loops and placed in a cooled nitrogen gas stream at 173 K on a Bruker D8 APEX II CCD sealed tube diffractometer. Data for $Mn^{III}Br(isq)_2$•0.42C_6H_{14} was obtained with graphite monochromated Cu Kα (λ = 1.54178 Å) radiation while diffraction data for all the others were collected using

graphite monochromated Mo Kα (λ = 0.71073Å) radiation. Data collection procedures, data processing and programs were the same for all samples. Frames were measured using a series of combinations of phi and omega scans with 10 s frame exposures and 0.5° frame widths. Data collection, indexing and initial cell refinements were all carried out using APEX II software.[47] Frame integration and final cell refinements were done using SAINT software.[48] The final cell parameters were determined from least-squares refinement on 9966 reflections for $Mn^{III}(isq)(ap)\bullet 1.25(C_7H_8$, 6409 reflections for $Mn^{III}(ap)(isq)(CH_3CN)$, 9007 reflections for $(Cp^*_2Co)[Mn^{III}(ap)_2]\bullet 2MeCN$, 2673 reflections for $Mn^{III}Br(isq)_2\bullet 0.42C_6H_{14}$ and 5961 reflections for $[Mn^{III}(OClO_3)(isq)_2]\bullet 0.25CH_2Cl_2\bullet 0.25C_7H_8$. The structures were solved using direct methods and difference Fourier techniques with the SHELXTL program package.[49] Hydrogen atoms were placed in their expected chemical positions using the HFIX command and were included in the final cycles of least-squares with isotropic U_{ij}'s related to the atoms ridden upon. All non-hydrogen atoms in $Mn^{III}(ap)(isq)(CH_3CN)$ and $(Cp^*_2Co)[Mn^{III}(ap)_2]\bullet 2MeCN$ were refined anisotropically, but only the metal-containing fragments in the others were refined anisotropically. Scattering factors and anomalous dispersion corrections are taken from the *International Tables for X-ray Crystallography.*[50] Other details of data collection and structure refinement are provided in **Table 4.2**.

4.5.9 Catalytic Aerobic Homocoupling Reactions.

In a representative procedure, a J. Young brand NMR tube with a Teflon screw cap was charged with 0.011 M $Mn^{III}Br(isq)_2$ (0.70 mL, 0.0073 mmol) in THF–d_8 and 0.92 M PhMgBr (0.160 mL, 0.15 mmol) in THF was added. The tube was sealed under N_2 and an initial ^1H NMR spectrum was acquired. The sample was subsequently degassed on a high-vacuum line by three freeze–pump–thaw cycles, backfilled with 1 atm of O_2, and shaken vigorously. The reaction progress was monitored by ^1H NMR spectroscopy over 10 min. During the course of the reaction, the tube was shaken periodically to maintain the concentration of dissolved O_2.

Table 4.2. Crystallographic Data and Structure Parameters for $Mn^{III}(isq)(ap)\bullet 1.25(C_7H_8)$, $Mn^{III}(ap)(isq)(CH_3CN)$, and $(Cp^*_2Co)[Mn^{III}(ap)_2]\bullet 2MeCN$

Complex	$Mn^{III}(isq)(ap)\bullet 1.25(C_7H_8)$	$Mn^{III}(isq)(ap)\bullet(CH_3CN)$	$CoCp^*_2[Mn^{III}(ap)_2]\bullet 2(CH_3CN)$
Identification code	cjr1166	cjr1185	cjr931s
Empirical formula	$C_{60.75}H_{84}N_2O_2Mn$	$C_{54}H_{77}N_3O_2Mn$	$C_{76}H_{110}N_4O_2MnCo$
Formula weight	929.24	855.13	1225.55
Temperature (K)	173(2)	173(2)	173(2)
Crystal system	Monoclinic	Triclinic	Monoclinic
Space group	PC	P-1	P2(1)
Unit cell dimensions			
a (Å)	11.8819(13)	11.9952(14)	10.967(2)
b (Å)	18.726(2)	12.2986(14)	27.726(6)
c (Å)	17.0248(14)	18.844(2)	13.207(3)
a (°)	90	90.663(2)	90
b (°)	129.544	102.355(2)	113.718(3)
g (°)	90	106.702(2)	90
Volume ($Å^3$)	2921.1(5)	2593.1(5)	3676.5(13)
Z	2	2	2
Calculated Density (g cm^{-1})	1.056	1.095	1.107
Absorption coefficient (mm^{-1})	0.265	0.294	0.442
Crystal size (mm)	0.38 x 0.36 x 0.10	0.30 x 0.23 x 0.11	0.33 x 0.15 x 0.13
θ range for data collection (°)	1.89-27.88	1.90-27.88	1.47-30.47
Index ranges	-15<=h<=15, -24<=k<=24 -22<=l<=22	-15<=h<=15, -16<=k<=16 -24<=l<=24	-15<=h<=15 -39<=k<=39 -18<=l<=18
Reflections collected/unique	49244/13956	44268/12327	74125/22245
Goodness-of-fit on F2	1.099	1.055	1.024
Final R indices [I>2sigma(I)]	0.0691	0.0511	0.0652
R indices (all data)	0.2134	0.1503	0.1736

Table 4.2. Crystallographic Data and Structure Parameters for $Mn^{III}Br(isq)_2 \bullet 0.42C_6H_{14}$ and $[Mn^{III}(OClO_3)(isq)_2] \bullet 0.25CH_2Cl_2 \bullet 0.25C_7H_8$

Complex	$Mn^{III}Br(isq)_2 \bullet 0.42(C_6H_{14})$	$Mn^{III}OClO_3(isq)_2 \bullet 0.25(CH_2Cl_2)0.25(C_7H_8)$
Identification code	final	cjr926_1s
Empirical formula	$C_{54.52}\ H_{79.88}\ N_2O_2BrMn$	$C_{54}H_{76.50}Cl_{1.50}N_2O_6Mn$
Formula weight	930.17	957.79
Temperature (K)	173(2)	173(2)
Crystal system	Monoclinic	Monoclinic
Space group	P2(1)/n	P2(1)
Unit cell dimensions		
a (Å)	16.1855(18)	11.4685(17)
b (Å)	20.6757(17)	23.313(4)
c (Å)	17.2044(17)	20.068(3)
a (°)	90	90
b (°)	91.203(8)	94.309(2)
g (°)	90°	90
Volume ($Å^3$)	5756.1(10)	5350.4(14)
Z	4	4
Calculated Density (g cm^{-1})	1.073	1.189
Absorption coefficient (mm^{-1})	2.94	0.369
Crystal size (mm)	0.22 x 0.11 x 0.09	0.37 x 0.18 x 0.01
θ range for data collection (°)	3.34-66.55	1.75-27.87
Index ranges	19<=h<=18	-15<=h<=15
	-24<=k<=23	-30<=k<=30
	-20<=l<=20	-26<=l<=26
Reflections collected/unique	35726/10034	91288/25468
Goodness-of-fit on F2	1.067	1.008
Final R indices [I>2sigma(I)]	0.0782	0.0624
R indices (all data)	0.2835	0.1311

4.6. Works Cited.

1. Stang, P., *Metal-Catalyzed Cross-Coupling Reactions*. Wiley-VCH Verlag GmbH: 1998.

2. Jana, R.; Pathak, T. P.; Sigman, M. S., Advances in Transition Metal (Pd,Ni,Fe)-Catalyzed Cross-Coupling Reactions Using Alkyl-organometallics as Reaction Partners. *Chemical Reviews* **2011,** *111* (3), 1417-1492, doi:10.1021/cr100327p.

3. Tamao, K.; Hiyama, T.; Niegishi, E.-i., Preface. *Journal of Organometallic Chemistry* **2002,** *653* (1-2), 1-4, doi:10.1016/s0022-328x(02)01391-8.

4. Littke, A. F.; Fu, G. C., Palladium-Catalyzed Coupling Reactions of Aryl Chlorides. *Angewandte Chemie International Edition* **2002,** *41* (22), 4176-4211, doi:10.1002/1521-3773(20021115)41:22<4176::aid-anie4176>3.0.co;2-u.

5. Halford, B., Nobel Prize in Chemistry. *Chemical & Engineering News* **2010,** *88* (41), doi:10.1021/cen-v088n041.p007.

6. Ashenhurst, J. A., Intermolecular oxidative cross-coupling of arenes. *Chemical Society Reviews* **2010,** *39* (2), 540-548,

7. Liu, C.; Zhang, H.; Shi, W.; Lei, A., Bond Formations between Two Nucleophiles: Transition Metal Catalyzed Oxidative Cross-Coupling Reactions. *Chemical Reviews* **2011,** *111* (3), 1780-1824, doi:10.1021/cr100379j.

8. Yeung, C. S.; Dong, V. M., Catalytic Dehydrogenative Cross-Coupling: Forming Carbon−Carbon Bonds by Oxidizing Two Carbon−Hydrogen Bonds. *Chemical Reviews* **2011,** *111* (3), 1215-1292, doi:10.1021/cr100280d.

9. Hull, K. L.; Sanford, M. S., Mechanism of Benzoquinone-Promoted Palladium-Catalyzed Oxidative Cross-Coupling Reactions. *Journal of the American Chemical Society* **2009,** *131* (28), 9651-9653, doi:10.1021/ja901952h.

10. Wei, Y.; Su, W., Pd(OAc)2-Catalyzed Oxidative C−H/C−H Cross -Coupling of Electron-Deficient Polyfluoroarenes with Simple Arenes. *Journal of the American Chemical Society* **2010,** *132* (46), 16377-16379, doi:10.1021/ja109383e.

11. Kim, S. H.; Yoon, J.; Chang, S., Palladium-Catalyzed Oxidative Alkynylation of Heterocycles with Terminal Alkynes under Air Conditions. *Organic Letters* **2011,** *13* (6), 1474-1477, doi:10.1021/ol200154s.

12. Tsou, T. T.; Kochi, J. K., Mechanism of biaryl synthesis with nickel complexes. *Journal of the American Chemical Society* **1979,** *101* (25), 7547-7560, doi:10.1021/ja00519a015.

13. Stahl, S. S., Palladium Oxidase Catalysis: Selective Oxidation of Organic Chemicals by Direct Dioxygen-Coupled Turnover. *Angewandte Chemie International Edition* **2004,** *43* (26), 3400-3420, doi:10.1002/anie.200300630.

14. Gilman, H.; Lichtenwalter, M., Relative Reactivities of Organometallic Compounds. XXV. Coupling Reaction with Halides of Group VIII Metals. *Journal of the American Chemical Society* **1939,** *61* (4), 957-959, doi:10.1021/ja01873a056.

15. Kharasch, M. S.; Fields, E. K., Factors Determining the Course and Mechanisms of Grignard Reactions. IV. The Effect of Metallic Halides on the Reaction of Aryl Grignard Reagents and Organic Halides1. *Journal of the American Chemical Society* **1941,** *63* (9), 2316-2320, doi:10.1021/ja01854a006.

16. Seyferth, D., The Grignard Reagents. *Organometallics* **2009,** *28* (6), 1598-1605, doi:10.1021/om900088z.

17. Truong, T.; Alvarado, J.; Tran, L. D.; Daugulis, O., Nickel, Manganese, Cobalt, and Iron-Catalyzed Deprotonative Arene Dimerization. *Organic Letters* **2010,** *12* (6), 1200-1203, doi:10.1021/ol902970z.

18. Cahiez, G.; Moyeux, A.; Buendia, J.; Duplais, C., Manganese- or Iron-Catalyzed Homocoupling of Grignard Reagents Using Atmospheric Oxygen as an Oxidant. *Journal of the American Chemical Society* **2007,** *129* (45), 13788-13789, doi:10.1021/ja075417k.

19. Do, H.-Q.; Daugulis, O., An Aromatic Glaser–Hay Reaction. *Journal of the American Chemical Society* **2009,** *131* (47), 17052-17053, doi:10.1021/ja907479j.

20. King, A. E.; Huffman, L. M.; Casitas, A.; Costas, M.; Ribas, X.; Stahl, S. S., Copper-Catalyzed Aerobic Oxidative Functionalization of an Arene C–H Bond: Evidence for an Aryl-Copper(III) Intermediate. *Journal of the American Chemical Society* **2010,** *132* (34), 12068-12073, doi:10.1021/ja1045378.

21. Sherry, B. D.; Fürstner, A., The Promise and Challenge of Iron-Catalyzed Cross Coupling. *Accounts of Chemical Research* **2008,** *41* (11), 1500-1511, doi:10.1021/ar800039x.

22. Cahiez, G.; Duplais, C.; Buendia, J., Manganese-Catalyzed Oxidative Cross-Coupling of Grignard Reagents with Oxygen as an Oxidant. *Angewandte Chemie International Edition* **2009,** *48* (36), 6731-6734, doi:10.1002/anie.200902188.

23. Liu, W.; Lei, A., Efficient Fe-catalyzed homo-coupling of aryl Grignard reagents using O2 as the oxidant. *Tetrahedron Letters* **2008,** *49* (4), 610-613, doi:10.1016/j.tetlet.2007.11.144.

24. Yoshikai, N.; Matsumoto, A.; Norinder, J.; Nakamura, E., Iron-Catalyzed Direct Arylation of Aryl Pyridines and Imines Using Oxygen as an Oxidant. *Synlett* **2010,** *2010* (EFirst), 313,316, doi:10.1055/s-0029-1219184.

25. Chirik, P. J.; Wieghardt, K., Radical Ligands Confer Nobility on Base-Metal Catalysts. *Science* **2010,** *327* (5967), 794-795, doi:10.1126/science.1183281.

26. Smith, A. L.; Hardcastle, K. I.; Soper, J. D., Redox-Active Ligand-Mediated Oxidative Addition and Reductive Elimination at Square Planar Cobalt(III): Multielectron Reactions for Cross-Coupling. *Journal of the American Chemical Society* **2010,** *132* (41), 14358-14360, doi:10.1021/ja106212w.

27. Smith, A. L.; Clapp, L. A.; Hardcastle, K. I.; Soper, J. D., Redox-active ligand-mediated Co-Cl bond-forming reactions at reducing square planar cobalt(III) centers. *Polyhedron* **2010,** *29* (1), 164-169, doi:10.1016/j.poly.2009.06.046.

28. Blackmore, K. J.; Lal, N.; Ziller, J. W.; Heyduk, A. F., Catalytic reactivity of a zirconium(IV) redox-active ligand complex with 1,2-diphenylhydrazine. *Journal of the American Chemical Society* **2008,** *130* (9), 2728-+, doi:10.1021/ja710611v.

29. Haneline, M. R.; Heyduk, A. F., C-C bond-forming reductive elimination from a zirconium(IV) redox-active ligand complex. *Journal of the American Chemical Society* **2006,** *128* (26), 8410-8411, doi:10.1021/ja061107a.

30. Nguyen, A. I.; Blackmore, K. J.; Carter, S. M.; Zarkesh, R. A.; Heyduk, A. F., One- and Two-Electron Reactivity of a Tantalum(V) Complex with a Redox-Active Tris(amido) Ligand. *Journal of the American Chemical Society* **2009,** *131* (9), 3307-3316, doi:10.1021/ja808542j.

31. Zarkesh, R. A.; Ziller, J. W.; Heyduk, A. F., Four-electron oxidative formation of aryl diazenes using a tantalum redox-active ligand complex. *Angew. Chem.-Int. Edit.* **2008,** *47* (25), 4715-4718, doi:10.1002/anie.200800812.

32. Bart, S. C.; Bowman, A. C.; Lobkovsky, E.; Chirik, P. J., Iron Diazoalkane Chemistry: N−N Bond Hydrogenation and Intramolecular C−H Activation. *Journal of the American Chemical Society* **2007,** *129* (23), 7212-7213, doi:10.1021/ja070056u.

33. Bouwkamp, M. W.; Bowman, A. C.; Lobkovsky, E.; Chirik, P. J., Iron-Catalyzed [2π + 2π] Cycloaddition of α,ω-Dienes: The Importance of Redox-Active Supporting Ligands. *Journal of the American Chemical Society* **2006,** *128* (41), 13340-13341, doi:10.1021/ja064711u.

34. Bowman, A. C.; Milsmann, C.; Atienza, C. C. H.; Lobkovsky, E.; Wieghardt, K.; Chirik, P. J., Synthesis and Molecular and Electronic Structures of Reduced Bis(imino)pyridine Cobalt Dinitrogen Complexes: Ligand versus Metal Reduction. *Journal of the American Chemical Society* **2010,** *132* (5), 1676-1684, doi:10.1021/ja908955t.

35. Manuel, T. D.; Rohde, J.-U., Reaction of a Redox-Active Ligand Complex of Nickel with Dioxygen Probes Ligand-Radical Character. *Journal of the American Chemical Society* **2009,** *131* (43), 15582-15583, doi:10.1021/ja9065943.

36. Chaudhuri, P.; Hess, M.; Müller, J.; Hildenbrand, K.; Bill, E.; Weyhermüller, T.; Wieghardt, K., Aerobic Oxidation of Primary Alcohols (Including Methanol) by Copper(II)− and Zinc(II)−Phenoxyl Radical Catalysts. *Journal of the American Chemical Society* **1999,** *121* (41), 9599-9610, doi:10.1021/ja991481t.

37. Mukherjee, C.; Pieper, U.; Bothe, E.; Bachler, V.; Bill, E.; Weyhermüller, T.; Chaudhuri, P., Ligand-Derived Oxidase Activity. Catalytic Aerial Oxidation of Alcohols (Including Methanol) by Cu(II)-Diradical Complexes. *Inorganic Chemistry* **2008,** *47* (19), 8943-8956, doi:10.1021/ic8009767.

38. Mukherjee, C.; Weyhermüller, T.; Bothe, E.; Chaudhuri, P., Targeted Oxidase Reactivity with a New Redox-Active Ligand Incorporating N2O2 Donor Atoms. Complexes of Cu(II), Ni(II), Pd(II), Fe(III), and V(V). *Inorganic Chemistry* **2008,** *47* (24), 11620-11632, doi:10.1021/ic8011734.

39. Abakumov, G. A.; Cherkasov, V. K.; Poddel'sky, A. I.; Bubnov, M. P.; Abakumova, L. G.; Fukin, G. K., A Novel Five-Coordinate Manganese(III) Complex with 4,6-Di-(2,6-di-isopropylphenyl)-1,2-iminobenzoquinone: Reversible Interaction

with Dioxygen. *Doklady Chemistry* **2004,** *399* (1), 207-210, doi:10.1023/b:doch.0000048078.97268.86.

40. Abakumov, G. A.; Poddel'sky, A. I.; Bubnov, M. P.; Fukin, G. K.; Abakumova, L. G.; Ikorskii, V. N.; Cherkasov, V. K., Manganese(III) and rhenium(II) complexes with bulky 4,6-di-tert-butyl-N-(2,6-di-iso-propylphenyl)-o-iminobenzoquinonato ligands via carbonyls of corresponding metals. *Inorganica Chimica Acta* **2005,** *358* (13), 3829-3840, doi:10.1016/j.ica.2005.07.003.

41. Bhattacharya, S.; Gupta, P.; Basuli, F.; Pierpont, C. G., Structural Systematics for o-C_6H_4XY Ligands with X,Y= O, NH, and S Donor Atoms. o-Iminoquinone and o-Iminothioquinone Complexes of Ruthenium and Osmium. *Inorganic Chemistry* **2002,** *41* (22), 5810-5816, doi:10.1021/ic025766+.

42. Poddel'sky, A. I.; Cherkasov, V. K.; Abakumov, G. A., Transition metal complexes with bulky 4,6-di-tert-butyl-N-aryl(alkyl)-o-iminobenzoquinonato ligands: Structure, EPR and magnetism. *Coordination Chemistry Reviews* **2009,** *253* (3-4), 291-324, doi:10.1016/j.ccr.2008.02.004.

43. Chun, H.; Chaudhuri, P.; Weyhermüller, T.; Wieghardt, K., o-Iminobenzosemiquinonato Complexes of Mn(III) and Mn(IV). Synthesis and Characterization of [MnIII(LISQ)2(LAP)] (St = 1) and [MnIV(LISQ)2(LAP-H)] (St = 1/2). *Inorganic Chemistry* **2002,** *41* (4), 790-795, doi:10.1021/ic010860w.

44. Abakumov, G.; Cherkasov, V.; Bubnov, M.; Abakumova, L.; Ikorskii, V.; Romanenko, G.; Poddel'sky, A., Synthesis and structures of five-coordinate bis-iminobenzosemiquinone complexes M(ISQ-R)X (X = Cl, Br, I, or SCN; M = Co, Fe, or Mn;). *Russian Chemical Bulletin* **2006,** *55* (1), 44-52, doi:10.1007/s11172-006-0213-3.

45. Scaiano, J. C.; Stewart, L. C., Phenyl radical kinetics. *Journal of the American Chemical Society* **1983,** *105* (11), 3609-3614, doi:10.1021/ja00349a043.

46. Abakumov, G. A.; Druzhkov, N. O.; Kurskii, Y. A.; Shavyrin, A. S., NMR study of products of thermal transformation of substituted N-aryl-o-quinoneimines. *Russian Chemical Bulletin* **2003,** *52* (3), 712-717, doi:10.1023/a:1023979311368.

47. APEX II, Analytical X-Ray Systems, Brukers AXS, Inc., Madison, WI, 2005.,

48. SAINT Version 6.45A, Analytical X-ray Systems, Brukers AXS, Inc., Madison, WI,

2003.,

49. SHELXTL Version 6.12, Analytical X-ray Systems, Bruker AXS, Inc., Madison, WI,
2002.,

50. Wilson, J. C., *In International Tables for X-ray Crystallography, Volume C;*. Academic Publishers: Dordrecht, The Netherlands, 1992.

CHAPTER 5

REACTIONS OF MANGANESE(III) AMIDOPHENOLATE COMPLEXES WITH DIOXYGEN

5.1 Introduction.

The activation of O_2 by transition metals is of fundamental importance to chemistry and biology.[1-6] Mononuclear metal-dioxygen adducts are observed as key intermediates in the catalytic cycles of dioxygen activation by metalloenzymes.[1-6] Manganese, iron and copper based enzymes are able to use O_2 as the primary oxidant in various biochemical transformations.[5-8] Peroxometal species are often proposed as key intermediates for many of these processes. Intermediates of dioxygen adducts are highly reactive and many synthetic chemists have been attracted design complexes in which O_2 adducts are observable; to understand mechanisms in biological processes and to help develop strategies for new catalyst design.[7-18]

In Chapter 4, the ability of $Mn^{III}(ap)(isq)$ to reversibly bind O_2 to form an η^2-$[O_2]^{2-}$ peroxo complex $Mn^{IV}(O_2^{2-})(isq)_2$ was observed.[19-20] This complex is prone to overoxidation and yields the free iminobenzoquinone ligand. The rate of overoxidation can be reduced by the addition of $MgBr_2$, which affords $Mn^{III}Br(isq)_2$, by formally reducing the manganese center and displacing the dioxygen adduct as $[O_2]^{\bullet-}$. However, the addition of excess $MgBr_2$ also results in degradation of the catalyst, which might be due to ligand substitution chemistry. In this chapter, I looked at isolating the Mn-O_2

adduct and stabilizing the $[Mn^{III}(isq)_2]^+$ core by synthesizing new $Mn^{III}(ap)(isq)$ derivatives.

5.2 Results.

5.2.1 Attempted Isolation of $Mn^{IV}(O_2^{2-})(isq)_2$.

Green solutions of $Mn^{III}(ap)(isq)$ in THF placed under an atmosphere of oxygen immediately lead to the formation of the red $Mn^{IV}(O_2^{2-})(isq)_2$. At room temperature, the O_2 adduct decomposes within minutes to afford the orange iminobenzoquinone. However, $Mn^{III}(ap)(isq)$ solutions oxygenated at –78 C resulted in the persistence of the red $Mn^{IV}(O_2^{2-})(isq)_2$. Reactions of $Mn^{III}(ap)(isq)$ with O_2 in diethyl ether at –78 C were stored at –50 C and allowed to slowly evaporate to afford red crystals suitable for X-ray analysis (**Scheme 1, Figure 5.1**).

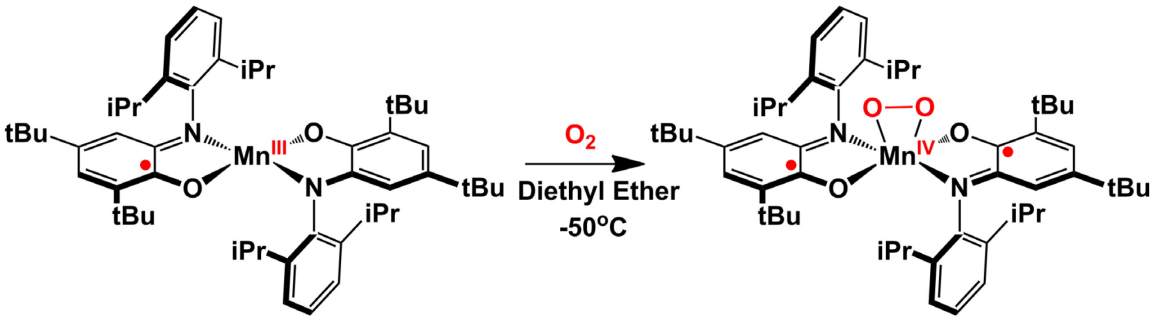

Scheme 1. Syntheisis of $Mn^{IV}(O_2^{2-})(isq)_2$

The crystals yielded low-quality data and the structure was only sufficient to assign atom connectivity. Within the structure there are two crystallographically unique molecules in the unit cell. Each molecule in the structure contains a six coordinate manganese ion

°

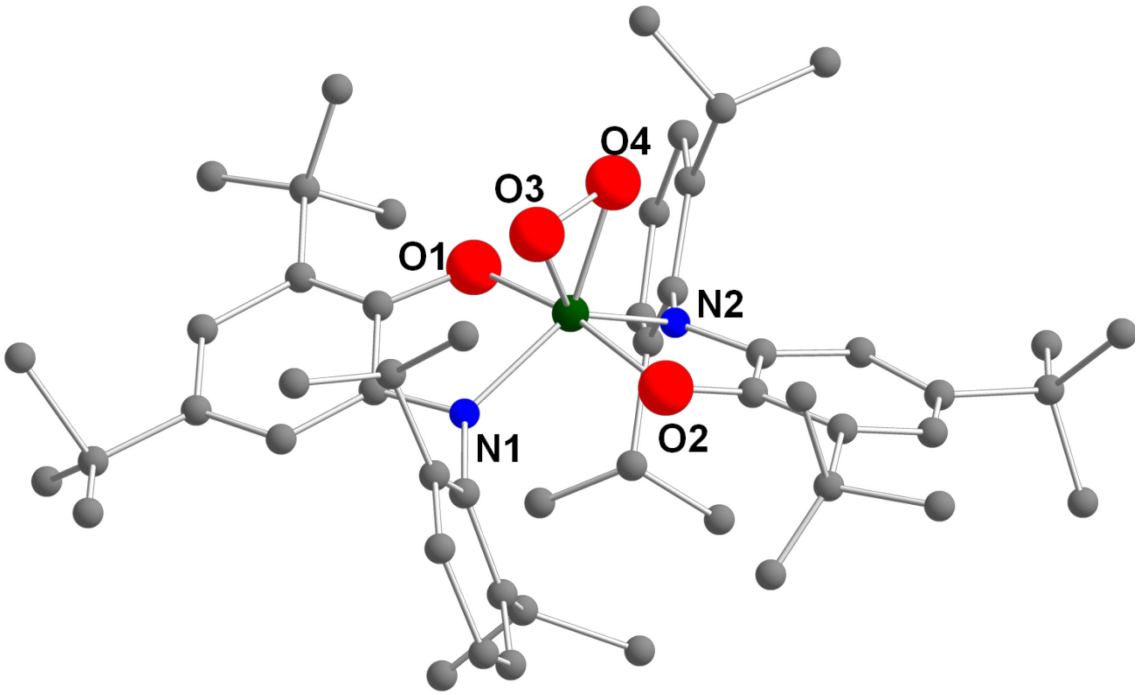

Figure 5.1 (a) Ball-and-stick representation of the solid-state data from a single crystal of $Mn^{IV}(O_2^{2-})(isq)_2$. The hydrogen atoms are omitted for clarity. All attempted syntheses yielded only low-quality crystals.

where each manganese center is coordinated by two aminophenolate ligands and an oxygen adduct in bound in an η^2 fashion. While the low quality data obtained was useful in assigning connectivity, it is not sufficient to assign ligand or O_2 oxidation states. X-Ray analysis of multiple crystals of $Mn^{IV}(O_2^{2-})(isq)_2$ using the same synthetic procedure consistently lead to only low quality data.

5.2.2 Preparation and Characterization of Bidentate Manganese Amidophenolate Complexes.

New Mn^{III}(ap)(isq) derivatives were prepared with different *N*-aryl-o-iminobenzoquinone ligands to examine substituent effects on O_2 oxidation (**Figure 5.2**).

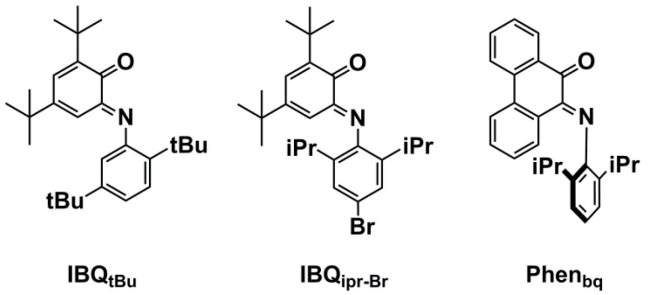

Figure 5.2. Series of *N*-aryl-o-iminobenzoquinone ligands.

Each Mn^{III}(ap)(isq) analog was prepared by irradiating toluene solutions containing 1 equiv of Mn_2CO_{10} with 4 equiv of the respective *N*-aryl-o-iminobenzoquinone with UV light over the course of two days.

In the case of 2,4-di-*tert*-butyl-6-(2,5-ditertbutylphenylimino)quinone (**IBQ_{tBu}**), the reaction afforded purple crystals in 42% yield that were characterized using UV-Vis, elemental analysis and X-ray crystallography (**Figure 5.3**).

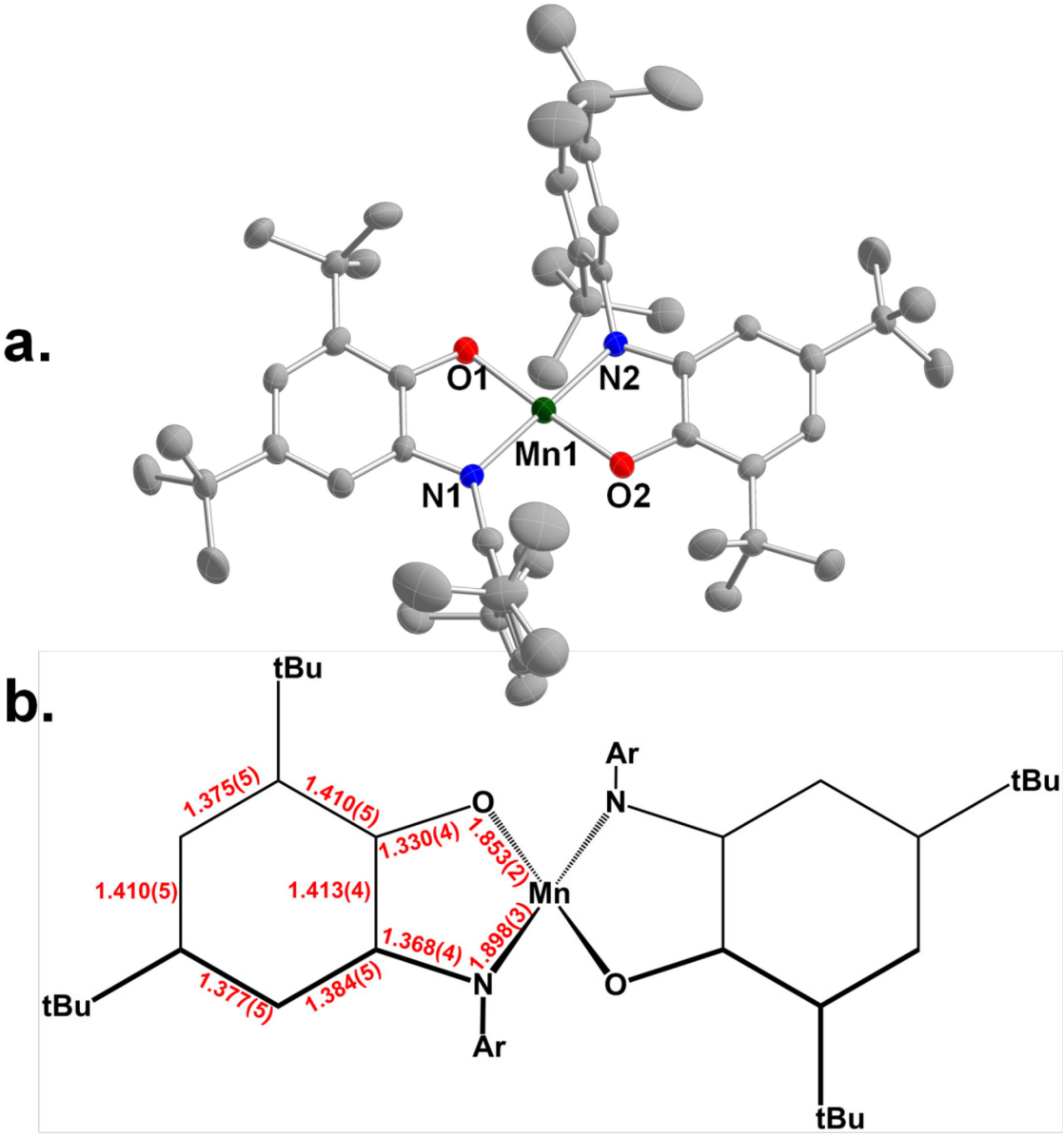

Figure 5.3 (a) Solid-state structure of $Mn^{III}(ap_{tBu})(isq_{tBu})$ drawn with 50% probability ellipsoids. The hydrogen atoms and toluene solvate molecule are omitted for clarity. (b) Schematic of selected bond lengths (Å) in $Mn^{III}(ap_{tBu})(isq_{tBu})$drawn to correspond to Figure 5.3a

Within the structure there are also two crystallographically unique molecules in the unit cell of the same crystal. Each molecule in the structure contains a four coordinate manganese ions where each manganese center is ligated by two aminophenol ligands which are crystallographically indistinguishable. The crystal structure shows that the N1–Mn–N2 and O1–Mn–O2 angles for are both 180(1) and 172(1) . The sum of the bond angles around the metal based on N1–Mn–O1, N1–Mn–O2, N2–Mn–O1 and N2–Mn–O2 is 360(1) , which is typical for a square planar environment. The C–N bond length in one of the molecules is 1.368(4) Å, which is between the C–N bond lengths commonly observed in reduced amidophenolate(2–) ligands (1.39 Å) and oxidized iminosemiquinonate(1–) (1.34 Å) ligand in transition metal complexes.[21-23] The C–O bond lengths of 1.330(4) Å observed also lies between C–O bond lengths commonly observed in amidophenolate(2–) ligands (1.35 Å) and iminosemiquinonate(–)ligands (1.30 Å) in transition metal complexes. Because the ligands display bond lengths that are between in amidophenolate(2–) ligands and iminosemiquinonate(–)ligands we can conclude that a single ligand centered oxidation is observed in this charge neutral complex. Therefore, the overall oxidation state of the complex is best described as $Mn^{III}(ap_{tBu})(isq_{tBu})$.

Reactions with N-(2,6-di-*iso*-propylphenyl)-9,10-iminophenanthraquinone (**Phen$_{BQ}$**) ligand yielded brown crystals in 40% yield that were characterized using UV-Vis, elemental analysis and X-ray crystallography **(Figure 5.4)**. The crystal structure contains a four coordinate manganese complex with two coplanar ligands. The structure shows that the N1–Mn–N2 and O1–Mn–O2 angles for both are 180(1) . The sum of the bond angles around the metal based on N1–Mn–O1, N1–Mn–O2, N2–Mn–O1 and N2–

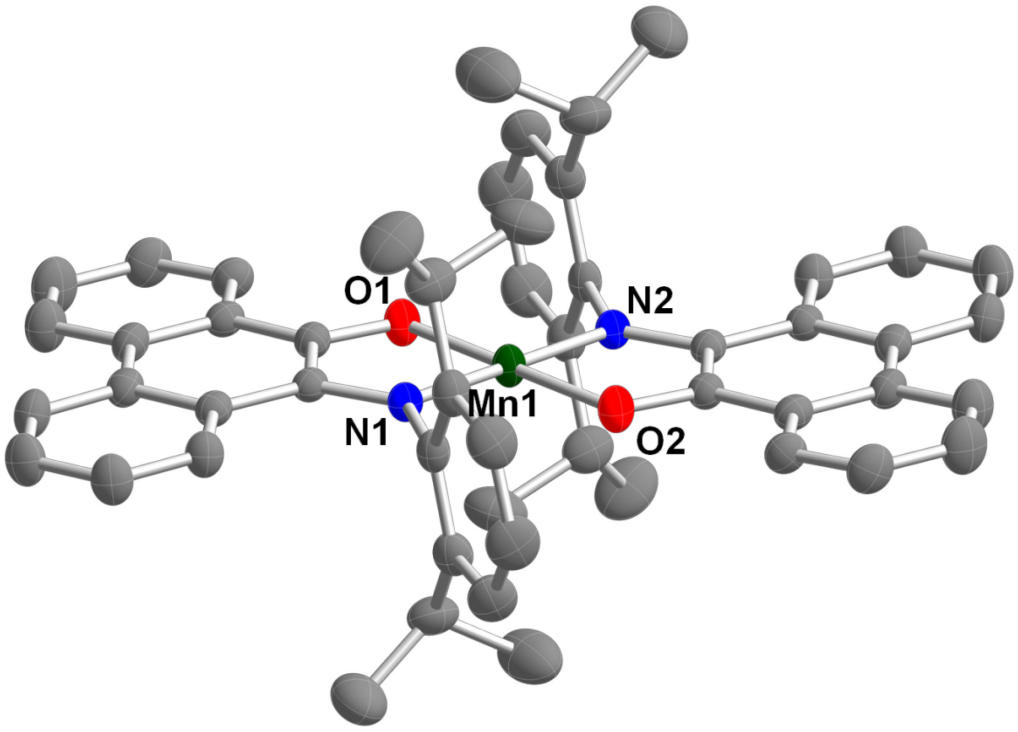

Figure 5.4 (a) Solid-state structure of $Mn^{III}(Phen_{ap})(Phen_{isq})$ drawn with 50% probability ellipsoids. The hydrogen atoms are omitted for clarity.

Mn–O2 is 360(1) , which is typical for the observed square planar environment. The manganese lies on an inversion center making the two ligands crystallographically identical. The C–N bond length of 1.378(4) Å is between the C–N bond lengths commonly observed in reduced amidophenolate(2–) ligands (1.39 Å) and oxidized iminosemiquinonate(1–) (1.34 Å) ligand in transition metal complexes.[21-23] The C–O bond lengths of 1.330(4) Å is also between C–O bond lengths expected for amidophenolate(2–) ligands (1.35 Å) and iminosemiquinonate(–)ligands (1.30 Å) in transition metal complexes. Because the C–N and C–O bond lengths are between amidophenolate(2–) ligands and iminosemiquinonate(–)ligands, we can conclude that the complex has one ligand centered oxidation. Therefore, the overall oxidation state of the complex is best described as $Mn^{III}(phen_{ap})(phen_{isq})$.

Reactions using 2,6-diisopropyl-4-bromo)quinone (**$IBQ_{iPr\text{-}Br}$**) as a ligand yielded purple microcrystals in 56% yield. A portion was recrystallized in acetonitrile to yield crystals suitable for X-ray crystallography **(Figure 5.5)**. The crystal structure shows that the complex is square pyramidal with an acetonitrile bound in the axial position. An additional acetonitrile solvate in the crystal stucture makes the two aminophenol ligands crystallographically unique. The C–N and C–O bond lengths in each ligand are significantly different from each other when an acetonitrile is bound, which is a feature that was also observed in the five coordinate $Mn^{III}(ap)(isq)(CH_3CN)$ in Chapter 4. One ligand has C–N and C–O bond lengths of 1.390(2) Å and 1.349(2) Å respectively, which coincide with average C–N (1.39 Å) and C–O (1.35 Å), typically observed for fully reduced amidophenolate(2–) ligands in transition metal complexes. The other ligand has C–N and C–O bond lengths of 1.357(2) Å and 1.314(2) Å respectively, which agree with

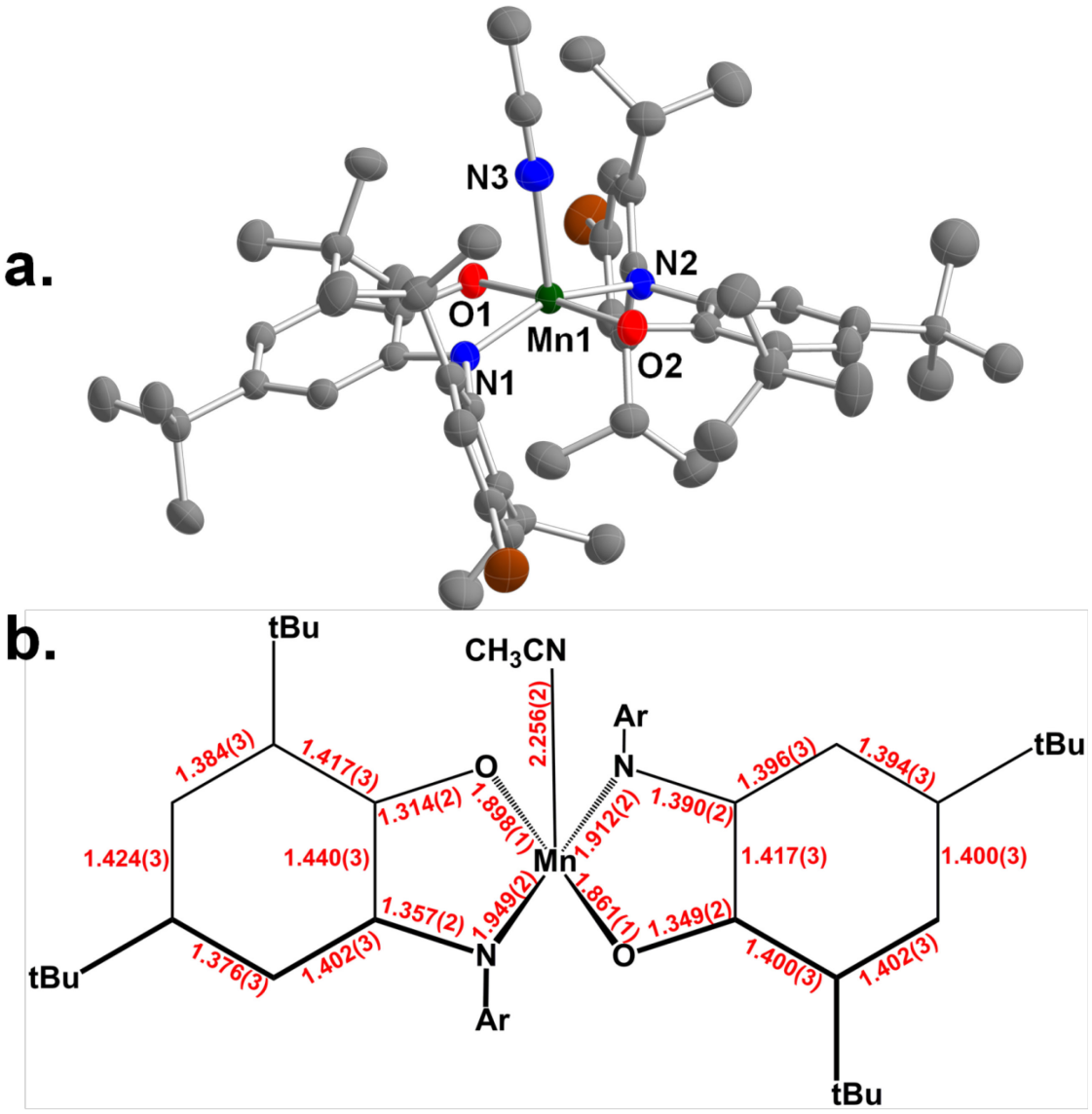

Figure 5.5 (a) Solid-state structure of $Mn^{III}(ap_{iPr\text{-}Br})(isq_{iPr\text{-}Br})$ drawn with 50% probability ellipsoids. The hydrogen atoms and acetonitrile solvate molecule are omitted for clarity. (b) Schematic of selected bond lengths (Å) in $Mn^{III}(ap_{iPr\text{-}Br})(isq_{iPr\text{-}Br})$drawn to correspond to Figure 5.5a

average C–N (1.34 Å) and C–O (1.30 Å), typically observed for iminosemiquinonate(1–) ligands in transition metal complexes. This structure clearly has ligands in two different oxidation states and the complex can best be described as $Mn^{III}(ap_{iPr\text{-}Br})(isq_{iPr\text{-}Br})(CH_3CN)$.

5.2.3 Preparation and Characterization of Tetradentate Manganese Amidophenolate Complexes.

In Chapters 2, 3 and 4, reactions of bidentate catecholate and amidophenolate type ligands were prone to over oxidation, ultimately leading to quinone formation. In an attempt to overcome this limitation, I investigated the coordination and reaction chemistry of the tetradentate *N*,*N*_-bis(3,5-di-*tert*-butyl-2-phenoxy)-1,2-phenylenediamide. Wieghardt and co-workers, studied complexes of this same ligand with copper and zinc.[24] Electrochemical data showed that up to four electrons can be removed from the ligand, in a series of one electron steps shown in **Scheme 2**.

Reactions of $Mn^{III}(OAc)_3 \cdot 2H_2O$ with *N*,*N*‘-bis(3,5-di-*tert*-butyl-2-hydroxyphenyl)-1,2-phenylenediamine(**H_4L**) and NaH as a base in THF affords dark brown solutions that precipitate solids upon the addition of pentane (**Scheme 3**). Recrystallization of the brown solids from THF/pentane solutions result in crystals suitable for X-ray crystallography.

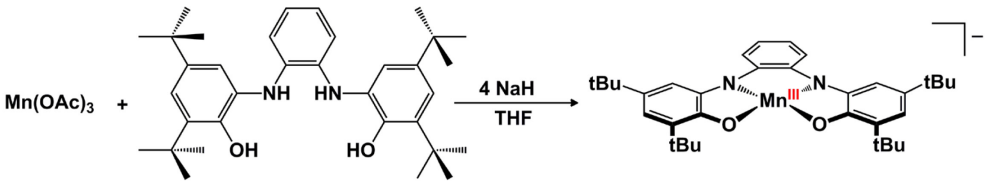

Scheme 3. Synthesis of $[Mn^{III}(L_4)]^-$

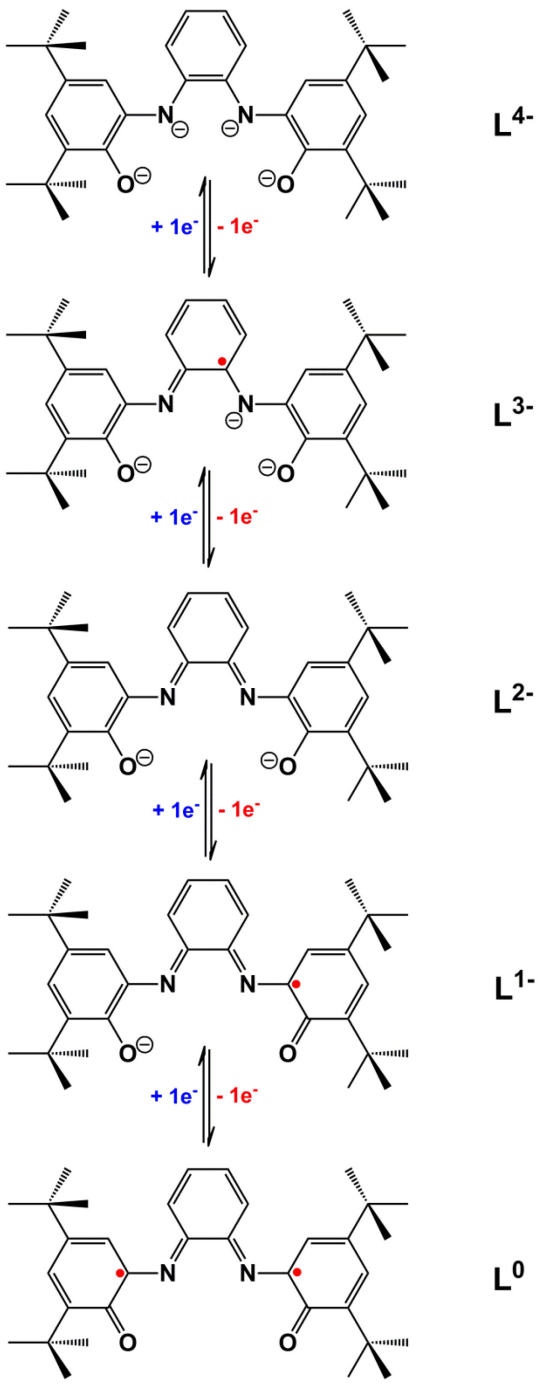

Scheme 2. The multiple oxidation states of L.

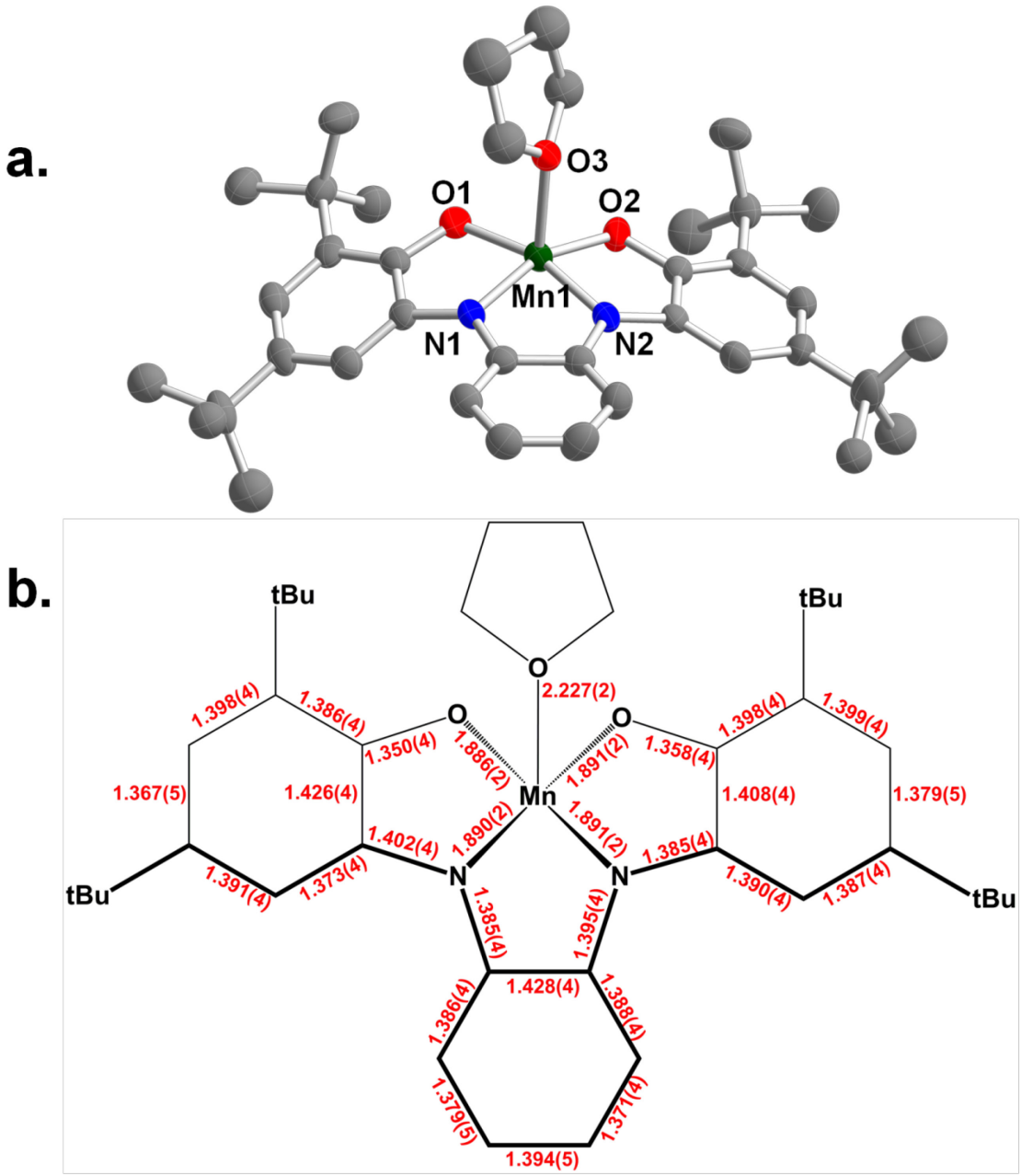

Figure 5.6 (a) Solid-state structure of PPN[$Mn^{III}(L_4)$(THF)]drawn with 50% probability ellipsoids. The hydrogen atoms and PPN counterion molecule are omitted for clarity. (b) Schematic of selected bond lengths (Å) of PPN[$Mn^{III}(L_4)$(THF)]drawn to correspond to Figure 5.6a

The crystal structure contains a five coordinate manganese complex with the tetradentate **(L^4)** ligand coordinated in a distorted square planar environment and THF coordinated the in axial position. The structure contains two crystallographically unique aminophenol fragments within the tetradentate ligand. The C–N bond lengths of 1.402 (4) Å and 1.385(4) Å are typical for fully reduced aminophenolate(2–) ligands (1.39 Å).[21-23] The C–O bond lengths of 1.358(4) Å and 1.350(4) Å are also commonly observed in reduced amidophenolate(2–) ligands (1.35 Å). The phenylenediamine bridge of the tetradentate ligand can also undergo ligand centered redox changes. The C–N bond lengths of 1.395 (4) Å and 1.385(4) Å are typical for fully reduced phenylenediamine(2–) ligands (1.39 Å). The structure is best described as $[Mn^{III}(L_4)]^-$, with L_4 containing two fully reduced aminophenol ligands and one fully reduced phenylenediamine bridge.

Alternatively, reactions of $Mn^{II}(OAc)_2 \cdot 4H_2O$ with *N*,*N*'-bis(3,5-di-*tert*-butyl-2-hydroxyphenyl)-1,2-phenylenediamine(**H_4L**) in methanol and air afford dark green solutions that precipitate green microcrystals with stirring **(Scheme 4)**. Recrystallization from methylene choride afforded crystals suitable for X-ray analysis.

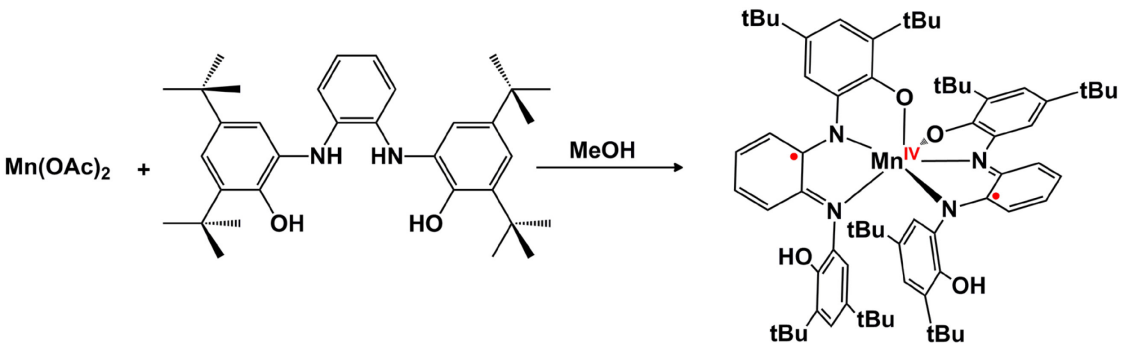

Scheme 4. Synthesis of $[Mn^{III}(L^3)_2]$

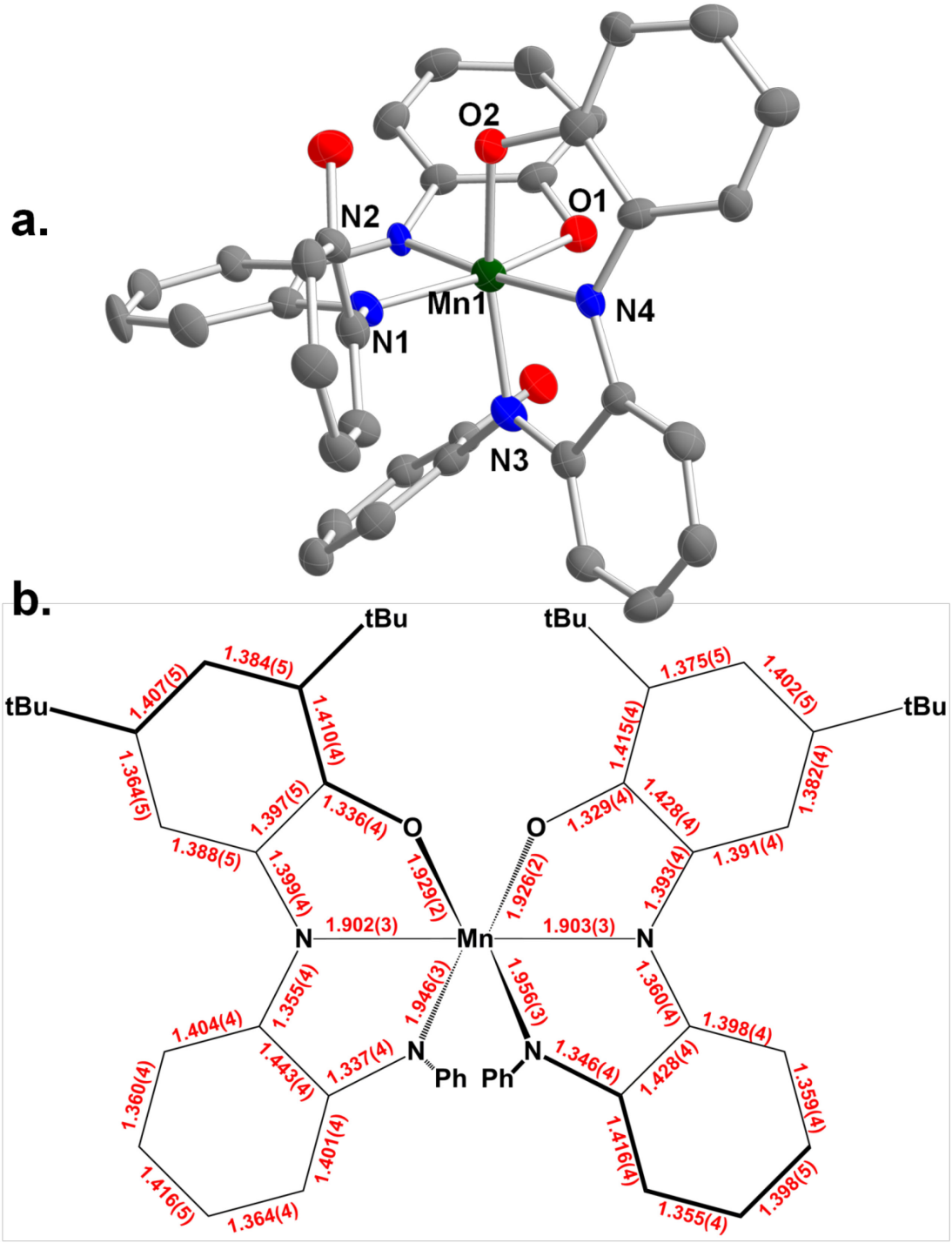

Figure 5.7 (a) Solid-state structure of $Mn^{IV}(L^3)_2$ drawn with 50% probability ellipsoids. The hydrogen atoms and tert-butyl groups in the molecule are omitted for clarity. (b) Schematic of selected bond lengths (Å) in $Mn^{IV}(L^3)_2$ drawn to correspond to Figure 5.7a

The crystal structure contains a six coordinate manganese complex with two tetradentate **(L)** ligands coordinated in a tridentate fashion. Both ligands are bound through the two Mn–N bonds of the phenylenediamine backbone and one Mn–O bond of the aminophenol ligand. The Mn–N bond distances range from 1.902 (4) Å and 1.956(4) Å, while the Mn–O bond length are 1.926(4) Å and 1.929(4) Å. In the structure, each ligand is crystallographically unique. The C–N bond lengths of the coordinated aminophenolate 1.399 (4) Å and 1.393(4) Å are typical for fully reduced aminophenolate(2–) ligands (1.39 Å).[21-23] The C–O bond lengths of 1.336(4) Å and 1.329(4) Å are lower that values commonly observed in bidentate reduced amidophenolate(2–) ligands (1.35 Å), but agree with values observed in L_4-derived. reduced amidophenolates(2–).[24] In the phenylenediamine bridge, the C–N bond lengths of 1.355 (4) Å and 1.337(4) Å for one ligand and 1.360 (4) Å and 1.346(4) Å for the other ligand are indicative of diiminosemiquinonate(1–) oxidation state, which have an average bond length of 1.34 Å.[24-25] The structure is best described as $Mn^{IV}(L^3)_2$, with L_4 containing two fully reduced aminophenol ligands and one oxidized phenylenediamine bridge

5.2.4 Reactions of Mn^{III}(ap)(isq) derivatives with O_2.

Reactions of THF solutions of $Mn^{III}(ap_{iPr\text{-}Br})(isq_{iPr\text{-}Br})$ placed under 1atm O_2 resulted in the formation of a new red solution with UV-Vis peaks at 663 nm, (3900ε) annd 505 nm (10700ε), which are very close to the previously observed $Mn^{IV}(O_2^{2-})(isq)_2$ complex. Degassing these solutions resulted in the reformation of the starting material. (**Figure 5.8, Scheme 5**)

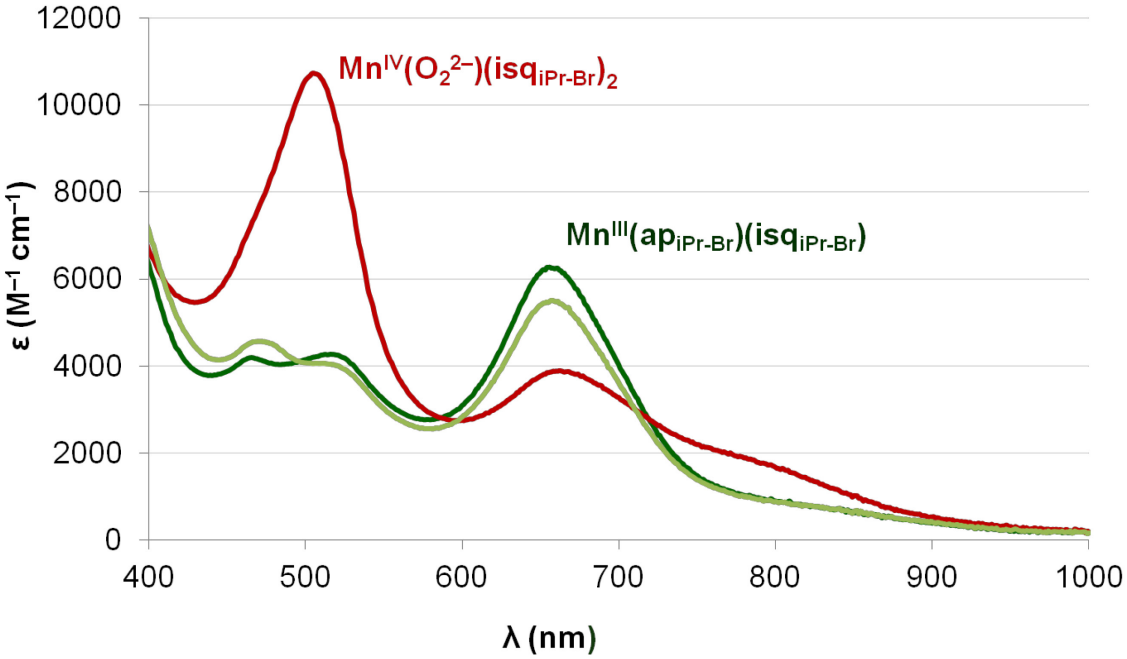

Figure 5.8. UV–vis absorption spectra showing reversible O_2 binding at $Mn^{III}(ap_{iPr\text{-}Br})(isq_{iPr\text{-}Br})$. Addition of 1 atm O_2 to 0.09 mM $Mn^{III}(ap_{iPr\text{-}Br})(isq_{iPr\text{-}Br})$ in THF (dark green line) generates $Mn^{IV}(O_2^{2-})(isq_{iPr\text{-}Br})_2$.(red line). Degassing the solution regenerates $Mn^{III}(ap_{iPr\text{-}Br})(isq_{iPr\text{-}Br})$ (light green line).

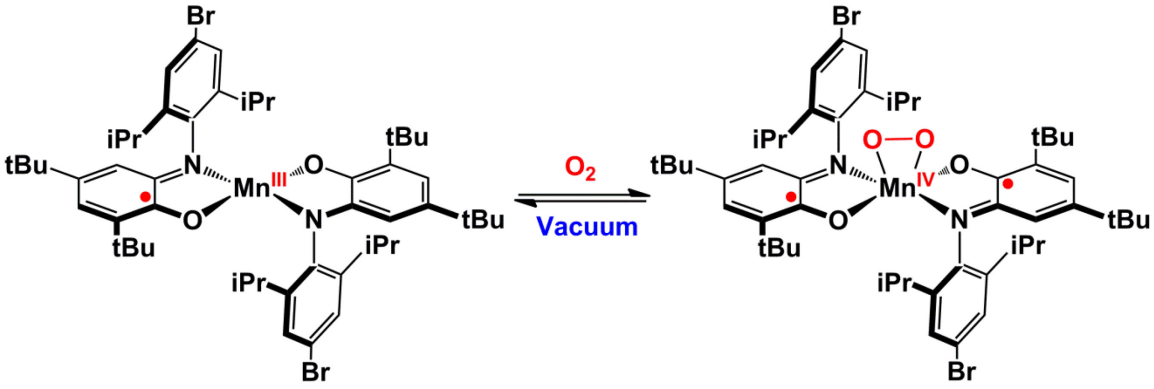

Scheme 5. The reversible binding of O_2 by $Mn^{III}(ap_{iPr\text{-}Br})(isq_{iPr\text{-}Br})$.

The stability of the O_2 adduct of $Mn^{III}(ap_{iPr\text{-}Br})(isq_{iPr\text{-}Br})$ was compared to parent $Mn^{III}(ap)(isq)$ complex. THF solutions of each complex were placed under an atmosphere of O_2 and monitored by UV-Vis over the course of 146 mins (**Figure 5.9**). The O_2 adduct of $Mn^{III}(ap_{iPr\text{-}Br})(isq_{iPr\text{-}Br})$ shows a marginal increase in stability when compared to the O_2 adduct of the parent $Mn^{III}(ap)(isq)$ complex. However, both complexes exhibit a significant increase in stability is observed in non-coordinating solvents, such as toluene and pentane. Reactions of $Mn^{III}(ap_{iPr\text{-}Br})(isq_{iPr\text{-}Br})$ with O_2 in pentane at −78 C were stored at 0 C and allowed to slowly evaporate to afford dark crystals suitable for X-ray analysis **(Figure 5.10)**. The data obtained was of higher quality when compared to the parent $Mn^{III}(ap)(isq)$ complex and useful in assigning both the ligand and O_2 oxidation states.

The crystal structure shows that the complex is distorted octahedral in wich a manganese ion is coordinated to two aminophenolate ligands and a dioxygen adduct in bound in an η^2 fashion. The two aminophenol ligands in the structure are crystallographically unique. The C–N bond lengths for each ligand are 1.349(2) Å and 1.347(2) Å, which is typical for the C–N bond lengths (1.34 Å) observed in oxidized

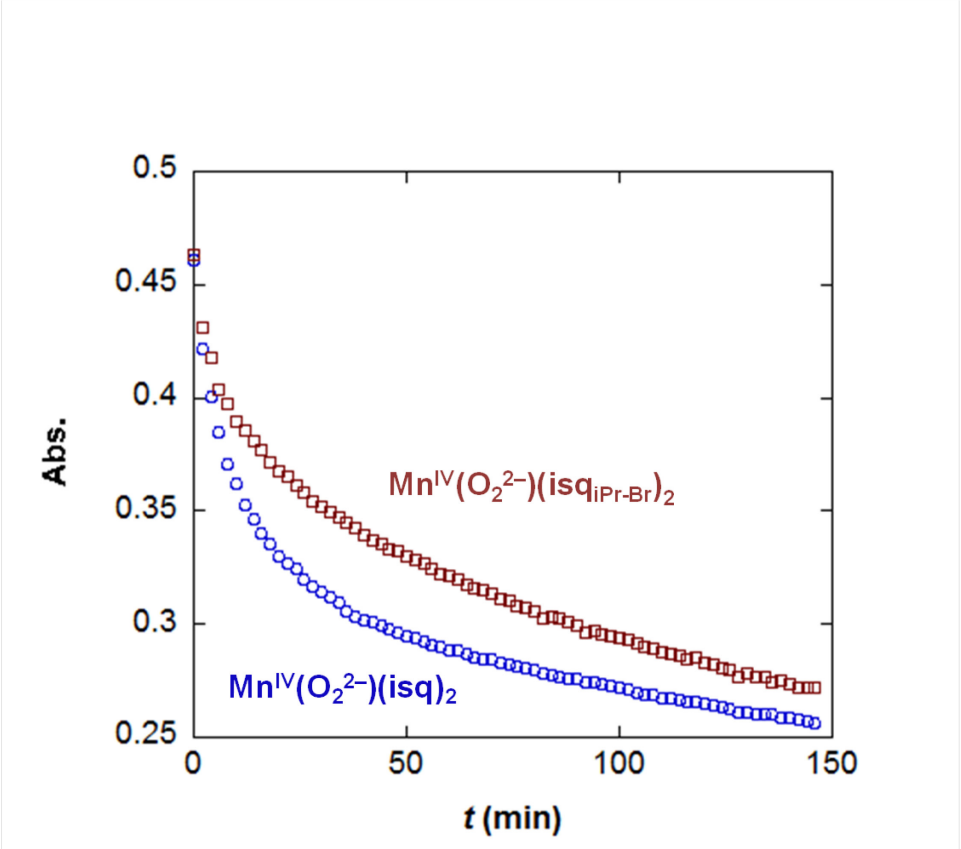

Figure 5.9. Time-resolved data at 663 nm showing the decomposition of 0.08 mM solution of $Mn^{III}(ap_{tBu})(isq_{tBu})$ in THF under 1 atm O_2 (red) and a 0.08 mM solution of $Mn^{III}(ap)(isq)$ in THF (blue).

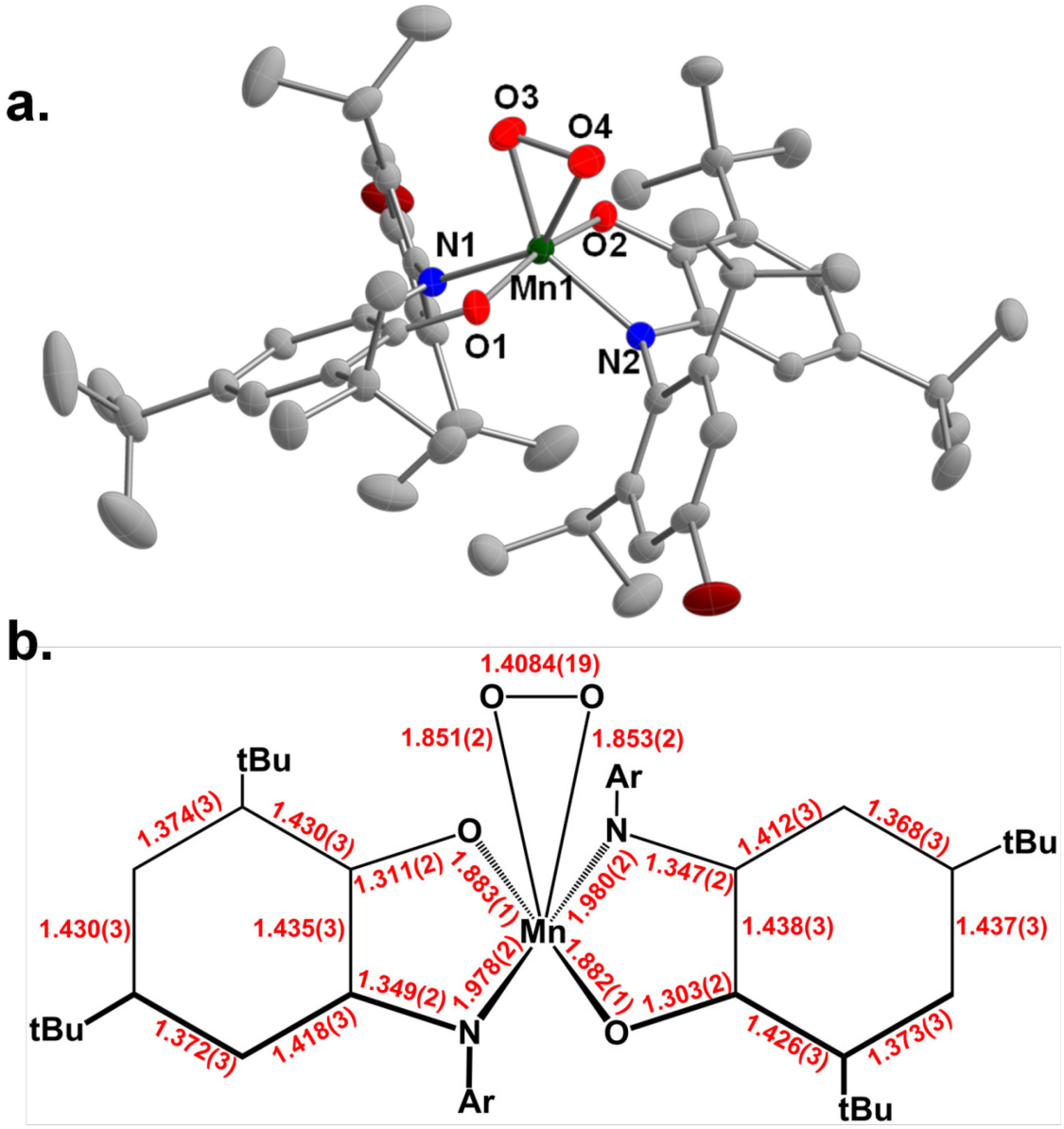

Figure 5.10 (a) Solid-state structure of $Mn^{IV}O_2(isq_{iPr\text{-}Br})_2$ drawn with 50% probability ellipsoids. The hydrogen atoms and pentane solvent molecule are omitted for clarity. (b) Schematic of selected bond lengths (Å) of $Mn^{IV}O_2(isq_{iPr\text{-}Br})_2$ drawn to correspond to Figure 5.10a.

iminosemiquinonate(1–) ligands.[21-23, 26] The C–O bond lengths for both complexes are from 1.303(2) Å to 1.311(2) Å, which is also typical for oxidized iminosemiquinonate(–1) ligands (1.30 Å).[21-23, 26] The O–O bond length of the dioxygen adduct is 1.408(2) Å is best describe as peroxo ligand. The complex is best described as $Mn^{IV}O_2(isq_{iPr\text{-}Br})_2$.

Red THF solutions of $Mn^{III}(Phen_{ap})(Phen_{isq})$ placed under 1atm O_2 results in the immediate decomposition of the metal complex to yield green solutions containing the free $Phen_{bq}$ form of the ligand. (**Scheme 6**). The reaction was monitored by UV-vis spectroscopy, and no evidence for any intermediates, including an O_2 adduct, was observed.

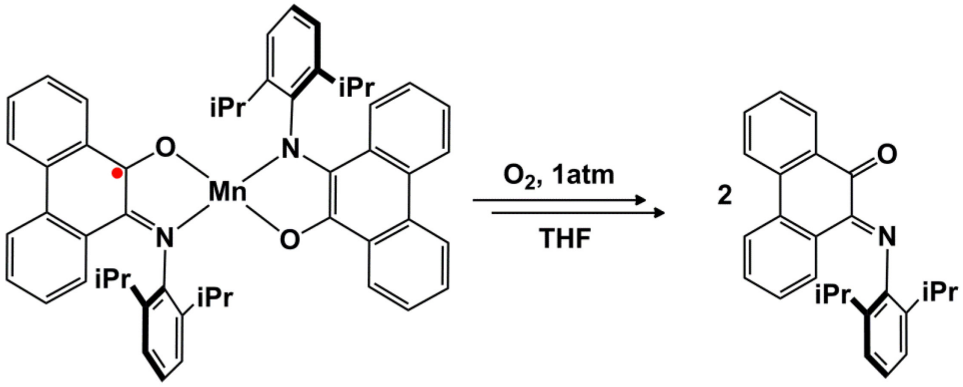

Scheme 6. Oxidative decomposition of $Mn^{III}(Phen_{ap})(Phen_{isq})$ by O_2 to form $Phen_{bq}$.

Similarly, THF solutions of $Mn^{III}(ap_{tBu})(isq_{tBu})$ placed under 1atm O_2 also results in rapid decomposition of the metal complex. Red solutions containing the free (BQ_{tBu}) form of the ligand are observed via UV-Vis. Monitoring by UV-vis spectroscopy revealed evidence for an O_2 adduct as an intermediate, however when attempting to degas solutions of $Mn^{III}(ap_{tBu})(isq_{tBu})$ under O_2, reformation of the starting material was not observed **(Scheme 7)**.

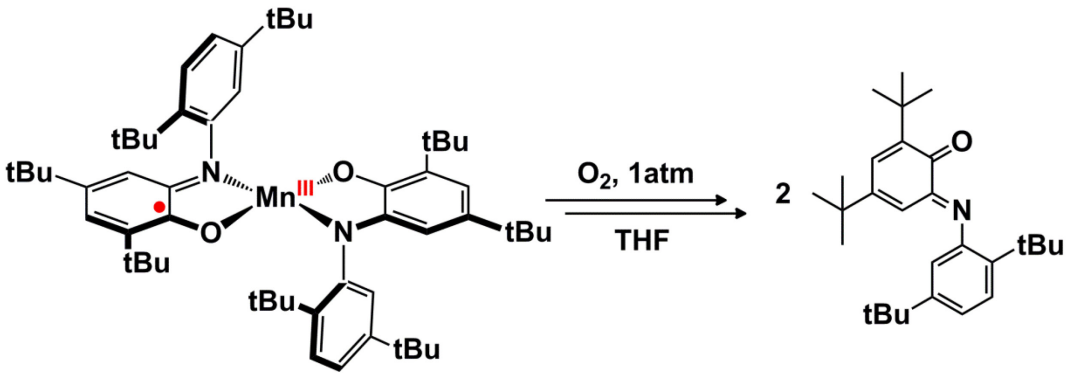

Scheme 7. Oxidative decomposition of $Mn^{III}(ap_{tBu})(isq_{tBu})$ by O_2 to form BQ_{tBu}.

5.2.5 Reactions of $[Mn^{III}(L^4)]^-$ With O_2.

Brown THF solutions of **$[Mn^{III}(L^4)]^-$** placed under 1atm O_2 was followed by UV-Vis spectroscopy and resulted in the immediate formation of a new purple solution **(Figure 5.11).** Degassing purple solutions did not result in the reformation of the starting material. Multiplte attempts to isolate crystals suitable for X-ray analysis from the purple solution were unsuccessful. The reaction of $[Mn^{III}(L^4)]^-$ with O_2 was then examined by ESI-MS in order to determine whether the complex was still intact after aerial oxidation. The spectra revealed two major peaks at 567 *m/z* and 602 *m/z*, which coincide with the molecular weights for $[Mn^{III}(L^4)]^-$ and $[Mn^{III}(L^4)]^-$ + Cl. The Cl adduct was suspected to be an impurity based on the PPN-Cl counterion used in crystallization, however solutions of $[Mn^{III}(L^4)]^-$ with O_2 that were derived without any source of Cl^- also yielded 602 *m/z* as the major peak. Elemental analysis also confirmed that no chloride was in the sample, which suggested the source of chloride was from the mass spectrometer.

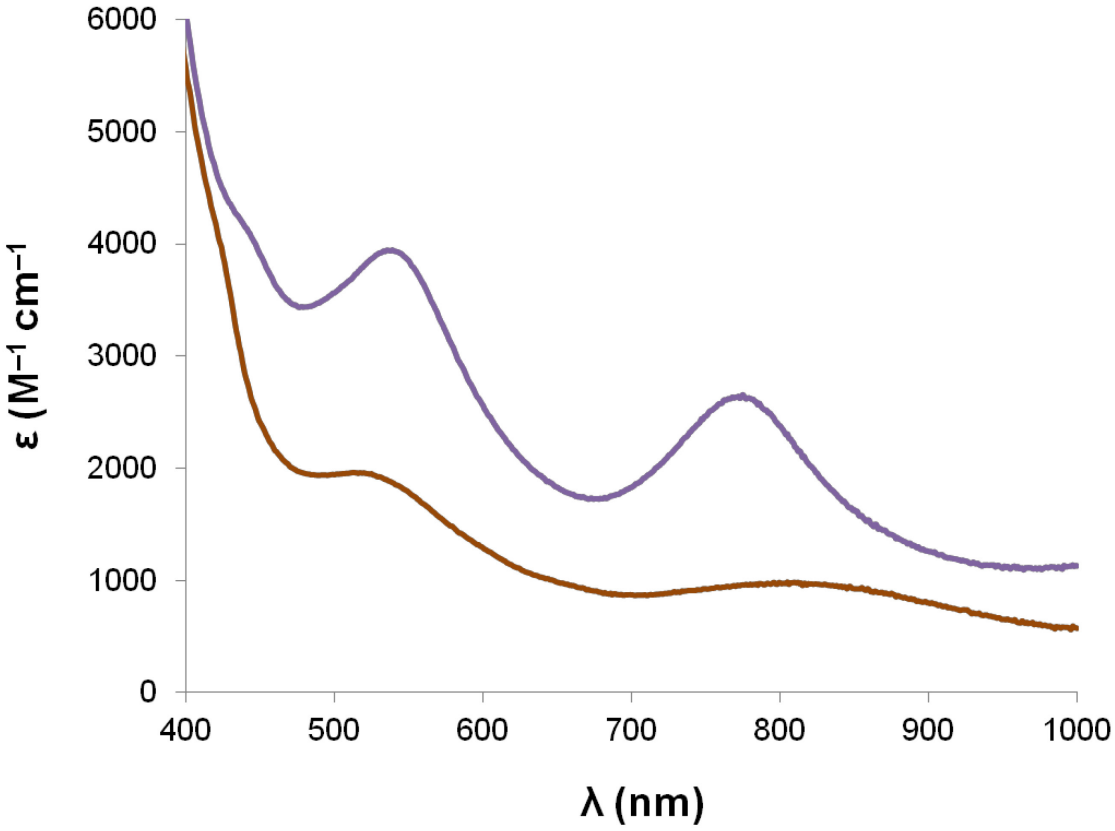

Figure 5.11. UV–vis absorption spectra showing reaction of $[Mn^{III}(L^4)]^-$ with O_2. Addition of 1 atm O_2 to 0.09 mM $[Mn^{III}(L^4)]^-$ in THF (brown line) a new purple species.(purple line).

Addition of MgX_2 salts to purple THF solutions of $[Mn^{III}(L^4)]^-$ with O_2, result in formation of a green solution. The solution was examined by UV-Vis and the spectra matched that of the previously isolated $Mn^{IV}(L^3)_2$ **(Scheme 8).**

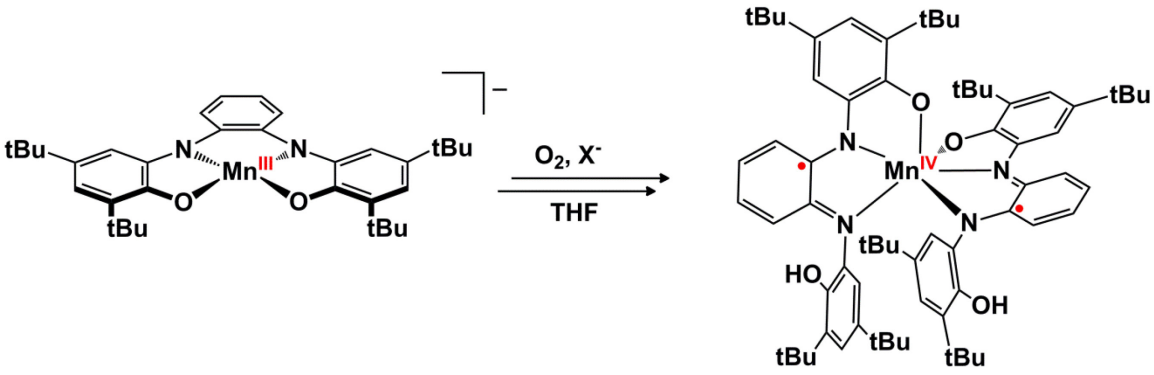

Scheme 8. Conversion of $[Mn^{III}(L^4)]^-$ to $Mn^{IV}(L^3)_2$.

5.3 Discussion

5.3.1 Synthesis of Mn(III) aminophenol complexes.

A series of bidentate Mn^{III}(ap)(isq) complexes were synthesized and characterized using X-ray crystallographically. The oxidation state of each of these complex was determined to be the same, by examining the bond distances in C–O, C–N and aromatic C–C bonds in each structure. Each complex was prepared similarly by reacting Mn_2CO_{10} with 4 equiv of the respective iminoquinone to afford the Mn^{III}(ap)(isq). This reaction pathway provides an excellent route to the synthesis of Mn complexes using both quinones[27] and iminoquinones[22] and is easily adaptable to a range of derivatives. In contrast, $[Mn^{III}(L^4)]^-$ was prepared from using $Mn^{III}(OAc)_3 \cdot 2H_2O$ and a reduced aminophenol derivative. The collection of four-coordinate manganese(III) complexes

with various redox active aminophenol ligands allowed us to pursue the effect that structural changes of the ligand would have on reactions with oxygen.

5.3.2 Reactions of Mn^{III}(ap)(isq) derivatives with O_2.

Reactions of Mn^{III}(ap)(isq) with O_2 afforded a dioxygen adduct previously assigned as $Mn^{IV}(O_2^{2-})(isq)_2$. The crystal structure of this complex revealed that O_2 was bound as η^2 species, however oxidation state of the aminophenol ligands and O_2 were not able to be determined from the low quality structure. The O_2 adduct degrades over time to afford free iminobenzoquinone. The derivatives of Mn^{III}(ap)(isq) also react with O_2 to afford free iminobenzoquinones. The rate of decomposition can observed in these complexes can be correlated to the difference in the reduction potentials of $Phen_{BQ}$(1.08 V) vs. BQ_{tBu}(0.99 V) vs. BQ_{iPr}(0.94 V).[28] Using $BQ_{iPr\text{-}Br}$ as a ligand offers a slight improvement in the decomposition of $Mn^{IV}(O_2^{2-})(isq)_2$, which suggest that aminophenol ligands with more stronger electron withdrawing groups should help to increase stability. The rate of decomposition is also dependent on solvent. Solutions of $Mn^{IV}(O_2^{2-})(isq)_2$ are more stable in non-coordinating solvents such as toluene and pentane vs THF. It is possible that coordinating solvents can react with $Mn^{IV}(O_2^{2-})(isq)_2$ to convert η^2-peroxo species into a η^1-peroxo species that is bound directly to an aminophenol ligand Literature precendent for this type of coordination has been observed in antimony complexes containing aminophenol ligands.[29-30] It is likely that the bridging η^1-peroxo species is responsible for the degradation of aminophenol type ligands in coordinating solvents **(Scheme 9)**.

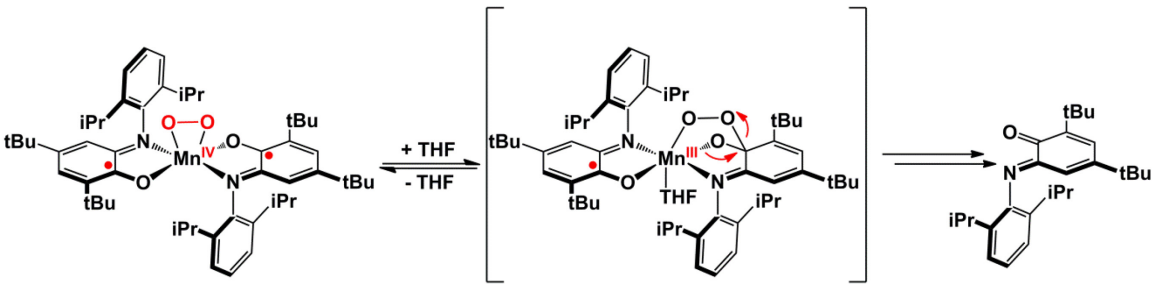

Scheme 9. Degradation pathway of $Mn^{IV}(O_2^{2-})(isq)_{2\ in}$ THF solutions.

The crystals structure of $Mn^{IV}O_2(isq_{iPr\text{-}Br})_2$ allowed me to determine that the binding of O_2 leads to a two electron oxidation of the metal complex. This is different from other isolated Mn-O_2 adducts which are either comprised of multiple Mn centers, use sacrificial reductants in conjuction with O_2 or use superoxide to generate similar Mn-peroxide adducts.[5] The $2e^-$ reduction of O_2 is facilitated by the metal and ligand in a cooperative fashion.

5.3.3 Reactions of $[Mn^{III}(L^4)]^-$ with O_2

Reactions of $[Mn^{III}(L^4)]^-$ with O_2 resulted in the immediate formation of new purple species. ESI-MS was used to determine that $Mn^{III}(L)$ core was intact in the purple solution, however attempts to isolate the complex and crystallographically characterize the complex were unsuccessful. The preservation of $Mn^{III}(L)$ core suggest that using macrocyclic ligands can be an effective approach to reduce the formation free iminoquinone observed in the oxidation chemistry. However, the oxidized fragment was prone to ligand redistribution in the presence of MgX_2 or MeOH to afford $Mn^{IV}(L^3)_2$ in the presence of air. The rearrangement can be attributed to the fact that high spin d^4

complexes are substitionally labile and steric bulk of the tetradentate ligand is insufficient to prevent two ligands from binding in a tridentate fashion.

5.4. Conclusions.

In conclusion, Mn(III) with redox active aminophenol-derived ligands are able to mediate e^- transfer reactions with dioxygen. $Mn^{IV}(O_2^{2-})(isq)_2$ intermediates can be isolated, which provides insight into the nature of the inner sphere of O_2 activation. Although $Mn^{IV}(O_2^{2-})(isq)_2$ complexes are prone to overoxidation to release free iminoquinone, future efforts can be based on using more electron deficient aminophenol type ligands to increase stability. Macrocyclic ligands can also be used as an effective strategy to avoid overoxidation, however sterically bulky ligands should be considered to avoid problems of ligand redistribution.

5.5 Experimental Details.

5.5.1 General Considerations.

Unless otherwise specified, all manipulations were performed under anaerobic conditions using standard vacuum line techniques, or in an inert atmosphere glove box under purified nitrogen. NMR spectra were acquired on a Varian Mercury 300 spectrometer (300.323 MHz for ^1H) at ambient temperature. Chemical shifts are reported in parts per million (ppm) relative to TMS, with the residual solvent peak serving as an internal reference. UV–visible absorption spectra were acquired using a Varian Cary 50 spectrophotometer equipped with a water-jacketed cell holder fitted to a Peltier

temperature controller. All electronic absorption spectra were recorded at 25 °C in 1 cm quartz cells unless specified otherwise. IR spectra were obtained by attenuated total reflection (ATR) through a diamond plate on a Bruker Optics Alpha-P FTIR spectrometer. Elemental analyses were performed by Atlantic Microlab, Inc. in Norcross, GA. All analyses were performed in duplicate, and the reported compositions are the average of the two runs.

5.5.2. Methods and Materials.

Anhydrous acetonitrile (MeCN), tetrahydrofuran (THF), dichloromethane (CH_2Cl_2), toluene, and pentane solvents for air- and moisture-sensitive manipulations were purchased from Sigma-Aldrich, further dried by passage through columns of activated alumina, degassed by at least three freeze-pump-thaw cycles, and stored under N_2 prior to use. Oxygen (ultra high purity) was used as received from Airgas, Inc. Deuterated tetrahydrofuran (THF–d_8) was purchased from Cambridge Isotope Laboratories, degassed by three freeze-pump-thaw cycles, vacuum distilled from CaH_2 or $Na_{(s)}$, respectively, and stored under a dry N_2 atmosphere prior to use. Mn^{III}(ap)(isq)[20] and 2,4-di-*tert*-butyl-6-(2,5-di-tert-butylphenylimino)benzoquinone (**ibq$_{tBu}$**), N-(2,6-di-*iso*-propylphenyl)-9,10-iminophenanthraquinone[31] (**Phen$_{BQ}$**), *N*,*N*-bis(3,5-di-*tert*-butyl-2-phenoxy)-1,2-phenylenediamide[24] (**H$_4$L**) were prepared by literature methods. All characterization data matched those referenced. Mn_2CO_{10} and $Mn^{III}(OAc)_3$•$2H_2O$ were purchased from Strem Chemical, Inc. All other chemicals were purchased from Sigma-Aldrich and used as received.

5.5.3. Synthesis of $Mn^{IV}(O_2^{2-})(isq)_2$.

Under N_2, in a 100mL round bottom flask $Mn^{III}(ap_{ipr})(isq_{ipr})$ (0.147 g, 0.76 mmol), was dissolved in a diethyl ether (10mL) to afford a green solution. The solution was degassed via 3 freeze-pump-thaw cycles. The reaction mixture was cooled to −78 °C and placed under an atmosphere of O_2, immediately resulting in a red solution. The solution was allowed to slowly evaporate −50 °C affording dark crystals. The crystals are temperature sensitive and degrade rapidly at room temperature. The crystals were kept cold until analyzed by X-ray diffraction.

5.5.4. Synthesis of $Mn^{III}(ap_{tBu})(isq_{tBu})$.

Under N_2, a 100 mL heavy-walled reaction flask fitted with a Teflon stopcock was charged with Mn_2CO_{10} (0.147 g, 0.38 mmol), ibq_{tBu} (0.619 g, 1.52 mmol) a stir bar, and toluene (20 mL) to afford a dark red solution. Irradition of the solution with a UV-lamp over 48 hrs afforded a purple-red solution. The solution was reduced in volume and stored at –25 °C for 48 h to deposit $Mn^{III}(ap_{tBu})(isq_{tBu})$. (0.28 g, 0.322 mmol, 42%) as purple single crystals suitable for X-ray diffraction analysis. UV-vis (THF) λ_{max}, nm (ε, M^{-1} cm^{-1}): 658 (4500), 517 (4100), 476 (3900).. Anal. Calcd for $C_{56}H_{82}MnN_2O_2$: C, 77.29; H, 9.50; N, 3.22; Found: C, 76.00; H, 9.61; N 2.96.

5.5.5. Synthesis of $Mn^{III}(phen_{ap})(phen_{isq})$.

Under N_2, a 100 mL heavy-walled reaction flask fitted with a Teflon stopcock was charged with Mn_2CO_{10} (0.20 g, 0.51 mmol), $phen_{Bq}$ (0.755 g, 2.05 mmol) a stir bar, and toluene (20 mL) to afford a dark blue-green solution. Irradition of the solution with a UV-lamp over 48 hrs afforded a brown solution. The solution was reduced in volume and stored at –25 °C for 48 h to deposit $Mn^{III}(phen_{ap})(phen_{isq})$ (0.32g, 0.41 mmol, 40%) as brown crystals. A single crystal suitable for X-ray diffraction analysis was grown by recrystallation in toluene. UV-vis (THF) λ_{max}, nm (ε, M^{-1} cm^{-1}): 589 (400). (Toluene) λ_{max}, nm (ε, M^{-1} cm^{-1}): 595 (320). A single crystal of the same sample of used for elemental analysis was determined. Anal. Calcd for $C_{52}H_{50}MnN_2O_2$: C, 79.07; H, 6.38; N, 3.55; Found: C, 75.53; H, 6.33; N 3.45.

5.5.6. Synthesis of $Mn^{III}(ap_{iPr\text{-}Br})(isq_{ipr\text{-}Br})$.

Under N_2, a 100 mL heavy-walled reaction flask fitted with a Teflon stopcock was charged with Mn_2CO_{10} (0.20 g, 0.51 mmol), $ibq_{iPr\text{-}Br}$ (0.94 g, 2.1 mmol) a stir bar, and toluene (20 mL) to afford a dark red solution. Irradition of the solution with a UV-lamp over 48 hrs afforded a purple-red solution. The solution was reduced in volume and stored at –25 °C for 48 h to deposit $Mn^{III}(ap_{iPr\text{-}Br})(isq_{iPr\text{-}Br})$. (0.54 g, 0.56 mmol, 56%) as purple single crystals. A portion was recrystallized in acetonitrile to afford green crystals suitable for X-ray diffraction analysis. UV-vis (THF) λ_{max}, nm (ε, M^{-1} cm^{-1}): 658 (4500), 517 (4100), 472 (3900).

5.5.7. Synthesis of PPN[$Mn^{III}(L^4)$].

Under N_2, bis(3,5-di-*tert*-butyl-2-phenoxy)-1,2-phenylenediamide **(H_4L)** (0.28g, 0.56 mmol) was combined with NaH (0.0053g, 2.2 mmol) in CH_3CN in 100mL round bottom flask, resulting in the evolution of H_2 Once hydrogen production ceased $Mn^{III}(OAc)_3 \cdot 2H_2O$ (0.15g, 0.56 mmol) was added directly to the reaction mixture with stirring, resulting in a brown solution. The reaction was stirred for 24 h and then filtered to remove unwanted salts. PPN-Cl (0.32g, 0.56 mmol) was added resulting in additional precipitates that were also removed by filteration. Next the solution was evaporated to dryness and redissolved in a minimal amount of THF. The solution was added dropwise to a solution of pentane to afford brown solids. The brown powder was filtered and washed with pentane. Recrystallization of the brown powder was performed by slow diffusion of pentane into a THF solution of **PPN[$Mn^{III}(L^4)$].** (0.28 g, 0.25 mmol, 45%) UV-vis (THF) λ_{max}, nm (ε, M^{-1} cm^{-1}): 832 (1000), 520 (2100)

5.5.8 Synthesis of $Mn^{IV}(L^3)_2$.

$Mn^{II}(OAc)_2 \cdot 4H_2O$ (0.10g, 0.41 mmol) and bis(3,5-di-*tert*-butyl-2-phenoxy)-1,2-phenylenediamide(0.42g, 0.82 mmol) were combined in 20mL MeOH in a 100mL round bottom flask, resulting in a green solution. The reaction was stirred for 24 h affording a green precipitate. The green powder was filtered and washed with MeOH. Recrystallization of the powder was performed by slow evaporation o from CH_2Cl_2 solutions. **$Mn^{IV}(L^3)_2$** (0.32g, 0.295 mmol, 73%) UV-vis (THF) λ_{max}, nm (ε, M^{-1} cm^{-1}): 858 (10000), 588 (9500) 434 (15000) Anal. Calcd for $C_{68}H_{90}MnN_4O_4$: C, 75.45; H, 8.38; N, 5.18; Found: C, 73.37; H, 8.17; N 4.92.

5.5.9. X-Ray Crystallography.

Crystals of $Mn^{IV}(O_2^{2-})(isq)_2$, $Mn^{III}(ap_{tBu})(isq_{tBu})$, $Mn^{III}(phen_{ap})(phen_{isq})$, $Mn^{III}(ap_{iPr\text{-}Br})(isq_{ipr\text{-}Br})$, PPN[$Mn^{III}(L^4)$and $Mn^{IV}(L^3)_2$, suitable for X-ray diffraction analysis were coated with Paratone N oil, suspended on small fiber loops and placed in a cooled nitrogen gas stream at 173 K on a Bruker D8 APEX II CCD sealed tube diffractometer. Data for $Mn^{III}(phen_{ap})(phen_{isq})$, and $Mn^{III}(ap_{iPr\text{-}Br})(isq_{ipr\text{-}Br})$ was obtained with graphite monochromated Cu Kα (λ = 1.54178 Å) radiation while diffraction data for all the others were collected using graphite monochromated Mo Kα (λ = 0.71073 Å) radiation. Data collection procedures, data processing and programs were the same for all samples. Frames were measured using a series of combinations of phi and omega scans with 10 s frame exposures and 0.5° frame widths. Data collection, indexing and initial cell refinements were all carried out using APEX II software.[32] Frame integration and final cell refinements were done using SAINT software.[33] The final cell parameters were determined from least-squares refinement on 9982 reflections for $Mn^{IV}(O_2^{2-})(isq)_2$, 2153 reflections for $Mn^{III}(ap_{tBu})(isq_{tBu})$, 4505 reflections for $Mn^{III}(phen_{ap})(phen_{isq})$, 3358 reflections for $Mn^{III}(ap_{iPr\text{-}Br})(isq_{ipr\text{-}Br})$, 6550 reflections for PPN[$Mn^{III}(L^4)$ and 2377 reflections for $Mn^{IV}(L^3)_2$. The structures were solved using direct methods and difference Fourier techniques with the SHELXTL program package.[34] Hydrogen atoms were placed in their expected chemical positions using the HFIX command and were included in the final cycles of least-squares with isotropic U_{ij}'s related to the atoms ridden upon. All non-hydrogen atoms $Mn^{III}(ap_{tBu})(isq_{tBu})$, ($Mn^{III}(phen_{ap})(phen_{isq})$, $Mn^{III}(ap_{iPr\text{-}Br})(isq_{ipr\text{-}Br})$ and $Mn^{IV}(L^3)_2$ were refined anisotropically, but only the metal-containing fragments in

the others were refined anisotropically. Scattering factors and anomalous dispersion corrections are taken from the *International Tables for X-ray Crystallography.*[35] Other details of data collection and structure refinement are provided in **Table 5.2**.

Table 5.1. Crystallographic Data and Structure Parameters for $Mn^{IV}(O_2^{2-})(isq)_2$, $Mn^{III}(phen_{ap})(phen_{isq})$, and $(Mn^{III}(ap_{tBu})(isq_{tBu})$.

Complex	$Mn^{IV}(O_2^{2-})(isq)_2$	$Mn^{III}(phen_{ap})(phen_{isq})$	$Mn^{III}(ap_{tBu})(isq_{tBu})$
Empirical formula	C52 H74 Mn N2 O4	C52 H50 Mn N2 O2	C56 H82 Mn N2 O2
Formula weight	846.07	789.88	870.18
Temperature (K)	173(2) K	173(2)	173(2)
Crystal system	Monoclinic	Orthorhombic	Monoclinic
Space group	P2(1)/c	Pccn	C2/c
Unit cell dimensions			
a (Å)	26.073(12)	20.7750(7)	90
b (Å)	26.075(12)	21.7236(7)	123.380(12)
c (Å)	16.772(8)	9.2274(3)	90
a (°)	90	90	29.350(3)
b (°)	100.259(7)	90	15.108(2)
g (°)	90	90	27.808(4)
Volume ($Å^3$)	11220(9) Å3	4164.4(2)	10297(2)
Z	8	4	8
Calculated Density (g cm^{-1})	1.002	1.26	1.123
Absorption coefficient (mm^{-1})	0.273	2.907	0.297
Crystal size (mm)	0.48 x 0.42 x 0.14	0.12 x 0.10 x 0.07	0.408 x 0.126 x 0.09
θ range for data collection (°)	1.11 to 28.33	2.94 to 69.71	1.57 to 28.28
Index ranges	-34<=h<=34	-25<=h<=19	-39<=h<=39
	-34<=k<=34	-25<=k<=25	-20<=k<=20
	-22<=l<=22	-11<=l<=10	-37<=l<=37
Reflections collected/unique	184302/27394	32359/3878	88548/12755
Goodness-of-fit on F2	2.499	1.067	1.028
Final R indices [I>2sigma(I)]	0.3533	0.0335	0.0776
R indices (all data)	0.7255	0.0957	0.21

Table 5.1. Crystallographic Data and Structure Parameters for $Mn^{III}(ap_{iPr\text{-}Br})(isq_{ipr\text{-}Br})$, PPN[$Mn^{III}(L^4)$, and $Mn^{IV}(L^3)_2$.

Complex	$Mn^{III}(ap_{iPr\text{-}Br})(isq_{ipr\text{-}Br})$	PPN[$Mn^{III}(L^4)$	$Mn^{IV}(L^3)_2$
Empirical formula	C56 H78 Br2 Mn N4 O2	C74 H82 Mn N3 O3 P2	C68 H90 Mn N4 O4
Formula weight	1053.98	1178.31	1082.38
Temperature (K)	173.15 K	173(2)	173(2) K
Crystal system	Monoclinic	Monoclinic	Triclinic
Space group	P21/n	P2(1)/n	P-1
Unit cell dimensions			
a (Å)	25.7130(5)	18.268(8)	86.689(9)
b (Å)	9.6762(2)	16.571(7)	81.304(9)
c (Å)	25.8767(1)	24.216(10)	74.961(9)
a (°)	90	90	10.128(5)
b (°)	118.499(1)	99.651(7)	12.617(7)
g (°)	90	90	25.459(13)
Volume ($Å^3$)	5658.1(2)	7227(5)	3105(3) Å3
Z	4	4	2
Calculated Density (g cm^{-1})	1.237	1.083	1.158
Absorption coefficient (mm^{-1})	3.859	0.271	0.262
Crystal size (mm)	0.198 x 0.196 x 0.09	0.22 x 0.21 x 0.16	0.30 x 0.24 x 0.13
θ range for data collection (°)	1.99 to 68.25	1.53 to 30.51	1.67 to 30.53
Index ranges	-30<=h<=30	-26<=h<=26	-14<=h<=14
	-11<=k<=11	-23<=k<=23	-17<=k<=17
	-29<=l<=29	-34<=l<=34	-36<=l<=36
Reflections collected/unique	16909/9805	143981/22067	34928/18508
Goodness-of-fit on F2	1.051	1.083	1.026
Final R indices [I>2sigma(I)]	0.0398	0.0876	0.0853
R indices (all data)	0.1086	0.2155	0.1756

5.6. Works Cited

1. Barton, D., H. R., Martell, A. E., Sawyer, D. T.,, *The Activation of Dioxygen and Homogeneous Catalytic Oxidation*. Plenum: New York, 1993.

2. Sawyer, D. T., *Oxygen Chemistry, International Series Of Monographs On Chemistry 26* Oxford University Press: New York, 1991.

3. Que, L.; Ho, R. Y. N., Dioxygen Activation by Enzymes with Mononuclear Non-Heme Iron Active Sites. *Chemical Reviews* **1996,** *96* (7), 2607-2624, doi:10.1021/cr960039f.

4. Simándi, L. I., *Advances in Catalytic Activation of Dioxygen by Metal Complexes*. Springer: New York, 2003.

5. Borovik, A. S. Z., P. J.; Zart, M. K., Dioxygen Binding and Activation: Reactive Intermediates. In *Activation of Small Molecules: Organometallic and Bioinorganic Perspectives*, Tolman, W. B., Ed. Wiley-VCH: Weinheim, Germany, 2006; pp 187–234.

6. Meunier, B., *Biomimetic Oxidations Catalyzed by Transition Metal Complexes*. Imperial College: London, 2000.

7. Kovaleva, E. G.; Neibergall, M. B.; Chakrabarty, S.; Lipscomb, J. D., Finding Intermediates in the O2 Activation Pathways of Non-Heme Iron Oxygenases. *Accounts of Chemical Research* **2007,** *40* (7), 475-483, doi:10.1021/ar700052v.

8. Costas, M.; Mehn, M. P.; Jensen, M. P.; Que, L., Dioxygen Activation at Mononuclear Nonheme Iron Active Sites: Enzymes, Models, and Intermediates. *Chemical Reviews* **2004,** *104* (2), 939-986, doi:10.1021/cr020628n.

9. Chufán, E. E.; Puiu, S. C.; Karlin, K. D., Heme–Copper/Dioxygen Adduct Formation, Properties, and Reactivity. *Accounts of Chemical Research* **2007,** *40* (7), 563-572, doi:10.1021/ar700031t.

10. Kieber-Emmons, M. T.; Riordan, C. G., Dioxygen Activation at Monovalent Nickel. *Accounts of Chemical Research* **2007,** *40* (7), 618-625, doi:10.1021/ar700043n.

11. Suzuki, M., Ligand Effects on Dioxygen Activation by Copper and Nickel Complexes: Reactivity and Intermediates. *Accounts of Chemical Research* **2007,** *40* (7), 609-617, doi:10.1021/ar600048g.

12. Stanciu, C.; Jones, M. E.; Fanwick, P. E.; Abu-Omar, M. M., Multi-electron activation of dioxygen on zirconium(IV) to give an unprecedented bisperoxo complex. *Journal of the American Chemical Society* **2007,** *129* (41), 12400-+, doi:10.1021/ja075396u.

13. Cho, J.; Sarangi, R.; Kang, H. Y.; Lee, J. Y.; Kubo, M.; Ogura, T.; Solomon, E. I.; Nam, W., Synthesis, Structural, and Spectroscopic Characterization and Reactivities of Mononuclear Cobalt(III)−Peroxo Complexes. *Journal of the American Chemical Society* **2010,** *132* (47), 16977-16986, doi:10.1021/ja107177m.

14. Donoghue, P. J.; Gupta, A. K.; Boyce, D. W.; Cramer, C. J.; Tolman, W. B., An Anionic, Tetragonal Copper(II) Superoxide Complex. *Journal of the American Chemical Society* **2010,** *132* (45), 15869-15871, doi:10.1021/ja106244k.

15. Cramer, C. J.; Tolman, W. B., Mononuclear Cu–O^2 Complexes: Geometries, Spectroscopic Properties, Electronic Structures, and Reactivity. *Accounts of Chemical Research* **2007,** *40* (7), 601-608, doi:10.1021/ar700008c.

16. Fukuzumi, S.; Kotani, H.; Lucas, H. R.; Doi, K.; Suenobu, T.; Peterson, R. L.; Karlin, K. D., Mononuclear Copper Complex-Catalyzed Four-Electron Reduction of Oxygen. *Journal of the American Chemical Society* **2010,** *132* (20), 6874-6875, doi:10.1021/ja100538x.

17. Korendovych, I. V.; Kryatov, S. V.; Rybak-Akimova, E. V., Dioxygen Activation at Non-Heme Iron: Insights from Rapid Kinetic Studies. *Accounts of Chemical Research* **2007,** *40* (7), 510-521, doi:10.1021/ar600041x.

18. F. Meyer, C. L., *Organometallic Oxidation Catalysis*. Springer-Verlag: Heidelberg, 2007; Vol. 22.

19. Abakumov, G. A.; Cherkasov, V. K.; Poddel'sky, A. I.; Bubnov, M. P.; Abakumova, L. G.; Fukin, G. K., A Novel Five-Coordinate Manganese(III) Complex with 4,6-Di-(2,6-di-isopropylphenyl)-1,2-iminobenzoquinone: Reversible Interaction with Dioxygen. *Doklady Chemistry* **2004,** *399* (1), 207-210, doi:10.1023/b:doch.0000048078.97268.86.

20. Abakumov, G. A.; Poddel'sky, A. I.; Bubnov, M. P.; Fukin, G. K.; Abakumova, L. G.; Ikorskii, V. N.; Cherkasov, V. K., Manganese(III) and rhenium(II) complexes with bulky 4,6-di-tert-butyl-N-(2,6-di-iso-propylphenyl)-o-iminobenzoquinonato ligands via carbonyls of corresponding metals. *Inorganica Chimica Acta* **2005,** *358* (13), 3829-3840, doi:10.1016/j.ica.2005.07.003.

21. Bhattacharya, S.; Gupta, P.; Basuli, F.; Pierpont, C. G., Structural Systematics for o-C_6H_4XY Ligands with X,Y= O, NH, and S Donor Atoms. o-Iminoquinone and o-Iminothioquinone Complexes of Ruthenium and Osmium. *Inorganic Chemistry* **2002,** *41* (22), 5810-5816, doi:10.1021/ic025766+.

22. Poddel'sky, A. I.; Cherkasov, V. K.; Abakumov, G. A., Transition metal complexes with bulky 4,6-di-tert-butyl-N-aryl(alkyl)-o-iminobenzoquinonato ligands: Structure, EPR and magnetism. *Coordination Chemistry Reviews* **2009,** *253* (3-4), 291-324, doi:10.1016/j.ccr.2008.02.004.

23. Chun, H.; Chaudhuri, P.; Weyhermüller, T.; Wieghardt, K., o-Iminobenzosemiquinonato Complexes of Mn(III) and Mn(IV). Synthesis and Characterization of [MnIII(LISQ)2(LAP)] (St = 1) and [MnIV(LISQ)2(LAP-H)] (St = 1/2). *Inorganic Chemistry* **2002,** *41* (4), 790-795, doi:10.1021/ic010860w.

24. Chaudhuri, P.; Hess, M.; Müller, J.; Hildenbrand, K.; Bill, E.; Weyhermüller, T.; Wieghardt, K., Aerobic Oxidation of Primary Alcohols (Including Methanol) by Copper(II)− and Zinc(II)−Phenoxyl Radical Catalysts. *Journal of the American Chemical Society* **1999,** *121* (41), 9599-9610, doi:10.1021/ja991481t.

25. Bill, E.; Bothe, E.; Chaudhuri, P.; Chlopek, K.; Herebian, D.; Kokatam, S.; Ray, K.; Weyhermüller, T.; Neese, F.; Wieghardt, K., Molecular and Electronic Structure of Four- and Five-Coordinate Cobalt Complexes Containing Two o-Phenylenediamine- or Two o-Aminophenol-Type Ligands at Various Oxidation Levels: An Experimental, Density Functional, and Correlated ab initio Study. *Chemistry – A European Journal* **2005,** *11* (1), 204-224, doi:10.1002/chem.200400850.

26. Abakumov, G.; Cherkasov, V.; Bubnov, M.; Abakumova, L.; Ikorskii, V.; Romanenko, G.; Poddel'sky, A., Synthesis and structures of five-coordinate bis-iminobenzosemiquinone complexes M(ISQ-R)X (X = Cl, Br, I, or SCN; M = Co, Fe, or Mn;). *Russian Chemical Bulletin* **2006,** *55* (1), 44-52, doi:10.1007/s11172-006-0213-3.

27. Attia; Pierpont, C. G., Valence Tautomerism within a Linear Polymer Consisting of Pyrazine-Bridged Manganese−Quinone Subunits. Synthesis and Characterization of

[MnIII(μ-pyz)(3,6-DBSQ)(3,6-DBCat)]n. *Inorganic Chemistry* **1997,** *36* (27), 6184-6187, doi:10.1021/ic970781d.

28. Smolyaninov, I.; Letichevskaya, N.; Kulakov, A.; Aref'ev, Y.; Pashchenko, K.; Berberova, N., Study of the mechanism of redox transformations of sterically hindered <i>N</i> -aryl- <i>o</i> -iminoquinones. *Russian Journal of Electrochemistry* **2007,** *43* (10), 1187-1199, doi:10.1134/s1023193507100138.

29. Abakumov, G. A.; Poddel'sky, A. I.; Grunova, E. V.; Cherkasov, V. K.; Fukin, G. K.; Kurskii, Y. A.; Abakumova, L. G., Reversible Binding of Dioxygen by a Non-Transition-Metal Complex. *Angewandte Chemie International Edition* **2005,** *44* (18), 2767-2771, doi:10.1002/anie.200462503.

30. Poddel'sky, A. I.; Kurskii, Y. A.; Piskunov, A. V.; Somov, N. V.; Cherkasov, V. K.; Abakumov, G. A., Triphenylantimony(V) o-amidophenolates with unsymmetrical N-aryl group for a reversible dioxygen binding. *Applied Organometallic Chemistry* **2011,** *25* (3), 180-189, doi:10.1002/aoc.1738.

31. Abakumov, G. A.; Cherkasov, V. K.; Druzhkov, N. O.; Kurskii, Y. A.; Fukin, G. K.; Abakumova, L. G.; Kocherova, T. N., Synthesis, Structures, and Properties of Novel *N*-Aryl-phenanthren-*o*-iminoquinones. *Synthetic Communications* **2006,** *36* (21), 3241-3247, doi:10.1080/00397910600908934.

32. APEX II, Analytical X-Ray Systems, Brukers AXS, Inc., Madison, WI, 2005.,

33. SAINT Version 6.45A, Analytical X-ray Systems, Brukers AXS, Inc., Madison, WI,
2003.,

34. SHELXTL Version 6.12, Analytical X-ray Systems, Bruker AXS, Inc., Madison, WI,
2002.,

35. Wilson, J. C., *In International Tables for X-ray Crystallography, Volume C;*. Academic Publishers: Dordrecht, The Netherlands, 1992.

CHAPTER 6

CONCLUSIONS AND FUTURE DIRECTIONS

6.1 Conclusions

In this work, I have synthesized new well-defined manganese(III) complexes that are active for selective aerobic oxidations of organic substrates. The use of redox active ligands are important for the multielectronic reaction with O_2. By understanding the mechanistic aspects of the reaction chemistry I was able to rationally design new complexes and pursue various oxidative transformations.

My initial work started with the robust $[Mn^{III}(Br_4cat)_2]^-$ fragment. The complex itself is inert to dioxygen, but in the presence of catechol substrates it reacts rapidly with O_2 to produce quinone and H_2O_2 in an oxidase-type dehydrogenation reaction. Although, the reaction proceeds via a series of $1e^-$ steps, the reaction is selective for the $2e^-$ dehydrogenation of catechols. Both metal- and ligand-centered redox events occur during catalytic turnover to facilitate the multielectron reaction chemistry. The ability of a coordinatively-unsaturated $[Mn^{III}(Br_4cat)_2]^-$ fragment to bind substrate prior to reaction with O_2 provided selectivity for O_2 intramolecular redox processes. This led me to pursue the development of new aerobic multielectron redox cycles using $[Mn^{III}(Br_4cat)_2]^-$.

The ability of the $[Mn^{III}(Br_4cat)_2]^-$ fragment to bind alcohols was observed, however deprotonation was required to initiate a reaction of the catalyst–substrate complex with O_2. The deprotonation of alcohol complexes result in the formation of a dimeric species. In the case of benzyl alcohol, the **$[Mn^{III}_2(\mu\text{-}OBn)_2]^{4-}$** anion dimer reacts

with O_2 to efficiently oxidize 1 equiv of $[OBn]^-$ to PhCHO. Selectivity in the net $2e^-$ reaction apparently derives from the ability of the $[Mn^{III}(Br_4cat)_2]^-$ fragment to bind BnOH and assemble a catalyst–substrate complex that initiates an inner-sphere reaction with O_2. Although the $[Mn^{III}(Br_4cat)_2]^-$ fragment is able to mediate stoichiometric oxidation of $[OBn]^-$, the complex is limited catalytically. This is because dimer formation requires a base to deprotonate the weakly acidic primary alcohols, but attempts to use excess bases lead to catalyst degradation. Because of this, the $[Mn^{III}(Br_4cat)_2]^-$ fragment is limited to only the selective aerobic oxidation of activated benzylic alcohols.

As a result, manganese(III) complexes with redox-active aminophenol ligands were pursued for catalytic oxidase-type oxidations. These ligands are able mediate the net $2e^-$ redox changes without a change in manganese(III) oxidation. $Mn^{III}Br(isq)_2$ is a uniquely well-defined metal catalyst for aerobic homocoupling of PhMgBr. Stoichiometric reactions of $Mn^{III}Br(isq)_2$ with PhMgBr result in the formation of $[Mn^{III}(ap)_2]^-$ and biphenyl. The reduced $[Mn^{III}(ap)_2]^-$ is oxidized by O_2 to regenerate $Mn^{III}Br(isq)_2$ in a series of $1e^-$ ligand-mediated reactions. Magnesium bromide generated during the reduction of PhMgBr is important in the reoxidation of $[Mn^{III}(ap)_2]^-$ because it acts as a trap and stabilizes the $[Mn^{III}(isq)_2]^+$ fragment against oxidative catalyst degradation. The Br^- trapping provides a mechanism for redox control in $2e^-$ reactions of $[Mn^{III}(ap)_2]^-$ with O_2 which can be applied for future reactions.

Reactions in the absence Br^- afford the dioxygen adduct $Mn^{IV}(O_2^{2-})(isq)_2$, which can be observed and partially isolated. Structural details of $Mn^{IV}(O_2^{2-})(isq)_2$ are necessary to provide insight into the nature of the inner sphere O_2 activation. $Mn^{IV}(O_2^{2-})(isq)_2$ complexes are prone to rapid overoxidation releasing free iminoquinone and ultimately

leading to catalyst degradation. Using more electron deficient aminophenol type ligands and macrocyclic ligands can be used as effective strategies to avoid overoxidation in future catalyst development.

6.2 Future Directions

Future efforts in this work should involve making the $Mn^{III}Br(isq)_2$ fragment more resistant to overoxidation. The modular design of aminophenol ligands has led to the synthesis of many derivatives recently.[1-4] New Mn(III) complexes can be prepared by using aminophenol-derived ligands containing electron deficient groups known in literature.[1] (**Figure 1)**

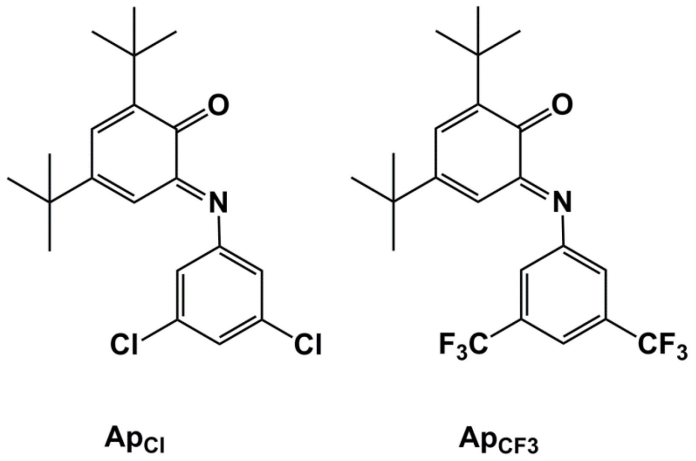

Figure 6.1 Ligands for the development of Mn(III) aminophenol complexes.

These ligands may help to stabilize the $Mn^{III}X(isq)_2$ fragment against oxidative degradation. However, if these ligands are not sterically bulky enough to avoid ligand redistribution that has been observed previously in other high spin d^4 complex efforts can be made to modify the existing $Mn^{III}Br(isq)_2$ fragment which contains the bulky

isopropyl groups. 4-bromo-2,6-diisopropylaniline can be used as a convenient precursor for the synthesis of new 2,6-iPr substituted aminophenol ligands that are electron deficient. **(Figure 2)**

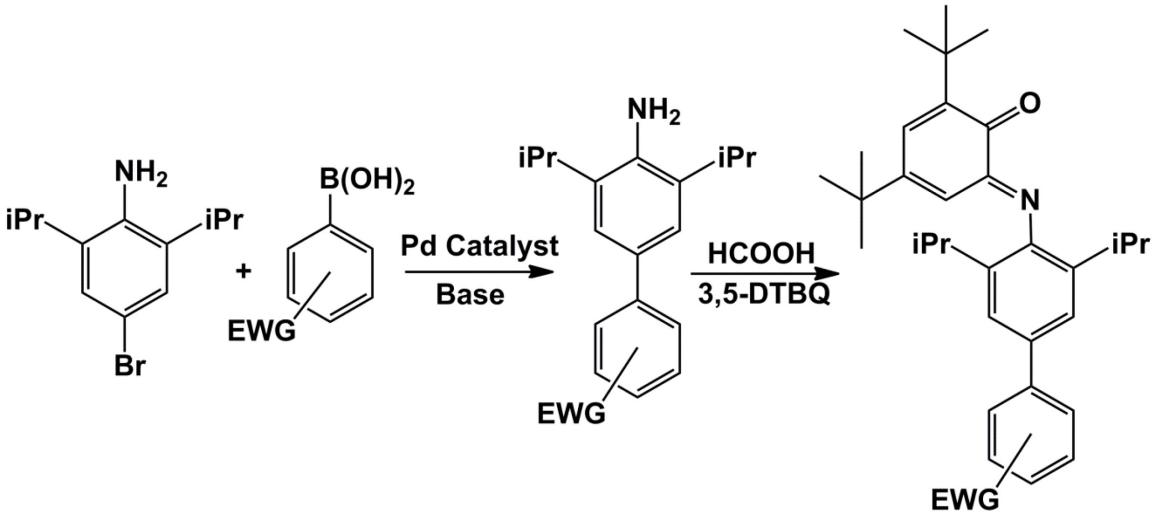

Figure 6.2. Proposed synthesis for new 2,6-iPr substituted aminophenol derivatives.

With new and more robust Mn(III) aminophenol complexes developed, efforts can be made to advance the oxidative coupling chemistry observed with $Mn^{III}Br(isq)_2$ and new oxidase-type transformations such as oxidative cross-coupling can be pursued.

6.3 Works Cited

1. Mukherjee, C.; Pieper, U.; Bothe, E.; Bachler, V.; Bill, E.; Weyhermüller, T.; Chaudhuri, P., Ligand-Derived Oxidase Activity. Catalytic Aerial Oxidation of Alcohols (Including Methanol) by Cu(II)-Diradical Complexes. *Inorganic Chemistry* **2008,** *47* (19), 8943-8956, doi:10.1021/ic8009767.

2. Blackmore, K. J.; Ziller, J. W.; Heyduk, A. F., "Oxidative addition" to a Zirconium(IV) redox-active ligand complex. *Inorganic Chemistry* **2005,** *44* (16), 5559-5561, doi:10.1021/ic050997c.

3. Poddel'sky, A. I.; Cherkasov, V. K.; Abakumov, G. A., Transition metal complexes with bulky 4,6-di-tert-butyl-N-aryl(alkyl)-o-iminobenzoquinonato ligands: Structure, EPR and magnetism. *Coordination Chemistry Reviews* **2009,** *253* (3-4), 291-324, doi:10.1016/j.ccr.2008.02.004.

4. Poddel'sky, A. I.; Kurskii, Y. A.; Piskunov, A. V.; Somov, N. V.; Cherkasov, V. K.; Abakumov, G. A., Triphenylantimony(V) o-amidophenolates with unsymmetrical N-aryl group for a reversible dioxygen binding. *Applied Organometallic Chemistry* **2011,** *25* (3), 180-189, doi:10.1002/aoc.1738.